

TECHNISCHE UNIVERSITÄT MÜNCHEN

Wissenschaftszentrum Weihenstephan für Ernährung, Landnutzung und Umwelt

Lehrstuhl für Lebensmittelverpackungstechnik

# **Texturization of pea protein isolates using high moisture extrusion cooking**

Raffael Josef Johannes Osen

Vollständiger Abdruck der von der Fakultät Wissenschaftszentrum Weihenstephan für Ernährung, Landnutzung und Umwelt der Technischen Universität München zur Erlangung des akademischen Grades eines

Doktor-Ingenieurs

genehmigten Dissertation.

Vorsitzender:

Prof. Dr.-Ing. U. Kulozik

Prüfer der Dissertation:

1. Prof. Dr. rer. nat. H.-Chr. Langowski

2. Prof. Dr.-Ing. H. Jäger

Die Dissertation wurde am 25.04.2017 bei der Technischen Universität München eingereicht und durch die Fakultät Wissenschaftszentrum Weihenstephan für Ernährung, Landnutzung und Umwelt am 29.08.2017 angenommen.



**Declaration**

I, the undersigned, hereby declare that the work contained in this thesis is my own original work and that I have not previously in its entirety or part of it submitted it to any university for a degree, and to the best of my knowledge, does not include material previously published or written by another person, except where due reference is made in the text.

---

Signature

---

Date

**Acknowledgements**

The present work was carried out in the department for Food Process Development at the Fraunhofer Institute for Process Engineering and Packaging (IVV).

I would like to express my gratitude to those who have contributed considerably to the successful completion of this thesis. In particular, I would like to express my sincere appreciation to the following:

First and foremost, I would like to thank my advisors Professor Langowski for the allocation of the topic and his continuous support of the thesis and PD Dr.-Ing. Peter Eisner for his confidence in the subject and myself as a researcher. Furthermore, I thank Professor Jäger for acting as second examiner and Professor Kulozik for chairing the examination committee.

In particular, my most sincere gratitude goes to Dr. Ute Schweiggert-Weisz for her excellent supervision during the course of the work. Ute's immense knowledge, her enthusiasm and her dedication to science is a great motivation for all young scientists under her supervision.

I would also like to thank Dr.-Ing. Florian Wild for his supervision and patience during the beginning of the project. Furthermore, I thank Dr. Simone Toelstede for her motivation and her support during the drafting of the publications.

Many thanks goes to the analytics team Elfriede Bischof, Evi Müller, Sigrid Bergmann and Sigrid Gruppe, the technical team led by Thomas Hubensteiner as well as a number of students that contributed by their accurate work: Katharina Rau, Stefanie Limbrunner, Katharina Auer, Anja Sraga, Rainer Giggenbach and Christian Hülsbergen.

Finally I'd like to thank my family and my wife Tharalinee for their love and support.

## Preliminary remarks

Parts of this thesis have been published in international peer reviewed journals, which are listed below.

## Peer-reviewed articles

Osen, R., Schweiggert-Weisz, U., 2016. High-Moisture Extrusion: Meat Analogues. *Reference Module in Food Sciences*. Elsevier, pp. 1–7.

Osen, R., Toelstede, S., Eisner, P., Schweiggert-Weisz, U. (2015). Effect of high moisture extrusion cooking on the protein composition and protein-protein interactions of pea (*Pisum Sativum* L.) protein isolates. *International Journal of Food Science and Technology* **50**, 1390-1396.

Osen, R., Toelstede, S., Wild, F., Eisner, P., Schweiggert-Weisz, U. (2014). High moisture extrusion cooking of pea protein isolates: Raw material characteristics, extruder responses, and texture properties. *Journal of Food Engineering* **127**, 67-74.

## Oral presentations

Osen, R. (2017) Texturization of plant protein using extrusion cooking. Innovations in Food Science and technology. Erding, Germany.

Osen, R. (2014). Texturization of pea proteins by high moisture extrusion cooking. Advances in Food Processing: Challenges for the Future; Campinas, Brasil

Osen, R. (2014). High moisture extrusion cooking of pea protein isolate: Effect of extrusion temperature on the protein composition and protein-protein interactions. IUFoST, Montreal, Canada

Mathmann K., Osen, R., Eisner, P., Briesen, H. (2013). Comparison of the microstructure of meat and meat-like extruded vegetable proteins. Delivery of Functionality in Complex Food Systems- Physically-Inspired Approaches from the Nanoscale to the Microscale, Haifa, Israel

Osen, R., Limbrunner, S., Wild, F., Ute Weisz (2012). Interactions of proteins during high-moisture extrusion cooking of pea protein. European Federation of Food Science and Technology (EFFoST), Montpellier, France

## Poster presentations

Osen, R., Toelstede, S., Wild, F., Eisner, P., Schweiggert-Weisz, U.(2014). High moisture extrusion cooking of pea protein isolates: Raw material characteristics, extruder responses, and texture properties. Food Structure Symposium: From molecules to functionality, Amsterdam, Netherlands

Osen, R., Limbrunner, S., Wild, F., Schweiggert-Weisz, U. (2013). The role of covalent disulfide-bonding during high-moisture extrusion cooking of pea protein isolate. Capabilities of Vegetable Proteins, 19th International Scientific Conference, IGV Institut für Getreideverarbeitung GmbH, Nuthetal, Germany



---

**Abstract**

The aim of this thesis was to elucidate the texturization of pea protein using high moisture extrusion cooking for the development of anisotropic fibrous structures. Three commercially available pea protein isolates were characterized regarding their chemical composition and technofunctional properties. Additionally, the viscoelastic properties of protein dispersions were evaluated as a function of temperature and moisture content typical for high moisture extrusion. Structure formation of anisotropic fibrous extrudates was analyzed by microscopic visualization as well as quantitative texture analysis and the flow behavior in the cooling die was visually inspected. Finally, protein reactions during texturization under high-moisture conditions were determined with focus on protein-protein interactions.

The comparison of pea protein ingredients revealed that the functional and rheological properties of the pea proteins correlated with their thermal properties. These in turn affected the rheological behavior below the denaturation temperature of the proteins. Small strain oscillatory experiments under thermal conditions similar to those during extrusion cooking were used to investigate thermally induced network formation of protein dispersions. Applying these findings to extrusion texturization suggested a plasticization of the protein dispersion in the cooking zone and a subsequent solidification of the fluid upon cooling. Texturization by high moisture extrusion cooking yielded extrudates with similar characteristics to meat in terms of fibrousness and microstructure. This demonstrated the potential of pea protein isolates as highly valuable protein ingredients for the development of fibrous meat substitutes. The fiber structure formation could be controlled in the confines of a relatively narrow process window mainly by the extrusion temperature.

Furthermore, the effect of high moisture extrusion cooking on the proteins with focus on the bonding nature was assessed. The legumin protein fraction participated in a macromolecular network in extruded protein that is aggregated and cross-linked via disulfide bonds; the vicilin and convicilin protein fractions did not contribute to a network formation. In addition to noncovalent interactions, covalent disulfide bonds were involved in the cross-linking of the legumin fraction in extrudates, stabilizing the fiber structures at extrusion temperatures above 110 °C. A temperature-induced damage of individual amino acids could not be observed under moderate thermal extrusion conditions below 140 °C, suggesting that high moisture extrusion cooking is a comparatively mild process compared to conventional thermoplastic extrusion for the production of high-quality meat substitutes.

**Kurzfassung**

Das Ziel dieser Arbeit war die Untersuchung von Faserstrukturbildungsprozessen bei der Nasstexturierung von Erbsenproteinisolat mittels Kochextrusion. Als Basis für weiterführende Texturierungsuntersuchungen erfolgte eine Charakterisierung kommerziell verfügbarer Erbsenproteinisolate. Die Rohstoffe zeichneten sich durch ähnliche Inhaltsstoffzusammensetzungen aus. Unterschiede zeigten sich in den technofunktionellen Eigenschaften, sowie im rheologischen Verhalten unterhalb der Denaturierungstemperatur, welche sich ursächlich auf den Denaturierungsgrad der Proteine zurückführen ließen. Weiterhin wurden die Vernetzungseigenschaften von Proteindispersionen unter extrusionsähnlichen Bedingungen in Bezug auf Temperatur und Druck anhand des viskoelastischen Verhaltens untersucht. Die temperaturinduzierte Erweichung der Masse, welche durch eine Reduzierung der Viskosität und der Fließgrenze gekennzeichnet war, lässt eine Plastifizierung der Extrusionsmasse in der Kochzone des Extruders vermuten. Aus den viskosen und elastischen Moduli lässt sich ableiten, dass die Extrusionsmasse unter den gegebenen Extrusionsbedingungen stets als viskoelastischer Feststoff vorliegt.

Unter Verwendung einer Laborextrusionsanlage ließen sich Extrudate mit unterschiedlichen Texturprofilen herstellen. Diese zeichneten sich durch faserige, fleischähnliche Textureigenschaften aus und zeigen damit das Potential von Erbsenprotein als alternative Proteinquelle zu Soja für die Entwicklung pflanzlicher Fleischalternativen auf. Die Faserstrukturbildung ließ sich in den Grenzen eines vergleichsweise engen Prozessfensters maßgeblich durch die Extrusionstemperatur steuern und anhand bildgebender und texturanalytischer Methoden quantifizieren. Um den Einfluss des Rohstoffs sowie der Extrusionstemperatur auf Änderungen in den Bindungsverhältnissen der Proteine bestimmen zu können, wurde der Anteil löslicher Proteine in selektiven Lösungsreagenzien bestimmt. Dabei zeigte sich, dass neben nicht-kovalenten Wechselwirkungen insbesondere kovalente Disulfidbrücken an der Quervernetzung der Leguminfraktion in kochextrudierten Nasstexturaten auf Erbsenbasis beteiligt sind, welche ab Extrusionstemperaturen größer 110 °C zur Stabilisierung der Faserstrukturen führen. Eine temperaturinduzierte Schädigung einzelner Aminosäuren unter extrusionstypischen Bedingungen konnte nicht beobachtet werden, was im Gegensatz zum konventionellen thermoplastischen Extrusionsprozess auf eine relativ niedrige thermische Belastung der Proteine schließen lässt.



---

**Index of Contents**

1	Introduction and objectives .....	1
2	State of the art.....	5
2.1	Physicochemical properties of food proteins .....	5
2.1.1	Protein conformation.....	5
2.1.2	Protein denaturation .....	8
2.1.3	Functional properties.....	8
2.2	Sources for plant proteins.....	11
2.2.1	Cereals.....	11
2.2.2	Legumes .....	13
2.3	Pea protein ingredients .....	17
2.3.1	Pea seeds .....	17
2.3.2	Fractionation and protein enrichment.....	18
2.3.3	Protein composition.....	20
2.3.4	Functional properties.....	24
2.3.5	Nutritional and anti-nutritional factors.....	26
2.4	Extrusion in food processing.....	28
2.4.1	Extruders and extrusion parameters .....	28
2.4.2	Texturization of food products during extrusion cooking.....	35
2.4.3	Rheological characterization of extruded food materials.....	38
2.5	High moisture extrusion cooking .....	48
2.5.1	Physico-chemical material properties .....	49
2.5.2	Texturization and fiber formation .....	51
2.5.3	Protein reactions during texturization .....	57
3	Materials and Methods .....	63
3.1	Characterization of pea protein ingredients.....	63
3.1.1	Chemical composition.....	63
3.1.2	Particle size distribution .....	63
3.1.3	Microstructure .....	64
3.1.4	Thermal properties .....	64
3.1.5	Functional properties.....	64
3.2	High moisture extrusion cooking .....	66
3.2.1	Extrusion procedure on laboratory scale .....	66
3.2.2	Extrusion procedure on pilot scale .....	71
3.3	Rheological measurements.....	73
3.3.1	Shear viscosity.....	73
3.3.2	Small amplitude oscillation .....	73
3.4	Characterization of high moisture extrudates.....	76
3.4.1	Qualitative microstructure analysis .....	76
3.4.2	Texture analysis.....	78

3.4.3	Water activity .....	79
3.4.4	Protein composition.....	79
3.4.5	Protein-protein interactions .....	80
3.4.6	Statistical Analysis .....	82
4	Results and discussion .....	83
4.1	Characterization of pea protein ingredients.....	83
4.1.1	Chemical composition .....	83
4.1.2	Particle size distribution .....	84
4.1.3	Thermal properties.....	85
4.1.4	Functional properties .....	86
4.2	Rheological properties of protein dispersions .....	92
4.2.1	Comparison of pea protein ingredients.....	93
4.2.2	Viscoelastic properties within a temperature range of 30-90 °C.....	98
4.2.3	Temperature sweep experiments within a temperature range of 50-150 °C.....	105
4.2.4	Residence time distribution during extrusion .....	111
4.3	Mechanical properties of high moisture extrudates.....	118
4.3.1	Visual microstructure and texture of extrudates and fibrous meat samples .....	118
4.3.2	Effect of protein ingredients and cooking temperature .....	120
4.3.3	Specific mechanical energy .....	123
4.3.4	Effect of cooling die and moisture content.....	125
4.3.5	Offline flow visualization in the cooling die .....	127
4.4	Protein reactions during high moisture extrusion.....	136
4.4.1	Amino acid composition.....	136
4.4.2	Molecular weight distribution .....	138
4.4.3	Degree of hydrolysis.....	141
4.4.4	Protein solubility.....	142
5	Conclusions.....	147
6	Summary .....	151
7	Literature.....	154
8	Appendix.....	173
9	Curriculum Vitae .....	175

## Index of Illustrations

Figure 1: Molecular structure of $\alpha$ -amino acids and a polypeptide chain bonded by peptide bonds .....	5
Figure 2: Production quantity of cereal grains (million tons) in 2014. ....	12
Figure 3: World pulse production (million tons) in 2014 .....	15
Figure 4: Longitudinal section of a pea seed.....	16
Figure 5: Worldwide production quantity of peas from 2004 until 2014 (FAO 2017).....	18
Figure 6: Flow diagram for processing of pea seeds into hulls, protein fraction and starch fractions..	19
Figure 7: Composition of pea globulins.....	21
Figure 8: SDS-PAGE pattern of pea protein products under reducing conditions.	20
Figure 9: Size exclusion chromatogram of protein isolates from field pea.....	23
Figure 10: Relative proportion of secondary structures of protein isolates from field pea.....	23
Figure 11: Gelling of globular proteins such as pea proteins.....	26
Figure 12: Schematic view of basic components of a food extruder. ....	28
Figure 13: Classification of extruders .....	29
Figure 14: Velocity profile in the extruder metering section. ....	30
Figure 15: Screw geometry of a conveying element.....	31
Figure 16: Effect of conveying elements with different pitch on filling degree in free screw volume.	31
Figure 17: Kneading blocks with different stagger and conveying direction .....	32
Figure 18: Clearance between screws and barrel in a co-rotating twin-screw extruder.....	32
Figure 19: Stimulus response techniques for the determination of residence time distribution.....	35
Figure 20: The glass transition and denaturation temperatures of the 11S broad bean globulin.....	36
Figure 21: The Two-Plates-Model for shear tests.....	38
Figure 22: Flow curves for classification of time-independent flow behavior of fluid foods.....	39
Figure 23: Typical RVA pasting profile of rice starch showing the commonly measured parameters.	41
Figure 24: Shear force, deformation and deformation angle in gap h.....	42
Figure 25: Preset shear strain function $\gamma$ and resulting shear stress function $\tau$ .....	42
Figure 26: Vector diagram showing $G'$ , $G''$ , the resulting vector $G^*$ .....	43
Figure 27: Stress amplitude sweep: linear viscoelastic range, the yield point and the flow point.....	44
Figure 28: Example for two polymers characterized using frequency sweeps .....	45
Figure 29: Viscoelastic response of a material undergoing gelation.....	46
Figure 30: Gelling properties of pea protein. ....	46
Figure 31: Early historical model for the structure formation mechanism during food processing.....	51
Figure 32: Schematic diagram of a protein molecule unfolding, aligning with the flow of the extruder barrel and forming new bonds with another molecule. ....	52
Figure 33: Model for phase separation mechanism during stream alignment in the cooling die.....	53
Figure 34: 2D-simulation of an extrusion process using the Generalized Material Point Method .....	54
Figure 35: Transmittance infrared spectra of extruded soy protein isolate .....	60

Figure 36: Screw profile showing the screw configuration and the location of thermocouples.....	66
Figure 37: Schematic screw profile showing the screw configuration, the heating profile and the image of gelled extruded material in the screw section .....	69
Figure 38: Screw profile during pilot-scale extrusion experiments.....	71
Figure 39: Components of a cooling die segment and connecting plate. ....	72
Figure 40: Stress amplitude sweep of a sample showing the yield stress and the flow point .....	75
Figure 41: Schematic sample preparation procedure for scanning electron microscopy. ....	76
Figure 42: Sample preparation for assessing the anisotropic structures.....	77
Figure 43: Schematic representation of anisotropic structures at the cutting side of extrudates from inside the die channel after a dead-stop.....	77
Figure 44: Evaluation of cutting strength of extrudates at room temperature. ....	78
Figure 45: Evaluation of cutting strength of meat samples parallel to the fibers and across the fibers	79
Figure 46: Volume fraction of particles from pea protein ingredients. ....	84
Figure 47: Scanning electron microscopy of pea protein isolates. ....	85
Figure 48: DSC thermograms of protein dispersions (30% w/w) heated at 5 °C/min.....	86
Figure 49: Protein solubility of protein ingredients as a function of pH. ....	87
Figure 50: RVA viscosity curves of pea protein isolates .....	89
Figure 51: Specific mechanical energy values of pea protein isolates during initial start-up .....	91
Figure 52: Viscosity curves of diluted protein dispersion obtained by shear rate sweep experiments..	93
Figure 53: Viscoelastic properties of protein dispersions with 65% w.b. moisture content obtained by stress amplitude sweep experiments.....	95
Figure 54: Viscoelastic properties of protein dispersion with w.b. moisture content of 65% (w/w) obtained by frequency sweep experiments .....	97
Figure 55: Viscoelastic properties of protein dispersion of PPI 1 obtained by stress amplitude sweep experiments with deformation at constant angular frequency .....	100
Figure 56: Viscoelastic properties of protein dispersion of PPI 1 obtained by frequency sweep experiments.....	103
Figure 57: Viscoelastic properties ( $G'$ , $G''$ ) of a protein dispersion of PPI 1 at 65% w.b. moisture content (w/w) obtained by temperature sweep experiments.....	106
Figure 58: Viscoelastic properties ( $\tan\delta$ , $ \eta^* $ ) of protein dispersion of PPI 1 at 65% w.b. moisture content (w/w) obtained by temperature sweep experiments.....	107
Figure 59: Apparent viscosity of PPI 2 at 65% w.b. moisture content (w/w) during temperature sweep experiments as a function of time at a shear rate of (a) $1\text{s}^{-1}$ and (b) $20\text{s}^{-1}$ .....	109
Figure 60: Residence time distribution function (a) and sum function (b) of pea protein isolate (PPI1) in the laboratory extrusion equipment. ....	112
Figure 61: Mean residence time of pea protein isolate (PPI1) in the laboratory extrusion equipment as a function of flow rate. ....	113

---

Figure 62: (a) Schematic screw profile showing and image of exemplary distribution of extruded material inside the barrel of the lab scale extruder.....	114
Figure 63: Cutting strength of different foods cut parallel to the visible fibers and cut perpendicular to the visible fibers. ....	118
Figure 64: SEM images of longitudinal sample sections of extrudate and chicken.....	119
Figure 65: Cutting strength of extrudates cut in longitudinal direction and in transverse direction ...	120
Figure 66: Scanning electron microscopic images of transverse sample sections of extruded PPI 1 .	121
Figure 67: Images of samples of pea protein isolate extruded at different cooking temperature.....	122
Figure 68: The effect of raw material and cooking temperature on specific mechanical energy.....	123
Figure 69: Effect of cooling die temperature on cutting strength of extrudates cut in transverse direction and cut in longitudinal direction .....	125
Figure 70: Effect of process parameters on the velocity profile of a non-Newtonian protein fluid in a cooled die channel.....	127
Figure 71: Image of extrudate stained with color tracer carmine.....	128
Figure 72: Residence time distribution function and sum function in the pilot scale extrusion equipment.....	129
Figure 73: Cutting strength of extrudates cut in longitudinal direction and cut in transverse direction from different axial positions along the die channel. ....	130
Figure 74: Side view of dissected extrudates from inside the die channel at different locations.....	131
Figure 75: Schematic illustration of a constant change of the velocity profile of a protein melt at different positions inside a die channel.....	132
Figure 76: Side view of extrudates from inside the die channel at different axial positions.....	133
Figure 77: Model for the effect of solidification on flow conditions of a non-Newtonian protein fluid in a cooled die channel.....	134
Figure 78: Amino acid composition of PPI 1 before and after extrusion.....	137
Figure 79: SDS-PAGE pattern of pea protein isolates under reducing and non-reducing conditions before and after extrusion at 60% w/w w.b. moisture content and 140 °C barrel temperature.....	138
Figure 80: SDS-PAGE pattern of PPI 1 as a function of cooking temperature under non-reducing and reducing conditions at 60% w/w w.b. moisture content.....	140
Figure 81: Effect of extrusion cooking on protein solubility from protein ingredients and their respective extrudates induced by extraction solvents.....	143
Figure 82: Effect of cooking temperature during HMEC of PPI 1 on protein solubilized induced by extracting solutions. ....	145
Figure 83: Cooling dies used for lab scale experiments.....	173
Figure 84: Schematic view of pressure cell for temperature sweep measurements at temperatures exceeding 100 °C .....	173

**Index of Tables**

Table 1: Bond-dissociation energy in protein-protein interactions and covalent bonds at 0 °C. ....	7
Table 2: Production quantity of selected crops in 2014 .....	11
Table 3: Typical protein contents of a selection of major cereal crops .....	12
Table 4: Typical protein contents of a selection of major legume crops .....	14
Table 5: Top ten pea producers in 2014 .....	18
Table 6: Average composition of pea protein ingredients .....	20
Table 7: Amino acid profile of pea seeds. ....	24
Table 8: Selection of typical functional properties of pea flour and pea protein products .....	25
Table 9: Effect of processing techniques on ANFs in raw pea seeds .....	27
Table 10: Selection of influencing variables and dependent parameters during extrusion cooking .....	29
Table 11: Types of interactions, amino acids and reagents able to break the interactions .....	59
Table 12: Temperature profile of the extruder barrel during initial start-up phase. ....	67
Table 13: Geometry of the cooling die channel attached to the lab-scale extruder .....	67
Table 14: Dimensions of the cooling die flow channel attached to the pilot-scale extruder .....	72
Table 15: Major chemical composition of pea protein isolates .....	83
Table 16: Average volume diameter of pea protein isolates. ....	84
Table 17: Functional properties of the protein ingredients .....	87
Table 18: Herschel–Bulkley parameters for diluted protein dispersions .....	94
Table 19: Viscoelastic properties of protein dispersions .....	96
Table 20: Regression parameters for frequency sweep data .....	98
Table 21: Viscoelastic properties of protein dispersion of PPI 1 .....	101
Table 22: Regression parameters for frequency sweep data .....	104
Table 23: Viscoelastic properties of a protein dispersion of PPI 1 at 65% w.b. moisture .....	107
Table 24: Screw filling degree in the cooking zone of the lab scale extruder .....	115
Table 25: Experimental mean residence time in the laboratory extruder equipment .....	115
Table 26: Experimental mean residence time in the pilot-scale extrusion equipment .....	116
Table 27: Comparison of mean residence time in laboratory and pilot-scale extrusion equipment .....	117
Table 28: Amino acid composition of pea protein isolates (PPI) and extrudates (EPPI). ....	136
Table 29: Degree of hydrolysis of pea protein isolates and extrudates. ....	141
Table 30: Degree of hydrolysis of PPI 1 at different cooking temperatures. ....	142
Table 31: Water activity of protein dispersions of PPI 1 as a factor of protein concentration. ....	174
Table 32: Screw elements used during pilot plant trials .....	174

**Abbreviations**

AACC	American Association of Cereal Chemists
BSA	Bovine serum albumin
DSC	Differential scanning calorimetry
DTT	Dithiothreitol
EPPI	Extruded pea protein isolate
Fmoc	Flourenylmethoxycarbonyl
HPLC	High pressure liquid chromatography
L/D-ratio	Length-diameter ratio
ND	Not determined
OPA	Ortho-phthaldialdehyde
PPI	Pea protein isolate
RTD	Residence time distribution
RVA	Rapid visco analyzer
SDS-PAGE	Sodium-dodecylsulphate-polyacrylamide-gel-electrophoresis
SEM	Scanning electron microscopy
U	Urea
w/v	Weight per volume
w/w	Weight per weight
w.b.	wet basis
d.b.	dry basis

**Units**

A	Surface area	cm <sup>2</sup>
D	Diameter	mm
D(v, 0.1)	Volume diameter	μm
DH	Degree of hydrolysis	%
EC	Emulsifying capacity	ml/g
F <sub>L</sub>	Longitudinal strength	N
F <sub>T</sub>	Transverse strength	N
G*	Complex shear modulus	Pa
G′	Elastic modulus	Pa
G″	Viscous modulus	Pa
H	Height	mm, cm
I	Electric current	mA
k	Consistency coefficient	Pa s <sup>n</sup>
L	Length	mm, cm
M	Molar mass	kg/mol
m	Mass	mg, g, kg
MW	Molecular weight	Da
N	Rotational screw speed	s <sup>-1</sup> /min <sup>-1</sup>
<i>n</i>	Flow behavior index	-
OBC	Oil binding capacity	ml/g
P	Pressure	bar, Pa
SME	Specific mechanical energy	kJ/kg
t	Time	h, min, s
T <sub>0</sub>	Onset temperature	°C
T <sub>d</sub>	Peak transition temperature	°C
U	Electric tension	kV
V	Volume	ml, l, cm <sup>3</sup>
W	Width	mm, cm



---

WBC	Water binding capacity	g/g
$\gamma$	Shear strain	-
$\Delta H$	Enthalpy of denaturation	J/g
$\eta$	Apparent viscosity	Pa s
$ \eta^* $	Complex viscosity	Pa s
$\lambda$	Wavelength	nm
$\rho$	Density	kg/m <sup>3</sup>
$\tau$	Shear stress	Pa
$\omega$	Angular frequency	s <sup>-1</sup>
$v$	Velocity	m/s
$\dot{\gamma}$	Shear rate	s <sup>-1</sup>
$\dot{m}$	Mass flow rate	g/min, kg/min, kg/h
$\bar{t}$	Mean residence time	s
$\dot{v}$	Volumetric flow rate	cm <sup>3</sup> /s, l/h
$\Delta T$	Heating rate	°C/min



# 1 Introduction and objectives

Proteins are an important component of the human diet and the vast majority is derived from animal products. Due to the growing demand for animal products accompanied by an increase in population, our society is faced with severe challenges since the mass production of meat has several negative impacts on the environment such as land use, freshwater depletion, global warming and loss of biodiversity (Steinfeld *et al.* 2006). One approach towards a more sustainable protein supply is the partial replacement of meat protein by plant protein (Smil 2000). Despite the increasing public awareness of the negative aspects associated with meat production, meat substitutes are still recognized as niche products which can be attributed to their atypical sensory attributes such as visual appearance, taste, aroma and texture. Hence, there is a need for technologies to transform plant protein into palatable products with a high consumer acceptance. While a meat-like taste can be achieved rather easily, the unique texture properties of muscle meat pose a particular challenge for product developers.

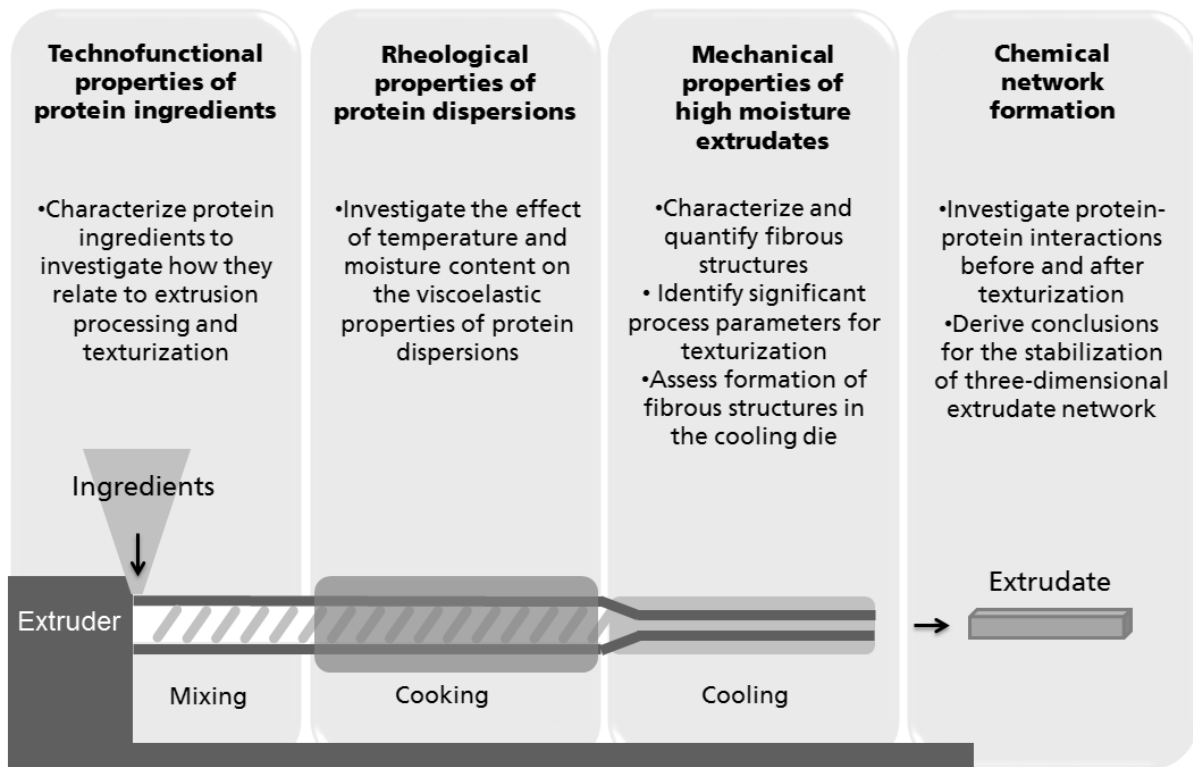
Since the 1960s extrusion cooking has been applied to produce meat substitutes using common starches and proteins as raw materials. The traditional extruded meat substitutes produced by low moisture extrusion, with a moisture content of about 30% w.b., have a sponge-like texture and require rehydration prior to consumption (Guy 2001). These products are used as meat extenders or ground meat substitutes. However, they fail to mimic the appearance and texture of fibrous muscle meat. One promising technology for obtaining high quality meat substitutes from plant proteins is the high moisture extrusion cooking (HMEC) process. The key feature of high moisture meat substitutes is their fibrous structure which resembles muscle meat e.g. chicken breast. The high similarity to muscle meat could not be achieved by previous technologies and raises the expectation of higher consumer acceptance. This could help to slow down the increase of meat production towards a more sustainable protein supply based on plant proteins.

Previous studies under high moisture extrusion conditions have been limited to soy and wheat gluten as plant protein sources which are associated with a number of disadvantages. From a European perspective, field pea (*Pisum sativum* L.) could play an important role as a substitute for meat protein among the various sources of plant proteins due to its nutritional characteristics and low potential for allergic responses (Nowak-Wegrzyn *et al.* 2003). In order to generate a fibrous texture, the proteins are heated in the extruder under high water conditions of >50% w.b. and texturized in a cooling die by varying the moisture, temperature, pressure and shear, respectively (Noguchi 1990). The combination of these

process variables results in molecular transformation and chemical reaction of the protein molecules. It was suggested that the proteins are plasticized inside the extruder and subsequently solidified during the passage through a cooling die (Akdogan 1999). However, there is still limited knowledge on the melting and solidification temperatures, viscosities and flow profiles inside the extruder and cooling die which are detrimental for the formation of the characteristic fibrous structure. For the structural stabilization of extrudates, alterations of both covalent bonds e.g. peptide-, disulfide bonds as well as noncovalent bonds such as hydrogen-, hydrophobic- and ionic linkages could be expected (Liu and Hsieh 2007; Chen *et al.* 2011).

Although high moisture extrusion cooking has been recently introduced in the food industry, the processes underlying the fiber structure formation are not yet elucidated sufficiently. This could be mainly attributed to the difficulty of studying the protein properties under high temperature, pressure and shear conditions inside the extruder as well as the complexity of the extrusion process, which is characterized by interactions between several process variables, measured feed and process parameters, and product characteristics. These dependencies impede to state the effect of a single process variable or parameter and the limited understanding of the relationships between ingredients, processing and structure formation stands in the way of target-focused product development. Altogether, a comprehensive investigation of the fiber structure formation process using pea protein as a promising protein source has not yet been described and therefore provides the basis for the present work.

The general objective of this thesis is to assess the effect of temperature and moisture content on the texturization process for the generation of fibrous meat-like structures during high moisture extrusion cooking. The following illustration gives an overview of the high moisture extrusion process and the sub-objectives during this research.



The first objective is to provide the basis for the assessment of the relationship between protein properties, extruder responses, product texture properties and protein-protein interactions by characterizing pea protein ingredients regarding their technofunctional properties. Against the background of the limitation in direct investigations of material properties inside the extruder, rheological data are to be generated by assessment of viscoelastic properties of protein dispersions using high pressure rheology as a function of temperature and moisture content typical for high moisture extrusion. Information on how long the protein dispersion is subjected to thermomechanical processing is to be provided by assessing the residence time distribution in the extruder barrel and the cooling die. The main scope of this thesis is to study the effect of temperature and moisture content during extrusion processing on the structure formation of anisotropic fibrous extrudates by means of microscopic visualization as well as quantitative texture analysis. Additionally, further insight into the texturization mechanism is to be provided by visual inspection of the flow behavior of the extruded mass in the cooling die channel. Finally, the objective is to assess the texturization process under high moisture conditions by studying the thermally-induced changes of the protein-protein interactions after extrusion texturization.



## 2 State of the art

The following chapter is devoted to the background and recent findings regarding the physicochemical properties of food proteins that are important for the texturization during extrusion. Furthermore, an overview of potential protein sources is provided with a focus on pea protein as a model ingredient for high moisture extrusion. Finally, the basics of extrusion cooking with a focus on texturization of plant proteins are described and the latest developments in high moisture extrusion are discussed.

### 2.1 Physicochemical properties of food proteins

#### 2.1.1 Protein conformation

Proteins are large biopolymers which play several fundamental roles in the structure and function of biological cells. These include amongst others biocatalysts e.g. enzymes, structural components e.g. collagen, contractile proteins such as actin and myosin as well as storage proteins like seed proteins (Yada 2004).

Unlike polysaccharides which contain only the glucose monomer, most proteins consist of 20 proteinogenic L- $\alpha$ -amino acids bonded together by peptide bonds. These protein-building amino acids possess common structural features, having both a primary amino group ( $\text{NH}_2$ ) and a carboxyl group ( $\text{COOH}$ ) attached to the first ( $\alpha$ )- carbon atom as well as a side chain ( $\text{R}_x$ ) specific to each amino acid as shown in Figure 1 (Cheftel 1992).

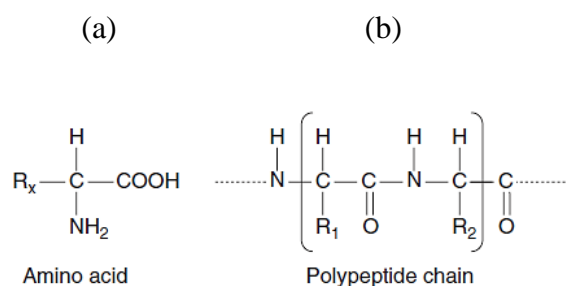


**Figure 1: Molecular structure of  $\alpha$ -amino acids (a) and a polypeptide chain bonded by peptide bonds (b). Reprinted from Bouvier and Campanella (2014) with permission of Wiley.**

Every amino acid is characterized by its side chain which determines its physicochemical properties e.g. charge, solubility and chemical reactivity and therefore the properties of the respective protein to which it belongs. Amino acids can be classified into four groups, based

on the polarity of the side chain. These are amino acids with hydrophobic, hydrophilic, positively charged and negatively charged side chains (Sikorski 2001).

The sequence of amino acids results in a specific three-dimensional structure that determines its chemical reactivity. The shape into which a protein naturally folds under normal conditions regarding pH and temperature is known as its native conformation. This corresponds to a thermodynamically stable and organized state with a minimal free energy (Yada 2004).

There are four levels of a protein's structural hierarchy. The primary structure of a protein denotes the linear sequential order in which the constituent amino acids are linked. The spatial arrangement of the polypeptide chain is referred to as secondary structure with regularly repeating local structures, most commonly  $\alpha$ - helix and  $\beta$ - sheet stabilized by hydrogen bonds. The tertiary structure refers to the three-dimensional arrangement of the polypeptide chains. The folding is driven by the thermodynamic requirement to minimize the free energy of the molecule by relocation of the nonpolar residues at the interior and disposal of the hydrophilic residues at the surface of the protein molecule. Although a majority of hydrophobic groups are buried in the protein interior, analysis of the surfaces of several globular proteins indicated that about 40-50% of the water-accessible protein surface is occupied by nonpolar residues. The distribution of hydrophilic and hydrophobic residues at the protein surface influences several physicochemical properties, such as shape, surface topography, and solubility of the protein. The conformation is stabilized mainly by non-covalent interactions and covalent disulfide bonds between the various groups in the protein. The association of several protein subunits usually linked by non-covalent bonds leads to the formation of quaternary structures which function as a single protein complex (Zayas 1997; Nakai and Modler 2000; Sikorski 2001; Yada 2004).

The structural and thermodynamic stability of a native protein is given by a number of intermolecular and intramolecular interactions. These protein-protein interactions are classified in covalent disulfide bonds and non-covalent interactions including electrostatic interactions, hydrogen bonds as well as hydrophobic interactions. Electrostatic interactions occur between oppositely charged groups such as dipoles or ions. They may be either attractive or repulsive and have been shown to immensely contribute to the thermostability of proteins. The charge of the protein molecule highly depends on the pH and the ionic strength of the surrounding solution. At their isoelectric point (pI), the net charge of proteins is zero. Above the pI, proteins are negatively charged, below it they are positively charged. Hydrogen bonds are formed between a hydrogen atom and a pair of electrons on an electronegative atom



e.g. oxygen. Hydrogen bonding in protein predominantly exists in secondary structures of polypeptide chains stabilizing  $\alpha$ - helix and  $\beta$ - sheet structures. Disulfide bonds (-S-S-) between the free thiol group (-SH) of two cysteine molecules account for the most important covalent link between two proteins and are characterized by a high bond-dissociation energy compared to non-covalent protein-protein interactions (Table 1).

**Table 1: Bond-dissociation energy in protein-protein interactions and covalent bonds at 0 °C (Cheftel 1992; Riedel 2010).**

Bonding type		Bond-dissociation energy [kJ/mol] (per bond)
Non-covalent interaction	Van-der Waals repulsion	0.5-5
	Hydrophobic interactions	4-12
	Hydrogen bonds	8-40
	Electrostatic interactions	40-80
Covalent bond	Disulfide bonds	268
	Peptide bonds	305

Under alkaline conditions, free thiol groups can also participate in thio-disulfide interchanges with disulfide bonds. Depending on the conditions, proteins are able to form both intramolecular and intermolecular bonds by an oxidation reaction. In a native protein, free thiol groups are located in the interior of the folded protein and are unavailable for interaction. Upon unfolding of the protein molecule, reactive sulfhydryl groups expose to the aqueous phase and become accessible for new linkages (Bryant and McClements 1998). The formation of covalent disulfide bonds is limited to the amount of cysteine residues but is essential for the stabilization of spatial arrangement. Protein molecules with 5 to 7 disulfide bonds of hundred amino acids are extremely stable, particularly with regard to high temperatures and extreme pH values (Cheftel 1992). Hydrophobic interactions between nonpolar sidechains of amino acids such as alanine, valine, leucine or phenylalanine contribute to the folding of proteins as well as their reactivity. Hydrophobic molecules in an aqueous solution cause the water molecules in close range to rearrange and minimize the contact area between water and non-polar groups and therefore increasing the attractive force between non-polar groups. The latter tend to increase in strength as the temperature is raised up to 60-70 °C. At higher temperatures they begin slowly to lose strength (Damodaran 1997; Zayas 1997; Bryant and McClements 1998; Nakai and Modler 2000; Sikorski 2001).

### **2.1.2 Protein denaturation**

Changes in a protein's environment such as temperature, pH, ionic strength and solvent composition can induce conformational changes in the protein which affect biological functions in the case of enzymes and functional properties of food proteins. Denaturation of food proteins is defined as a process in which the conformation of polypeptide chains within a molecule is changed from that typical of the native protein to a more disordered arrangement not accompanied by the rupture of peptide bonds involved in the primary structure (Cheftel 1992). Denaturation of food proteins usually causes insolubilization and loss of some functional properties. The unfolded protein molecules associate through intermolecular interactions into aggregates which may lead to precipitation, coagulation or gelation.

Apart from either the native or the fully denatured forms, partially folded stable conformations have been found with various levels of denaturation according to the structural level that is involved in the process. For example, the molten globule state refers to a compact intermediate protein conformation with a secondary structure content similar to the native state but with a poorly defined tertiary structure. The term "globule" refers to the native compactness and "molten" refers to the increased enthalpy and entropy on transition from the native structure to the intermediate state. Partial denaturation of food proteins can be desirable since partially denatured proteins are generally more digestible and possess better functional properties, such as foaming and emulsifying properties compared to their native counterpart (Damodaran 1997).

### **2.1.3 Functional properties**

Several definitions for functional properties of proteins exist in literature. Kinsella and Melachouris (1976) defined protein functionality as "those physical and chemical properties of proteins that affect their behavior in food systems during processing, storage, preparation, and consumption". These properties result from interactions between the protein and other food components and depend on intrinsic physicochemical properties characterizing the protein structure and conformation as well as extrinsic factors of the environment that the proteins are exposed to. Important physicochemical properties include the amino acid composition, net charge and hydrophobicity while extrinsic factors include temperature, pH, ionic strength and the presence of other constituents (Kinsella and Whitehead 1989). Hence, the application of proteins allows the modification of food properties such as solubility, water binding, fat binding, emulsification, foaming, gelation and thickening.

A high solubility is considered a prerequisite for further technofunctional properties such as gelling, emulsification or foaming. It is usually determined via the soluble nitrogen fraction in a standard buffered solution and depends on the distribution and accessibility of polar and nonpolar groups at the surface of the molecule as a result of its three-dimensional folding. The solubility of proteins is highly affected by extrinsic factors such as temperature, pH, and ionic strength that determine the folding of the molecule (Cheftel 1992; Damodaran 1997; Yada 2004).

The water binding capacity depends both on the macroscopic particle surface where water is physically bound in the cavities and capillaries of the protein particles as well as protein-water interactions. The ability of protein to bind oil and to function as a food emulsifier follows similar principles which are governed by its structure and properties at colloidal interfaces. Their amphiphilic nature allows proteins to be adsorbed at the oil/water interface and form an interfacial layer that lowers the surface tension (Day 2013).

Among the functional protein properties, the ability to form gels is of special interest for the preparation of many foods. Application examples for protein gelation extend from the boiling of an egg to more sophisticated applications such as the replacement of animal protein in dairy and meat products (Clark et al. 2001). The gel structure is based on the protein network in which water, amongst other minor components such as sugars or starch, becomes entrapped while contributing to the overall consistency. Food protein gels can be classified into fine-stranded cross-linked polymer networks or particle gels consisting of strands or clusters of aggregated protein. Heat-induced gelation of globular proteins typically yields turbid gels and follows three consecutive steps. Those are (1) temperature induced unfolding of the protein with exposure of hydrophobic residues, (2) interaction of these side chains forming aggregates, and (3) arrangement of the aggregates into a three-dimensional network (O'Kane et al. 2004).

Besides the physicochemical properties that determine the protein-protein interactions as well as protein-non-protein associations, extrinsic factors such as heating/cooling rate, pH and ionic strength influence the network formation (Renkema 2004).

Until now, the gelation behavior of plant proteins in general is not fully understood and there have been great efforts to assess the chemical forces that are involved in protein gels. Renkema and van Vliet (2002) studied heat-induced gel formation of soy protein and found that an increase in the elastic modulus during cooling was thermo-reversible at neutral pH. This indicated that disulfide bonding and rearrangements do not occur during gelation.

Catsimpolas and Meyer (1970) proposed that thermal gelation of soy protein starts with initial unfolding and dissociation leading to reversible aggregation and formation of an intermediate progel that involves non-covalent bonding. Upon further heating the progel is disrupted, followed by an irreversible gel formation involving covalent disulfide bonding. Utsumi and Kinsella (1985) studied the gelling behavior of fractions of soy protein. These protein fractions can be classified according to their sedimentation coefficient in two main groups, which are the 11S size fraction and the 7S size fraction. It was suggested that gelation of soy protein isolate is based on hydrogen bonding and hydrophobic interactions, while 11S globulins mainly involve electrostatic interactions and disulfide bonds and 7S gels involve mostly hydrogen bonding. Sheard *et al.* (1986) studied macromolecular changes during heat treatment of soy protein and proposed that, while heat-treated soy proteins were primarily aggregated by hydrophobic interactions, increasing the protein concentration seemed to increase disulfide linkages in stabilizing the protein aggregates.

The current position of understanding is that the main protein-protein interactions responsible for gelation of plant protein are mainly non-covalent interactions such as hydrogen bonds and hydrophobic interactions and to a small extent covalent disulfide crosslinking. It was suggested that the relative proportion of each type of bond in their structure is important in terms of thermal reversibility and structural rigidity (Liu and Hsieh 2007).

## 2.2 Sources for plant proteins

The suitability of the protein source for plant protein ingredients depends on a number of factors such as the economic potential for commercial protein production, nutritive properties, the functionality of the protein as well as environmental aspects regarding cultivation and manufacturing of the crops. The following chapter aims to provide an overview of a selection of crops that are used for the production of plant protein ingredients and covers the major cereals and legumes including oilseeds and pulses.

### 2.2.1 Cereals

In terms of production yield, cereals are the most important crops with a total annual grain yield of 2780 million tons in 2014 (Table 2).

**Table 2: Production quantity of selected crops in 2014 (FAO 2017).**

Region	million tons		
	Cereals	Oil crops	Pulses
Africa	189	12	17
America	723	64	16
Asia	1339	97	35
Europe	529	27	7
Oceania	40	3	2
<b>Total</b>	<b>2820</b>	<b>203</b>	<b>77</b>

Cereals are commonly used as a source of energy and contain an average of about 10-12% d.b. of protein, which is relatively little compared to legume seeds. Cereal proteins are mostly a by-product of the starch production industry (Day 2013). Depending on their solubility in different solvents, seed storage proteins fall into four solubility classes called Osborne fractions: albumins (water-soluble), globulins (salt-soluble), prolamins (alcohol-soluble), and glutelins (alkali-soluble). Prolamins are the predominant fraction in all the major cereals except oats and rice. They tend to be rich in sulphur-containing amino acids and deficient in the essential amino acids lysine as well as threonine and tryptophan, which can result in nutritional deficiencies in some developing countries (Shewry and Halford 2002).

Despite the wide variety of edible cereal species, almost 90% of the total production is based on maize, rice and wheat (Figure 2).

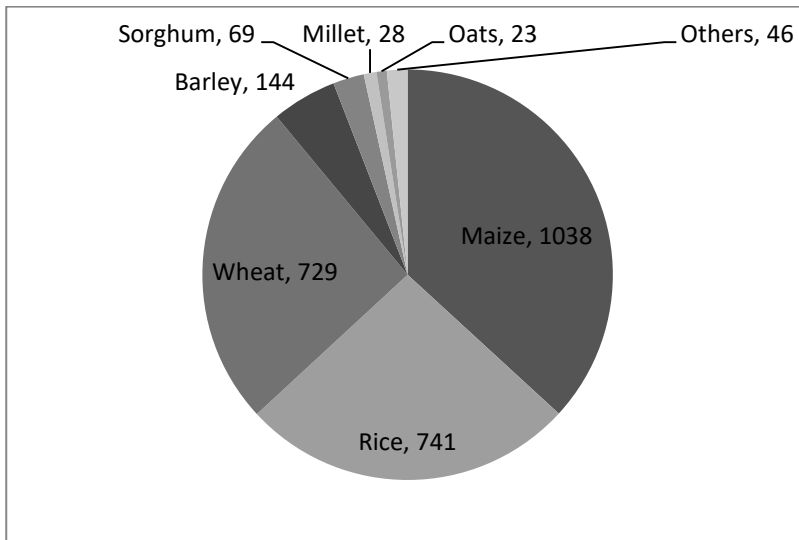


Figure 2: Production quantity of cereal grains (million tons) in 2014 (FAO 2017).

Among all cereals, maize or corn (*Zea mays* L.) is the single most important food crop in human nutrition worldwide. It contains 9-12% d.b. protein with zein as the major class of prolamins. Although zein is industrially produced as a clear, odorless and tasteless powder, it is rarely used directly for human consumption due to its poor solubility in water. The major applications of zeins are polymer films, coatings and plastics (Day 2013).

Rice (*Oryza sativa* L.) is the second largest cereal crop in terms of production quantity with the lowest protein content of 7-9% d.b. among the major cereals (Table 3).

Table 3: Typical protein contents of a selection of major cereal crops and approximate distribution of protein fractions according to the Osborne classification (Day 2013).

Plant source	Protein content* [%d.b.]	Osbourne fraction [%d.b.]			
		Albumins	Globulins	Prolamins	Glutelins
Maize	9-12	4	4	60	26
Wheat flour	8-15	6-10	5-8	35-40	40
Rice	7-9	2-6	12	4	80
Barley (dehulled)	8-15	3-5	10-20	35-45	35-45
Sorghum	9-17	2-7	2-10	35-60	20-35

Rice protein mainly consists of a high-molecular-weight glutelin fraction (~80% d.b.) and a low-molecular-weight globulin fraction (~12% d.b.). Some rice protein ingredients are

available that are applied in gluten-free food products. These are produced by alkaline extraction from rice flour and precipitation at the isoelectric point or enzymatic removal of non-protein components (Shih and Daigle 2000).

The third largest cereal crop is wheat. Depending on grain variety, it contains 8-15% d.b. gluten protein. Due to the simple protein enrichment process by washing out the starch fraction with water, commercial wheat gluten has been available since the 1850's. The composite of the storage proteins gliadin and glutenin in the endosperm of the seed possesses a unique functional property. When wheat flour is mixed with water to form a dough, the gluten proteins form a cohesive proteinaceous network with visco-elastic properties which allows the dough to expand during fermentation and baking. The unique visco-elastic properties of wheat gluten are of fundamental interest to cereal scientists and depend on the amount of high molecular mass glutenin polymers (Van Der Borgh *et al.* 2005; Day *et al.* 2006). In summary, cereal proteins are a cheap by-product of starch manufacturing, however their unique functional properties are determined by their water-insoluble prolamin and glutelin fractions, which limits their application as protein ingredients for food applications.

### **2.2.2 Legumes**

Commonly used in traditional diets, legumes have been a cheap and valuable source of protein in many regions throughout the world (El-Niely 2007). The crop plants belong to the botanical family of Leguminosae (nom. alt.: Fabaceae) and are further subdivided into three subfamilies: Mimosoidae, Caesalpinioideae and Faboideae (nom.alt.: Papilionoideae). Among those, the Faboideae are the largest subfamily that include the majority of plants which are cultivated mainly for their edible seeds, such as bean, pea or chickpea (Berrios 2011).

Many legumes contain symbiotic soil bacteria (Rhizobia) inside their root nodules with the ability to fix nitrogen from atmospheric nitrogen. The ability for nitrogen fixation enables the plants to grow on relatively poor soil and to use nitrogen for the production of amino acids. Hence, legumes are rich in protein (Table 4) which is beneficial for the production of plant protein ingredients (Kinkema *et al.* 2006).

**Table 4: Typical protein contents of a selection of major legume crops and approximate distribution of protein fractions according to the Osborne classification (Day 2013).**

Plant source	Protein content [% <sup>*1</sup> ]	Osbourne fraction [%]			
		Albumins	Globulins	Prolamins	Glutelins
<b>Soybean</b>	35-40		90		
<b>Lupine</b>	35-40	25	75		
<b>Pea</b>	20-30	15-25	50-60		
<b>Dry bean<sup>*2</sup></b>	20-30	10-30	45-70		
<b>Chickpea</b>	20-25	8-12	53-60	3-7	19-25

<sup>\*1</sup> = information on reference of percentage not available <sup>\*2</sup> = data from Sathe (2002)

Furthermore, legumes can be used as part of a pasture improvement process by serving as natural fertilizers for future crops. Their cultivation can help to promote a more sustainable food production by contributing to a decrease in greenhouse gas production, since the manufacture and application of synthetic nitrogen fertilizer has been accounted for a number of negative environmental effects (Abberton 2010).

When these legumes are harvested at maturity and used as a dry commodity, they are referred to as pulses, whereas legumes harvested green such as green beans or green peas are considered vegetable crops. According to the definition of the FAO, the term “pulse” also excludes those legume crops which are mainly grown for the production of oil used for food, feed as well as oleochemicals such as soybeans. Nevertheless, these crops can also be used as a source for plant protein ingredients after the oil is removed (FAO 2011).

Globally, soy (*Glycine max* L.) is the economically most important legume because of its high oil and protein content. The main product is oil for human consumption. The remaining press cake is high in protein and primarily used as defatted soybean meal in livestock feed. In contrast to most cereals, soy protein mainly consists of globulins. The two major types of soy globulins, the 11S glycinin and 7S  $\beta$ -conglycinin, have been studied extensively in scientific literature. The remaining proteins are low-molecular weight fractions including antinutritional factors such as trypsin inhibitors and lectins (Petruccioli and Anon 1995).

A small, but culturally and historically significant amount of soy has been used to produce protein-rich products such as tofu, tempeh and miso, which are primarily consumed in Asia. The main soy protein ingredients are defatted soy flour, protein concentrate, protein isolate as well as texturized and hydrolyzed soy proteins (H. Aiking *et al.* 2006). However, a number of drawbacks are associated with the use of soybeans such as the presence of antinutritional factors, their allergenic potential, and the introduction of genetically modified organisms (Martínez-Villaluenga *et al.* 2008). Furthermore, cultivation of soy is taking place almost



exclusively in America and in Asia due to climatic requirements and is therefore not adequate as the only source of plant protein to supply the global market (H. Aiking *et al.* 2006).

Compared to oilseeds and cereals, the production amount of pulses is rather low, despite their traditional importance as a protein-delivering foodstuff. Figure 3 shows the worldwide production amounts of a selection of pulse crops in 2014.

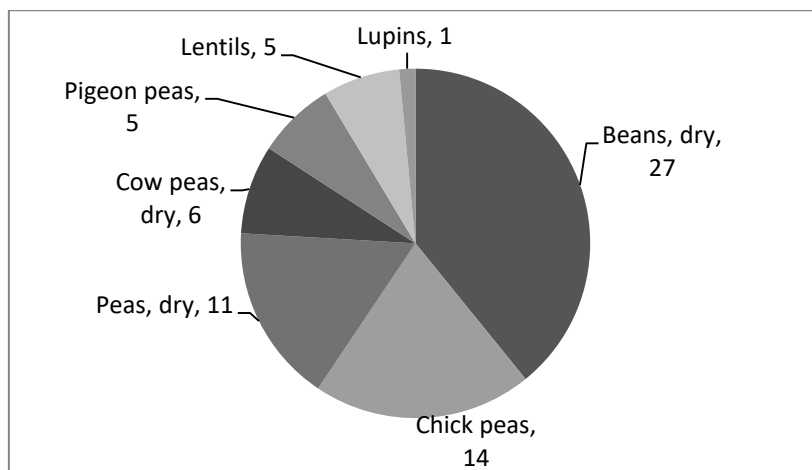


**Figure 3: World pulse production (million tons) in 2014 (FAO 2017).**

Among pulses, dry common beans of the species *Phaseolus vulgaris* L. were the most cultivated crops in 2013, followed by chick peas (*Cicer arietinum* L.) and dry peas (*Pisum sativum* L.). Beans are a highly variable species consisting of several genetic variations that have been cultivated in most countries with Brazil and India as the top producers. The major types of commercially grown beans include kidney beans, navy beans, pinto beans or wax beans which contain up to 60% starch, 20-30% protein, ~ 5% crude fiber and <2% lipids (Van Der Poel 1990). The proteins are composed of the major storage fraction vicilin, or sometimes called phaseolin, and the minor fraction legumin (Yin *et al.* 2008). Other commercially grown species are *Vicia faba* (broad bean) and *Vigna sinensis* (cow pea).

Chickpeas are the second largest pulse crop in terms of production quantity, being mostly consumed in the Indian sub-continent as well as the Mediterranean region. The two major types of chickpea are the larger kabuli varieties and the smaller and darker des varieties. The seeds contain around 40-50% carbohydrate and 20-25% protein with globulins as the major fraction (El-Adawy 2002; Boye *et al.* 2010).

Despite low production quantities, lupines (*Lupinus sp.*) are gaining interest due to their high amount of protein of ~ 40% d.b., which is similar to that of soybeans while the fat content of lupine seeds is significantly lower (4-11%). Globulins represent the major storage proteins of

lupine seeds with three main fractions conglutin  $\alpha$ ,  $\beta$  and  $\gamma$ . Albumins amount to 5 to 13% of the total lupine proteins which comprise biologically active proteins of the seeds. In contrast to yellow lupines (*Lupinus luteus* L.), which contain quinolizidinic alkaloids and are grown in Europe and South America mostly for animal feed, white lupines (*Lupinus albus* L.) contain low levels of alkaloids and are primarily cultivated for direct food uses (Day 2013).

Altogether, these pulses show a high potential as future protein ingredients. However, as their commercial availability is still limited, prices for protein ingredients made thereof are on a high level compared to e.g. soy or wheat gluten. In contrast, pea seeds have been exploited more extensively as a source for protein ingredients and there are several commercial protein products available on the market.

From a European perspective, pea protein could be an economic source of protein that is readily available for the production of meat substitutes. Hence, this thesis uses pea seed as a model protein source to study the texturization to meat substitutes using HMEC. Therefore, the following chapter describes pea seeds in more detail with a focus on pea protein properties in the light of their application for extrusion texturization.

## 2.3 Pea protein ingredients

### 2.3.1 Pea seeds

Pea (*Pisum sativum L.*) is a pulse crop of the family *Leguminosae* that is widely grown for human consumption as well as animal feeding. The pea seed consists of two cotyledons, the embryo (hypocotyl, radicle) and the seed hull or testa (Figure 4).

Dry pea seeds contain mainly starch (~50%), which is located in the storage cotyledons. The amount of protein and dietary fiber account for ~24% (N x 6.25\*) and 20%, respectively, whereas lipids are present in lower amounts (~6 %) (Kosson *et al.* 1994). Both starch and protein contents can vary due to the diversity of breeds and growing conditions. The garden pea (*Pisum sativum ssp. hortense*) and the field pea (*Pisum sativum ssp. arvense*) are cultivated in many regions of the world in cool climates with an optimum daily temperature of roughly 17 °C. Under irrigation, dry pea yields 0.6 to 0.8 tons/ha (12% moisture) with a growing period of 85 to 120 days (Cousin 1997).

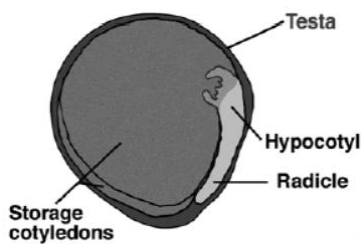


**Figure 4: Longitudinal section of a pea seed. Reprinted from Finch-Savage and Leubner-Metzger (2006) with permission of Wiley.**

---

\* Protein content of most foods is determined on the basis of total nitrogen content (AOAC, 2000). Nitrogen content is then multiplied by a factor to calculate the protein content, which is based on the assumptions that all of the nitrogen in the sample can be attributed to amino acids in proteins. The average nitrogen (N) content of proteins was found to be around 16 percent, hence the calculation  $N \times 6.25$  ( $1/0.16 = 6.25$ ) to convert nitrogen content into protein content (Moore *et al.* 2010).

The total production of dry peas was around 11 million tons in 2014 (Figure 5).

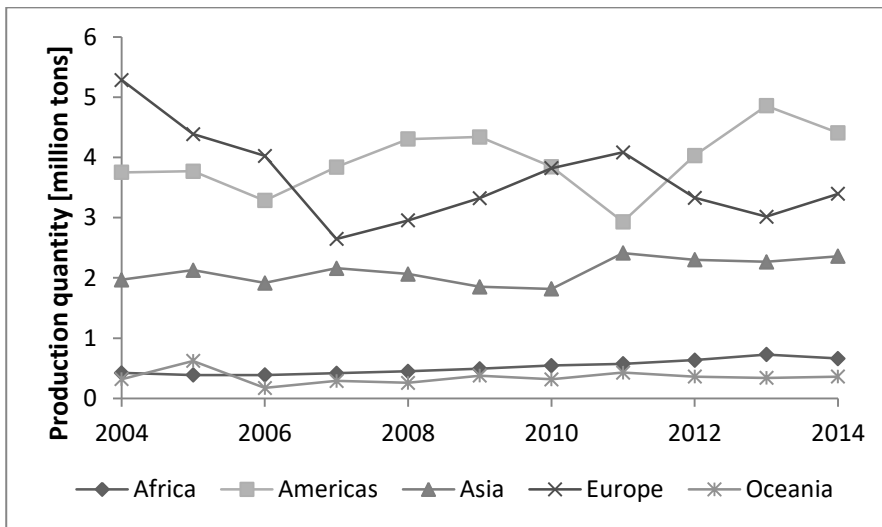


Figure 5: Worldwide production quantity of peas from 2004 until 2014 (FAO 2017).

The biggest producer of peas is America, followed by Europe and Asia. In 2014, the biggest producer of peas was Canada, followed by China and the Russian Federation. In Europe, France was the biggest producer (Table 5).

Table 5: Top ten pea producers in 2014 (FAO 2017).

Country	Production quantity [million tons]
Canada	3.4
Russian Federation	1.5
China, mainland	1.4
USA	0.8
India	0.6
France	0.5
Ukraine	0.4
Ethiopia	0.3
Australia	0.3
Iran	0.2

### 2.3.2 Fractionation and protein enrichment

Peas are commercially fractionated into their major components starch, protein and hulls. Pea globulins in the protein fraction are of special interest to the food industry as they exhibit nutritional as well as functional properties that can add extra value to food products. In contrast, pea starch is mainly used in industrial applications instead of food products due to its limited functional properties. It is mainly available as a by-product of protein extraction and is used as a relatively cheap source of starch compared to corn, wheat and potato starches (Ratnayake *et al.* 2002).

Commonly protein concentrates are produced by air classification of pea flour into a starch-rich fraction and a protein-rich fraction with a protein content of ~ 50% d.b.. Using wet fractionation can yield higher protein concentrations of ~ 85% d.b. (O'Kane *et al.* 2004). Figure 6 shows exemplary flow diagrams for the fractionation of pea seeds by dry and wet milling processes.

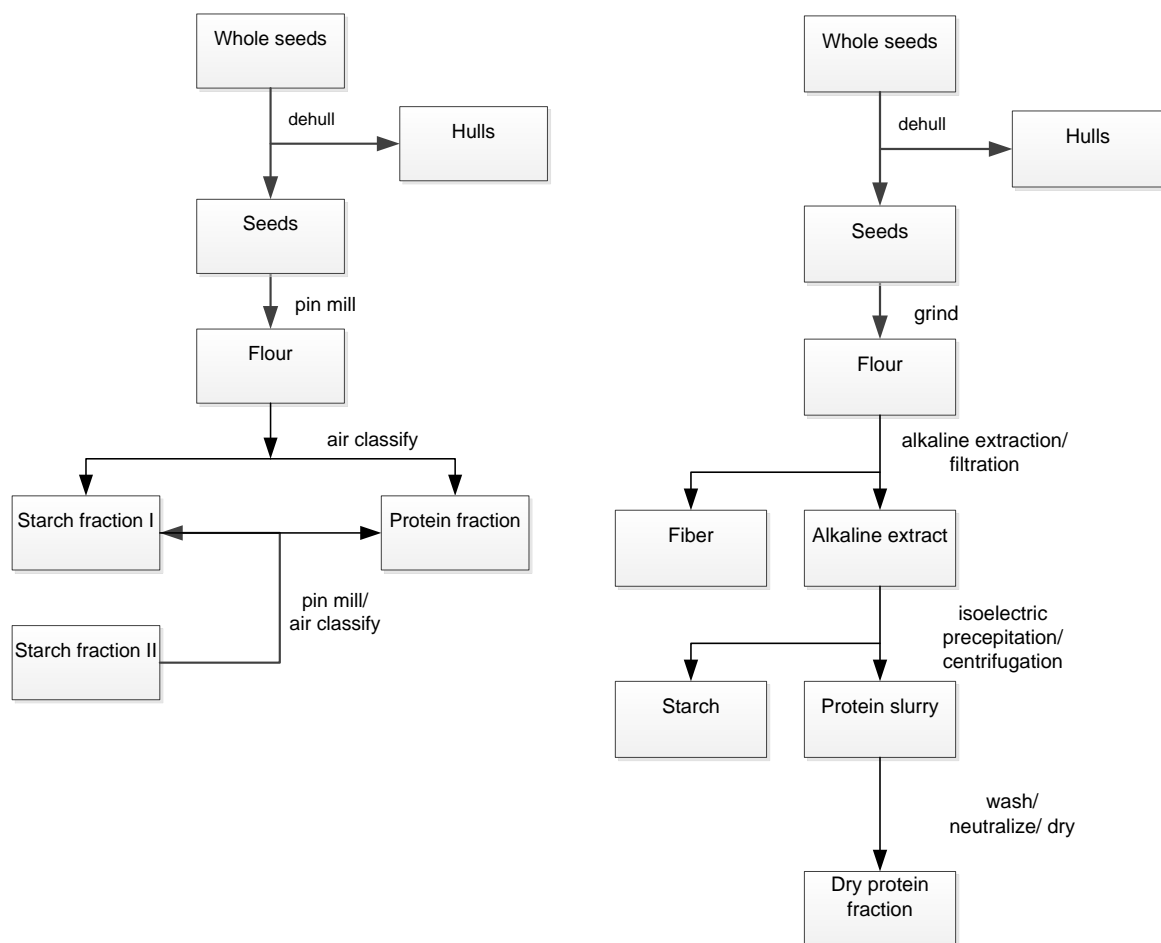


Figure 6: Flow diagram for processing of pea seeds into hulls, protein fraction and starch fractions by (a) dry fractionation and (b) wet fractionation. Modified from Sosulski and Mcurdy (1987) with permission of Wiley.

Dry fractionation uses milling and air classification to separate particles by their density. Whole seeds are de-hulled and finely ground in a pin mill to achieve a complete cellular disruption of the cotyledons. During air classification, the flour is subsequently separated in a spiral air stream into a light protein-rich fraction and a heavy starch-rich fraction. The separation efficiency can be improved by repeating the process several times as the protein bodies tend to stick to the starch granules (Sosulski and Mccurdy 1987; Pelgrom *et al.* 2015; Schutyser *et al.* 2015).

Wet fractionation takes advantage of the pH-dependent protein solubility. Again, the seeds are ground and dispersed in water. The pH of the mixture is adjusted to alkaline to facilitate the solubilization of the proteins. During this step, increasing the temperature can further enhance protein solubilization and extraction, although temperature-induced denaturation should be avoided for the sake of protein functionality. The mixture is then filtered to remove insoluble compounds such as plant fibers and the pH of the extract is adjusted to the isoelectric point to induce protein precipitation. The solution is then centrifuged to recover the protein, washed to remove salts, neutralized and dried into a protein powder. The processing conditions such as temperature, time, flour to solvent ratio etc. can be adjusted to increase the protein yield and purity (Sosulski and Mccurdy 1987). Typical compositions of protein ingredients obtained after fractionation are shown in Table 6.

**Table 6: Average composition of pea protein ingredients (O'Kane *et al.* 2004).**

	Whole dry peas [% d.b.]	Concentrate [% d.b.]	Isolate [% d.b.]
<b>Protein</b>	25	50	85
<b>Starch</b>	50	17	0
<b>Lipids</b>	5-6	4	<3

### 2.3.3 Protein composition

Pea protein mainly consists of globular storage proteins and albumins. The salt extractable globular storage proteins account for 65-80% of the total extractable protein in the seeds (Owusu-Ansah and McCurdy 1991). Based on their sedimentation coefficient, the globulins can be subdivided into the 11S size fraction legumin and the 7S size fraction vicilin and convicilin (Figure 7).

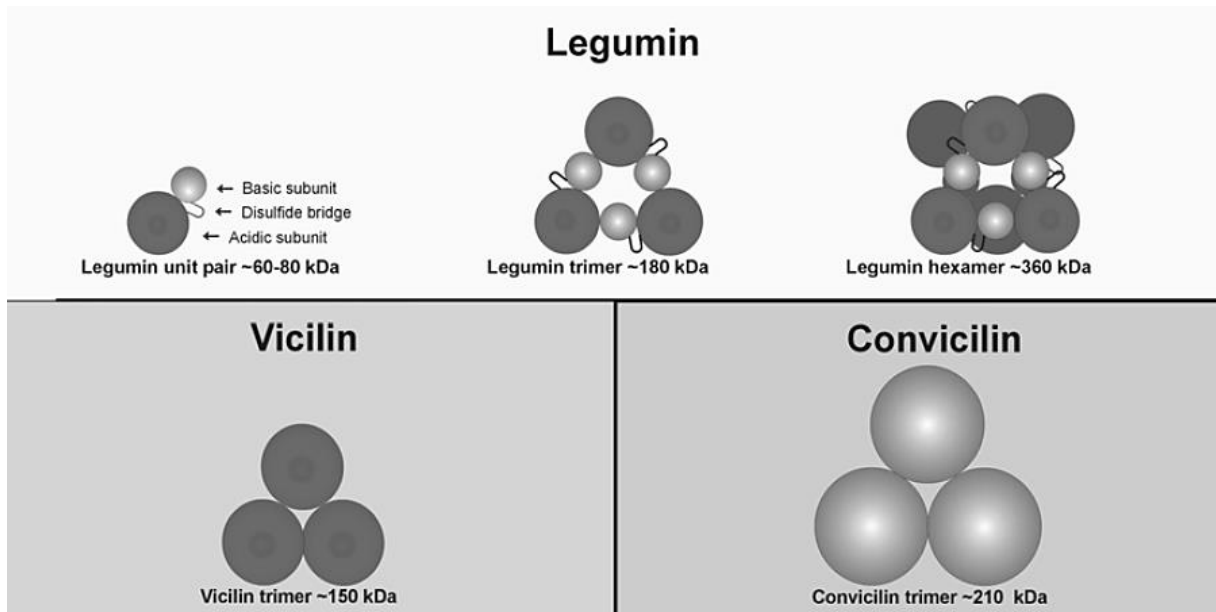
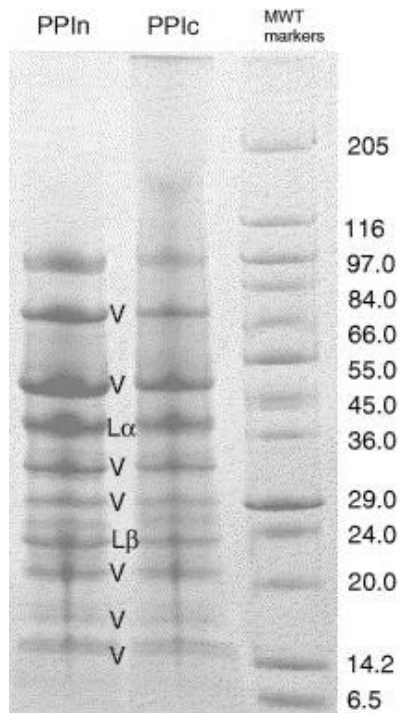


Figure 7: Composition of pea globulins (Tsitzikas 2005).

Pea legumin is a protein of ~60 kDa that is associated in trimers or hexamers, depending on the pH. It consists of an acidic ( $L\alpha$ ) and basic ( $L\beta$ ) subunit covalently linked by a disulfide bond under participation of its sulphur containing amino acids cysteine and methionine. In contrast, the protein fractions vicilin and convician are both covalently associated trimers containing only few methionine residues and no cysteine residues. The albumin fraction accounts for 20-35% of the total protein. Although albumins are predominantly storage proteins, they also contain a variety of bioactive proteins such as lipoxygenases and other enzymes, lectins and trypsin inhibitors (Mariotti *et al.* 2001). The protein fractions of native and commercial pea protein isolates after electrophoresis are shown in Figure 8.



**Figure 8: Sodium dodecylsulfate-polyacrylamide gel electrophoresis (SDS-PAGE) pattern of pea protein products under reducing conditions. In the lanes of PPIC (pea protein isolate commercial) and PPIIn (pea protein isolate native), V = bands from vicilin protein, L $\alpha$  = legumin acidic subunit and L $\beta$  = legumin basic subunit. MWT = molecular weight markers. Reprinted from Shand *et al.* (2007) with permission of Elsevier.**

Shand *et al.* (2007) found the major polypeptides of the vicilin fraction (7S) with a molecular mass of 71, 50 and 33 kDa and minor components of lower molecular mass (19–12.5 kDa). During manufacturing of pea protein isolate some protein fractions associate into high molecular weight proteins (Figure 9).



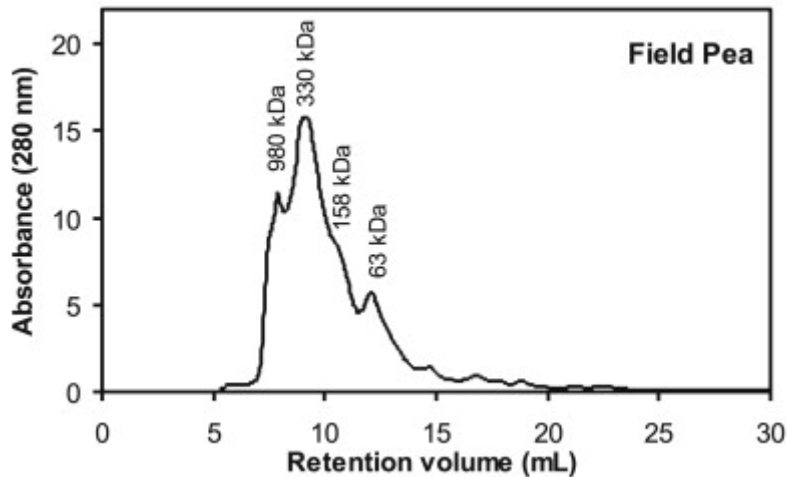


Figure 9: Size exclusion chromatogram of protein isolates from field pea. Reprinted from Shevkani *et al.* (2015) with permission of Elsevier.

The chromatogram shows peaks that are attributed to high molecular protein aggregates fractions of ~980, ~330, ~158 kDa.

Recent work has been published on the structural characterization of pea protein isolates using infrared spectroscopy (Shevkani *et al.* 2015; Yu *et al.* 2015). Information about the secondary structure of proteins was obtained by Fourier transform infrared spectroscopy (FTIR) (Barth 2007). FTIR-spectra of protein isolates from field pea are shown in Figure 10.

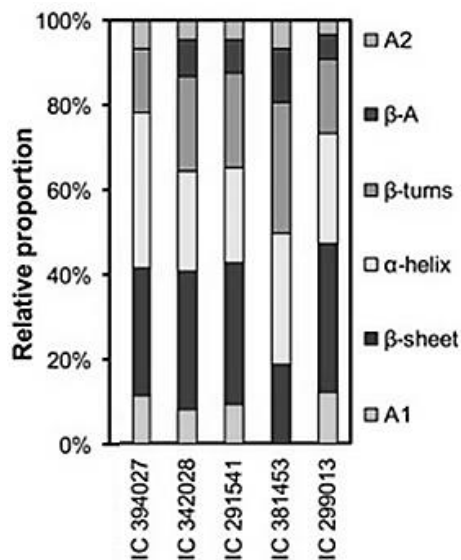


Figure 10: Relative proportion of secondary structures of protein isolates from different field pea lines. Reprinted from Shevkani *et al.* (2015) with permission of Elsevier.

Figure 10 shows the mean relative proportion of secondary structures in pea protein consisting of:  $\beta$ -sheets 30%,  $\alpha$ -helix 28%,  $\beta$ -turns 22%,  $\beta$ -A 7%, A1 8% and A2 5%. The results indicated that pea proteins, like most of the other plant globulins, have greater proportion of  $\beta$ -conformations than  $\alpha$ -helix (Shevkani *et al.* 2015) .

Compared to other legume seeds, the amino acid profile of peas (Table 7) is high in lysine and low in cysteine (Schneider and Lacampagne 2000).

**Table 7: Amino acid profile of pea seeds.**

Amino acid	Content [g/16g N]	
	Ref a	Ref b
Cys	1.2	1.6
Asn	ND	10.7
Gln	ND	16.9
Ser	ND	4.8
Gly	4.5	4.3
His	2.4	2.5
Thr	3.7	3.6
Arg	10.0	6.8
Ala	4.4	4.3
Tyr	0.0	3.2
Val	4.7	3.9
Phe	4.6	4.2
Ile	3.9	3.3
Leu	7.1	6.6
Lys	7.3	6.8
Pro	ND	3.8

Ref a: Holt and Sosulski (1979), Ref b: .Leterme *et al.* (1990)

Fractionation of the proteins showed that pea albumins contain more of the essential amino acids tryptophan, lysine, threonine, cysteine and methionine while the globulin proteins are rich in arginine, phenylalanine, leucine and isoleucine (Swanson 1990).

#### 2.3.4 Functional properties

The functional properties of pea proteins have been the focus of a number of studies (Naczka *et al.* 1986; Sosulski and Mccurdy 1987; Swanson 1990; Owusu-Ansah and McCurdy 1991; Alonso *et al.* 2000; O'Kane *et al.* 2004; Maninder *et al.* 2007; Shand *et al.* 2007; Aluko *et al.* 2009; Barac *et al.* 2010; Sun and Arntfield 2010; Sun and Arntfield 2011; Barac *et al.* 2012; Munialo *et al.* 2014). Generally, pea protein ingredients have been reported to exhibit comparable and complementary functional properties to their soy counterparts.

The solubility of native pea protein isolate is similar to that of most pulse proteins and follows a typical U-shaped curve with a lowest solubility at the isoelectric point around pH 4-5 which increases at low acidic and high alkaline pH-values to around 80% (Shand *et al.* 2007). Table 8 shows typical values of a selection of functional properties of pea flour and pea protein products.

**Table 8: Selection of typical functional properties of pea flour and pea protein products (Owusu-Ansah and McCurdy 1991).**

	<b>Water binding capacity [g H<sub>2</sub>O/g sample]</b>	<b>Oil binding capacity [g oil/g sample]</b>	<b>Emulsifying capacity (ml oil/g sample)</b>
<b>Pea flour</b>	0.8-1.2	0.4-1.0	346
<b>Pea protein concentrate</b>	0.7-1.1	0.6-0.9	372
<b>Pea protein isolate</b>	1.1-3.3	0.9-2.3	366

Heat treatment during fractionation and drying of the protein ingredients highly affects their functionality. For instance, a temperature induced unfolding of a protein molecule would increase the number of hydrophobic side chains at the molecule surface. Hence, the solubility in water of denatured proteins is generally lower than that of native proteins and both oil binding and emulsifying capacity increase with increasing thermal energy input.

The functional properties can be further affected by the isolation method. Fractionation into of pea protein into water-, salt-, alkaline- and ethanol-soluble protein fractions yielded pea protein fractions with a wide range of emulsifying capacity and foaming stability (Adebiyi and Aluko 2011).

Due to their application in meat products and meat alternatives, the gelation behavior of pea protein has been widely studied (O'Kane *et al.* 2004; Shand *et al.* 2007; Munialo *et al.* 2014; Munialo *et al.* 2015). During gelation, both globulins and albumins in pea protein isolates contribute to gel formation depending on extrinsic factors including pH, presence of ionic species, heating temperature and heating rate (Shand *et al.* 2007; Sun and Arntfield 2011) (Figure 11).

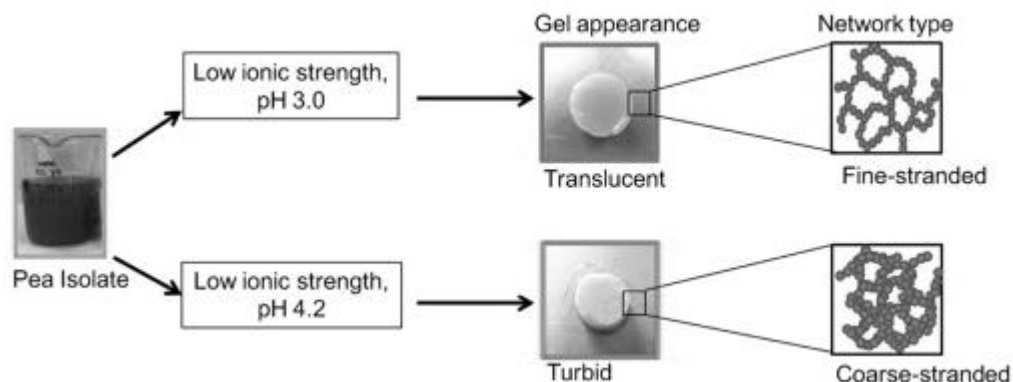


**Figure 11: Gelling of globular proteins such as pea proteins form gels varying in appearance from transparent to opaque. Reprinted from Munialo *et al.* (2015) with permission of Elsevier.**

Compared to soy, pea protein forms weak, heat induced gels with a minimum gelation concentration of commercial pea protein isolate of ~ 14.5% w.b. while that of salt-extracted pea protein isolate was 5.5% w.b. (Sun and Arntfield 2011). Heating and cooling rates were minor factors influencing the gelation properties of pea protein. By blocking sulfhydryl groups using N-ethylmaleimide, O'Kane *et al.* (2004) showed that covalent disulfide bonds were not essential within the network strands of pea legumin and soy glycinin gels. Similar observations in gels made of soy protein isolate were described by Liu and Hsieh (2007).

### 2.3.5 Nutritional and anti-nutritional factors

In many parts of the world, pea seeds are important sources of energy and protein in human nutrition, besides providing fiber, minerals and vitamins. The amino acid profile of pea protein is characterized by high amounts of lysine and arginine, whereas the content of the sulfur-containing amino acids cysteine and methionine as well as tryptophan is comparatively low. However, the consumption of proteins from legumes in combination with cereals such as corn, oats, rice, or wheat complements the amino acids profile (Mensa-Wilmot *et al.* 2001). Despite their nutritional potential, several undesirable compounds are present in pea seeds that are typically found in most legumes. Among these are phytic acid and compounds in the low-molecular albumin fractions such as protease inhibitors (trypsin, chymotrypsin),  $\alpha$ -amylase inhibitors, saponins and lectins, (Alonso *et al.* 1998). A comprehensive review on the presence of several important anti-nutritional factors in food legumes is provided by Gupta (1987).

When consumed in high amounts, their anti-nutritional affect is based on their interference with the absorption of certain nutrients in the gastrointestinal tract. For example, phytic acid

or inositol hexakisphosphate, which serves as a principal storage form of phosphorus in cereals and grains, can inhibit trace element and mineral absorption by forming insoluble precipitates that are less absorbable in the intestines. Protease and amylase inhibitors prevent the actions of the respective enzymes and therefore reduce the absorption of protein and sugar. The anti-nutritional activity of lectins is due to gastrointestinal distress through their interaction with the epithelial gut cells as well as their hemagglutinating activity which can lead to the agglutination of red blood cells. Saponins are glycosides with a bitter taste and pronounced foaming properties. These Saponins are known to cause haemolysis of red blood cells (Alonso *et al.* 1998; Vidal-Valverde *et al.* 2003). However, during traditional processing techniques for legumes such as de-hulling, soaking or heating, the levels of these anti-nutritional compounds can be reduced as shown in Table 9.

**Table 9: Effect of processing techniques (de-hulling, soaking, germination, extrusion) on the amount trypsin inhibitors [TU/mg d.b.], lectins [HU/mg d.b.] and phytic acid [g/100g d.b.] in raw pea seeds *Pisum sativum* L. ssp Solara (Alonso *et al.* 1998).**

Treatment	Trypsin inhibitors <sup>a</sup>	Haemagglutinating activity <sup>b</sup>	Phytic acid
Raw seeds	2.80±0.09	6.2±0.0	1.33±0.01
Dehulling	2.82±0.06	6.2±0.0	1.50±0.01
Soaking	2.25±0.06	6.2±0.0	1.18±0.01
Germination (48h)	1.88±0.06	6.2±0.0	0.88±0.02
Extrusion	0.16±0.06	0.1±0.0	1.15±0.01

a: One trypsin unit was defined as the increase by 0.01 absorbance unit at 410 nm of the reaction mixture.

b: One unit of haemagglutinating activity [HU] was defined as that present in the last dilution giving 50% agglutination of the blood cells.

It was reported that thermal processing of pea seeds using extrusion cooking (148 °C, 24% w.b. moisture content) effectively reduced the content of enzyme inhibitors and lectins due to thermal inactivation of the proteins. The reduction in phytic acid content compared to raw seeds could be explained by a thermally induced hydrolysis of the inositol hexaphosphate to penta- and tetraphosphates (Alonso *et al.* 1998). Besides food processing, the dietary pattern mainly affects the intake of anti-nutritional compounds. Taking phytic acid as example, the Recommended Daily Intake (RDI) of varies from one country to another and average phytate intake can range from as little as 219 to 746 mg per day in Sweden and the United Kingdom, respectively (Onomi *et al.* 2004).

## 2.4 Extrusion in food processing

### 2.4.1 Extruders and extrusion parameters

Food extrusion has been practiced since the middle of the last century. Initially, cold extrusion was used for the continuous mixing and forming of pasta products (Harper 1989). Today, extrusion cooking is considered a high-temperature short-time process in which food ingredients are continuously cooked and forced through a die that forms and texturizes the ingredients (Akdogan 1999; Guy 2001). Extrusion technology is widely used due to its versatility, high productivity and energy efficiency with a broad range of products such as breakfast cereals, baby food or ready-to-eat snacks (Akdogan 1999).

Food extruders mainly comprise of a temperature controlled barrel, one or more rotating screws, a feeding hopper and a die (Figure 12).

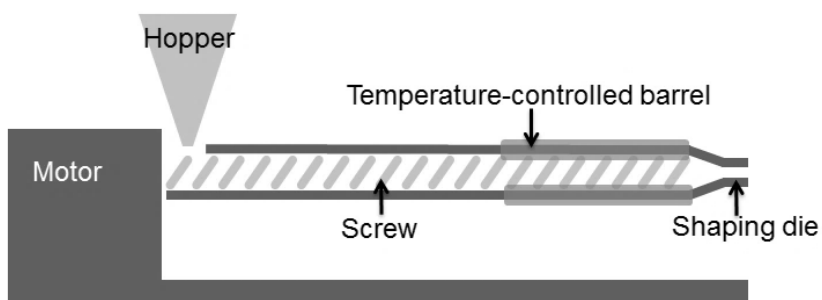


Figure 12: Schematic view of basic components of a food extruder.

The rotation of the screw in a single-screw extruder transports the material from the feed hopper through the barrel until it is pushed through a shaping die. Today, co-rotating twin-screw extruders with a smooth barrel wall are most commonly used in the food industry (Guy 2001; Moscicki 2011; Bouvier and Campanella 2014). These types of extruders provide good pumping efficiency, control over residence time distribution, self-cleaning mechanism and process stability. When co-rotating twin-screw extruders are used, one screw flight interacts with the flow channel in the adjoining screw. This facilitates to wipe off material stuck to the screw surface, thus transporting the extrudate forward. Counterrotating twin-screw extruders are frequently used for processing materials that require high pumping pressures (Riaz 2000; Guy 2001). Accordingly, extruders can be classified by the amount of screws into single-, double- and multiple-screw extruders (e.g. planetary extruder), shown schematically in Figure 13.

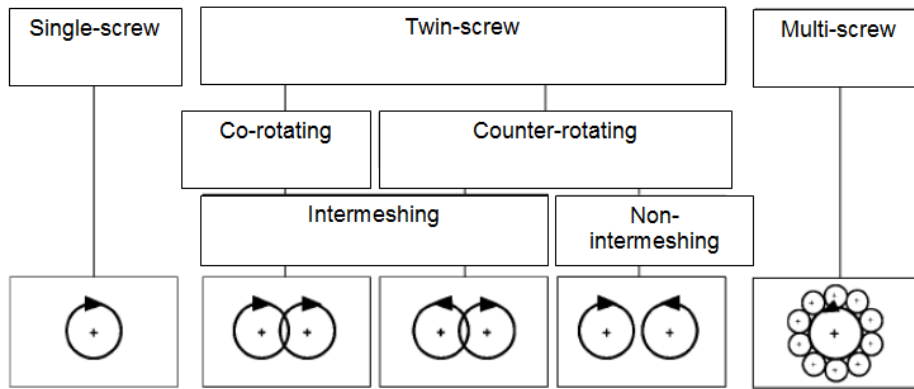


Figure 13: Classification of extruders based on the number of screws, direction of screw rotation and the degree of intermeshing. Adapted from Schuchmann (2008) with permission of Wiley.

Food extruders can be further characterized by the geometrical dimensions of the barrel. The length-to-diameter-ratio (L/D -ratio) is the distance from the internal rear edge to the discharge end of the barrel, divided by the diameter of the bore. Typical food extruder L/D-ratios range from 1 : 1 up to 40 : 1 (Guy 2001). The screw profile is usually built with different screw elements comprising of conveying, mixing, kneading or recirculation elements according to the processing requirements.

Extrusion cooking is a multi-step operation that includes conveying, mixing, kneading, cooking, compression, shearing and stream alignment before pumping out of a die for shaping. These operations depend on a number of independent variables of the machinery and the raw material such as e.g. barrel temperature of the extruder, rotational screw speed, feed rate, and various feed properties (Meuser and Van Lengerich 1984; Camire 1991; Schuchmann 2008). The variables affect a range of dependent parameters in the barrel, such as the material temperature, residence time, pressure and shear (Table 10).

Table 10: Selection of influencing variables and dependent parameters during extrusion cooking (Camire 1998; Schuchmann 2008; Bouvier and Campanella 2014).

Machine	Independent variables		Dependent parameters
	Feed	Process	System
Extruder type	Chemical composition	Mass flow	Pressure
L/D-ratio	Physical properties	Temperature	Torque
Screw profile	Functional properties	Rotational screw speed	Residence time
Die design	Moisture content		Mass temperature
			Shear
			Specific mechanical energy (SME)
			Melt viscosity
			Flow properties
			Filling degree

The combination of these parameters results in molecular transformation and chemical reaction of the feed materials which contributes to stabilization of the three-dimensional network formed during cooling after the extrusion step. Hence, the characteristics of the extruded products e.g. size, shape, texture, and moisture level, that directly determine the properties of the end-product, result from the dependent system parameters. Therefore, the selection of suitable extrusion equipment, the characterization of the feed materials and the control of the process parameters is fundamental to achieve the desired product quality (Camire 1998; Schuchmann 2008; Bouvier and Campanella 2014).

#### 2.4.1.1 Screw design

The conveying and mixing characteristics of intermeshing co-rotating twin screw extruders are attributed to the open screw channel in the axial direction that provides the possibility of axial mixing in the lengthwise direction. The material inside the extruder barrel is moved by the screw rotation creating a drag flow minus the pressure flow generated by the die. The polymer velocity profile in the metering section is shown in Figure 14.

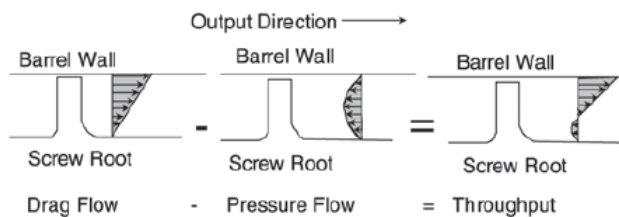


**Figure 14: Velocity profile in the extruder metering section.**  
Reprinted from Giles *et al.* (2004) with permission of Elsevier.

The polymer flow is driven by drag flow with a high velocity along the barrel wall as the material is scraped off the barrel with the screw flight and zero velocity at the screw root. Pressure flow is the result of die pressure forcing the material backward into the metering zone. The combination of these two velocity profiles forms the throughput velocity profile in the metering section with a high flow velocity at the barrel and a negative velocity near the screw root (Giles *et al.* 2004). During extrusion, the material is conveyed from one screw towards the lower wedge where the material is compressed and transported to the other screw. The number of flights per unit length and therefore the width of the screw crest affect the free volume of material that can be transported. Single-flight elements provide advantages for processing materials with poor flow properties such as powders with a low bulk density and are often used in the feed section for maximum free volume. Increasing the number of screw



flights increases the screw surface-to-volume ratio and therefore the conversion of mechanical energy to heat through friction. At the same time, the free volume decreases which reduces the conveying rate and increases the mixing efficiency (Wang 2000; Breitenbach 2002). Conveying elements are characterized by a distinct pitch, a defined length and a specific conveying direction (Figure 15).

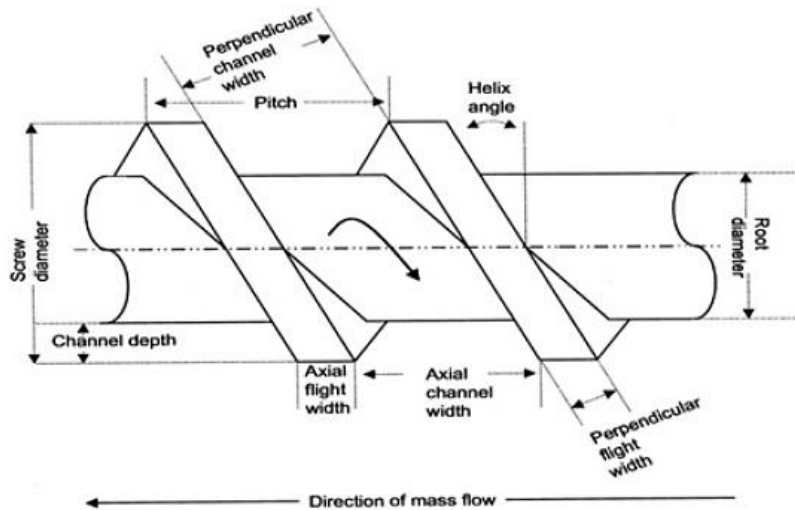


Figure 15: Screw geometry of a conveying element (Breitenbach 2002).

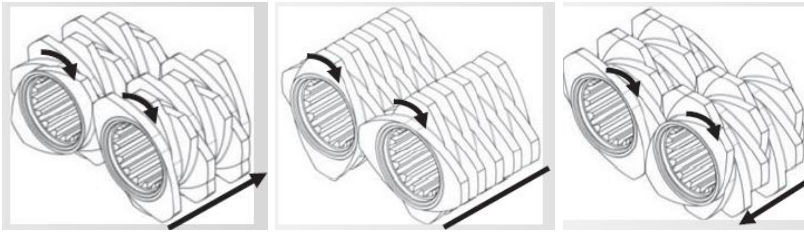
The pitch influences the filling degree in intermeshing extruders as the reduction of the pitch leads to an increased fill of the free screw volume. At reduced pitch, more revolutions around the screw shaft are necessary to transport the material the same distance resulting in a slower conveying rate of the material (Figure 16).



Figure 16: Effect of conveying elements with different pitch on filling degree in free screw volume. Reprinted from Giles *et al.* (2004) with permission of Elsevier.

The material transport efficiency of conveying elements in twin screw extruders is related to the conversion of mechanical energy into heat through friction as well as the residence time in different zones in the extruder barrel (Giles *et al.* 2004). In order to increase shearing, mixing, heating and pressure build-up of the material, mixing or kneading elements can be used. These elements can vary in their design and function according to the specific processing requirements. Kneading blocks are the most common mixing elements and characterized by

their length, number and width of discs, stagger, and conveying direction (Bouvier and Campanella 2014) (Figure 17).



**Figure 17: Kneading blocks with different stagger and conveying direction. Reprinted from Bouvier and Campanella (2014) with permission of Wiley.**

The highest pressure build up can be achieved by reverse-flight or left-handed elements that increase the degree of fill in that region of the screw. These elements are typically used as a seal lock before a degassing zone. The reverse flight elements may cause excessive pressure and shear conditions in that area with negative consequences such as thermal damage of the material, excessive screw and barrel wear and the inability of the extruder to empty (Riaz 2000).

#### 2.4.1.2 Shear rate

The shear rate in the extruder results from the velocity gradient between the screws and the barrel. The use of a selection of screw elements with different geometries as well as different degrees of fill over the length of the screw poses a difficulty for the calculation of the actual shear stress of the materials during the whole process (Wang 2000). However, the shear stress can be estimated from the geometry of the screws and the rotational screw speed (Figure 18).

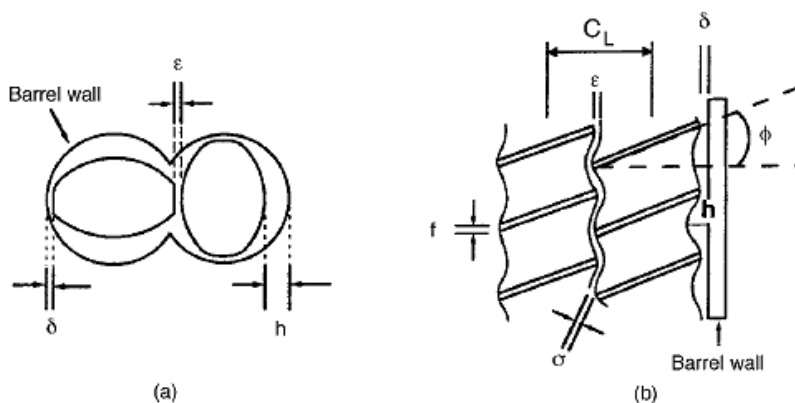


**Figure 18: Clearance between screws and barrel in a co-rotating twin-screw extruder: (a) front view, (b) axial view. Reproduced with permission from Guy (2001); permission conveyed through Copyright Clearance Center, Inc.**

Based on the screw geometry shown in Figure 18, the shear rate can be estimated in the different zones of the screw elements (Martelli 1983). The highest shear rate occurs at the clearance between the screw tips and the barrel wall  $\delta$  as well as the clearance between the screw tips and channel bottom  $\varepsilon$ . The shear rate  $\dot{\gamma}$  [ $s^{-1}$ ] can be calculated as follows:

$$\text{Shear rate barrel wall:} \quad \dot{\gamma}_{\delta}[s^{-1}] = \frac{\pi \cdot d \cdot N}{\delta} \quad 2.1$$

$$\text{Shear rate clearance:} \quad \dot{\gamma}_{\varepsilon}[s^{-1}] = \frac{\pi \cdot 2 \cdot C_L \cdot N}{\varepsilon} \quad 2.2$$

with  $d$  = outer diameter of the screw element [mm],  $N$  = rotational screw speed [ $s^{-1}$ ],  $\varepsilon$  = clearance between the screw tips and channel bottom,  $\delta$  = clearance between the screw tips and the barrel wall and  $C_L$  = the distance between the screw shafts [mm].

#### 2.4.1.3 Thermal and mechanical energy transfer

The energy transferred into the material is of thermal origin by conduction of heat from hot surfaces such as the barrel wall as well as mechanical origin through dissipation of heat caused by the shearing of polymeric material in the screw channel. Bouvier and Campanella (2014) used the term "thermomechanical" to qualify both thermal and mechanical energy inputs in food extrusion.

The understanding and control of energy transfer during food extrusion cooking is important for generating the desired product properties. The levels of both mechanical and thermal energy can be quantified throughout the extruder including heating, cooling, losses and changes in the internal energy of the material. In order to quantify the energy levels, an energy balance may be obtained from heat transfer experiments or models involving parameters related to the extruder (i.e. geometry) and to the material (thermal/rheological properties). An approach is described in Guy (2001) to determine the energy consumption of the process and to quantify the energy into the material using the following power values:

- The mechanical energy supplied by the motor,  $E_{\text{mechanical}}$
- The thermal energy supplied by the heating system,  $E_{\text{heating}}$
- The thermal energy absorbed by the cooling circuit,  $E_{\text{cooling}}$
- The thermal losses to the environment,  $E_{\text{losses}}$
- The energy absorbed by the material,  $E_{\text{material}}$

The resulting energy balance equation is:

$$\text{Energy balance: } E_{\text{mechanical}} + E_{\text{heating}} = E_{\text{cooling}} + E_{\text{losses}} + E_{\text{material}} \quad 2.3$$

This method has been used to characterize the extent of starch gelatinization by deducting the power absorbed by the material from the other measured power levels which represents the quantity of heat necessary for starch gelatinization as it passes through the extruder. The extent of mechanical energy input into the material is usually expressed by the specific mechanical energy as the energy going into the extrusion system per unit mass in the form of work from the motor.

The power transferred between the material and the barrel is proportional to the transfer area and the degree of fill of the screws defined by the operational conditions such as rotational speed, pitch of the screws, material throughput and material density. A lower degree of fill usually results in a higher mixing rate of the material. In partially filled screw elements, the mean residence time depends on the pitch and the rotational screw speed and is independent of the feeding rate. A higher degree of fill increases the shear stress on the material. If the screws are fully filled with material, the residence time depends on the feeding rate (Guy 2001). The mean residence time in fully filled screw sections can be calculated based on the free volume between the extruder barrel and the screw profile, and the flow rate (Bialleck 2012).

#### 2.4.1.4 Residence time distribution

Residence time is largely the result of the distribution of the velocities inside the device and the length of the screw. Residence time distribution (RTD) is a measure of the time the extruded material spends in the extruder until it exits from the die. Particularly in food extrusion it is important to assess the time the extruded biopolymer is exposed to local mechanical and thermal loads in the different zones of the extruder. Based on the RTD, it is possible to estimate the degree of mixing of the material, to anticipate the course of plasticization as well as the stream of liquid material during extrusion (Moscicki 2011; Gao *et al.* 2012).

The RTD is determined by measuring the output response of a change in the input, which is referred to as the pulse input and the step input (Figure 19).

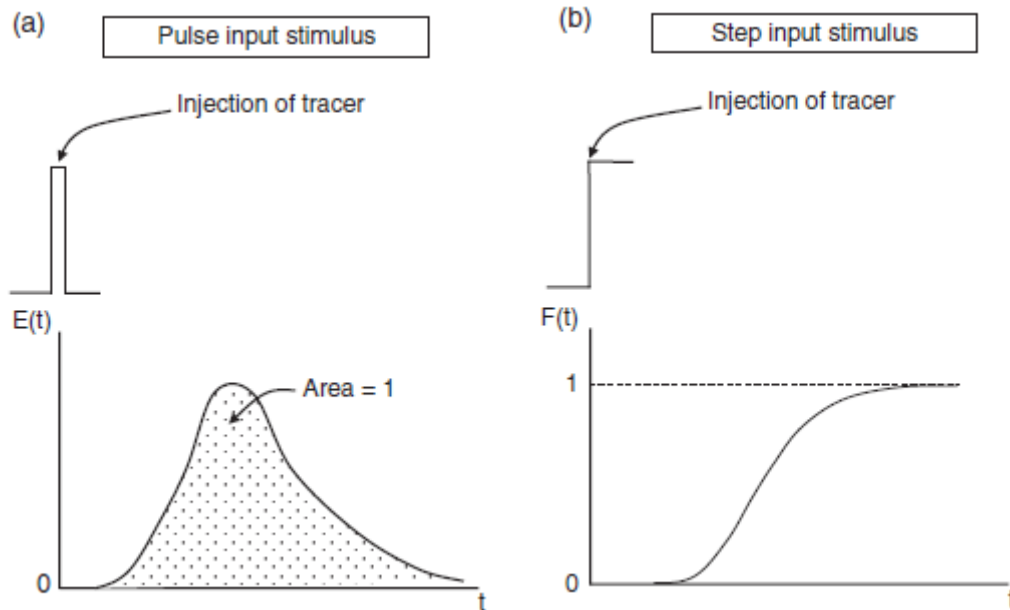


Figure 19: Stimulus response techniques for the determination of residence time distribution. Reprinted from Bouvier and Campanella (2014) with permission of Wiley.

The pulse input stimulus consists of injecting a tracer in one shot into the feed at  $t = 0$  and measuring the signal at the outlet versus time which usually gives a bell-shaped curve. The step input stimulus refers to a constant tracer addition to the feed that is initiated at  $t = 0$  until the tracer concentration in the effluent is similar to that in the feed (Bouvier and Campanella 2014). The most common method for experimental determination of the residence-time is adding color tracer by pulse injection and measuring the time when the color can be observed at the extruder outlet (Aigner *et al.* 2015). The method allows the visualization of the residence time distribution (Bouvier and Campanella 2014). Furthermore, various measurement technologies have been reported that are based on properties of the tracer such as radioactivity (Wolf and White 1976; Thompson *et al.* 1995) color (Mélo and Canevarolo 2002), conductivity (Leeb *et al.* 2008) and fluorescence (Bur and Gallant 1991; Hu *et al.* 1999).

#### 2.4.2 Texturization of food products during extrusion cooking

Extrusion cooking allows the development of unique texture properties, which are usually formed from starches and protein. The thermomechanical process can be generally divided into two different types of processing, depending on the amount of water added. Against this background it is important to differentiate between the moisture content in a dry base, which

corresponds to the intrinsic quantity of water present in the raw materials, from the moisture content on a wet basis (w.b.) which corresponds to the total water after it has been added to the material (Guy 2001). Conventional low moisture extrusion cooking, which is a form of thermoplastic extrusion, is characterized by a composition comprising water contents lower than 40% w.b.. The raw materials are usually preconditioned and extruded using typically single-screw extruders under high shear rate and pressure conditions (up to 200 bar) as well as elevated temperature (<200 °C) conditions (Moscicki 2011). As the hot plasticized mass exits the extruder through a shaping die, the superheated entrapped water vaporizes instantly due to a sudden pressure drop to normal atmosphere (Guy and Horne 1988; Davidson 1992; Lillford 2008).

The sudden evaporation of the included water facilitates the formation of a porous network after its solidification at ambient temperature (Areas 1992). These expanded products exhibit a brittle cellular structure with a crunchy appearance (Barrett *et al.* 1994).

During thermoplastic extrusion, water serves several essential functions. These are the reduction of the glass transition temperature (Figure 20), melting of the polysaccharides and protein as well as the reduction of the viscosity of the extruded mass (Tolstoguzov 1993).

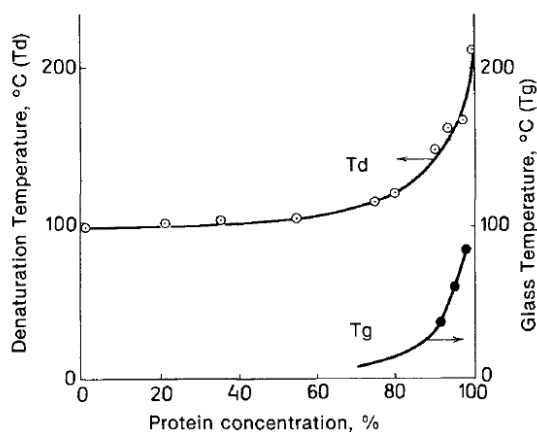


**Figure 20: The glass transition ( $T_g$ ) and denaturation ( $T_d$ ) temperatures of the 11S broad bean globulin. Reprinted from Tolstoguzov (1993) with permission of Springer.**

The glass transition temperature corresponds to the reversible transition of a brittle, glassy solid state of an amorphous material to a rubber-like or a viscous liquid state. This transition results in a change in various physical properties such as the coefficient of thermal expansion and density of biopolymers within a specific temperature range characterized as the glass transition temperature (Tolstoguzov 1993). A glass transition temperature of about 150 °C obtained by dynamic mechanical thermal analysis has been reported for unplasticized soy

protein isolate (Su *et al.* 2010). The term “melting” commonly corresponds to a first order phase transition of crystalline or partly crystalline materials with a sudden change of enthalpy at the characteristic melting temperature (Figura and Teixeira 2007). Regarding extrusion texturization of food materials, a minimum amount of water is necessary as dry proteins and polysaccharides cannot be melted because their melting temperatures exceed the temperatures of their thermal decomposition (Tolstoguzov 1993).

Extrusion cooking of cereal starches to expanded products using low moisture extrusion has been investigated to a great extent (Guy and Horne 1988; Lai and Kokini 1991; Moraru and Kokini 2003; Schuchmann 2008). Another application of this technology is the texturization of proteins to expanded products that are used as meat extenders or ground meat substitutes. The minimal temperature for extrusion texturization seems to be universal for all globular native and denatured proteins and is about 130-140 °C. This temperature range corresponds to the change of water-plasticized food biopolymers as well as to the melting temperature of many protein gels (Tolstoguzov 1993). The textured vegetable protein products are mainly obtained from defatted soy flour and require rehydration prior to consumption resulting in a sponge-like texture. A recent development in food extrusion is the processing of starch or protein based raw materials with high moisture levels up to 80% w.b. using twin screw extruders (Bouvier and Campanella 2014). In starch-based high moisture extrusion, the extruder is considered as a continuous bioreactor. During the process called continuous liquefaction, cereal starches are extruded in the absence or presence of enzymes such as thermostable  $\alpha$ -amylases to convert starch into dextrans in order to produce a soluble, low viscosity hydrolysate that can be further processed to e.g. maltodextrins (Akdogan 1999).

In contrast, the extrusion of proteins with high moisture levels is focused on texture formation. Unlike the textured vegetable protein from low moisture extrusion, the products from high moisture extrusion are not expanded. This is achieved by the use of a cooling die in order to reduce the temperature of the extruded mass to an exit temperature below 100 °C and prevent water from flashing off at ambient pressure. These products are characterized by anisotropic structures with a fibrous texture. These products have the potential to resemble chicken or turkey breast meat and therefore exhibit enhanced visual appearance and taste sensations (Noguchi 1990; Cheftel *et al.* 1992; Thiebaud *et al.* 1996; Akdogan 1999; Lin *et al.* 2002; Yao *et al.* 2004; Ranasinghesagara *et al.* 2005; Liu and Hsieh 2008; Chen *et al.* 2011). Besides high moisture extrusion, the generation of anisotropic structures was reported for other techniques i.e. spinning (Hartman 1978; Tolstoguzov 1988; Huang *et al.*) and shearing (Grabowska *et al.* 2014; Krintiras *et al.* 2015; Grabowska *et al.*; Krintiras *et al.* 2016).

### 2.4.3 Rheological characterization of extruded food materials

During extrusion, food material is exposed to thermal and mechanical stresses that are responsible for the changes in the physical and chemical structure of the material through various mechanisms such as gelatinization, melting, fragmentation/degradation, protein denaturation, lipid oxidation, and formation of flavors (Emin 2015). Hence, measuring the thermal and mechanical stresses and material properties in extruders is of crucial importance for the investigation of molecular changes during processing, process control and optimization as well as the development of new extruded food products (Faller and Unlu 2010). The viscosity of the extruded material depends on both the temperature and shear rate. Knowledge of the viscosity over industrially relevant range of shear rates and temperature is important for controlled processing. However, due to the wide viscosity range of food materials resulting from the thermal and mechanical stresses during extrusion, their rheological characterization is a difficult task and remains challenging (Emin 2015). The following section covers a selection of rheological approaches in order to investigate the properties of food materials during extrusion cooking.

#### 2.4.3.1 The concept of shear stress, shear rate and apparent viscosity

The fundamental rheological parameters are defined using the Two-Plates-Model (Figure 21).

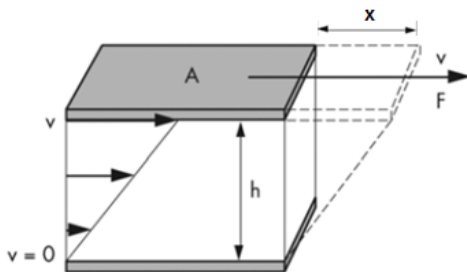


**Figure 21: The Two-Plates-Model for shear tests to illustrate the velocity distribution of a flowing fluid in the shear gap with shear area  $A$ , shear force  $F$ , gap height  $h$ , deformation  $x$  and velocity  $v$ . Modified from Mezger (2006) with permission of Vincentz.**

When a force  $F$  is acting on area  $A$  to effect a movement in the fluid between two plates with the gap size  $h$  [m], the velocity  $v$  [m/s] of the movement is controlled by the internal forces of the material. The apparent viscosity of a fluid is a measure of its resistance to a deformation by shear stress (Mezger 2006):

$$\text{Shear stress} \quad \tau \text{ [Pa]} = \frac{F}{A} \quad 2.4$$



Shear rate	$\dot{\gamma}[s^{-1}] = \frac{v}{h}$	2.5
------------	--------------------------------------	-----

Apparent viscosity	$\eta[Pa\cdot s] = \tau/\dot{\gamma}$	2.6
--------------------	---------------------------------------	-----

The major types of fluid flow behavior can be described by plotting the shear rate versus shear stress. The shear viscosity of a fluid depends on the concentration of macromolecular constituents, temperature, pressure, time and shear rate. If an ideally viscous material is subjected to a shear stress, a shear gradient of a viscous flow is generated which is proportional to the applied shear stress as described by Newton's law of viscosity. Examples of Newtonian materials are water, mineral oil or bitumen (Mezger 2006). In contrast, most foods are structurally complex, non-Newtonian mixtures of fluid and solids with different rheological states including solid, gel, liquid, emulsion and their associated rheological behaviors (Rao 2007). Non-Newtonian fluids can exhibit a variety of different correlations between shear stress and shear rate (Figure 22).

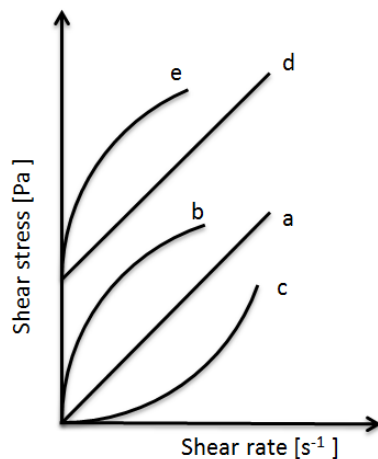


**Figure 22:** Flow curves for classification of time-independent flow behavior of fluid foods with Newtonian (a), shear thinning or pseudoplastic (b), shear thickening or dilatant (c) behavior as well as Bingham (d) and Herschel-Bulkley flow (e) with a yield stress that must be exceeded for flow to occur. Modified from Sahin and Sumnu (2006) with permission of Springer.

Starch dispersions typically exhibit shear thickening behavior. The flow curve shows an increasing slope and the apparent viscosity increases with increasing load. In contrast, protein dispersions exhibit shear thinning behavior typical for polymer solutions due to a partial disentanglement and orientation of macromolecules with increasing shear rates. The flow curve shows a decreasing curve slope and the viscosity correspondingly decreases with increasing load (Sahin and Sumnu 2006).

For some materials, a threshold stress value is necessary to initiate flow which is referred to as the yield stress. Many foods exhibit shear thinning with yield stress behavior (Herschel-

Bulkley flow) such as tomato concentrates, tomato ketchup, mustard, and mayonnaise (Rao 2007). The Herschel-Bulkley model is a generalized power law equation with a yield stress added and it is commonly used to describe the rheological properties of food products (Augusto *et al.* 2012).

Herschel-Bulkley model: 
$$\tau [Pa] = \tau_0 + K \dot{\gamma}^n \quad 2.7$$

with the shear stress  $\tau$ , yield stress  $\tau_0$ , consistency coefficient  $K$ , flow behavior index  $n$  and shear rate  $\dot{\gamma}$

The exponent  $n$  indicates shear thinning behavior with  $n < 1$ , shear thickening behavior with  $n > 1$  and Bingham-behavior with  $n = 1$  (Akdogan and McHugh 2000). The consistency coefficient  $K$  indicates the viscosity of the fluid at a shear rate of  $1\text{s}^{-1}$ .

The rheological methods to assess extruded foods can be divided into offline measurements using typically rotational rheometers, on-line measurements in a bypass loop from the main process line as well as inline measurements directly in the process line (Roberts 2001).

#### 2.4.3.2 Offline-measurement

The most common offline-rheometers based on the application of steady shear rate to the fluid are capillary and rotational rheometers. Typically, rotational measurements are applied to investigate the viscosity of flowable liquids. As most food compositions for extrusion are solid under room temperature and start to flow only at elevated temperatures above  $100\text{ }^\circ\text{C}$ , the food materials need to be diluted for rotational testing. In the context of extrusion, rotational rheometers have been used to investigate temperature-induced changes in rheological behavior of diluted starch or protein suspensions as a result of starch granule swelling, gelatinization or protein denaturation that occurs during extrusion cooking. This can provide valuable information about technofunctional properties of the raw materials (Bourne 2002; Tabilo-Munizaga and Barbosa-Cánovas 2005; Sorba and Sopade 2013).

Common empirical instruments for routine rheological analyses of extruded foods are the Brabender ViscoAmylograph and the Rapid Visco Analyzer (RVA) (Biliaderis 2009). These instruments are used to characterize the hydrated raw material in its preprocessed state as well as the postprocessed state (Borwankar 1992). Changes in viscosity are monitored under constant stirring and following a programmed heating and cooling cycle. In contrast to common rotational rheometers using plate, cone or cylinder probes, the rotating paddles may prevent sedimentation of dispersed particles. The pasting properties characteristics of extruded products have been reported in several publications (Moisio *et al.* 2015; Wu *et al.*

2015; Román *et al.* 2016). Pasting is a phenomenon following gelatinization, involving granular swelling, amylose leaching, and total disruption of the starch granule. A typical pasting viscosity profile of a starch suspension is shown in Figure 23.

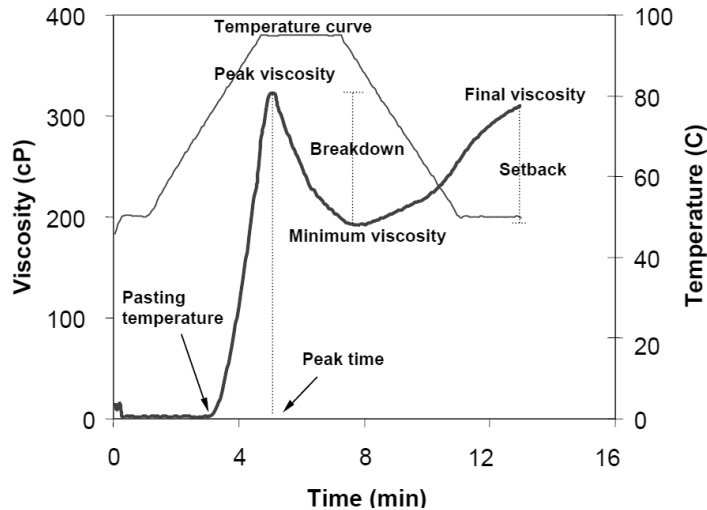


**Figure 23:** Typical RVA pasting profile of rice starch showing the commonly measured parameters. Reprinted from Copeland *et al.* (2009) with permission of Elsevier.

The RVA curve shows an increase of viscosity that relates to the onset of starch gelatinization. The peak viscosity indicates the maximum swelling of the hydrated starch granules followed by a breakdown due to their disintegration into amylose and amylopectine. Upon cooling, the viscosity increases due to gelling until a final viscosity is reached (Saunders *et al.* 2011). Although the viscosity response of diluted fluids can help to determine structural changes occurring in the biopolymer structure, the rheological behavior of food materials during extrusion requires approaches to assess the rheological properties in both the liquid as well as the solid state. Another approach to characterize extruded foods is based on the investigation of their viscoelastic properties.

#### 2.4.3.3 Small strain oscillation

Viscoelastic materials such as food gels exhibit some of the elastic properties of an ideal solid and some of the flow properties of an ideal liquid (Bourne 2002). Small strain oscillatory shear, also called dynamic rheological experiments, can be used to determine viscoelastic properties of foods. In contrast to rotational measurement, the test material is exposed to a

small strain oscillation about a central point with a sinusoidal velocity while the shear stress is measured (Figure 24).

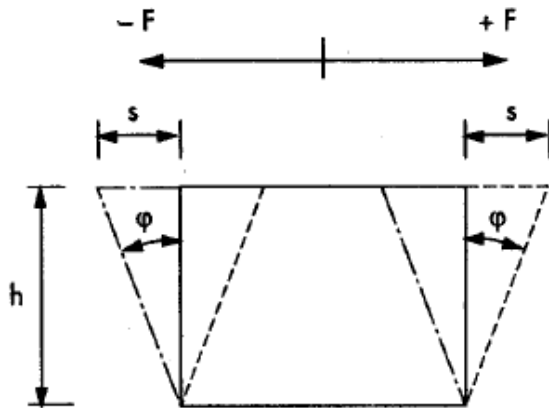


Figure 24: Shear force  $\pm F$ , deformation  $\pm s$  and deformation angle  $\pm\phi$  in gap  $h$ . Reprinted from Mezger (2006) with permission of Vincentz.

The properties of viscoelastic materials can be described by their response to sinusoidal inputs depending on both shear frequency and rate of shear strain. For ideal-elastic materials, the stress and strain are in phase whereas for ideal-viscous materials, the strain lags stress by a  $90^\circ$  phase lag. In the case of viscoelastic fluids the shear stress lags behind the strain by an angle between  $0^\circ$  and  $90^\circ$  (Figure 25).

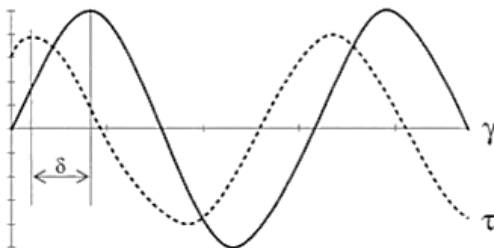


Figure 25: Preset shear strain function  $\gamma$  and resulting shear stress function  $\tau$  showing the same frequency but between the preset and the resulting curve occurs the phase shift angle  $\delta$ . Reprinted from Mezger (2006) with permission of Vincentz.

The resulting function for oscillatory measurement is derived from:

$$\text{Measuring with controlled strain: } \gamma(t) = \gamma_A \cdot \sin\omega t \quad 2.8$$

$$\text{Measuring with controlled stress: } \tau(t) = \tau_A \cdot \sin\omega t \quad 2.9$$

with  $\gamma_A$  = amplitude of deformation [%],  $\tau_A$  = amplitude of shear stress [Pa] and  $\omega$  = radial frequency [ $s^{-1}$ ]. Differentiation of equation 2.7 yields the function of the deformation or shear rate:

$$\text{Deformation/shear rate:} \quad \dot{\gamma}(t) = \gamma_A \cdot \omega \cdot \cos\omega t \quad 2.10$$

The stress component in phase with the shear strain is defined as the storage (or elastic) modulus  $G'$ , the stress component  $90^\circ$  out of phase is the loss (or viscous) modulus  $G''$ :

$$\text{Storage modulus:} \quad G'[Pa] = \frac{\tau_A}{\gamma_A} \cdot \cos\delta \quad 2.11$$

$$\text{Loss modulus:} \quad G''[Pa] = \frac{\tau_A}{\gamma_A} \cdot \sin\delta \quad 2.12$$

The  $G'$  value is a measure of the deformation energy that is stored in the sample during the shear process representing the elastic behavior of a sample while the  $G''$  value is a measure of the deformation energy used up in the sample during the shear and lost to the sample afterwards, representing the viscous behavior of a sample (Mezger 2006).

For strain values within the linear range of deformation,  $G'$  and  $G''$  are independent of strain. The loss tangent  $\tan\delta$  is calculated as the quotient of the lost and the stored deformation energy and reveals the ratio of the viscous and the elastic portion of the viscoelastic deformation behavior (Rao 2007).

$$\text{Loss tangent:} \quad \tan\delta [-] = G''/G' \quad 2.13$$

The value of  $\tan\delta$  is infinite for an ideal liquid and approximates zero for a solid matter. Materials in the liquid state exhibit  $\tan\delta > 1$  ( $G'' > G'$ ) and materials in the gel or solid state exhibit  $\tan\delta < 1$  ( $G' > G''$ ). The point when  $\tan\delta = 1$  is the sol/gel transition point, which is important for the characterization of viscoelastic material behavior (Shevkani *et al.* 2015).

The complex shear modulus  $G^*$  characterizes the complete viscoelastic behavior consisting of both the elastic and the viscous portion as illustrated by the vector diagram in Figure 26.

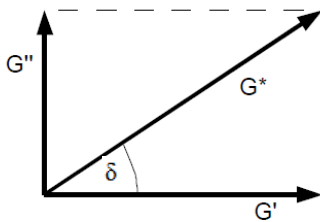


Figure 26: Vector diagram showing  $G'$ ,  $G''$ , the resulting vector  $G^*$  and the phase shift angle  $\delta$ . Modified from Mezger (2006) with permission of Vincentz.

$$\text{Absolute value of the complex shear modulus: } |G^*| [\text{Pa}] = \sqrt{(G')^2 + (G'')^2} \quad 2.14$$

$$\text{Absolute value of the complex viscosity: } |\eta^*| [\text{Pa s}] = |G^*|/\omega \quad 2.15$$

When plotted as a function of angular frequency,  $|\eta^*|$  can be correlated to the steady shear viscosity as a function of shear rate. This empirical relationship, known as the Cox/Merz relation for polymer and melt solutions, states that the absolute value of the complex shear viscosity at a given frequency is equal to the steady shear viscosity at the same shear rate. It enables the generation of viscosity/shear rate profiles from oscillation frequency sweeps in the low shear range for some materials that cannot be tested using rotational techniques.

$$\text{Cox/Merz relation:} \quad \eta[\dot{\gamma}] = |\eta^*(\omega)| \quad 2.16$$

The relationship has been applied to a number of polymers, solutions and complex food systems (Tiziani and Vodovotz 2005; Yaşar *et al.* 2009; Storz *et al.* 2010). However, it can only be applied to viscoelastic liquids with  $G'' > G'$  in the low-shear range (Kulicke and Porter).

Common tests for characterizing the viscoelastic properties of materials include amplitude sweep and frequency sweep. The linear viscoelastic range with constant values for  $G'$ - and  $G''$  is determined by means of an amplitude sweep as shown in Figure 27.

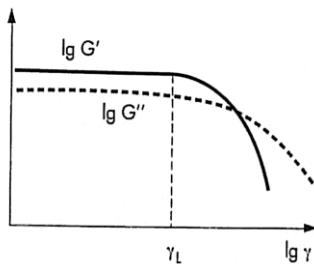


**Figure 27: Stress amplitude sweep of a sample showing linear viscoelastic range, the yield point  $\gamma_L$  and the flow point when  $G' = G''$ . Reprinted from Mezger (2006) with permission of Vincentz.**

At low amplitude values, both  $G'$ - and  $G''$ -curves typically show constant plateau values, i.e. the structure of the sample shows stability under this condition. At amplitudes higher than  $\gamma_L$ , the limit of the linear viscoelastic range is exceeded and the sample structure is irreversibly changed. At the crossover point of  $G'$  and  $G''$ , the material starts to flow, hence the term flow point is used. The corresponding shear stress values are the yield stress  $\tau_\gamma$  at the yield point and the flow stress  $\tau_f$  at the flow point when  $G' = G''$ .

Frequency sweeps are used to evaluate time-dependent deformation of a sample such as the consistency of a material at rest, its short-time behavior (high frequencies) or long-term behavior (low frequencies).

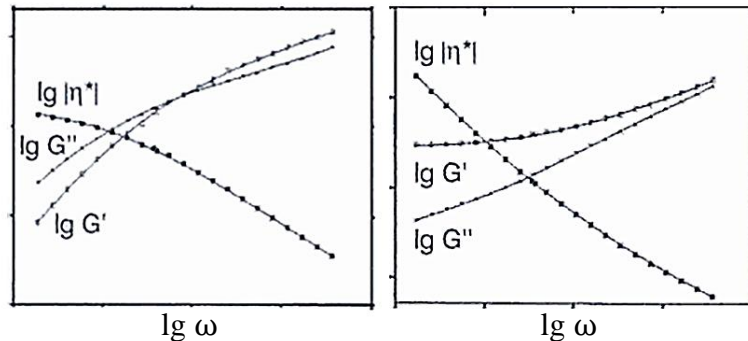


**Figure 28:** Example for two polymers characterized using frequency sweeps in the low-frequency range. **Left:** In the low frequency region,  $G'' > G'$  indicates viscous properties and the  $|\eta^*|$ -function approaches a plateau value at zero shear, a behavior typical for unlinked molecules. **Right:**  $G' > G''$  indicates elastic behavior and the  $|\eta^*|$ -function rises towards infinitely high values, which is typical for cross-linked molecules with a gel character and form-stability at rest. Reprinted from Mezger (2006) with permission of Vincentz.

For describing the time-dependent viscoelastic behavior of dispersions, the storage and loss modulus can be modeled as a power function of oscillatory frequency (Rao 2007):

$$G'[\text{Pa}] = K' \omega^{n'} \quad 2.17$$

with behavior index  $n' = \text{slope of } G'$  and consistency index  $K' = \text{intercept with ordinate}$ .

Both indices can help to characterize and compare the viscoelastic properties of fluids. The behavior index  $n'$  in the power law model of the viscoelastic properties- that is the slope of  $\log G' \text{ vs } \log \omega$  - is supposed to be zero for pure elastomers, while weak gels and highly concentrated solutions exhibit positive slopes. The consistency coefficient  $K'$  in the power law model of the viscoelastic properties gives the intercept with the ordinate and indicates the consistency at a shear rate of  $1 \text{ s}^{-1}$  (Rao and Cooley 1992; Ahmed *et al.* 2006; Augusto *et al.* 2012; Augusto *et al.* 2013; Ahmed *et al.* 2016).

A common method to study the gelation behavior of food polymers, particularly the temperature-induced phase transition from sol to gel, uses the crossover of the storage modulus  $G'$  and the viscous modulus  $G''$  during a temperature sweep (Figure 29).

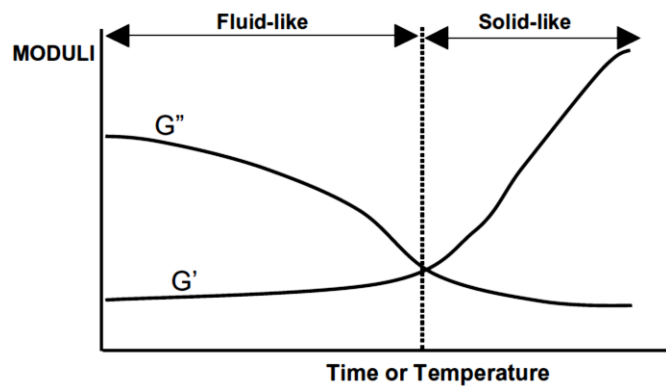


Figure 29: Viscoelastic response of a material undergoing gelation. Reprinted from Tabilo-Munizaga and Barbosa-Cánovas (2005) with permission of Elsevier.

The temperature at which  $G'$  becomes greater than  $G''$  is determined as the initiation of gelation or the gel point (Stephen and Phillips 2006). A typical temperature sweep to monitor the gel formation is shown in Figure 30.

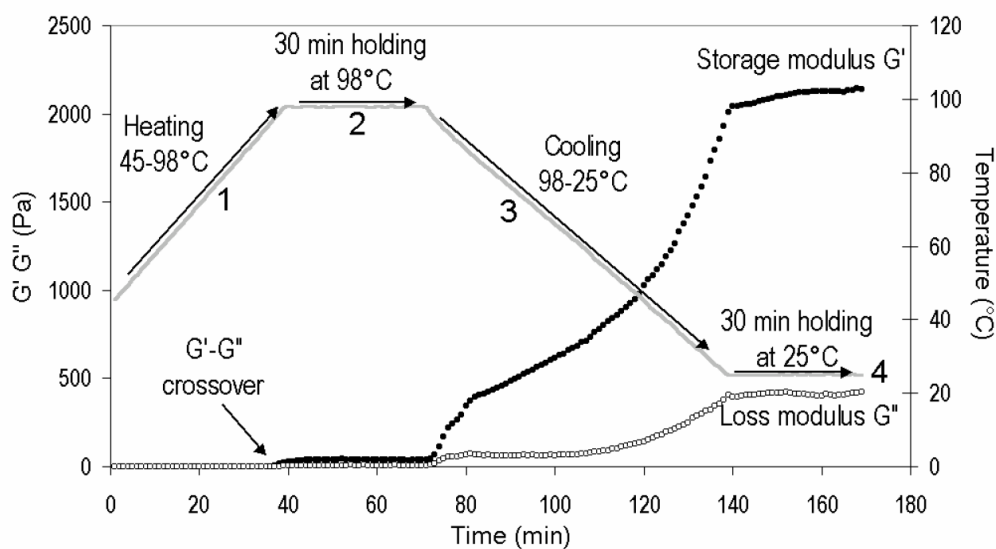


Figure 30: Gelling properties of pea protein. Storage ( $G'$ ) and loss ( $G''$ ) moduli as a function of time and temperature (O'Kane *et al.* 2004).

For native proteins, the temperature at which  $G'$  starts to increase can be attributed to the onset of gel formation, which is usually between the onset and peak denaturation temperature of the major protein fraction of the respective protein (Renkema and van Vliet 2002).

The characterization of the viscoelastic properties of materials can help to determine structural changes occurring in the biopolymer structure due to thermomechanical processing during extrusion. However, the wide viscosity range of biopolymeric materials, which result from specific extrusion conditions such as shear rate, temperature and pressure, can only be



studied within the limits of the rheological equipment (Davidson 1992). This will be further addressed in chapter 4.2.

#### 2.4.3.4 Online rheometry

One example for a capillary instrument to determine the melt-flow rate or mass-flow rate of thermoplastic polymers is an extrusion plastometer or melt-flow indexer. The melt-flow test measures the weight of the polymer extruded in ten minutes through a capillary of specific diameter and length by pressure applied through a specific load and temperature conditions. During testing, the polymer sample is preheated in the apparatus for a specified amount of time at 190 °C or 230 °C; depending on the material (Shenoy *et al.* 1983). In contrast to polymer melts, the composition of extruded food products usually contains water as a plasticizer. Accordingly, melt-flow tests are not suitable for food materials due to water flashing off as soon as the temperature reaches 100 °C (Bouvier and Campanella 2014).

In contrast, online rheometry using pressure transducers along a slit- or capillary die which is attached to the extruder allows the investigation of the rheological properties during the process. Slit die geometries are usually preferred due to flush-mounted pressure transducers (Horvat *et al.* 2013a). The measured pressure drop resulting from fully developed laminar flow of a fluid through a straight section of a known length and flow rate under constant temperature conditions is used to calculate viscosity (Li *et al.* 2004; Chen *et al.* 2010b; Fang *et al.* 2014).

Online viscosity: 
$$\eta[\text{Pas}] = \frac{\tau}{\dot{\gamma}} = \frac{\Delta PH}{2L} / \frac{6\dot{v}}{WH^2} \quad 2.18$$

In this formula,  $\eta$  is the apparent viscosity (Pa s);  $\tau$  is the shear stress (Pa);  $\dot{\gamma}$  is the shear rate ( $\text{s}^{-1}$ );  $\Delta P$  is the die pressure drop (Pa); H, L, and W (height, length, width) are the known geometries of the die channel (mm); and  $\dot{v}$  is the volumetric flow rate ( $\text{mm}^3/\text{s}$ ).

Several studies use online rheometry for the measure of rheological properties of starch during extrusion cooking (González *et al.* 2006; Horvat *et al.* 2013a; Horvat *et al.* 2013b; Hochstein *et al.* 2015). However, a number of drawbacks are associated with online rheometry during food extrusion. For instance, the variable output flowrates during most extrusion processes can complicate data interpretation. Furthermore, the geometrical requirements of the slit die (large length, small gap) increase the pressure in the extruder which might change the nature and structure of the material compared to extrusion conditions without the device (Horvat *et al.* 2013a; Horvat *et al.* 2013b).

## 2.5 High moisture extrusion cooking

In order to texturize proteins under high moisture conditions, it is important to prevent the expansion of the subcritical water in the extruded materials at the exit of the die. This is achieved by using a long cooling die that reduces the temperature and viscosity of the feed in order to shape the biopolymeric material inside the die channel. An early model for the texturization process of protein during high moisture extrusion was proposed by Noguchi (1990). They proposed that the proteins are plasticized and texturized by varying different process variables, which directly influence both the pressure and shear inside the extruder resulting in a molecular transformation and chemical reaction of the protein molecules. By means of a proper adaptation of the process variables such as moisture content of the feed and cooking temperature, fibrous meat-like structures could be obtained (Noguchi 1990; Cheftel *et al.* 1992).

The specific requirements for high moisture extrusion equipment have been described by several authors (Noguchi 1990; Cheftel *et al.* 1992; Akdogan and McHugh 1999; Bouvier and Campanella 2014). In contrast to low moisture extrusion where the feed temperature increases mainly due to mechanical energy input through the screws, the large amount of moisture (50-80% w.b.) reduces the shear due to the low viscosity of the feed mixture. This requires thermal energy supplied by the temperature-controlled barrel to increase the feed temperature in the cooking zone. Hence, extruders are configured with a high length/diameter ratio between 25 and 40 (Bouvier and Campanella 2014). Twin screw extruders provide improved conveying properties compared to single screw extruders and are usually used for high-moisture extrusion applications to ensure a proper process control (Noguchi 1990; Akdogan 1999). Besides the extruder, the cooling die has several functions during the texturization of proteins and plays a crucial role during high moisture extrusion cooking. When the extruded material is pushed through the cooling die channel, the reduction of the feed temperature increases the feed viscosity which prevents an expansion of the feed at the die outlet (Cheftel *et al.* 1992). At the die exit, the solidified extrudate is shaped based on the die geometry into the desired product appearance (Akdogan 1999).

The following sections provide an overview of the fundamental work as well as the latest studies in the field of high moisture extrusion cooking of protein.

### 2.5.1 Physico-chemical material properties

In most food extrusion processes as well as in high moisture extrusion cooking, agricultural materials are converted from a solid, granular state into a flowable viscoelastic state by a combination of heat, shear, pressure and moisture (Bouvier and Campanella 2014). Despite previous studies on high moisture extrusion cooking, there is only a small amount of published data about the physical state of the protein-water mixture in the cooking zone of the extruder during high moisture extrusion conditions (Kitabatake and Doi 1991; Cheftel *et al.* 1992). This is because the high vapor pressure of the subcritical water in the extruded biopolymeric material impedes a direct investigation of the physico-chemical material properties in the cooking zone, as it would cause an expansion and subsequent drying upon opening the extruder barrel at temperatures higher than 100 °C. This section summarizes the previous work on this topic. It should be noted that in the original studies, some of the terms to describe phase transitions have been used on the basis of visual observation rather than analytical data. Keeping that in mind, the same terms will be used in this summary as the basis for a detailed discussion in the results and discussion part in section 4.2.

Based on indirect measurements, Cheftel *et al.* (1992) observed that an increase of the cooking temperature caused the torque to decrease, which is indicative for a weakening of the cohesion of the paste-like protein-water mixture. Moreover, occasional leaks of fluid protein material between the barrels in the cooking zone were observed during extrusion. Hence, several authors described the protein-water mixture in the cooking zone as a “plasticized mass” or “protein melt” at temperatures between 140-180 °C (Noguchi 1990; Cheftel *et al.* 1992; Hayashi *et al.* 1993; Thiebaud *et al.* 1996; Chen *et al.* 2011). Based on the change of appearance of the protein-water mixture from a kind of coarse protein paste before, to a rigid elastic product after extrusion, it was assumed that the protein melt solidifies during the passage through the cooling die channel.

These observations raised the question at which temperature range these physical transitions - that means melting and solidification - occur during high moisture extrusion cooking. Based on a study on soy protein isolate, it was suggested that the melting temperature of the proteins correlates with the denaturation temperature of the proteins (Kitabatake and Doi 1992). Therefore, the temperature needed for texturization by extrusion cooking was proposed to be in the same range as the denaturation temperature of the proteins, which causes the protein-water mixture to plasticize inside the extruder (Kitabatake and Doi 1992). Considering the thermo-reversibility of the phase transitions, it was shown that the rigid structure of the extrudates can be broken down and reformed as the texture and appearance of extrudates were

similar after repeated extrusion cycles (Isobe and Noguchi 1987). In the context of food processing, the term phase transition refers to a change in the physical state and the transition of concern is often either from liquid to solid, solid to liquid or solid to solid (Roos and Drusch 2015).

The current understanding of the physico-chemical material properties during high moisture extrusion cooking were summarized by Bouvier and Campanella (2014). Initially, the bio-based polymers are in either amorphous or partially crystalline solid state, depending on their microstructure and composition. During heating in the extruder, the materials are converted from solid to liquid state while undergoing physical transitions such as glass transition or, in the case of partially crystalline polymers, melting transition. During cooling, they are converted back to solid or rubbery state through physical transitions leading to physical characteristics which may differ from those of the original solid state (Bouvier and Campanella 2014).

As described in 2.4.3, changes in physical material properties can be monitored by their rheological properties. Up to now, there is only a small amount of published data on the rheological properties of the protein-water mixture in the cooking zone as well as the cooling die under high moisture conditions. Recent studies applied a slit die rheometer that was cooled to 80 °C to study the effect of specific mechanical energy and moisture content on the online-viscosity of soy protein isolate during high moisture extrusion (Chen *et al.* 2010b; Fang *et al.* 2014). With increased specific mechanical energy using different screw configurations, the online viscosity at the die significantly decreased from 997 to 867 Pa s. Similar observations of a negative correlation between online viscosity and specific mechanical energy were described in several studies on extrusion cooking of starch-based materials and attributed to a reduction of the size of macromolecules under high specific mechanical energy conditions causing the online viscosity to decrease (Wang *et al.* 1990; Chang *et al.* 1999; Rosentrater *et al.* 2009). Under high moisture conditions of 60% w.b. and 140 °C cooking temperature, the online viscosity at the die was around 1000 Pa s and increased to around 2500 Pa s when the moisture content of the extrudate was reduced to 28% w.b.. When the cooking temperature was increased from 140 to 160 °C, the online viscosity decreased below 500 Pa s at the die.

Currently, several research projects funded by the Research Association of the German Food Industry (Rauh *et al.* 2015) and others focus on methods to acquire rheological data of the

fluid properties during high moisture extrusion in order to provide a better understanding of the texturization mechanisms.

## 2.5.2 Texturization and fiber formation

### 2.5.2.1 Structure formation mechanism

Extrusion cooking of food mixes with high moisture levels requires the use of a cooling die in order to prevent expansion. The combination of heating and subsequent cooling of the protein-water mixture facilitates the texturization to layered or fibrous structures with a meat-like appearance (Cheftel *et al.* 1992). However, the mechanisms of the texturization process into fibrous structures during high moisture extrusion cooking are not clearly understood up to now (Lin *et al.* 2002; Chen *et al.* 2010b; Fang *et al.* 2014).

Tolstoguzov *et al.* (1985) initially suggested a model for the mechanism of protein texturization in thermoplastic extrusion based on the spinneretless spinning process. The model is based on the deformation and orientation of emulsion droplets during flow until they take a filamentous form. This would require phase separation of the polymers in the liquid medium based on their thermodynamic incompatibility, thus forming a water-in-water emulsion that can be spun. This behavior of thermodynamically incompatible components led to the suggestion that phase separation of protein above a certain concentration forming water-in-water emulsions could occur in the die. This was suggested as the mechanisms for the filamentous structure of thermoplastic protein extrudates, even when only one type of protein was present (Tolstoguzov *et al.* 1985; Tolstoguzov 1988; Tolstoguzov 1993).

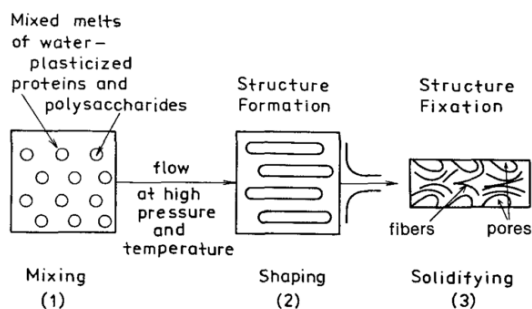


Figure 31: Early historical model for the structure formation mechanism during food processing including thermoplastic extrusion. Reprinted from Tolstoguzov (1993) with permission of Springer.

Based on this hypothesis, Mitchell and Areas (1992) proposed the “suspension model” for biopolymer extrusion and texturization. They considered the extruded mass as a two-phase

system, suggesting that insoluble protein- or nonprotein particulates act as fillers in a continuous molten mass flowing through the extruder.

They described that soy yielded a relatively small amount of indeterminate insoluble material based on protein resolubilization by selective reagents. As the proportion of the insoluble material depended on the extrusion temperature, they proposed that an increase of the volume fraction of the insoluble phase would be expected to reduce extrudate expansion and stability.

Based on these observations, Camire (1991) proposed a model for the crosslinking of protein texturization during extrusion cooking as shown in Figure 32.

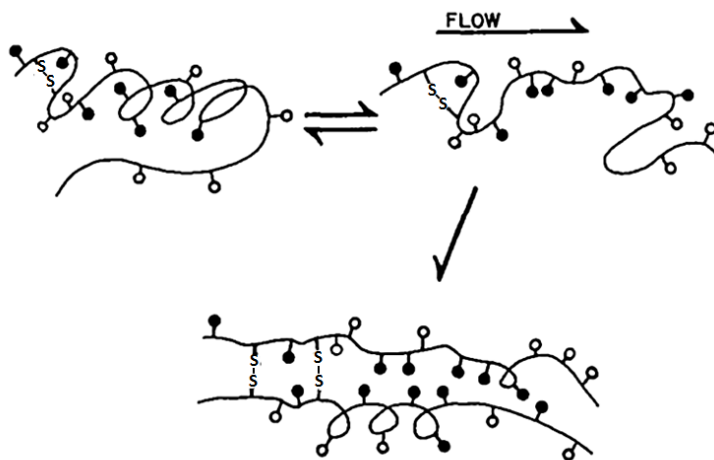


**Figure 32:** Schematic diagram of a protein molecule unfolding, aligning with the flow of the extruder barrel and forming new bonds with another molecule. Open circles represent hydrophilic amino acid residues, closed circles hydrophobic residues and S-S disulfide bridges. Adapted from Camire (1991), with permission of Springer.

Early work on the formation of fibrous structures during high moisture conditions suggested that the protein bodies are first melted and then fused to each other creating a larger elastic protein mass. This mass is then stretched in the extrusion direction forming the observed fibers (Noguchi 1990). Bounie and Van Hecke (1997) adapted these models to the process of high moisture extrusion cooking to further explain the texturization and fiber formation mechanism (Figure 33).

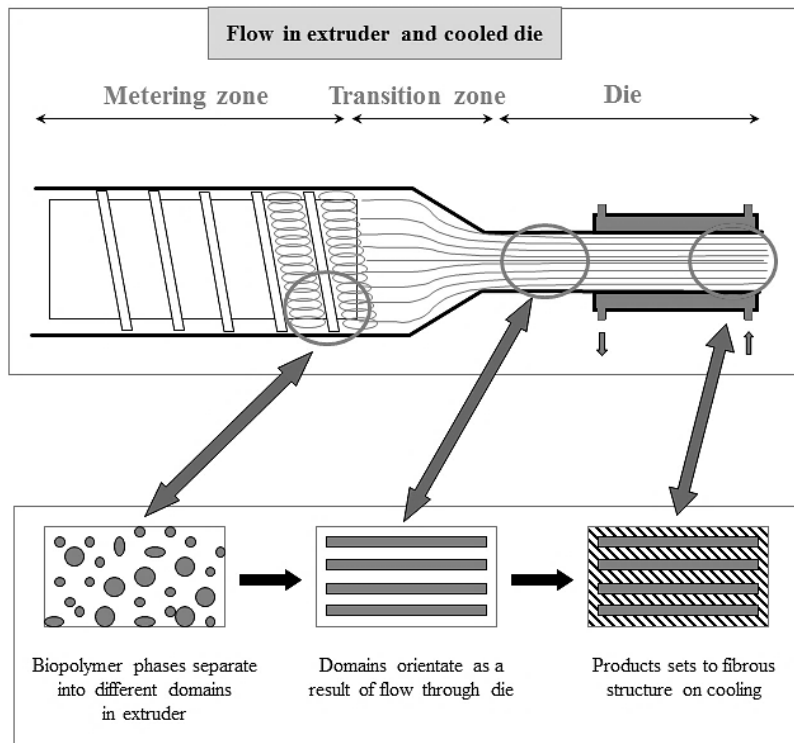


**Figure 33: Model for phase separation mechanism during stream alignment in the cooling die. Reprinted from Bounie and Van Hecke (1997) with kind permission.**

They proposed that during texturization, the proteins separate from other components such as starch and insoluble fiber into two phases that are rich in the individual components during stream alignment in the die (Tolstoguzov 1993). Due to shearing at the die entrance, proteinaceous fibrous structures are formed by the separated proteins that are interrupted by e.g. gelatinized starch layers (Bounie and Van Hecke 1997).

Recent studies on the formation of anisotropic structures based on plant protein were conducted by a shear-induced structuring technique (Grabowska *et al.* 2014; Krintiras *et al.* 2014; Krintiras *et al.* 2015; Grabowska *et al.* 2016; Krintiras *et al.* 2016). A shearing device with a couette design was used to initiate laminar flow of a protein mass in the space between two plates. They reported that the creation of anisotropic structures requires the presence of structural domains that are susceptible to shear flow. The alignment of domains such as particles or micelles depends on the interactions between the domains as well as the magnitude of the shear flow (Grabowska *et al.* 2016).

#### 2.5.2.2 Flow properties in the cooling die

The cooling die plays an important role during the fiber formation process as it affects the flow properties of the melt during high moisture food extrusion (Akdogan 1999).

Measurements of polymers using capillary flow rheometers showed that Newtonian fluids generate a parabolic velocity profile, shear thinning a flattened parabolic profile and shear thickening an extended parabolic velocity profile. The most important polymer flow in an extruder is shear flow where molten polymer layers slide against each other (Giles et al. 2004).

The flow velocity profile across the die channel therefore depends on the polymer rheology, shear rate as well as the temperature distribution of the fluid in the cooling die channel. In addition, understanding the flow properties in a cooling die is complicated by unique material properties such as shear thinning behavior of the proteinaceous material as the fluid is sheared inside die channel as well as viscoelastic behavior in the sol/gel state as the temperature of the fluid is reduced. Therefore, information on the temperature distribution in the cooling die is of crucial importance for the flow properties of the melt and coherent fiber formation process. Based on a 2D-simulation of a simplified high moisture extrusion process, Figure 34 shows the temperature distribution of a Newtonian fluid during the laminar flow through a cooling die.

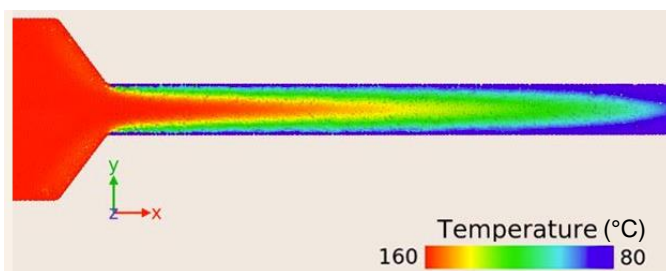


**Figure 34:** 2D-simulation of an extrusion process using the Generalized Material Point Method (Buzzi *et al.*). The constitutive behavior of the material is modelled using a linearly elastic equation of state with Newtonian viscosity. The heat transfer equation in its discrete form was used to compute the temperature distribution. An algorithm was employed to represent the surfaces corresponding to the extruder, nozzle and cooling channel and simulates the interactions with the material, namely: contact, Coulomb and viscous friction, and heat transfer (Unpublished data).

It can be seen that the temperature distribution of the fluid in the cooling die channel affects the material viscosity and the flow velocity distribution. The average velocity in the die channel typically ranges between 30 – 80 mm/s under laminar flow conditions of the viscous melt (Bouvier and Campanella 2014). The velocity gradient and shear forces developed in the peripheral zones of the die allow the orientation and alignment of the protein macromolecules in the flow direction (Akdogan 1999). Cooling of the viscous melt under laminar flow conditions reduces the viscosity and a phase transition from a liquid into a gel state occurs which results in the fiber formation of the extrudate (Bouvier and Campanella 2014).



### 2.5.2.3 Raw materials

The raw materials greatly affect the fiber formation during high moisture extrusion cooking (Noguchi 1990; Areas 1992; Cheftel *et al.* 1992). The major components of fibrous meat analogues are proteins from either animal or plant origin with concentrations from 50 up to 95% (dry matter). Common formulations consist of a plant protein concentrate or isolate, insoluble fiber, starch and further ingredients for taste and texture. Early studies on extrusion cooking of defatted soy flour with high moisture levels date back to the 1980s (Kitabatake *et al.* 1985; Noguchi *et al.* 1986; Isobe and Noguchi 1987). Later on, the majority of research was published using a combination of soy protein isolate, wheat gluten and wheat starch (Lin *et al.* 2000; Lin *et al.* 2002; Yao *et al.* 2004; Ranasinghesagara *et al.* 2005; Ranasinghesagara *et al.* 2006; Liu and Hsieh 2007; Ranasinghesagara and Yao 2007; Liu and Hsieh 2008; MacDonald *et al.* 2009; Chen *et al.* 2010a; Chen *et al.* 2010b; Fang *et al.* 2013; Fang *et al.* 2014).

Both the protein type and further additives such as starch or lipids have an impact on texturization (Akdogan 1999). Noguchi (1990) studied the effect of soybean oil addition during high moisture extrusion of defatted soybean flour and found that oil addition up to 10% into the formulation resulted in a reduction of fibrousness as evaluated by tensile strength measurement in the longitudinal and transverse direction. They proposed that the orientation of the proteins depends on the shearing at the die. The oil acts as a lubricant and decreases the friction and shearing below the level necessary to align the protein. The tensile strength of extrudates was highest at pH 7 and decreased upon a shift of the pH in either direction (Noguchi 1990).

Proteins with different conformation and solubility characteristics such as soy protein concentrate and gluten could be easily texturized both separately or in combination, while soy protein isolate, myofibrillar proteins from mechanically deboned meat or calcium caseinate require the presence of other food constituents or additives (Cheftel *et al.* 1992). As reported for low moisture extrusion of soy, sulfur and sulfur-containing additives as well as mono- or bivalent salts can be used to modify the processing behavior and texture properties of extrudates (Riaz 2006). The underlying protein reactions are based on covalent disulfide bonding and ionic interactions and will be further addressed in the following section.

#### 2.5.2.4 Quantification of fiber formation

A critical requirement for the acceptance of meat substitutes is that consumers can recognize them as being a product that should be eaten instead of meat, meaning that appearance and preparation should be similar to meat (Elzerman *et al.* 2011). A meat-like appearance covers the sensory properties of the substitute including visual appearance, taste, aroma and texture (Bredahl *et al.* 1998). One characteristic property of animal meat is structural anisotropy, which is the tendency of a material to exhibit different physical properties depending upon the orientation or position of the material. The filamentous proteins of muscle cells form into a structure depending upon the orientation of the axis (Aguilera and Stanley 1999). Plant based meat substitutes produced by high moisture extrusion cooking show the potential for a meat-like appearance due to their fibrous structure which resembles the structural anisotropy of animal meat.

In order to extract information from complex foods with anisotropic structures, several characterization techniques are applied including texture analysis, light microscopy or scanning electron microscopy (Krintiras *et al.* 2014). Texture analysis is commonly used for quantification of mechanical properties (stress, strain) by several measuring procedures. Texture profile analysis, a common method that determines the compression force of a probe during repeated compression cycles, does not sufficiently reflect the fiber formation under high moisture extrusion conditions (Lin *et al.* 2000). Another approach is to measure the tensile stress or strain, which is the force and deformation at rupture upon stretching of extrudates. Due to high variability of the results, Thiebaud *et al.* (1996) suggested texture determination by shearing, a common objective method for the evaluation of beef tenderness. This imitates the sensation when food is cut by the front incisors during mastication (Caine *et al.* 2003; de Huidobro *et al.* 2005). The determination of the cutting strength in longitudinal and transverse directions, with respect to the flow direction in the cooling die, has been used to assess the quality of fiber formation (Chen *et al.* 2010b; Fang *et al.* 2014; Osen *et al.* 2014).

Several microscopic methods have been used to study the microstructure of high moisture extrudates such as light microscopy (Noguchi 1990; Lin *et al.* 2002) and scanning electron microscopy (Lin *et al.* 2002). Although the degree of fiber formation can be recorded using a high-resolution camera, visual examination is subjective and does not provide a numeric index for accurate and convenient comparison among products. In order to improve the visual examination of samples, Ranasinghesagara *et al.* (2005) described an image-processing technique to characterize sample fiber formation using digital images, which is based on the detection of linear lines and curves on the sample surface. However, the method requires

partly destructive preparations of the samples prior to analysis. The authors suggest this method to be used as a standard quantitative method for the evaluation of other nondestructive methods. A nondestructive approach to quantify the fiber formation of extruded meat substitutes was developed using fluorescence polarization spectroscopy (Yao *et al.* 2004). The method is based on the relationship of the fluorescence emission light intensity and the structure orientation of the sample. The degree of polarization is determined from emitted fluorescence intensities of a sample parallel and perpendicular with respect to the plane of linearly polarized excitation light. As several measurements with different polarization directions are needed to quantify the degree of fiber formation, the method could not be implemented in a production line. In order to monitor fiber formations in an industrial setting, Ranasinghesagara *et al.* (2006) described another nondestructive method using a real-time scanning system based on photon migration to map fiber formations in meat substitutes.

The method uses light that propagates in a turbid media and is absorbed and randomly scattered. When light escapes from the sample surface and is measured as the optical reflectance, those scattered photons carry vital information about optical properties of the media, which can be derived from reflectance measurements based on light transportation theories. With the use of a laser as light source, the method allows a 2-dimensional mapping of the fiber formation and their orientation over the entire sample in real time. This method could be used as a fast and noninvasive method for online monitoring of fiber formation in meat analogs (Ranasinghesagara *et al.* 2009). However, these nondestructive methods are limited to an optical quantification of the fiber formation on the surface of the extrudates.

Another recent development in the field of food structure analysis is the application of micro-computed tomography ( $\mu$ CT) (Mathanker *et al.* 2013). Three-dimensional insight into products and processes by means of non-destructive micro-computed tomography offers great potential for a better understanding of the relationship between macro- and microstructure. Mathmann *et al.* (2014) investigated the influence of the process parameter temperature on the resulting texture and showed that image analysis of micro-computed tomography measurements is able to differentiate between extrusion samples reliably.

### **2.5.3 Protein reactions during texturization**

During extrusion cooking, the protein matrix undergoes chemical and structural changes that greatly influence the texture quality of the extruded products (Ilo and Berghofer 2003). Native proteins are denatured and the forces which stabilize the tertiary and quaternary structures of the proteins are weakened by a combination of temperature and shearing inside the extruder.

The individual protein molecules unfold and align themselves with the flow of material towards the die (Camire 1991). For the structural stabilization of extrudates, existing protein linkages have to be cleaved in the cooking zone and new chemical bonds have to be formed in the cooling die. Alterations of both covalent bonds (peptide bonds, disulfide bonds) as well as non-covalent interactions such as hydrogen-, hydrophobic-, and ionic linkages have been expected (Areas 1992; Liu and Hsieh 2008).

The way proteins interact during extrusion and structural stabilization to fibrous extrudates has been the focus of many studies since the introduction of protein extrusion in the 1960s (Harper and Harmann 1973; Kinsella and Melachouris 1976; Harper 1989; Camire 1991). Up to now, some controversy exists in the literature with regard to the relative importance of non-covalent interactions, intermolecular disulfide bonds, and possible formation of other covalent bonds for structural stabilization of extrudates. One reason for the poor understanding of protein-protein interactions during extrusion is the difficulty of studying the interactions due to the high temperature and pressure conditions inside the extruder (Liu and Hsieh 2007; Liu and Hsieh 2008). Monitoring possible chemical interactions between amino acid residues should be performed before, after, and, if possible, during extrusion which remains to be a difficult task (Areas 1992).

The most common approach to study protein-protein interactions is based on protein solubilization by selective agents with known mechanisms of protein solubilization (Liu and Hsieh 2008). The soluble protein in extruded and non-extruded material is quantified in buffer systems containing three types of extraction reagents. The first type is a salt buffer with the ability to extract protein molecules that are loose and not in a stable network. The insoluble fraction is considered to be the protein linked to the three-dimensional protein network structure. The second type is a reagent known to break non-covalent interactions such as sodium dodecyl sulfate (SDS) or urea and the third type is a reducing agent with the ability to cleave disulfide bonds such as 2-mercaptoethanol and dithiothreitol (Areas 1992). Table 11 shows the types of protein-protein interactions, amino acids capable of engaging in them and reagents able to break the interactions.

**Table 11: Types of interactions, amino acids capable of engaging in them and reagents able to break the interactions (Liu and Hsieh 2008).**

<b>type of interaction</b>	<b>specific interaction</b>	<b>amino acids</b>	<b>reagents capable of breaking up the interaction</b>
<b>covalent</b>	disulfide bonding	cysteine/cysteine	oxidizing or reducing agents, e.g. performic acid, 2-mercaptoethanol, DTT*
<b>non-covalent neutral</b>	hydrogen bonding	asparagine, glutamine, threonine, serine, cysteine	strong H- bonding agents, e.g. urea, thiourea, SDS**
<b>non-covalent neutral</b>	hydrophobic interactions	tyrosine, tryptophan, phenylalanine, proline, methionine, leucine, isoleucine, valine, alanine, glycine	ionic and nonionic detergents, e.g. SDS, thiourea
<b>non-covalent electrostatic</b>	acid hydrophilic; basic hydrophilic	aspartic acid, lysine, arginine, histidine, glutamic acid	acids, alkali or salt solutions

\* DTT = dithiothreitol; \*\*SDS = sodium dodecyl sulfate,

A protein solubility profile using a combination of the above reagents for protein samples before and after extrusion allows to estimate the approximate contribution of each of the most important interactions during protein texturization (Areas 1992).

Protein solubility studies were used as early as 1966 to investigate the fiber formation of spun soy fibers (Kelley and Pressey 1966). They found that hydrogen bonds, ionic interactions and disulfide bonds contribute to the formation of spun soybean fibers. Another proposed mechanism for protein texturization claimed that disulfide bonds were of negligible importance for the structural stability of soy protein extruded at temperatures as high as 180 °C. Instead, the formation of newly formed intermolecular peptide bonds was suggested (Burgess and Stanley 1976; Smonskey and Stanley 1982). These claims were based on three observations: First, the increase of free sulfhydryl groups after extrusion which indicated the cleavage of disulfide bonds instead of disulfide crosslinking. Second, the addition of reducing reagents to the feed was found to improve product characteristics, further suggesting that disulfide bonds were of minor importance during texturization. Third, the decrease in texture formation after blocking free amino and carboxyl groups using ninhydrin and citric acid which indicated that the structural stability of extrudates was driven by peptide bond formation. However, the proposed mechanism of intramolecular peptide formation during thermoplastic extrusion was widely disputed in numerous following studies. This was based on the observation that proteins could be resolubilized from extruded products with extracting solutions containing an agent capable of destroying hydrogen bonds and hydrophobic interaction in combination with an agent capable of disrupting disulfide linkages (Jeunink and Cheftel 1979; Hager 1984; Areas 1992; Prudencio-Ferreira and Areas 1993; Li and Lee

1996). The discrepancy in the proposed mechanisms was attributed to the high extrusion temperature of 180 °C used by Burgess and Stanley (1976) which might have provided the energy necessary for peptide bonding (Prudencio-Ferreira and Areas 1993).

As reported in previous studies, the processing conditions used in thermoplastic extrusion under low moisture conditions can favor the Maillard reactions leading to amino acid loss, in particular of lysine (Björck *et al.* 1983; Ilo and Berghofer 2003). Maillard reactions may occur even without the addition of reducing sugars based on the reactivity of some starch and fiber fragments (Camire 1991). Higher temperature, shear and longer residence time during extrusion increase the rate of Maillard reactions, but this effect may be offset by increased moisture content (Camire 1991). In contrast to protein reactions during extrusion, there is little information on the structural conformation of extruded protein. Infrared spectroscopy of soy protein extruded at temperatures between 140-180 °C at 30-40% w.b. moisture content revealed peaks that were attributed to anti parallel  $\beta$ -sheet structures (Figure 35).

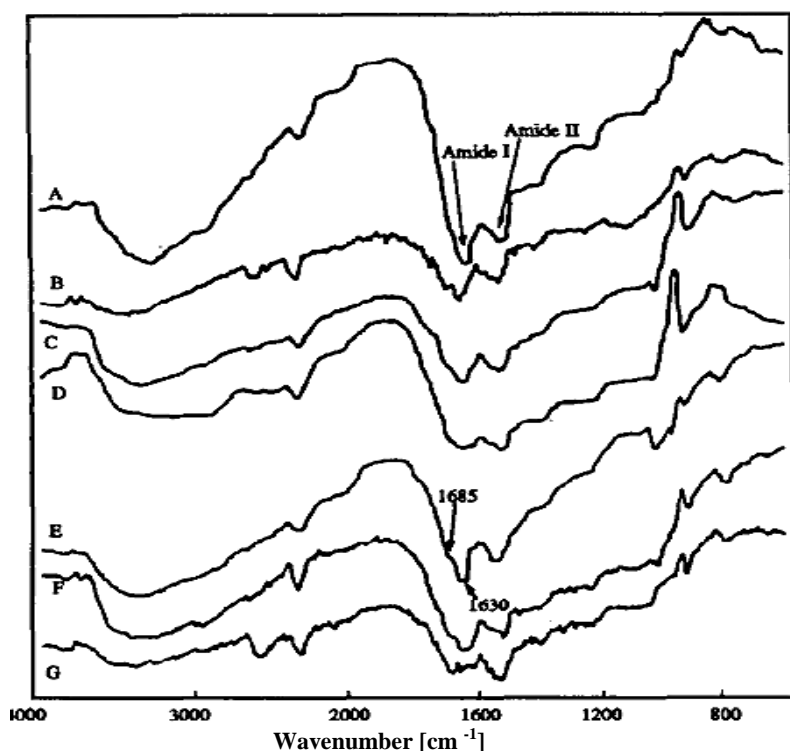


Figure 35: Transmittance infrared spectra of soy protein isolate (A); extruded at 140 °C and 30% w.b. moisture (B); extruded at 140 °C and 40% w.b. moisture (C); extruded at 160 °C and 30% w.b. moisture content (D); extruded at 160 °C and 40% w.b. moisture content (E); extruded at 180 °C and 30% w.b. moisture content (F) and extruded at 180 °C and 40% w.b. moisture content (G). Extruded proteins show peaks at 1685 cm<sup>-1</sup> with a shoulder at 1630 cm<sup>-1</sup> that are attributed to  $\beta$ -sheet structures. Reprinted from Prudencio-Ferreira and Areas (1993) with permission of Wiley.

Although the high energy input and shearing may have induced a high degree of denaturation along with a breakdown of the secondary protein structure, the process appeared to allow

protein interactions to stabilize the three-dimensional structure to include anti parallel  $\beta$ -sheet conformations (Prudencio-Ferreira and Areas 1993).

#### 2.5.3.1 Protein-protein interactions during high moisture extrusion

Since the early work on high moisture extrusion of Noguchi (1990) and Cheftel *et al.* (1992), efforts have been made to study the protein reactions that stabilize fibrous high moisture extrudates. Compared to thermoplastic extrusion, the water during high moisture extrusion has a protective effect on the amino acids during processing as the water reduces the shear forces in the extruder (Noguchi *et al.* 1982; Björck and Asp 1983). Furthermore, the formation of peptide bonds is not favored by wet conditions and there was no evidence for newly formed peptide bonds in extrudates from high moisture extrusion (Noguchi 1990). This was based on the observation that high moisture extrudates from soy protein isolate were completely soluble in extracting solutions containing agents capable of destroying hydrogen bonds and hydrophobic interaction in combination with agents capable of disrupting disulfide linkages, indicating that there are no other covalent bonds involved besides disulfide bonds (Lin *et al.* 2000; Liu and Hsieh 2007; Liu and Hsieh 2008; Chen *et al.* 2011).

In contrast to the expanded and sponge-like extrudates produced from thermoplastic extrusion, high moisture extrudates are characterized by a rubbery gel-like texture. This led to the assumption that heat-induced soy protein gels and protein extrudates from high moisture extrusion have the same types of chemical bonds, namely disulfide bonds, hydrogen bonds, and hydrophobic and electrostatic interactions. What sets the two apart from each other in terms of thermal reversibility and structural rigidity was the relative proportion of each type of bond in their structures (Liu and Hsieh 2007). Based on the methodology of protein solubilization in selective agents as previously described, it was found that non-covalent bonds played a dominant role over disulfide bonds in forming protein gels during heat-induced gelation, whereas in forming the fibrous structure of protein extrudates, non-covalent and disulfide bonds were both important (Liu and Hsieh 2007).

With regard to the relative importance of non-covalent interactions, intermolecular disulfide bonds, and possibly other covalent bonds for structural stabilization of extrudates, Liu and Hsieh (2008) suggested that disulfide bonds play a more important role than non-covalent interactions in the stabilization of the rigid structure. In contrast, Chen *et al.* (2011) claimed that the contribution of non-covalent bonds outweighs covalent bonds. Until now, a disagreement in literature with regard to the relative importance of the individual kind of linkages still exists.

### 2.5.3.2 Influence of pressure and shear on protein reactions

As extrusion technology is a multivariable process, it is difficult to study the isolated effects of individual system parameters such as pressure or shear on the protein reactions. One attempt to investigate the complex processes inside the extruder is the simulation of the extrusion process using non-continuous experimental setups. The maximal pressure in the compression zone of the extruder under high moisture conditions is usually below 20 bar. Using a temperature-controlled pressure cell to simulate the effect of pressure during extrusion, it was shown that pressures between 20 – 80 bar do not affect protein reactions. Hence, it can be concluded that the effect of pressure on protein reactions inside the extruder plays a minor role (Noguchi 1990).

Besides pressure, the extent of shear affects protein reactions during extrusion cooking. In contrast to conventional protein extrusion, a high moisture content reduces the shear which can be monitored indirectly by the system mechanical energy (Noguchi *et al.* 1982; Björck and Asp 1983).

Fang *et al.* (2013) studied the effect of mechanical shear on molecular characteristics of soy protein extruded at 50% w.b. moisture content indirectly using different screw configurations. They subsequently replaced 3 conveying elements by kneading elements (25 mm length, 45° staggering angle) in the cooking zone of the extruder. Different values of specific mechanical energy ranging from 840 to 1277 kJ/kg were transferred into the product by changing screw configurations. A higher specific mechanical energy led to an increased proportion of low molecular weight fractions of 17.43 kDa suggesting that increasing shear can increase the extent of molecular breakdown of protein aggregates. Increasing the specific mechanical energy also reduced the viscosity of the mass at the die exit and resulted in extrudates with an increased tensile strength (Fang *et al.*, 2014; Fang *et al.*, 2013). In summary, it could be concluded that the pressure during high moisture extrusion cooking plays a minor role, but the extent of shear affects the molecular breakdown of the protein aggregates indicating that protein was partly depolymerized by mechanical shear.

In summary a disagreement in literature with regard to the relative importance of the individual kind of linkages still exists. More research activities are required to get more insights into chemical changes during high moisture extrusion. These findings might be very important for an understanding and a concerted handling of the process and the ingredients used to obtain high quality meat-like products.



## 3 Materials and Methods

### 3.1 Characterization of pea protein ingredients

Three commercial pea protein isolates (*Pisum sativum* L.) were used: Pisane®M9 (Cosucra Groupe, Warcoing, Belgium), Emvital®E7 (Emsland-Stärke GmbH, Emilchheim, Germany), and Nutralys®F85M (Roquette Frères S.A., Lestrem, France). These were designated PPI 1, PPI 2, and PPI 3. Additionally, soy protein concentrate (Alpha 10 IP, Solae, USA) and defatted soy flour (Supro TB 200, Solae, USA) was used during pilot-plant trials instead of pea protein isolate as a model formulation for the assessment of the offline flow visualization in the cooling die in section 4.3.5.

#### 3.1.1 Chemical composition

The total dry matter was analyzed according to the German Food Act (2005). Samples were dried to weight constancy at 105 °C in a thermogravimetric system (TGA 601, Leco Corporation, St. Joseph, MI, USA). The ash contents were determined in a thermogravimetric system (TGA 601, Leco Corporation, St. Joseph, MI, USA) at 950 °C until weight constancy (AOAC International 1990). The protein contents were calculated based on the nitrogen content according to the Dumas combustion method described in the German Food Act (2005) using a Protein/Nitrogen Analyzer FP 528 (Leco Corporation, St. Joseph, MI, USA) with a conversion factor of 6.25 (Sumner *et al.* 1981; Shand *et al.* 2007). The total lipid content was determined including fatty acids from phospholipids according to the method of Caviezel, DGF K-I 2c (00) (DGF-Einheitsmethoden 2004). Native and partially hydrolyzed starch was analyzed by determination of glucose units following complete hydrolysis with amyloglucosidase, using a Biopharm assay kit (R-Biopharm AG). All analyses were performed in duplicate.

#### 3.1.2 Particle size distribution

The particle sizes of the protein powders were determined using a Malvern laser diffraction particle size analyzer (Mastersizer S Long Bed Version 2.15, Malvern Instruments Ltd., Malvern, UK). Powders were dispensed in a wet dispersion unit using 1-butanol (VWR, Germany). The particle size distribution function was plotted from the particles volume diameter. The volume median diameter  $D(v, 0.5)$  was calculated for each protein ingredient.

$D(v, 0.1)$  was calculated referring to the 10% of the samples smaller than that value, and  $D(v, 0.9)$  indicating that 90% are smaller and 10% are larger than that value.

### 3.1.3 Microstructure

The microstructure of the protein powders was qualitatively assessed using a scanning electron microscope type SEM ABT-55 (ISI ABT, Akashi Beam Technology, Japan). 0.5 g of powder was mounted on a sample holder and sputter coated with 5 nm of platinum at 2.5 kV and 20 mA for 1.5 min. The SEM was operated at 10 kV accelerating voltage.

### 3.1.4 Thermal properties

Differential scanning calorimetry (DSC) was used to determine the thermal properties of pea protein dispersions according to the method of Sousa *et al.* (1995). The w.b. moisture content was adjusted to 70% (w/w). Approximately 10 mg of the protein dispersion was weighed into aluminum pans. The pans were hermetically sealed and heated from 40 °C to 120 °C at a rate of 5 °C/min on a DSC instrument (Q2000, TA Instruments, USA). Each sample was reheated to verify that there was no reversibility of denaturation. The peak transition temperature or denaturation temperature ( $T_d$ ) and enthalpy of denaturation ( $\Delta H$ ) were computed from the thermograms. Triplicate measurements were carried out for each sample.

### 3.1.5 Functional properties

#### 3.1.5.1 Protein solubility

Protein solubility was determined according to the procedure used by Morr *et al.* (1985) by mixing an aliquot of 1 g of protein with 50 ml 0.1 M sodium chloride solution and incubating at ambient temperature in a shaking water bath for 60 min. The pH was adjusted using 0.1 M hydrogen chloride or sodium hydroxide solution respectively. The non-dissolved fraction was separated by centrifugation at 20000 g for 15 min at ambient temperature. The protein content in the supernatant was measured by a combustion method based on an AOAC method using a Protein/Nitrogen Analyzer FP 528 (Leco Corporation, St. Joseph, MI, USA). Duplicate measurements were undertaken for each sample.

### 3.1.5.2 Water binding capacity, oil binding capacity, emulsifying capacity

The determination of the water binding capacity (WBC) was performed according to the AACC (1982) method and expressed as the weight of water bound by 1 g of dry sample.

$$\text{WBC [g/g]} = \frac{\text{Weight of sample + bound water [g]} - \text{Initial sample weight [g]}}{\text{Dry sample weight [g]}} \quad 3.1$$

The oil binding capacity (OBC) was determined by the procedure used by Lin *et al.* (1974) and expressed as ml of oil bound by 1 g dry sample. The protein sample was dispersed using excess oil (Canola oil, Mazola, Unilever, Germany) until a homogeneous mixture was achieved. After centrifugation the volume of free oil was read.

$$\text{OBC [ml/g]} = \frac{\text{Initial oil volume [ml]} - \text{Nonbound oil volume [ml]}}{\text{Dry sample weight [g]}} \quad 3.2$$

The emulsifying capacity (EC) was determined according to the method of Wäsche *et al.* (2001) by continuous addition of oil to an oil-in-water emulsion to the point of phase inversion of the emulsion. The phase inversion was detected by an abrupt breakdown of the electrical conductivity below 10  $\mu\text{S}$  using a conductivity meter (LF 521 with electrode KLE 1/T, WTW GmbH, Weilheim). The volume of oil needed for phase inversion was used to calculate the emulsifying capacity (ml oil per g dry sample).

$$\text{EC [ml/g]} = \frac{\text{Oil volume [ml]}}{\text{Dry sample weight [g]}} \quad 3.3$$

In order to compare the functional properties of the protein ingredients at the same pH value, the pH of PPI 2 was adjusted using 0.1 M sodium hydroxide solution. Duplicate measurements were undertaken for each sample.

### 3.1.5.3 RVA viscosity

The viscosity of protein dispersions as a function of temperature were determined on a Rapid Visco Analyzer (Newport Scientific Pty. Ltd., Warriewood, Australia) using the AACC Method 76-21 STD 2 (AACC 1997). The RVA is used as a common empirical instrument for routine rheological analyses of extruded foods (Biliaderis 2009) as described in 2.4.3.2. In contrast to common rotational rheometers using plate, cone or cylinder probes, rotating paddles are used to prevent sedimentation of dispersed particles. The protein powders were suspended in demineralized water to the desired w.b. moisture content (w/w), heated to 50 °C and stirred at 960  $\text{min}^{-1}$  for 10 s for thorough dispersion. The slurry was held at 50 °C for 50 s, and then heated to 95 °C at 6 °C/min, held at 95 °C for 300 s, and finally cooled to 50 °C. Duplicate measurements were performed for each sample.

## 3.2 High moisture extrusion cooking

### 3.2.1 Extrusion procedure on laboratory scale

#### 3.2.1.1 Extruder

Extrusion experiments in laboratory scale with a mass flow rate of 1 kg/h were performed using a laboratory, co-rotating, intermeshing twin screw extruder (Haake Rheocord, Thermo Fisher Scientific, Inc., UK) with a screw diameter of 16 mm, a smooth barrel, and a length-diameter ratio of 25:1. All experiments were performed using protein ingredients described in 3.1.

#### 3.2.1.2 Screw profile

The screw profile was built with different screw elements that can be assembled on hexagonal-shaped shafts (Figure 36).

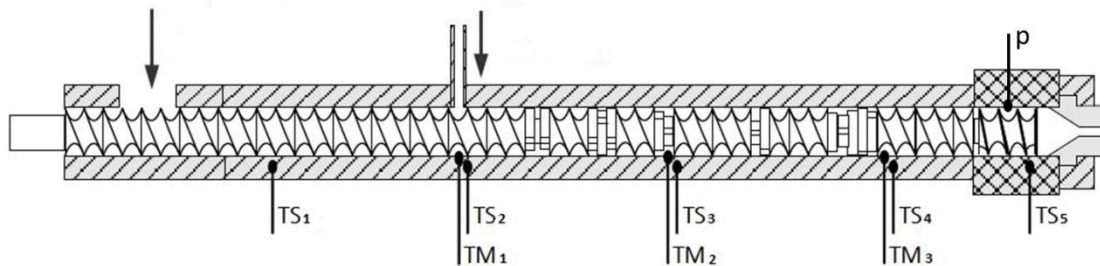


**Figure 36:** Screw profile showing the screw configuration, the location of thermocouples for measuring the barrel temperature (TS<sub>1</sub>-TS<sub>5</sub>) and the melt temperature (TM<sub>1</sub> – TM<sub>3</sub>) as well as the location of the pressure sensor p. Modified from Wild (2012).

The screw profile comprised (from feed to exit): 192 mm, twin lead feed screw elements; 8 mm, 45° forwarding kneading blocks; 16 mm, twin lead feed screw elements; 16 mm, 45° forwarding kneading blocks; 16 mm, twin lead feed screw elements; 8 mm, 45° forwarding kneading blocks; 32 mm, twin lead feed screw elements; 4 mm, 45° forwarding kneading blocks; 8 mm, twin lead feed screw elements; 8 mm, 45° forwarding kneading blocks; 64 mm, twin lead feed screw elements; and 24 mm, single lead screw elements.

#### 3.2.1.3 Configuration

The barrel is segmented into 5 temperature-controlled zones that are heated by an electric cartridge heating system and cooled with water.

A twin screw gravimetric feeder type KCM (K-tron, Niederlenz, Switzerland) was used to feed the dry protein ingredients into the extruder. While operating, water at ambient temperature was pumped into the top of the extruder barrel 130 mm downstream from the center of the feed port using a piston pump (Alpha 50 Plus, ECOM, Prague, Czech Rep.). The feeding rates of both protein powder and water were adjusted to the desired w.b. moisture content (w/w) of the protein dispersion while keeping the mass flow rate constant at 1 kg/h and the rotational screw speed at 150 min<sup>-1</sup> for all experiments. During the initial start-up phase until the experimental conditions were reached, barrel temperatures were stepwise increased from 40 °C to a temperature profile of 40, 60, 80 and 100 °C from the first (feeding zone) to the fourth zone (Table 12).

**Table 12: Temperature profile of the extruder barrel from zone 1 (feed) to zone 5 (exit) and cooling die (zone 6) during initial start-up phase.**

Time [min]	Temperature [ °C]					
	Zone 1	Zone 2	Zone 3	Zone 4*	Zone 5*	Zone 6**
0	40	40	40	40	40	40
5	40	60	60	60	60	50
10	40	60	80	80	80	60
15	40	60	80	100	100	70

\* = cooking zone, \*\* = cooling die

After the temperature was reached, the last cooking zone (fifth) was set at the desired cooking temperature of 100, 120, 140 or 160 °C, respectively.

To prevent expansion at the die exit, a cooling die (Figure 83) with a length of 21 cm was attached to the end of the extruder as a counter-flow heat exchanger with water at 80 °C as a cooling medium at a flow rate of 3.4 l/min. The dimensions of the cooling dies used for the experiments are shown in Table 13.

**Table 13: Geometry of the cooling die channel attached to the lab-scale extruder.**

Shape	Height [cm]	Length [cm]	Width [cm]	Cross sectional area [cm <sup>2</sup> ]	Volume [cm <sup>3</sup> ]	Inner surface area [cm <sup>2</sup> ]
Rectangular die	0.3	21.0	0.5	0.15	3.15	33.9
Slit die	0.2	21.0	1.9	0.38	7.98	89.0

### 3.2.1.4 Calculation of shear rate in the extruder barrel and the cooling die

The shear rate in the cooking zone of the extruder was estimated using the equation according to Martelli (1983) for calculating the shear rate at the barrel wall:

$$\text{Shear rate at barrel wall:} \quad \dot{\gamma}_{\delta} [s^{-1}] = \frac{\pi \cdot d \cdot n}{\delta} \quad 3.4$$

With the outer diameter of the conveying screw elements  $d = 15.6$  mm, rotational screw speed  $N = 2.5$  s<sup>-1</sup>, clearance between the screw tips and the barrel wall  $\delta = 0.2$  mm the shear rate  $\dot{\gamma}_{\delta}$  was 613 s<sup>-1</sup>.

The shear rate at the die wall was estimated from the geometry of the cooling die channel, using the equation for calculating the online viscosity in a slit capillary die {Li, 2004 #604} as described in section 2.4.3.4:

$$\text{Shear rate at die wall:} \quad \dot{\gamma} [s^{-1}] = \frac{6V}{WH^2} \quad 3.5$$

The mass flow rate  $\dot{m}$  was evaluated by taking samples every 10 s and measuring the sample weight.

The density  $\rho$  of the extruded samples was determined by water displacement according to a modified method by Zhang *et al.* (2015). Extrudates were weighed and put into a graduated cylinder filled with water. The displaced water was gravimetrically determined and the density of the samples was calculated from the weight of the samples and the displaced water. Measurements were performed in triplicate.

$$\text{Density:} \quad \rho \left[ \frac{kg}{m^3} \right] = m / V \quad 3.6$$

$$\text{Volumetric flow rate:} \quad \dot{v} \left[ \frac{cm^3}{s} \right] = \dot{m} / \rho \quad 3.7$$

With the channel height of 0.2 cm, channel width of 1.9 cm and the volumetric flow rate of 256 mm<sup>3</sup>/s the shear rate  $\dot{\gamma}$  was 20.2 s<sup>-1</sup> in the slit die.

### 3.2.1.5 Extruder responses

Once the extruder reached steady state conditions as indicated by constant extrusion system parameters, the extruder responses including torque (torque sensor between gear box and process section, strain-gauge principle, Thermo Fisher Scientific, Inc., UK) and pressure (flush mounted melt pressure sensor, capillary strain-gage principle, Thermo Fisher Scientific, Inc., UK) in front of the cooling die were measured and recorded inline (Polylab software, Thermo Fisher Scientific, Inc., UK).

The specific mechanical energy was calculated from the rotational screw speed  $N$  ( $\text{min}^{-1}$ ), motor torque  $T$  (kJ), and mass flow rate  $\dot{m}$  (kg/min) by the following equation (Godavarti and Karwe 1997; Chen *et al.* 2010b):

$$\text{Specific mechanical energy: } SME \left[ \frac{\text{kJ}}{\text{kg}} \right] = \frac{2\pi \times N \times T}{\dot{m}} \quad 3.8$$

### 3.2.1.6 Screw fill degree in the cooking zone

Based on the temperature profile of the extruder barrel during extrusion (Table 12), the cooking zone was defined as the section with a temperature of  $\geq 100$  °C. The screw elements in that section consisted of 64 mm twin lead feed screws and 24 mm single lead screw (Figure 37a).

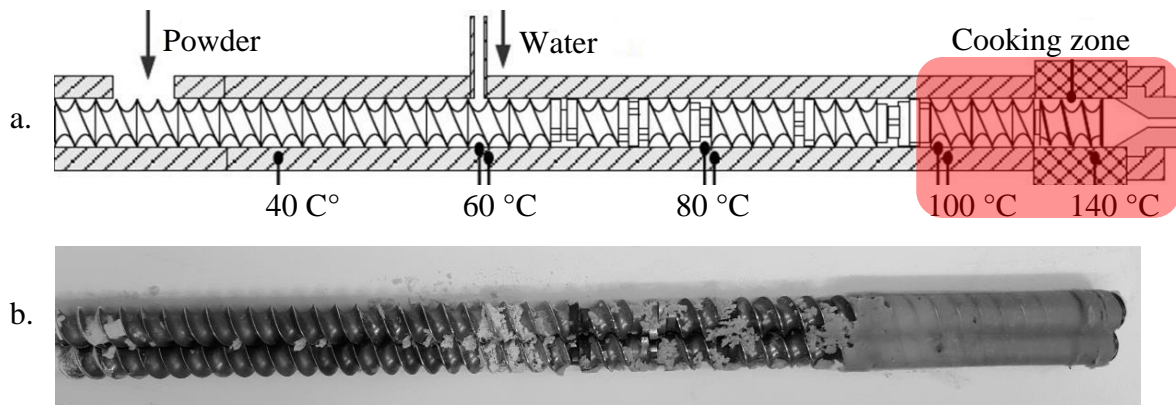


**Figure 37:** Schematic screw profile showing the screw configuration, the heating profile (a) and image of gelled extruded material in the screw section (b) from the cooking zone of the lab scale extruder after extrusion of pea protein isolates (mass flow rate 1kg/h, rotational screw speed 150  $\text{min}^{-1}$ , cooking temperature 140 °C, water content 60% w/w w.b.).

The screw fill degree in the cooking zone of the extruder, consisting of 88 mm screw length, was calculated by measuring the difference between the free screw volume before and after the extrusion experiment using the water replacement method as described by (Zhang *et al.* 2015). The volume of the screw section was determined by putting the screw sections into a graduated cylinder filled with water and the displaced water was gravimetrically determined. The weight of the displaced water represents the volume of screw section. Next, the screw section including the gelled extruded material from the cooking zone was measured. After the extruder reached steady state conditions, it was stopped and the screws were removed. The volume of the screw section was determined as described above. The weight of the replaced water represents the volume of screws and the attached sample material from the cooking zone.

The volume of the extruder barrel section was calculated using the inner barrel diameter  $d$  and the barrel section length  $L$ :

$$\text{Volume barrel:} \quad V_{\text{barrel}}[\text{m}^3] = \pi * \left(\frac{d}{2}\right)^2 * L \quad 3.9$$

The free volume  $V_{\text{free}}$  in the fully filled cooking zone of the extruder was calculated using the volume of the extruder  $V_{\text{barrel}}$  and the volume of the extruded material  $V_{\text{fill}}$  in the respective cooking zone.

$$\text{Free volume:} \quad V_{\text{free}}[\text{m}^3] = V_{\text{barrel}} - V_{\text{screws}} \quad 3.10$$

The screw fill degree in the cooking zone of the extruder was calculated from the volume of the extruder barrel section  $V_{\text{barrel}}$  and the filled screws in the cooking zone:

$$\text{Screw fill degree:} \quad \text{SFD} [-] = \frac{V_{\text{fill}}}{V_{\text{free}}} \quad 3.11$$

### 3.2.1.7 Residence time distribution

The experimental residence time distribution was determined by a manual impulse injection of 1 g of a color tracer (Carmin, Chr. Hansen, Germany) into the feeding zone of the extruder. The experiments were conducted using the rectangular cooling die. Extrusion operating conditions were set at  $150 \text{ min}^{-1}$ ,  $140 \text{ }^\circ\text{C}$  cooking temperature, 60% w.b. moisture content (w/w) and mass flow rates between 0.79 and 2 kg/h. After the extruder reached steady state conditions indicated by constant values for barrel pressure and torque, stripes of extrudates were collected from the die exit at intervals of 10 s until the color tracer was no longer visible. Samples were immediately packed in plastic zipper storage bags and stored at  $-20 \text{ }^\circ\text{C}$ . After thawing in a water bath at room temperature, the samples were analyzed spectrophotometrically in triplicate using a spectrophotometer (CM-700d, Konica Minolta Sensing Americas, Inc., NJ, USA).

By using experimental data, the residence time distribution function  $E(t)$ , the cumulative residence time distribution  $F(t)$ , the mean residence time  $\bar{t}$  and the variance  $\sigma_t^2$  were computed using the equations as described by Chao-Chi Chuang and Yeh (2004):

$$\text{Residence time distribution:} \quad E(t) = \frac{C}{\int_0^\infty C dt} = \frac{C_i}{\sum_0^\infty C_i \Delta t_i} \quad 3.12$$

where  $C$  is the intensity and  $t$  is the time.



$$\text{Cumulative distribution: } F(t) = \int_0^t E(t)dt = \frac{\sum_0^t c_i \Delta t_i}{\sum_0^\infty c_i \Delta t_i} \quad 3.13$$

$$\text{Experimental mean residence time: } \bar{t}_e \text{ [s]} = \int_0^\infty tE(t)dt = \frac{\sum t_i c_i \Delta t_i}{\sum c_i \Delta t_i} \quad 3.14$$

$$\text{Variance: } \sigma^2 = \frac{\sum (t_i - \bar{t})^2 c_i \Delta t_i}{\sum c_i \Delta t_i} \quad 3.15$$

The theoretical mean residence time  $\bar{t}_a$  in the fully filled screw section in the cooking zone of the extruder barrel was estimated using the free volume  $V_{free}$  of the cooking zone and the die as well as the volumetric flow rate  $\dot{v}$  according to Kao and Allison (1984). They suggest a number of assumptions and simplifications to be considered such as an incompressible Newtonian fluid, a constant free screw volume and a steady isothermal operation due to the complexity of screw geometry and rheological behavior of food materials.

$$\text{Theoretical mean residence time: } \bar{t}_t \text{ [s]} = \frac{V_{free}}{\dot{v}} \quad 3.16$$

### 3.2.2 Extrusion procedure on pilot scale

#### 3.2.2.1 Extruder

Extrusion experiments on pilot scale with a mass flow rate of 10 kg/h were performed using a co-rotating, intermeshing twin screw extruder (ZSK 26, Coperion GmbH, Stuttgart) with a screw diameter of 26 mm, a smooth barrel, and a length-diameter ratio of 25:1.

#### 3.2.2.2 Screw profile

The screw profile was built as described by Bouvier *et al.* (2003) with some modifications comprising twin lead feed screws and kneading blocks (Figure 38).

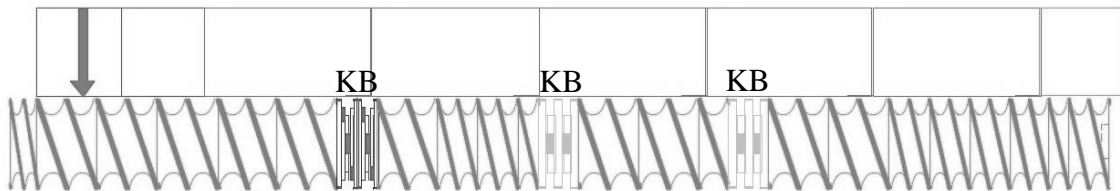


**Figure 38:** Screw profile during pilot-scale extrusion experiments comprising twin lead feed screws and kneading blocks (KB).

The designation for each screw element in the screw profile is attached in the appendix (Table 32).

### 3.2.2.3 Configuration

The barrel is segmented into 5 temperature-controlled zones that are heated by an electric cartridge heating system and cooled with water. To prevent expansion at the extruder exit, a cooling die was attached to the end of the extruder, with water as a cooling medium at a flow rate of 3.4 l/min at 80 °C. The die was built from individual parts that enable different flow channel dimensions (Figure 39). To adjust the length, 3 segments with a length of 30 cm each were used. The width of the cooling die channel was 40 mm and the height could be adjusted to 5 or 10 mm using metal spacers that separate the top from the bottom part.

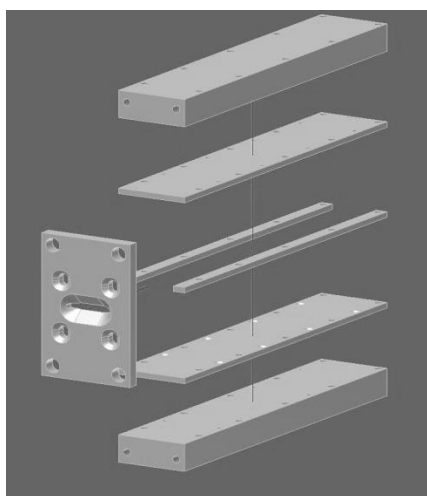


**Figure 39: Components of a cooling die segment and connecting plate.**

The dimensions of the flow channel are shown in Table 14.

**Table 14: Dimensions of the cooling die flow channel attached to the pilot-scale extruder.**

Height [cm]	Number of segments	Total length [cm]	Width [cm]
0.5	1	30	4
1	1	30	4
0.5	2	60	4
1	2	60	4
0.5	3	90	4
1	3	90	4

The dry ingredients were fed into the extruder using a twin screw gravimetric feeder (DDW-MD5- DSR67-35, Brabender GmbH & Co. KG, Duisburg, Germany). While operating, water at ambient temperature was pumped (FD-DKMP-6, Brabender GmbH & Co. KG, Duisburg, Germany) into the top of the extruder barrel 225 mm downstream from the center of the feed port. The feeding rates of both protein powder and water were adjusted to the desired w.b.

moisture content (w/w) of the protein dispersion (55-70%) while keeping the mass flow rate constant at 10 kg/h and the rotational screw speed at 180 min<sup>-1</sup> for all experiments. Once the extruder reached steady state conditions as indicated by constant extrusion system parameters, samples were collected from the die exit, immediately packed in plastic zipper storage bags and stored at -20 °C.

#### 3.2.2.4 Residence time distribution

The residence time distribution was determined as described in section 3.2.1.7 by a manual impulse injection of 1 g of a color tracer (Carmin, Chr. Hansen, Germany) into the feeding zone of the extruder. The temperature profile was set at 100 °C – 120 °C – 140 °C – 160 °C – 150 °C from the feeding zone to the extruder exit. The w.b. moisture content was adjusted to 60 % (w/w) and the mass flow rate was 10 kg/h. The residence time in the extruder barrel and the cooling die were calculated as described in section 3.2.1.7, based on the configuration of the each cooling die.

### 3.3 Rheological measurements

Rheological properties were evaluated using a rheometer (Physica MCR 301, Anton-Paar, Graz, Austria). All samples were subjected to the same standard routine and experiments were performed at least in duplicate.

#### 3.3.1 Shear viscosity

Protein dispersions were adjusted to the desired w.b. moisture content (55-85% w/w) with deionized water and kept overnight at 10 °C for complete hydration. Flow properties were recorded at 30 °C using a concentric cylinder (CC27, Anton-Paar, Graz, Austria) as described by Herrmann *et al.* (2013). The apparent viscosity  $\eta$  was calculated as shear rate  $\dot{\gamma}$  was increased from 0.1 to 100 s<sup>-1</sup> using the RheoPlus software (Anton-Paar, Graz, Austria). The Herschel–Bulkley equation was applied to describe the shear rate dependent flow behavior as described in chapter 2.4.3.3.

#### 3.3.2 Small amplitude oscillation

Dynamic oscillatory analysis was applied as a common method to characterize the structure and network development of food gels, avoiding the problems associated with structural breakdown during measurement (see section 2.4.3.3). The energy stored due to elastic

deformation (storage or elastic modulus,  $G'$ ) and the energy dissipated due to viscous flow (loss or viscous modulus,  $G''$ ) were determined in order to characterize the elastic and the viscous proportions of a viscoelastic sample (Stephen and Phillips 2006).

### 3.3.2.1 Sample preparation

Protein dispersions with moisture contents typical for high moisture extrusion (55-65% w/w w.b.) yielded materials with a dry, crumbly texture and a dough-like appearance. In order to generate samples with a homogenous shape and without air pockets that might interfere during rheological characterization, a laboratory extruder was used to mix the protein dispersion at room temperature and shape the materials into homogenous shape by means of the slit die (25 x 2 x 210 mm; W x H x L) attached to the extruder. The extrusion procedure was performed as described in section 3.2.1. Once the extruder reached steady state conditions as indicated by constant extrusion system parameters, samples were collected from the die exit, packed in plastic zipper storage bags and stored at -20 °C. Before rheological testing, the samples were defrosted in a water bath at room temperature. Defrosted samples were cut into specimen using a circular cutting probe with a diameter of 20 mm and loaded into the respective measuring system.

### 3.3.2.2 Amplitude sweep

The linear viscoelastic region (LVR) as well as the viscoelastic behavior in the linear viscoelastic region was assessed using dynamic oscillatory measurements with parallel plate geometry with 25 mm diameter (PP25, Anton-Paar, Graz, Austria). A constant normal force of 5 N was adjusted in order to compensate small variations of the sample height of the extruded samples.

Amplitude sweep tests were performed at an angular frequency of  $10 \text{ s}^{-1}$  at increasing strain ranging from 0.01 to 100% (logarithmic mode). The elastic modulus  $G'$  and the viscous modulus  $G''$  were determined as a function of oscillatory frequency within the linear viscoelastic range. The loss tangent  $\tan\delta$  was calculated from the ratio of  $G'$  and  $G''$ . The yield stress  $\tau_y$  at the yield point and the flow stress  $\tau_f$  at the flow point where determined as shown in Figure 40.

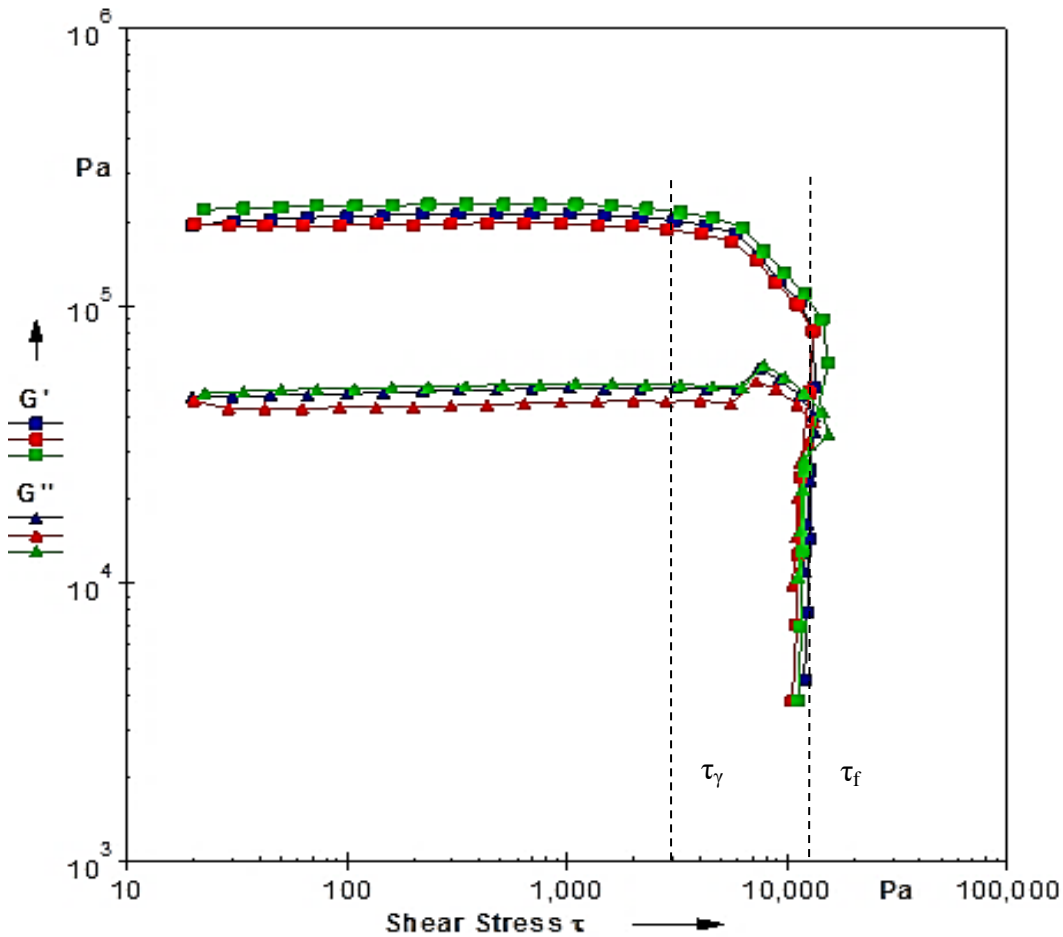


Figure 40: Stress amplitude sweep of a sample measured in triplicate showing the yield stress  $\tau_y$  at the limit of the viscoelastic range and the flow point  $\tau_f$  ( $G' = G''$ ) as described by (Mezger 2006).

### 3.3.2.3 Frequency sweep

A small strain frequency sweep test at a stress within the linear viscoelastic range was used to characterize the time-dependent behavior of the samples at constant temperature and shear strain. Measurements were performed using parallel plate geometry with 25 mm diameter (PP25, Anton-Paar, Graz, Austria) and a constant normal force of 5 N. Angular frequency was decreased from 500 to  $0.05 \text{ s}^{-1}$ . The elastic modulus  $G'$ , the viscous modulus  $G''$ , the complex modulus  $G^*$  and loss modulus  $\tan\delta$  were obtained.  $G'$  was modeled as a power function of angular frequency  $\omega$  as described in chapter 2.4.3.3.

### 3.3.2.4 Temperature sweep experiments within a temperature range of 50-150 °C

The viscoelastic properties were evaluated after a modified method from Morales and Kokini (1999) at a fixed frequency as a function of temperature using a rheometer (Physica MCR 301, Anton-Paar, Germany). The device was equipped with a pressure cell (Pr150, Anton-Paar, Graz, Austria) and a nitrogen head pressure of 15 bar was applied in order to prevent water from evaporation. Heating profile was holding at 50 °C for 45 minutes, heating to 150 °C at 2 °C/minute, holding at 150 °C for 45 minutes, cooling to 50 °C and finally holding at 50 °C for 45 minutes. The rheological material properties were assessed by small strain oscillation using a plate geometry with 20 mm diameter (PP20, Anton-Paar, Graz, Austria) at 1 mm gap height at a constant deformation  $\gamma = 1\%$  as well as constant angular frequency  $\omega = 10 \text{ s}^{-1}$ . Furthermore, rotational measurements were applied using a concentric cylinder (CC25, Anton-Paar, Graz, Austria) at two constant shear rates ( $\omega = 20 \text{ s}^{-1}$  or  $1 \text{ s}^{-1}$ ). Both plate and cylinder were driven by an indirect drive (magnetic coupling) as shown in Figure 84. Triplicate measurements were performed for each sample.

## 3.4 Characterization of high moisture extrudates

### 3.4.1 Qualitative microstructure analysis

#### 3.4.1.1 Scanning electron microscopy

Qualitative analysis of microstructure of high moisture extrudates as well as chicken breast samples were assessed using a scanning electron microscope type SEM ABT-55 (ISI ABT, Akashi Beam Technology, Japan). Preliminary studies showed that sample preparation using freeze drying resulted in a better visualization of fibrous structures compared to direct fixing procedure with cryo-scanning electron microscopy. The samples were freeze-dried at  $-50 \text{ °C}$  for 72 h in a freeze drier (Beta 1-8, Christ GmbH, Osterode, Germany) and cut into small pieces with a dimension of 5 x 2 x 5 mm (W x H x L). The samples were mounted on a sample holder with the cutting side facing up (Figure 41).

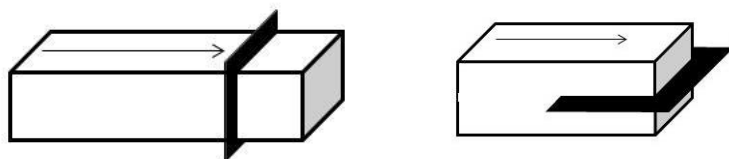


**Figure 41:** Schematic image of sample preparation procedure for imaging the (a) transverse and (b) the longitudinal section. The black rectangle indicates the cutting side and the arrow indicates the flow direction of the extrudate.

### 3.4.1.2 Anisotropy pattern of extrudates inside the cooling die

The velocity gradient and shear forces inside the die determine the flow properties of the viscous fluid along the length of the cooling die channel. A direct visual investigation of the flow properties inside the die is inherently difficult due to increasing vapor pressure of the material at temperatures  $> 100\text{ }^{\circ}\text{C}$ . However, visual and textural investigation of the extruded mass could be achieved when the mass was solidified inside the cooling die after a sudden stop of the extruder. This would provide an image of the flow pattern in different axial positions from inside the cooling die at the moment the extruder was stopped. Therefore, the anisotropic structures were studied by visual assessment of gelled extrudate from inside the cooling die after the extruder was stopped. A dead-stop was initialized by first stopping the screws and then the feeder and water dosage immediately. The cooling die was quickly disassembled and the extrudate removed from inside the cooling die. The extrudate was cut into pieces with dimensions of  $20 \times 10 \times 40\text{ mm}$  (W x H x L). The cutting side shown in Figure 42 (black rectangle) was used to visually assess the anisotropy pattern of the sample.



**Figure 42:** Sample preparation for assessing the anisotropic structures. The black rectangle indicates the cutting side used for assessing the flow profile. The arrow indicates the flow direction of the extrudate.

The cutting side of the samples showed anisotropic patterns as schematically shown in Figure 43.

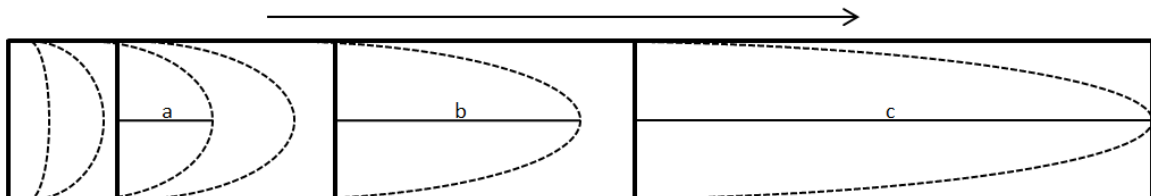


**Figure 43:** Schematic representation of anisotropic structures at the cutting side of extrudates from inside the die channel after a dead-stop. Anisotropic patterns consisting of visible fibers could be described approximately by a nearly parabolic shape (a: flattened shape, c: extended shape).

The anisotropy pattern was assessed by measuring the axial length in the centerline of the visible contours of the fiber orientation (a-c) at the cutting side as shown in Figure 42. Samples were taken from different axial positions along the length of the cooling die channel.

### 3.4.2 Texture analysis

The investigation of the texturization process during high moisture extrusion requires a method which allows for quantitative comparison of different product samples in terms of structure formation (Krintiras *et al.* 2016). As discussed in section 2.5.2.4, samples with fibrous structures will show differences between samples in stress or strain values obtained parallel or perpendicular to the formed fibers. Therefore, the cutting strength of the extrudates (Figure 44) were evaluated using a TA.XT plus Texture Analyzer (Stable Micro Systems, UK) according to the modified procedure of Thiebaud *et al.* (1996) and Chen *et al.* (2010b).

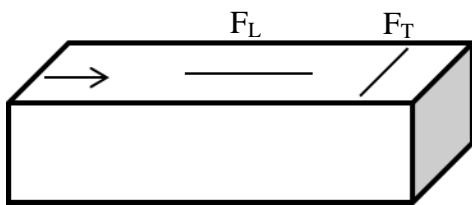


Figure 44: Evaluation of cutting strength of extrudates at room temperature. Samples were cut in longitudinal direction ( $F_L$ ) and in transverse direction ( $F_T$ ) with respect to the flow direction in the cooling die channel.

Samples were cut in longitudinal ( $F_L$ ) and in transverse direction ( $F_T$ ) with respect to the direction of extrudate outflow from the extruder. Equal values ( $F_L = F_T$ ) indicate uniform texture with low material anisotropy and without fibrous texture, whereas  $F_L > F_T$  indicates predominantly transverse fibers and  $F_T > F_L$  predominantly longitudinal fibers. Extrudates from pilot-scale trials (40 x 40 mm) were cut in half along the extrusion direction. Each half was used to evaluate  $F_L$  and  $F_T$  respectively as described above.

Once the extruder reached steady state conditions as indicated by constant extrusion system parameters, samples were collected from the die exit and packed in plastic zipper storage bags. As preliminary studies showed no significant effect of freezing and thawing of the extrudates on the cutting strength  $F_L$  and  $F_T$  ( $p < 0.05$ ), samples were stored at  $-20\text{ }^\circ\text{C}$  until texture analysis. After thawing in a water bath at room temperature, extrudates from laboratory trials (19 x 19 mm) were cut using a knife blade (A/LKB probe, Winopal Forschungsbedarf GmbH, Germany) to 75% of its original thickness at a speed of 2 mm/s and the cutting strength was recorded.



For comparison, foods with visible anisotropy structures (beef, chicken) as well as without visible anisotropy structures (flat pasta) were evaluated accordingly as shown in Figure 45.

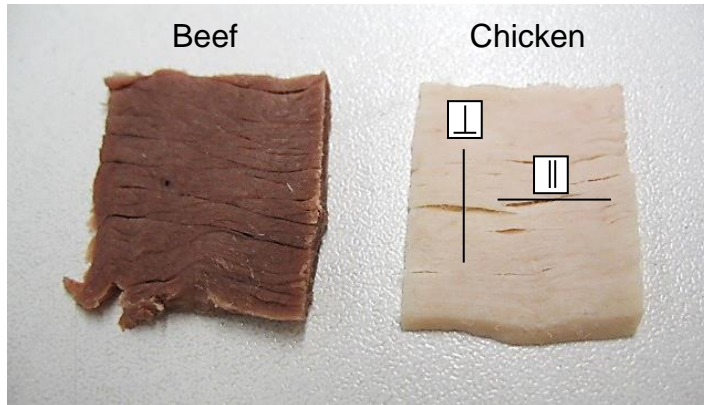


Figure 45: Evaluation of cutting strength of meat samples parallel to the fibers (||) and across the fibers (⊥).

All determinations were performed with at least 12 replicates.

### 3.4.3 Water activity

The water activity of extrudates was determined with a water activity meter (AquaLab 4TEV, Decagon Devices Inc., Pullman, USA) after samples equilibration at 25 °C. Sample preparation was conducted as described in 3.3.2.1 using a laboratory extruder and a slit die to mix the protein paste at room temperature and generate homogenous samples. Samples of PPI 1 were adjusted to the desired w.b. moisture content (55-65% w/w) with deionized water. Samples were packed in plastic zipper storage bags and stored at -20 °C. Prior to analysis, all samples were thawed at ambient temperature in a water bath. The measurements were performed in triplicate at 25 °C.

### 3.4.4 Protein composition

#### 3.4.4.1 Amino acid composition

Quantitative determination of amino acids from the protein isolates and extrudates was performed according to Köhler (2003) and Moore (1963) by reversed phase high-performance liquid chromatography (HPLC). Protein powders (ca. 1 mg) were hydrolyzed with 6 mol/l hydrochloric acid containing 0.1% (w/v) phenol at 110 °C for 24 h. To get reliable contents for cysteine and methionine, these amino acid residues were converted into cysteic acid and methionine sulfone by performic acid prior to hydrolysis. The results were expressed as cysteine and methionine.

Separation and quantification of amino acids was performed as pre-column derivatization with Flourenylmethoxycarbonyl (FMOC)-chloride for primary amino acids and o-phthaldialdehyde (OPA) for proline on an Ultimate 3000 HPLC system (Dionex, Idstein, Germany) equipped with a Dionex Acclaim RSLC 120 C<sub>18</sub> column (12 nm pore size and 2.2 µm particle size, 2.1 x 100 mm at 40 °C) and a pre-column (Sequant Exp Filter Cartridge, 0.2 µm). Injection volume was 0.5 µL and the mobile phase was composed of two eluents: an acetate buffer (4.2 g/L, pH 6) and acetonitrile/methanol/water (45/45/10, v/v/v). Gradient elution was performed as described by Köhler (2003). Amino acid derivatives were detected in a fluorescence detector at 338 nm (excitation wavelength) and 450 nm (emission wavelength). An amino acid mix (0.5 µmol/ml for each amino acid) was used for calibration. Four measurements were performed for each sample.

#### 3.4.4.2 Molecular weight distribution

The protein molecular weight distributions of the protein isolates and extrudates were determined according to Laemmli (1970) using sodium dodecylsulphate polyacrylamide gel electrophoresis (SDS-PAGE) under reducing (0.2 M DTT) and non-reducing conditions. The samples were suspended in treatment buffer (0.125 M Tris-CL, 4% (w/v) SDS, 20% (v/v) glycerine, 0.002% bromophenole blue, pH 6.8). The suspension was heated for 3 minutes in boiling water, centrifuged at 12100 g for 3 minutes and diluted with treatment buffer (6 µg protein/µL). 10% acryl amide gels were used to separate proteins using 1D gel electrophoresis (Hoefer SE 600 Ruby, Amersham Biosciences, GB). 10 µL of the supernatant was applied into each lane and 20 µL of the molecular weight marker (10-250 kDa, Kaleidoscope™, BioRad Laboratories Inc., Hercules, USA) was applied into a separate lane. Electrophoresis conditions were 300 V, 60 mA, 100 W at 10 °C and After separation, proteins were fixed and strained using coomassie blue.

### 3.4.5 Protein-protein interactions

#### 3.4.5.1 Covalent disulfide bonding and noncovalent interactions

The protein solubility of the protein isolates and extrudates was analyzed according to the method of Liu and Hsieh (2008) with some modifications. Different media (1-4) were used to solve specific chemical bonds within the protein network of the respective proteins. (1) 100 mM phosphate buffer consisting of KH<sub>2</sub>PO<sub>4</sub> and K<sub>2</sub>HPO<sub>4</sub> with a pH of 7.5 was used to extract the proteins in their native state (P). In addition, this buffer system was used for the

preparation of the following solvents: (2) 8 M urea known to dissolve proteins with hydrogen and hydrophobic interactions (PU); (3) 50 mM dithiothreitol (DTT) known to disrupt disulfide bonds (PD); (4) 8 M urea and 50 mM DTT known to disrupt both covalent and non-covalent interactions (PUD).

0.5 g of dry protein powder was extracted with 20 ml of the individual extraction media (1-4) at 40 °C for 2.5 h using a shaker at 100 min<sup>-1</sup>. Extruded samples were milled with liquid nitrogen. Due to the w.b. moisture content in extrudates of 50-60% w/w, the sample weight of ground extrudate was increased to 1g for the extraction procedure as described above. After extraction the dispersions were centrifuged at 10000 g for 30 min. The soluble proteins in the supernatants were determined using the Bio-Rad Protein Assay (Bio-Rad Laboratories GmbH, Munich, Germany). The absorbance was read at 595 nm in a microplate spectrophotometer (μQuant MQX200, BioTek Instruments Inc., USA) using bovine serum albumin (BSA) as standard protein.

The total protein content in the samples was calculated based on the nitrogen content according to the Dumas combustion method described in the German Food Act (2005) using a nitrogen analyzer type FP 528 (Leco Corporation, St. Joseph, MI, USA) with a conversion factor of 6.25 (Sumner *et al.* 1981; Shand *et al.* 2007). Each measurement was performed in duplicate. The protein solubility was calculated as the ratio of soluble protein in supernatant to total protein in the samples.

#### 3.4.5.2 Peptide bonding

The degree of hydrolysis (DH) is defined as the ratio of cleaved peptide bonds and the amount of free amino groups (Nielsen *et al.* 2001). DH of the protein isolates and extrudates was calculated by the determination of free α-amino groups with o-phthaldialdehyde (OPA) using serine as a standard according to Nielsen *et al.* (2001). The percentage of DH was calculated as follows:

$$DH[-] = h / h_{\text{tot}} \quad 3.17$$

where  $h_{\text{tot}}$  is the total number of peptide bonds per protein equivalent, and  $h$  is the number of hydrolyzed bonds. The  $h_{\text{tot}}$  factor was 7.8 (based on soy) according to Adler-Nissen (1986). Six measurements were performed for each sample.

### **3.4.6 Statistical Analysis**

Data were treated with Microsoft<sup>®</sup> Excel (Microsoft<sup>®</sup> Office, 2010) for calculation of means and standard deviation. Analysis of variance (ANOVA) was conducted for statistical significance using OriginPro Software, version 8.5 (OriginLab Corporation, Northampton, MA, USA) when indicated. Two-way ANOVA was used to determine the effect of protein ingredients, extrusion temperature and their interactions on the extruder responses (section 4.3.3), extrudate texture properties (section 4.3.2) and protein alteration (Chapter 4.3.5). Tukey's HSD (honestly significant difference) test ( $\alpha = 0.05$ ) was used to identify the significant difference of each treatment.

## 4 Results and discussion

### 4.1 Characterization of pea protein ingredients

The majority of research on high moisture extrusion cooking was published using a combination of soy protein isolate, wheat gluten and wheat starch as described in section 2.5.2.3. One hypothesis of this thesis is that texturization to extrudates with anisotropic structures could be achieved using pea protein isolate as an alternative protein source. In order to investigate the effect of raw materials on the texturization during extrusion cooking, this chapter covers the properties of protein ingredients made from pea seeds. Three commercially available pea protein isolates were characterized regarding their chemical composition, particle size distribution, thermal properties as well as their functional properties. Characterization and comparison of the protein ingredients were the basis for further studies in the following chapters to identify the protein properties that affect rheological properties (chapter 4.2), extrudate texture properties (chapter 4.3) and protein-protein interactions (chapter 4.4).

#### 4.1.1 Chemical composition

The chemical compositions of the protein ingredients were evaluated as described in 3.1.1 and are summarized in Table 15.

**Table 15: Major chemical composition of pea protein isolates (Osen *et al.* 2014).**

Material	Dry Matter [%]	Ash [%]	Protein [%]	Lipid [%]	Starch [%]
PPI 1	93.4±0.1	5.1±0.0	84.9±0.4	7.7±0.3	0.4±0.0
PPI 2	94.2±0.0	4.2±0.0	87.3±0.1	8.3±0.1	0.0±0.0
PPI 3	94.3±0.0	5.4±0.0	83.2±0.1	7.4±0.1	0.4±0.1

The data revealed only minor differences between the three protein isolates and were in similar range as reported by Shand *et al.* (2007). The total lipid content with 7-8% for pea protein isolates was relatively high compared to 3-4% lipids in pea seeds (Shand *et al.* 2007). As reported by Sosulski and Mccurdy (1987), alkaline solubilization and isoelectric precipitation tend to concentrate lipid in the pea protein products due to lipid-protein binding during protein extraction. PPI 1 and PPI 3 exhibited an almost identical major composition. In PPI 2, the fat content was slightly higher and ash lower compared to the other PPI. In

summary, the chemical compositions of pea protein ingredients used in this thesis revealed only minor differences among each other.

#### 4.1.2 Particle size distribution

Particle size is reported to play a significant role in low moisture extrusion with regard to the processing and texture properties of the extrudates. Some raw materials are as fine as 38 microns or as coarse as 180 microns (Yada 2004; Riaz 2006). The particle size distributions of pea protein powders were evaluated as described in section 3.1.2 and plotted from the particles' volume diameter as provided in Figure 46.

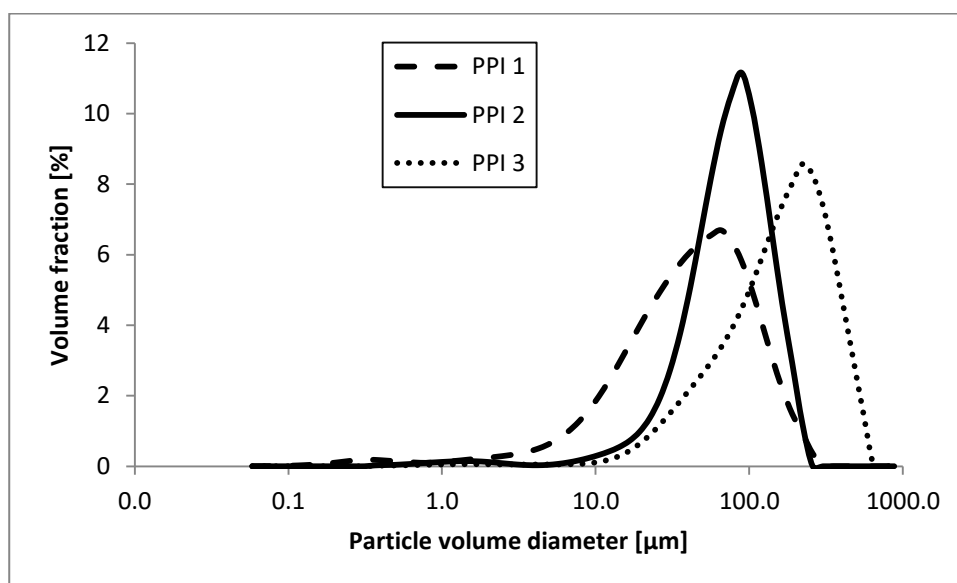


Figure 46: Volume fraction of particles from pea protein ingredients.

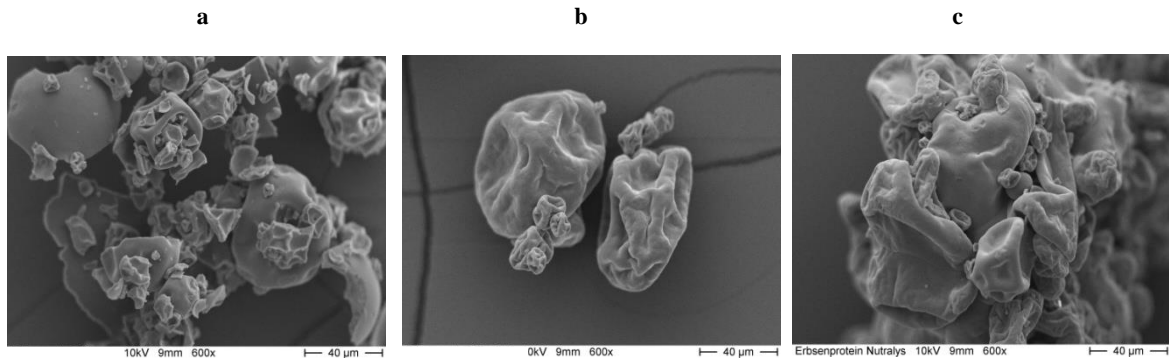
The distributions were different for the three powders. PPI 1 showed the broadest distribution, PPI 2 and PPI 3 were shifted towards bigger particles respectively. Table 16 shows the mean volume diameter  $D(v, 0.5)$ , as well as  $D(v, 0.1)$  and  $D(v, 0.9)$  values of the respective isolates.

Table 16: Average volume diameter of pea protein isolates.  $D(v, 0.1)$  was calculated referring to the 10% of the samples smaller than that value, and  $D(v, 0.9)$  indicating that 90% are smaller and 10% are larger than that value (Osen *et al.* 2014).

	$D(v, 0.1)$ [ $\mu\text{m}$ ]	$D(v, 0.5)$ [ $\mu\text{m}$ ]	$D(v, 0.9)$ [ $\mu\text{m}$ ]
PPI 1	9.1 $\pm$ 0.2	39.5 $\pm$ 0.9	108.7 $\pm$ 4.6
PPI 2	29.0 $\pm$ 0.0	71.8 $\pm$ 0.4	137.2 $\pm$ 1.1
PPI 3	40.8 $\pm$ 0.2	157.7 $\pm$ 1.7	344.5 $\pm$ 2.1

The average particle size of PPI 1 was the lowest, followed by PPI 2 and PPI 3 respectively. The differences in the particle size distributions can be attributed to the different

manufacturing methods, mainly the drying conditions. In Figure 47 microscopic images of the powder particles of the different pea protein isolates are shown as examples for a random assortment of particles.



**Figure 47: Scanning electron microscopy of pea protein isolates: (a) PPI 1, (b) PPI 2, (c) PPI 3.**

Differences in the visual appearance of the exemplary powder particles are clearly visible. The investigated sample of PPI 1 revealed small fractured particles to a great extent, whereas sample PPI 2 appeared to be less fractured with more uniformly shaped particles. In contrast, sample PPI 3 shows larger aggregates formed out of uniformly shaped bigger particles with attached finer particles.

### 4.1.3 Thermal properties

Differential scanning calorimetry (DSC) was used to analyze the thermal properties of pea protein dispersions as described in section 3.1.4. The DSC thermograms of the protein dispersions are shown in Figure 48. Peak transition temperature ( $T_d$ ) and enthalpy of denaturation ( $\Delta H$ ) were computed from the endothermic peaks observed in the thermograms.

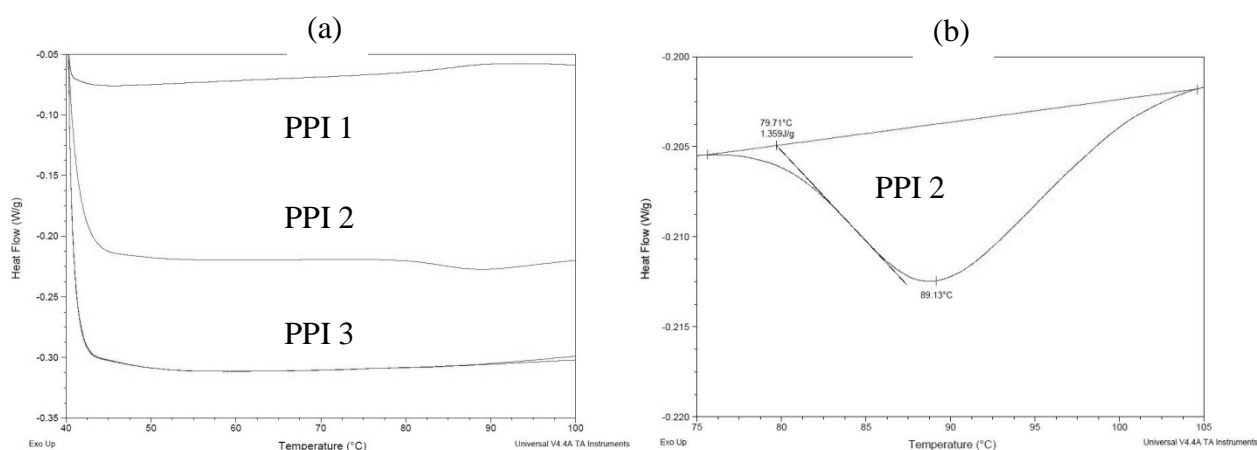


**Figure 48:** DSC thermograms of protein dispersions adjusted to 70% w.b. moisture content (w/w) heated at 5 °C/min. (a) PPI 1, PPI 2 and PPI 3 and (b) zoomed endothermic peak of PPI 2. Modified from Osen *et al.* (2014), with permission of Elsevier.

Among the three protein ingredients, only PPI 2 showed a small endothermic peak at  $88.5 \pm 0.2$  °C ( $\Delta H 1.3 \pm 0.0$  J/g). According to Arnfield and Murray (1981), a  $T_d$ -value of 86 °C was observed for air-classified pea protein. Shand *et al.* (2007) found two major peaks for laboratory prepared PPI, one at 67 °C for the non-globulin fraction and one at 85 °C for the globulin fraction. Considering these results, the endothermic peak obtained for PPI 2 may represent the thermal transition of the structural conformation of partly native globulin fractions. In contrast, the absence of any peaks in the thermograms of PPI 1 and PPI 3 indicates the denaturation of the respective protein fractions.

#### 4.1.4 Functional properties

According to Lampart-Szczapa *et al.* (2006), the functional properties of proteins in food products result from interactions between the protein and other food components, depending on the physicochemical properties characterizing the protein structure.

##### 4.1.4.1 Protein solubility

Protein quality for texturization of soy based protein ingredients is usually measured by the level of protein solubility and was determined according to the procedure described in 3.1.5.1 (Riaz 2004). Figure 49 shows the protein solubility curves in the pH-range of 3 to 8.



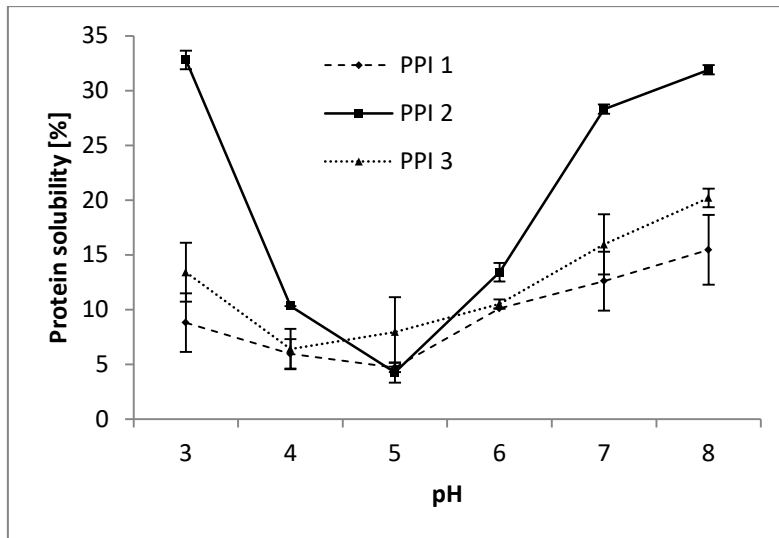


Figure 49: Protein solubility of protein ingredients as a function of pH. Reprinted from Osen *et al.* (2014) with permission of Elsevier.

The recorded protein solubility curves were in agreement with previous studies (Sosulski and Mccurdy 1987; Tomoskozi *et al.* 2001; Shand *et al.* 2007). PPI 1 and PPI 3 had lower solubility values than PPI 2, which can be attributed to their denatured state (Figure 48).

According to Yada (2004), protein solubility reflects the heat treatment history of proteins throughout the preparation process with a lower solubility following extensive heat treatment. The differences in solubility of the protein ingredients may have been the result of the processing conditions (mechanical loads from grinding, high temperatures e.g. during spray-drying).

#### 4.1.4.2 Water binding capacity, oil binding capacity, emulsifying capacity

Selected functional properties of the protein ingredients were compared and are summarized in Table 17.

Table 17: Functional properties of the protein ingredients (Osen *et al.* 2014).

Material	pH value	Water binding capacity [g/g]	Oil binding capacity [ml/g]	Emulsifying capacity [ml/g]
PPI 1	7.5	5.4±0.3	1.6±0.1	870.0±21.2
PPI 2	6.7	2.1±0.0	0.7±0.0	580.0±33.4
PPI 2*	7.5	2.5±0.1	1.3±0.0	395.0±28.3
PPI 3	7.4	5.0±0.1	1.7±0.0	725.0±0.0

\* = adjusted to pH 7.5 for comparison

The water binding capacity (WBC) depends on the number of polar sites interacting with water. PPI 1 exhibited the highest WBC of 5.4 g/g, followed by PPI 3 and PPI 2 with 5.0 and 2.1 g/g respectively. As shown in Figure 2, more protein was soluble at pH 7.5 for PPI 2 (~30%) compared to the other proteins (~15% w.b.). This affects the WBC determination, since the amount of soluble protein in the discarded supernatant is not available for binding water. Considering the thermal properties of PPI 2 its low WBC is in accordance with the findings of Sumner *et al.* (1981). The oil binding capacity (OBC) was between 0.7-1.7 ml/g and in the range reported by Owusu-Ansah and McCurdy (1991) and (Stone *et al.* 2015). Native proteins show lower OBC than their denatured counterparts because of their structural folding (Zayas 1997). Accordingly, the low OBC of PPI 2 correlates with its thermal properties and can be attributed to its structural folding with presumably a lower amount of hydrophobic groups on the molecule surface compared to the denatured PPI 1 and 3. Emulsification properties are reported to be partly improved by heat denaturation, correlating with an increase in surface hydrophobicity (Zayas 1997). This might explain the fact that PPI 2 had the lowest emulsifying capacity (EC) among the proteins. Similar findings were reported by Sumner *et al.* (1981). They stated that drum-dried PPI had the highest EC-values compared to spray-dried and freeze-dried PPI.

#### 4.1.4.3 Rheological behavior of diluted protein dispersions

As described in section 2.4.2, the viscosity response of diluted dispersions using a RVA (rapid visco analyzer) can be used to evaluate physicochemical changes such as denaturation of proteins or gelatinization of starch. Changes in viscosity of three protein ingredients were monitored under constant stirring to prevent sedimentation of dispersed particles according to the procedure described in section 3.1.5.3. The viscosity patterns of three protein ingredients are presented in Figure 50.

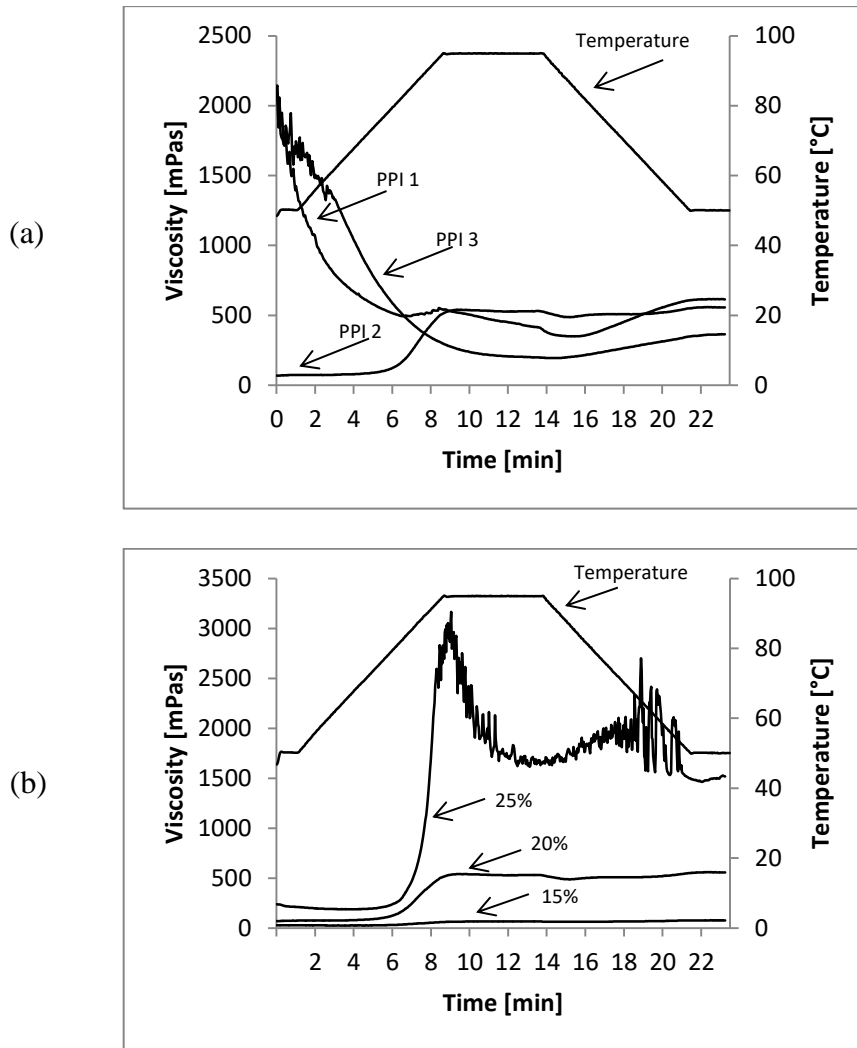


**Figure 50: RVA viscosity curves of pea protein isolates. (a) Paste profile of protein ingredients are shown with w.b. protein concentrations (15%;20%;15% (w/w) for PPI 1, PPI 2, PPI 3) giving smooth curves without sharp peaks. Viscosity profiles are displayed. (b) Paste profile of varied concentrations of PPI 2. Reprinted from (Osen *et al.* 2014) with permission of Elsevier.**

Both PPI 1 and 3 showed a high initial viscosity of around 2000 mPas that decreased upon heating to 95 °C. The pasting profiles as described in Figure 23 relate to the proteins' functional properties, particularly a low protein solubility and high water binding capacity. Upon hydration the powders absorb water and swell resulting in a high starting viscosity that subsequently decreases when the mechanical and thermal energy input increases. In contrast, PPI 2 exhibits a different viscosity profile. Following a low initial viscosity of <100 mPas, the viscosity increased sharply during heating to 95 °C. The viscosity curves of PPI 2 b) showed a sharp increase in viscosity at temperatures around 80 °C, depending on the protein content of the protein dispersion. The low starting viscosity of PPI 2 can be attributed to its high solubility compared to the other proteins. Furthermore, the sudden increase in viscosity at elevated temperatures can be explained by partly undenatured protein fractions as indicated by the protein's thermal properties (denaturation enthalpy  $\Delta H = 1.3 \pm 0.0$  J/g). When the

temperature increases above 75 °C, denaturation of the native proteins causes the protein solubility to decrease which results in an increase in viscosity. Similar findings have been recently reported by Pelgrom *et al.* (2015) who studied the effect of heating and cooling on the rheological properties of pea protein fractions using rapid visco analyzer experiments. They described a high initial degree of denaturation as well as initial high water absorption and viscosity of commercial pea protein isolates. Onwulata *et al.* (2014) studied food proteins by rapid visco analysis as well as small strain oscillation methods and showed that their viscoelastic responses could be characterized using the RVA to identify peak paste viscosity. They suggested that thermally induced changes of pasting viscoelastic behavior of food proteins could help predict the type of networks formed during food manufacturing and rapid assays of protein pastes could help to avoid flow problems that may result from protein coagulation during food processing. Regarding the high moisture extrusion process in this context, the observation of a sudden increase in viscosity could lead to processing difficulties especially during the starting sequence due to the higher protein concentration compared to the previously measured diluted protein dispersions.

The extrusion process usually starts at room temperature. Subsequently, the temperature is slowly increased until the final cooking temperature is reached. Based on the rather high initial viscosity of PPI1 and PPI3 in Figure 51, the hydrated feed mixture is expected to exhibit a rather high viscosity during the low starting temperature especially for denatured protein ingredients, which could lead to processing difficulties such as blocking in the extruder barrel or backing up of water during the heating phase. In order to monitor physicochemical changes at higher protein concentrations typical for high moisture extrusion, the specific mechanical energy was recorded during the initial start-up heating phase of the protein ingredients until a cooking temperature of 100 °C was reached (Figure 51).

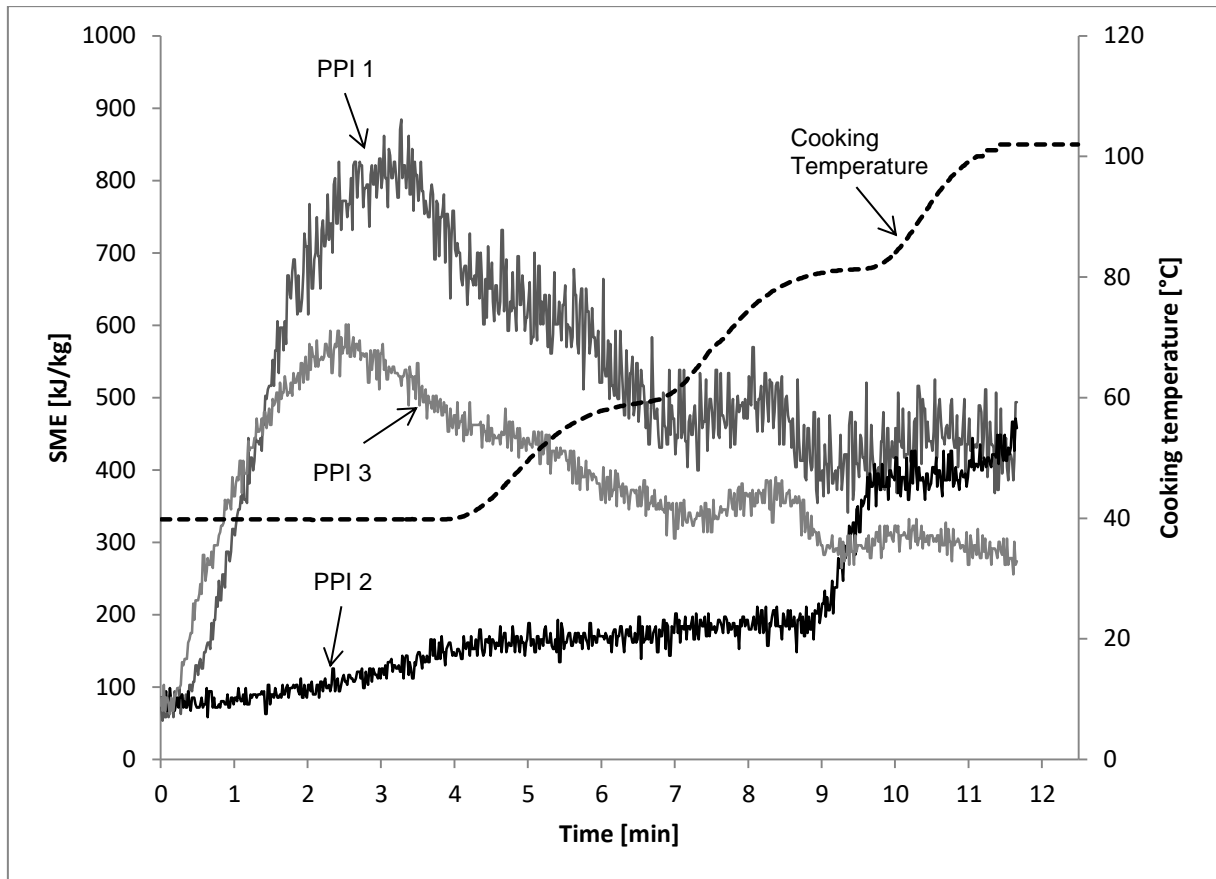


Figure 51: Specific mechanical energy values of pea protein isolates during initial start-up phase until the cooking temperature reached 100 °C. Specific mechanical energy profiles for each PPI were recorded during three consecutive experiments at a constant mass flow rate of 1 kg/h, rotational screw speed of 150 min<sup>-1</sup> and 65% w.b. moisture content (w/w). The cooking temperature was read in the 5th barrel section. During the heating phase, the temperature profile was set at 40,40,40,40,40; 40,60,60,60,60; 40,60,80,80,80 and 40,60,80,100,100 °C from the first to the fifth zone respectively. Reprinted from (Osen *et al.* 2014) with permission of Elsevier.

PPI 1 and PPI 3 exhibited similar specific mechanical energy-curves, showing a sharp increase during the first 4 minutes followed by a steady decrease upon further heating. In contrast, PPI 2 exhibited low energy consumption until a sharp increase at around 80 °C. The sudden rise in specific mechanical energy can be attributed to the denaturation of partly native proteins in PPI 2, as shown in Figure 48, which lead to a sudden decrease in protein solubility. This caused the required energy intake to increase rapidly, which corresponds to the RVA-viscosity curves in Figure 51. These findings suggest that at temperatures below the denaturation temperature of proteins, their thermal properties have great impact on the fluid properties of the feed especially during the initial phase of the extrusion process and should be taken into account to avoid blocking within the extruder barrel or backing up of water.

## 4.2 Rheological properties of protein dispersions

During high moisture extrusion of globular proteins, the biopolymers are converted from a solid granular state into a flowable viscoelastic state by a combination of heat, shear, pressure and moisture (Bouvier and Campanella 2014). Until now, there is only a small amount of published data on the physical state of the protein dispersion in the cooking zone of the extruder as well as in the cooling die channel (Kitabatake and Doi 1991; Cheftel *et al.* 1992). Although physico-chemical transitions such as melting, gelation or solidification could occur, as reported for thermoplastic protein extrusion, these changes have not been supported by experimental data yet for high moisture protein extrusion. Evidence could be provided e.g. by studying the materials' thermodynamic properties by calorimetry. Furthermore, rheological characterization can be applied to assess e.g. sol/gel-changes by studying the materials mechanical spectra.

This chapter describes the rheological properties of protein dispersions as a function of concentration, temperature and shear rate. The rheological characteristics of protein dispersions were evaluated using shear flow and dynamic measurements. First, rotational shear flow experiments of diluted protein dispersions were conducted in order to compare the protein ingredients characterized in the previous chapter regarding their viscous response to shear deformation. Based on the rheological data, mathematical models were applied to describe the shear rate dependent flow behavior. Consecutively, small strain amplitude oscillation experiments were applied to gain further insight into the viscoelastic properties of the protein dispersions in the concentration range used for high moisture extrusion processing. The protein ingredients characterized in the previous chapter were compared regarding their viscoelastic properties by means of amplitude and frequency sweep. The effect of protein concentration and temperature during amplitude and frequency sweep measurements were further investigated. Because of the difficulty of studying the physical changes of the protein dispersion inside the extruder as described in section 2.5.1, temperature-induced changes of the viscoelastic properties were examined in a pressure cell at 15 bar and elevated temperatures up to 150 °C by means of small amplitude oscillation. These conditions are similar to the temperature and pressure conditions during high moisture extrusion cooking. In order to assess the extent of thermal energy uptake of the extruded material, the residence time distribution as well as the mean residence time was evaluated. In addition, the filling degree in the cooking zone of the extruder was determined in order to calculate the associated theoretical mean residence time.

## 4.2.1 Comparison of pea protein ingredients

### 4.2.1.1 Rotational shear flow experiments

The rheological characterization by means of rotational shear flow experiments (section 3.3.1) was performed using PPI 1, PPI 2 and PPI 3. Figure 52 shows the changes in viscosity with increasing shear rate for diluted protein dispersions. As previously described in 4.1.4.3, the concentration had to be adjusted to lower protein concentrations compared to the usual concentration during high moisture extrusion in order to yield flowable protein dispersions with similar fluid properties without sedimentation by visual observation.

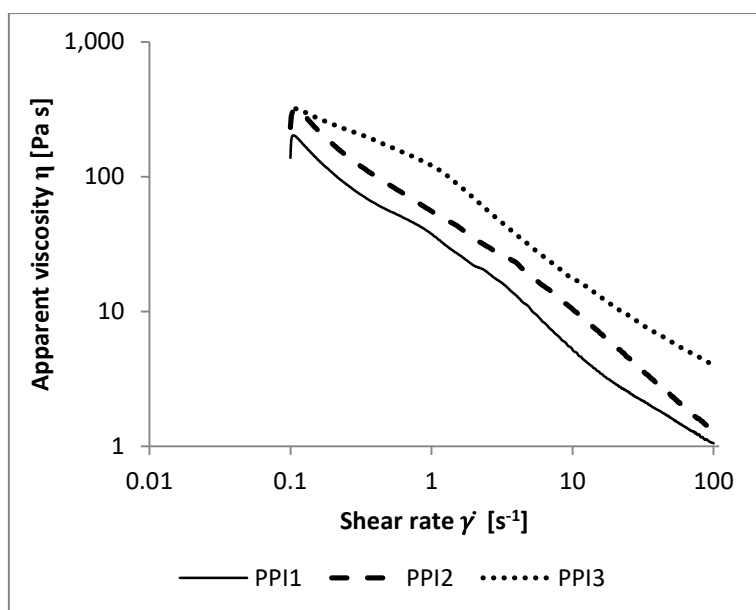


Figure 52: Viscosity curves of diluted protein dispersion with adjusted w.b. moisture content (PPI 1 (85 %), PPI 2 (70%) and PPI 3 (85%)) obtained by shear rate sweep experiments using a concentric cylinder (CC27, Anton-Paar, Graz, Austria) at 30 °C.

From the shear rate dependent viscosity profiles of the diluted protein dispersions, it can be seen that all the test samples exhibited flow curves showing decreasing values with increasing shear rate, typical for shear thinning behavior in the shear rate range from 0.1 to 100 s<sup>-1</sup>. The slope of the curves are in accordance with Pelgrom *et al.* (2015). They studied functional properties of pea protein fractions and reported that an aqueous suspension of pea protein isolate (30 g in 100 g water) exhibited a viscosity curve from ~ 1000 Pa s at a shear rate of 1 s<sup>-1</sup> to ~ 50 Pa s at 100 s<sup>-1</sup>. The rheological behavior of the pea protein follows the general observation of shear thinning behavior for most protein dispersions over a wide range of shear rates (Tung 1978). It was described that in polymer dispersions such as aqueous protein systems, molecules are randomly oriented and entangled at rest. With increasing shear rate,

the molecules tend to align themselves with the shear planes in order to reduce frictional resistance.

Several models are potentially applicable to describe the behavior of globular protein dispersions. The Bingham model is the simplest equation that accounts for a yield stress assuming that once the yield stress has been exceeded, Newtonian behavior occurs. Examples for Bingham-behavior are butter, margarine, and honey (Mackey 1989). The Herschel-Bulkley (HB) model is one of the most extensively used equations to describe the flow characteristics of shear thinning fluids with a yield stress over a wide shear rate range (Akdogan and McHugh 2000). Based on the rheological data, the Herschel–Bulkley equation was used to describe the shear rate dependent flow behavior with a yield stress (Table 18).

**Table 18: Herschel–Bulkley parameters for diluted protein dispersions with adjusted w.b. moisture content (PPI 1 (85 %), PPI 2 (70%) and PPI 3 (85%) obtained by shear rate sweep experiments with the yield stress  $\tau_0$ , flow index  $n$  and shear rate  $\dot{\gamma}$ . The exponent  $n$  indicates shear thinning behavior with  $n < 1$ , shear thickening behavior with  $n > 1$  and Bingham-behavior with  $n = 1$ . The goodness of fit was described by means of the coefficient of determination  $R^2$  (Akdogan and McHugh 2000).**

	PPI 1	PPI 2	PPI 3
$\tau_0$ (Pa)	47.49 ± 7.82	119.58 ± 11.43	84.73 ± 5.02
$n$	5.43 ± 2.71	0.95 ± 0.24	1.55 ± 0.14
$R^2$	0.94 ± 0.08	0.99 ± 0.01	0.95 ± 0.02

Application of the Herschel–Bulkley model suggested a yield stress for all protein concentrations. Magnitude of the yield stress varied from 48 Pa for PPI 1 to 120 Pa for PPI 2.

The exponent  $n$  suggests a shear thinning behavior for PPI 2 only, indicated by a value  $< 1$ , while both PPI 1 and PPI 3 had  $n$ -values  $> 1$  which is indicative for shear thickening behavior. This behavior is in contrast to the viscosity curves in Figure 59 showing a shear thinning behavior for all protein ingredients. One explanation could be found in the protein concentration which was adapted to lower protein concentration prior to the experiment for PPI 1 and PPI 3. It was suggested previously that the concentration may determine the type of flow behavior. For instance, Vélez-Ruiz and Barbosa-Cánovas (1998) described that concentrated milks showed Newtonian flow up to 22.3% solids, power-law flow from 22.3% to 30.5% solids, and Herschel–Bulkley flow above 42.4% solids. Similar observations were reported by Hermansson (1975) who studied the flow properties of soy protein isolate and observed an increasing deviation from Newtonian behavior and an increasing yield stress with increasing protein concentration. They interpreted these observations as strongly indicative of the presence of protein-protein interactions leading to the formation of a protein network at higher concentrations.



Regarding the rheological properties of the diluted proteins dispersions as described in 2.4.3.2, it could be concluded that the protein dispersions typically used for high moisture extrusion are expected to exhibit increasing network strength due to protein crosslinking with increasing protein concentration up to 50% w.b.

#### 4.2.1.2 Amplitude sweep

In order to investigate the rheological properties of protein dispersion in the concentration range that is used for high moisture extrusion (55-65% w.b. moisture content), small strain amplitude sweep experiments were performed as described in 3.3.2.2. By increasing the amplitude at a constant angular frequency, the viscoelastic properties of the protein ingredients were studied and the linear viscoelastic range was identified. Experiments were performed at 30 °C and 65% w.b. moisture content to compare the rheological properties of the protein ingredients.

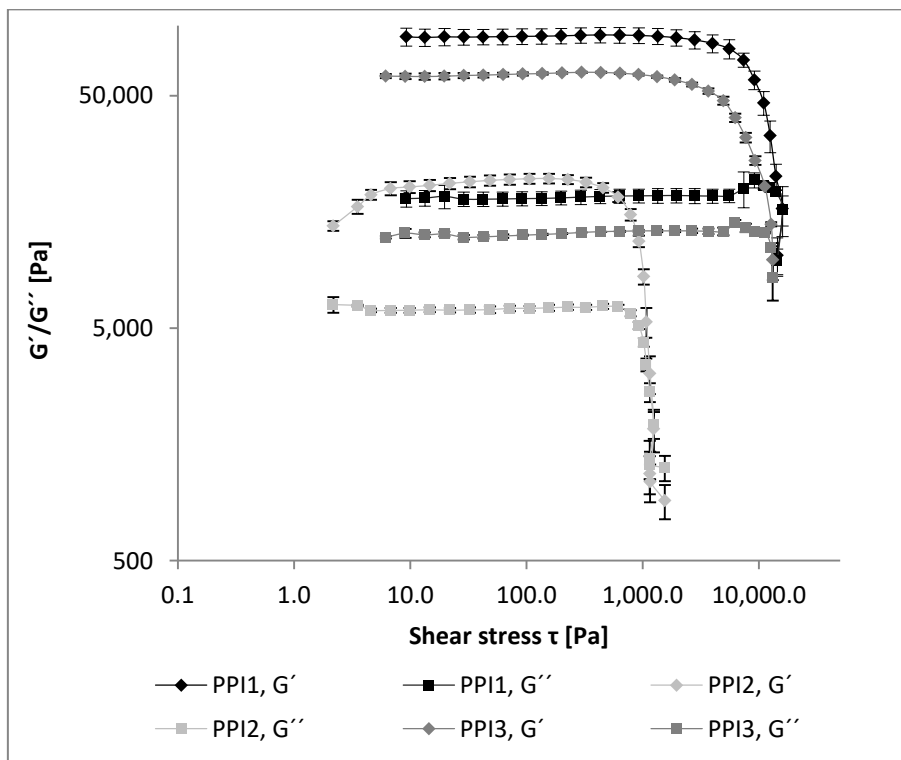


**Figure 53:** Viscoelastic properties of protein dispersions with w.b. moisture content of 65% w/w obtained by stress amplitude sweep experiments at constant angular frequency of  $10 \text{ s}^{-1}$  using a parallel plate geometry with 25 mm diameter (PP25, Anton-Paar, Graz, Austria) and a constant normal force of 5 N at 30 °C.

All samples exhibited a predominant gel-like behavior with the elastic modulus  $G'$  greater than the viscous modulus  $G''$  in the linear viscoelastic range. This viscoelastic response is typical for polymeric gel networks or viscous pastes with a yield flow (Mezger 2006).

Based on the amplitude sweep data, the average  $G'$  and  $G''$  values in the linear viscoelastic range, the modulus and the flow stress  $\tau_f$  at the flow point when  $G' = G''$ , as well as the yield stress  $\tau_y$  at the yield point (limit of the linear viscoelastic range) were determined (Table 19). Additionally, the loss tangent  $\tan\delta$  was calculated from  $G'/G''$ .

**Table 19: Viscoelastic properties of protein dispersions with w.b. moisture content of 65% (w/w) obtained by stress amplitude sweep experiments with deformation at constant angular frequency  $\omega$  of  $10 \text{ s}^{-1}$  using a parallel plate geometry with 25 mm diameter (PP25, Anton-Paar, Graz, Austria) and a constant normal force of 5 N at  $30 \text{ }^\circ\text{C}$ .**

	PPI 1	PPI 2	PPI 3
$G'$ [Pa]	$88392 \pm 5834$	$20179 \pm 2467$	$61555 \pm 1257$
$G''$ [Pa]	$18112 \pm 1193$	$6072 \pm 195$	$12697 \pm 321$
$G' = G''$ [Pa]	$15805 \pm 4419$	$2076 \pm 35$	27170*
Yield stress $\tau_y$ [Pa]	$926 \pm 73$	$325 \pm 15$	$782 \pm 250$
Flow stress $\tau_f$ [Pa]	$14145 \pm 148$	$1234 \pm 186$	12130*
Loss tangent $\tan\delta$ [-]	0.205	0.301	0.206

\*only a single crossover could be detected due to fluctuations of the curves at high amplitude

PPI 1 presented the highest viscoelastic parameters followed by PPI 3 and PPI 2. The lower gel strength of PPI 2 could be attributed to the protein solubility which was higher compared to the other protein ingredients. This is in accordance with the general observation that the formation of heat-set protein gels requires the denaturation of the proteins in order to crosslink and form a gel network (Renkema *et al.* 2000; Augusto *et al.* 2012; Pelgrom *et al.* 2015). With increasing amplitude, the limit of the linear viscoelastic range is depicted by the yield point where the sample structure is irreversibly changed and with further increasing amplitude the flow point ( $G' = G''$ ) were the material starts to flow, or in case of strong gels the material starts to become disintegrated. Again, similar trends could be observed with PPI 1 exhibiting the highest resistance against structural breakdown followed by PPI 3 and PPI 2 showing the weakest gel properties.

#### 4.2.1.3 Frequency sweep

After determination of the linear viscoelastic range, frequency sweep experiments were performed by decreasing the angular frequency from 500 to  $0.05 \text{ s}^{-1}$  at a constant amplitude in the linear viscoelastic range. Experiments were performed at  $30 \text{ }^\circ\text{C}$  and 65% moisture content to compare the rheological properties of the protein ingredients.

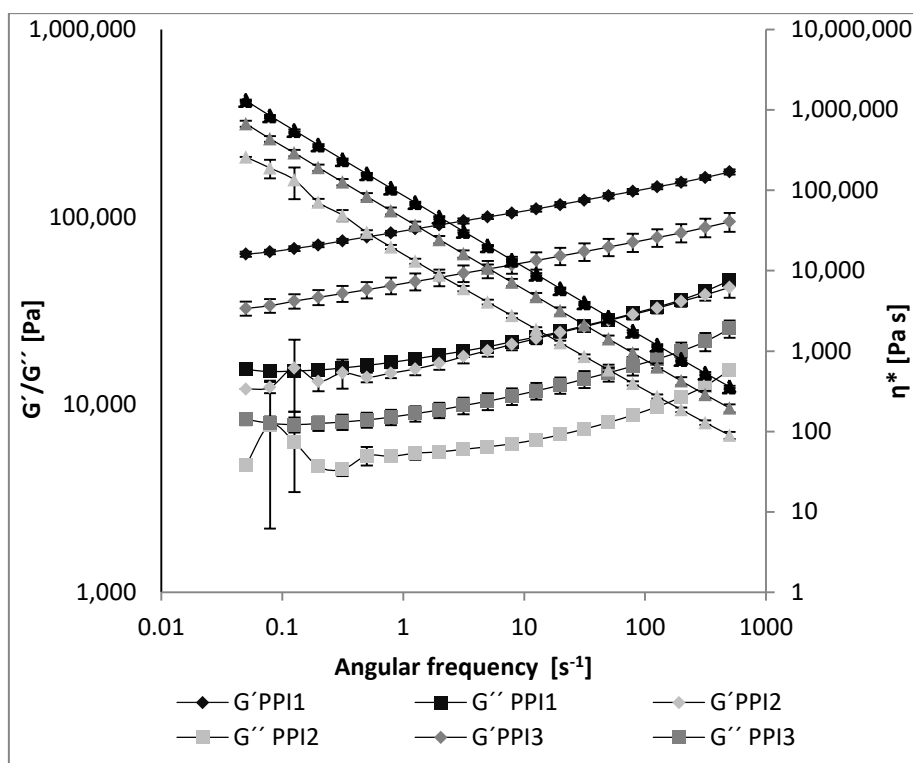


Figure 54: Viscoelastic properties of protein dispersion with w.b. moisture content of 65% (w/w) obtained by frequency sweep experiments using a parallel plate geometry with 25 mm diameter (PP25, Anton-Paar, Graz, Austria) and a constant normal force of 5N at 30 °C. Angular frequency was decreased from 500 to 0.05 s<sup>-1</sup> with deformation  $\gamma$  in the linear viscoelastic region of the respective protein ingredient (PPI 1 = 1%, PPI 2 = 0.5%, PPI 3 = 0.5%).

Comparison of the protein dispersions using frequency sweeps showed differences regarding their viscoelastic response. The elastic modulus  $G'$  dominated over the viscous modulus  $G''$  over the frequency range for all samples, which is a characteristic behavior typical of crosslinked networks with a gel- or paste like behavior. The apparent viscosity increased towards an infinitely high value at a low angular frequency indicating shear thinning behavior and structure stability at rest (Mezger 2006).

Both, the storage and loss modulus exhibited a pronounced frequency dependency, with  $G'$  and  $G''$  values rising gradually with increasing frequencies. One explanation is that at higher frequencies, molecular chains cannot disentangle during the short period of oscillation and the entanglement points may act as a temporary cross-linking junction zone, which would explain the increase observed for the elastic component (Rao 2007). With decreasing angular frequency, the  $G'$  curve approaches a constant value near the intercept with the ordinate further supporting the behavior of structure stability at rest.

The characteristics of the protein dispersion can be represented mathematically by a power-type equation relating elastic modulus ( $G'$ ) and angular frequency (Rao and Cooley 1992;

Ahmed *et al.* 2006; Augusto *et al.* 2012; Augusto *et al.* 2013; Ahmed *et al.* 2016). Linear regressions of  $\log \omega$  versus  $\log G'$  were performed and the magnitudes of slopes and intercepts were computed as described in chapter 2.4.3.3. The regression parameters obtained are reported in Table 20.

**Table 20: Regression parameters for frequency sweep data at 30 °C and w.b. moisture content of 65% (w/w). Behavior index  $n'$  = slope of  $G'$ , consistency index  $K'$  = intercept with ordinate,  $R^2$  = coefficient of determination and SD = standard deviation.**

PPI 1				PPI 2				PPI 3			
$n'$	$K'$	$R^2$	SD	$n'$	$K'$	$R^2$	SD	$n'$	$K'$	$R^2$	SD
0.111	1449.3	0.993	28.9	0.143	132.0	0.873	11.8	0.114	483.8	$0.975 \geq$	18.1

The moduli-frequency data fitted the power law model well for PPI 1 and PPI 3 ( $R^2 \geq 0.975$ ) and adequately for PPI 2 (section 2.4.3.3, equation 2.17). It was reported earlier that the slope of  $\log G'$  vs  $\log \omega$  - that is the behavior index  $n'$  - is supposed to be zero for pure elastomers, while weak gels and highly concentrated solutions exhibit positive slopes (Rao and Cooley 1992; Ahmed *et al.* 2006).

As  $n'$  was lowest for PPI 1, followed by PPI 3 and PPI 2, this suggests that PPI 1 behaves more like an elastomer and PPI 2 tends to behave more like a concentrated solution with PPI 3 in between. Similar flow behavior index values were reported by Hua *et al.* (2005) who studied heat and cooled set gels prepared from different soy protein isolates at concentrations of 120 mg/ml. They observed a behavior index  $n'$  in the range between 0.093 and 0.267. Additionally, the differences between the pea proteins are characterized by the consistency index  $K'$ . The consistency of PPI 1 was highest, followed by PPI 3 and PPI 2, which correlates with the behavior index.

#### 4.2.2 Viscoelastic properties within a temperature range of 30-90 °C

As reported in section 2.5.1, the temperature during extrusion of protein greatly affects the product properties. During heating in the extruder, the mechanical properties of the materials may change from a viscoelastic solid to a liquid while encountering physical transitions such as melting transition. During cooling, they are converted back to solid or rubbery state (Bouvier and Campanella 2014). Up to now, little is reported about the physical state of the protein-water mixture in the cooking zone of the extruder during high moisture extrusion conditions (Kitabatake and Doi 1991; Cheftel *et al.* 1992).

---

In the following section, the mechanical response of protein dispersion in the concentration range that is used for high moisture extrusion (55-65% w.b. moisture content) was investigated as a function of temperature and protein concentration exemplary using PPI 1. Amplitude and frequency sweep experiments were performed at temperatures below 100 °C due to the limitation of water evaporation. Consecutively, temperature sweep experiments were conducted until 150 °C using a pressure resistant measuring cell.

#### 4.2.2.1 Amplitude sweep

Small strain amplitude sweep experiments were conducted varying (a) the protein concentration under isothermal conditions as well as varying (b) the temperature (Figure 55).

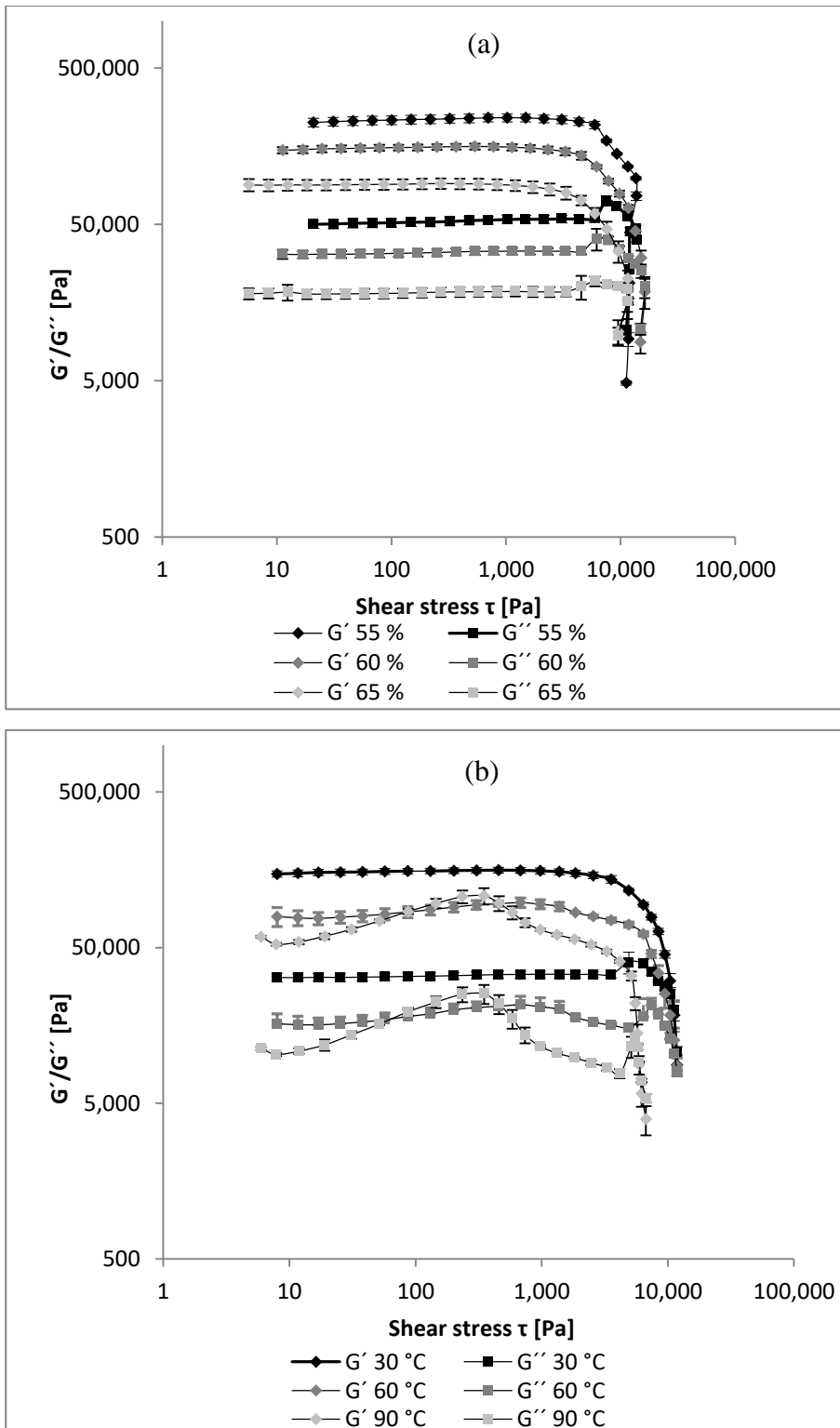


Figure 55: Viscoelastic properties of protein dispersion of PPI 1 obtained by stress amplitude sweep experiments with deformation at constant angular frequency  $\omega$  of  $10 \text{ s}^{-1}$  using a parallel plate geometry with 25 mm diameter (PP25, Anton-Paar, Graz, Austria) and a constant normal force of 5N. Variation of (a) w.b. moisture content (55%, 60%, 65%) w/w at isothermal conditions at 30 °C and (b) temperature (30 °C, 60 °C, 90 °C) with w.b. moisture content of 60% w/w.

As expected, both increasing water content and temperature affected the mechanical response of the samples by reducing the moduli of PPI 1. Figure 55a shows the effect of water content at isothermal conditions on the rheological properties. The samples could be characterized as

viscoelastic solids as the storage modulus was higher than loss modulus in the linear viscoelastic region. As expected, with increasing water content  $G'$ ,  $G''$  and the yield point decreased. This can be attributed to a dilution effect reducing protein-protein interactions leading to a lower gel network strength.

The effect of temperature on the moduli is shown in Figure 55b. As expected, the moduli decreased upon increasing the temperature. However,  $G'$  remained higher than  $G''$  even at 90 °C suggesting viscoelastic solid behavior. When the temperature was increased from 30 to 60 °C, the moduli decreased although a small shoulder appeared in the curve progression. At 90 °C, the curves showed a distinct shoulder in the linear viscoelastic range until the moduli decreased due to structural breakdown at the yield point. This behavior could be attributed to water evaporation and a resulting increase of the moduli. Hence, this temperature marks the limit of the experimental range for the applied method. Data from the mechanical response during amplitude sweep experiments are shown in Table 21.

**Table 21: Viscoelastic properties of protein dispersion of PPI 1 obtained by stress amplitude sweep experiments with deformation at constant angular frequency  $\omega$  of 10 s<sup>-1</sup> using a parallel plate geometry with 25 mm diameter (PP25, Anton-Paar, Graz, Austria) and a constant normal force of 5N. Variation of w.b. moisture content (55%, 60%, 65% w/w) and temperature (30 °C, 60 °C, 90 °C).**

Temperature [ °C]	30			60			90		
	Moisture content [%]	55	60	65	55	60	65	55	60
$G'$ [Pa]	233021 ± 1290	152940 ± 6849	88392 ± 5834	149596 ± 1274	85357 ± 9572	57913 ± 5476	112712 ± 2639	74725 ± 1904	87730 ± 4565
$G''$ [Pa]	52487 ± 3105	33012 ± 1549	18112 ± 1193	33117 ± 3469	18259 ± 2686	12124 ± 1741	23443 ± 7815	15685 ± 5527	20941 ± 1119
$G' = G''$ [Pa]	43657 ± 3902	21147 ± 2857	15805 ± 4419	19357 ± 1268	*1	9146*2	14787 ± 3849	9485 ± 1719	4931*2
$\tau_y$ [Pa]	2470 ± 156	1593 ± 70	926 ± 73	1593 ± 129	88 ± 7	58 ± 6	9 ± 1	6 ± 0.1	4 ± 1
$\tau_f$ [Pa]	19680 ± 946	18563 ± 2702	14145 ± 148	13657 ± 1822	*1	6917*2	8551 ± 3768	5959 ± 636	5892*2
$\tan\delta$ [-]	0.23	0.22	0.2	0.22	0.21	0.21	0.21	0.21	0.24

\*1 = no data available. \*2 = single determination

The data from the amplitude experiments show that the increase of temperature results in a weakening of the network strength as expressed by a reduction of  $G'$  as well as the yield point. This was expected, as the increasing temperature facilitates the weakening of the molecular interactions that stabilize the three-dimensional network. Consequently, it could be expected that  $\tan\delta$  would simultaneously increase towards unity which would indicate the

approach of a solid/liquid phase change. However,  $\tan\delta$  remained unaffected from both temperature and moisture content which could be further attributed to the characteristics of crosslinked networks with a gel- or paste like behavior.

Regarding the material behavior during extrusion processing, it can be inferred that elevated temperature conditions during high moisture extrusion cooking of up to 160 °C would lead to a further decrease of the network strength. Regarding the observed decrease of both yield- and flow stress at 90 °C, it can be assumed that the thermomechanical conditions during high moisture extrusion would facilitate a rather low-viscosity polymeric melt flow. Hence, it can be suggested that the forces stabilizing the network structure become weaker and a gel/sol transition might be possible with further increasing temperature.

#### 4.2.2.2 Frequency sweep

The mechanical response of PPI1 in the concentration range used for extrusion experiments was investigated as a function of temperature and protein concentration. In Figure 56,  $\log(G')$  and  $\log(G'')$  values were plotted against  $\log \omega$  as affected by moisture content (a) and temperature (b).



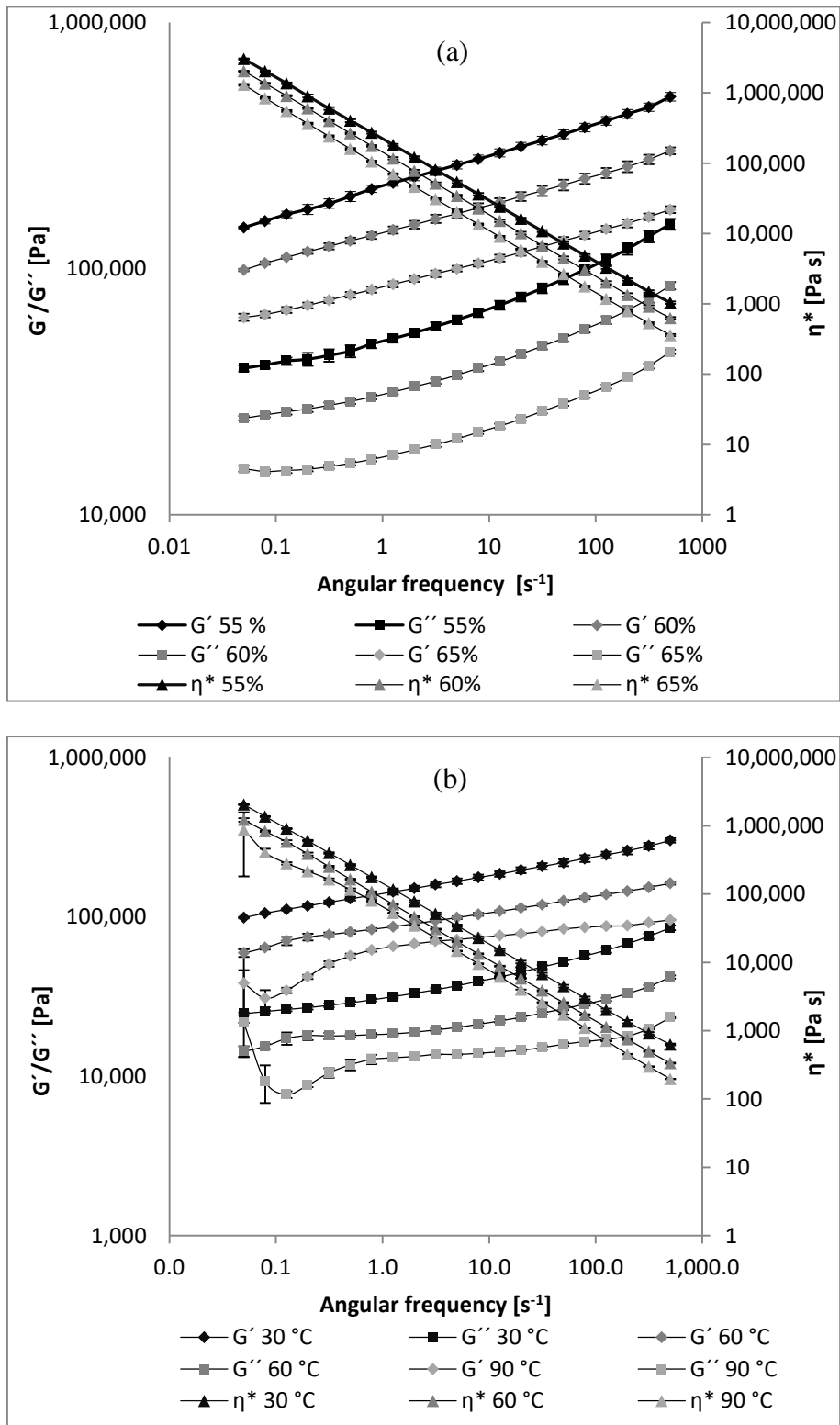


Figure 56: Viscoelastic properties of protein dispersion of PPI 1 obtained by frequency sweep experiments in the linear viscoelastic region using a parallel plate geometry with 25 mm diameter (PP25, Anton-Paar, Graz, Austria) and a constant normal force of 5N. Angular frequency was decreased from 500 to  $0.05 s^{-1}$  with deformation  $\gamma$  in the linear viscoelastic region (30 °C = 1%, 60 °C = 0.5%, 90 °C = 0.1%). Variation of (a) w.b. moisture content (w/w) at 30 °C and variation of temperature (b) at a constant w.b. moisture content of 60% (w/w).

The mechanical spectra showed characteristics typical for a viscoelastic gel, with dominant elastic properties over the viscous ones in the entire angular frequency range. All samples exhibited parallel curve progression which is typical for crosslinked polymer gels. Figure 56 a shows that  $G'$  and  $G''$  increase with increasing protein concentration indicating a stronger network. With increasing angular frequency the apparent viscosity decreased denoting shear thinning behavior of the samples which is in accordance with the flow behavior during rotational measurements. The temperature conditions seemed to have smaller effects on the viscoelastic response compared to the moisture content as shown in Figure 56 b.

Table 22 shows the values for the power-law model (section 2.4.3.3, equation 2.17) as a function of temperature and moisture content.

**Table 22: Regression parameters for frequency sweep data as a function of w.b. moisture content (w/w) and temperature. Behavior index  $n'$  = slope of  $G'$ , consistency index  $K'$  = intercept with ordinate,  $R^2$  = coefficient of determination and SD = standard deviation [%].**

Moisture content [%]	Temperature [ °C]											
	30				60				90			
	$n'$	$K'$	$R^2$	SD	$n'$	$K'$	$R^2$	SD	$n'$	$K'$	$R^2$	SD
55	0.128	4008	1.00	32.2	0.098	2142	0.98	57.3	0.087	1488	0.56	223.5
60	0.117	2471	1.00	38.4	0.101	1383	1.00	18.6	0.104	912	0.78	90.2
65	0.111	1449	0.99	28.9	0.080	835	0.83	66.1	0.013	543	0.21	122.3

At 30 °C and 60 °C,  $R^2$  regression values were  $\geq 0.98$  with the exception of the sample behavior at 60 °C and 65% moisture content. At 90 °C, the moduli showed low agreement with the power law model. This was expected as the rheological response of the samples showed comparatively high variability in the data due to potential water evaporation. Similar observations using meat puree based baby foods were reported by Ahmed and Ramaswamy (2007). They found that rheological data did not fit well at and above 65 °C, which they attributed to possible initiation or partial denaturation of meat protein.

As expected, the increase in temperature reduced the consistency coefficient ( $K'$ ) due to a decreased network stability of the sample (section 2.4.3.3, equation 2.17). Similar effects of temperature on the consistency coefficient were reported for soy protein isolate (Ahmed *et al.* 2006). The flow index  $n'$  showed a tendency to decrease with increasing temperature, but the effect was less pronounced. This is in contrast to other studies that show an angular frequency-independent flow behavior index (Ahmed *et al.* 2006; Augusto *et al.* 2012).

### 4.2.3 Temperature sweep experiments within a temperature range of 50-150 °C

The effect of temperature on protein dispersions results in thermal transitions responsible for rheological changes inside the extruder (Little *et al.* 1997). In order to study the material properties and possible phase changes during extrusion cooking, it is important to investigate the mechanical response of the protein dispersions in a temperature range similar to that during high moisture extrusion cooking, which may be as high as 160 °C. Previous researchers used pressure rheometers that permit moisture to be retained in the system at elevated pressure and temperature. This methodology allowed temperature sweep measurements of aqueous dispersions in a temperature range as high as 190 °C (Little *et al.* 1997; Morales and Kokini 1999). In this thesis, a similar approach was followed for the assessment of the mechanical response of pea protein isolate under temperature and moisture conditions similar to that during high moisture extrusion cooking (section 3.3.2.4). Small strain oscillatory temperature sweeps were performed to investigate the mechanical spectra as a function of temperature. Additionally, rotational steady shear experiments as a function of temperature were conducted to monitor the apparent viscosity of the protein dispersion.

#### 4.2.3.1 Small strain oscillation

Figure 57 shows the influence of temperature on storage modulus  $G'$  and loss modulus  $G''$  of a protein dispersion (PPI 1) with a moisture content of 65% following the procedure described in section 3.3.2.4.

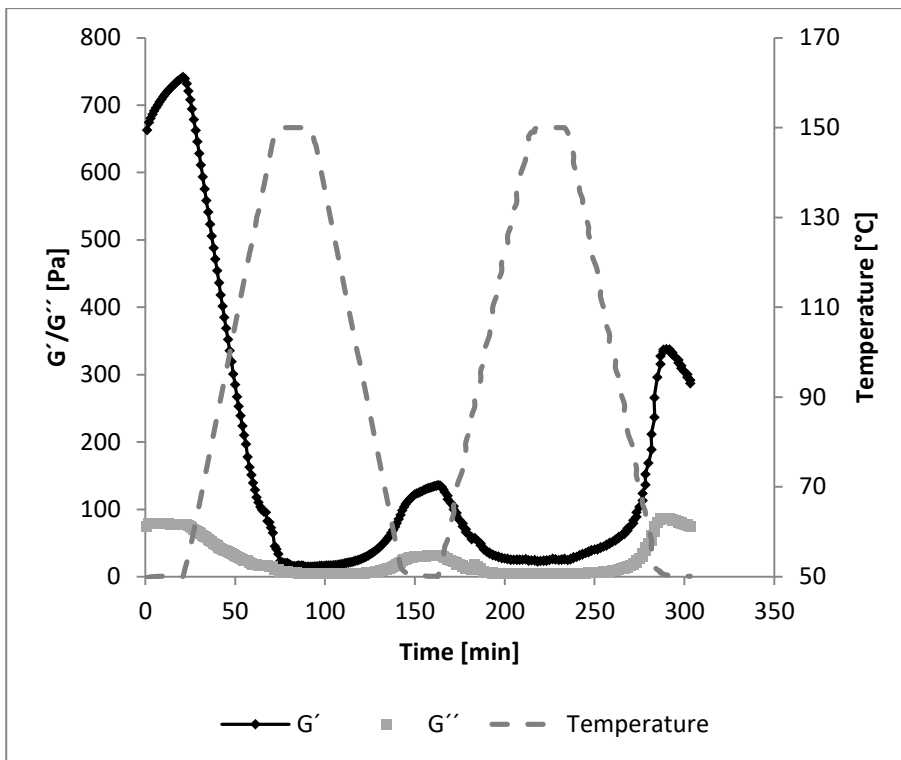


Figure 57: Viscoelastic properties of a protein dispersion of PPI 1 with w.b. moisture content of 65% w/w by temperature sweep experiments using a parallel plate geometry with 20 mm diameter (PP25, Anton-Paar, Graz, Austria) and 1 mm gap size at constant deformation  $\gamma = 1\%$  and constant angular frequency  $\omega = 10 \text{ s}^{-1}$ . Heating/cooling rate was  $2 \text{ }^\circ\text{C}/\text{min}$ . Head pressure of 15 bar using nitrogen was applied to prevent moisture evaporation.

The diagram shows the mechanical spectra during two subsequent heating and cooling cycles with temperatures between 50 and 150 °C (dotted line). It can be seen that the initial  $G'$  was higher than  $G''$  at 50 °C, indicating viscoelastic solid properties of the sample. As the temperature increased, both moduli decreased which is indicative for a weakening of the network structure. During the holding phase at 150 °C, both moduli remained low until they slightly increased upon cooling which could be attributed to crosslinking and formation of a viscoelastic solid network. During the first holding phase at 50 °C, both moduli were lower compared to the initial values at similar temperature. In the following consecutive heating and cooling cycle, the mechanical spectra followed similar curve progressions as affected by temperature, although higher moduli could be observed in the final holding phase at 50 °C compared to the previous one.

Additionally  $\tan\delta$  and the absolute value of the complex viscosity  $|\eta^*|$  are shown in Figure 58.

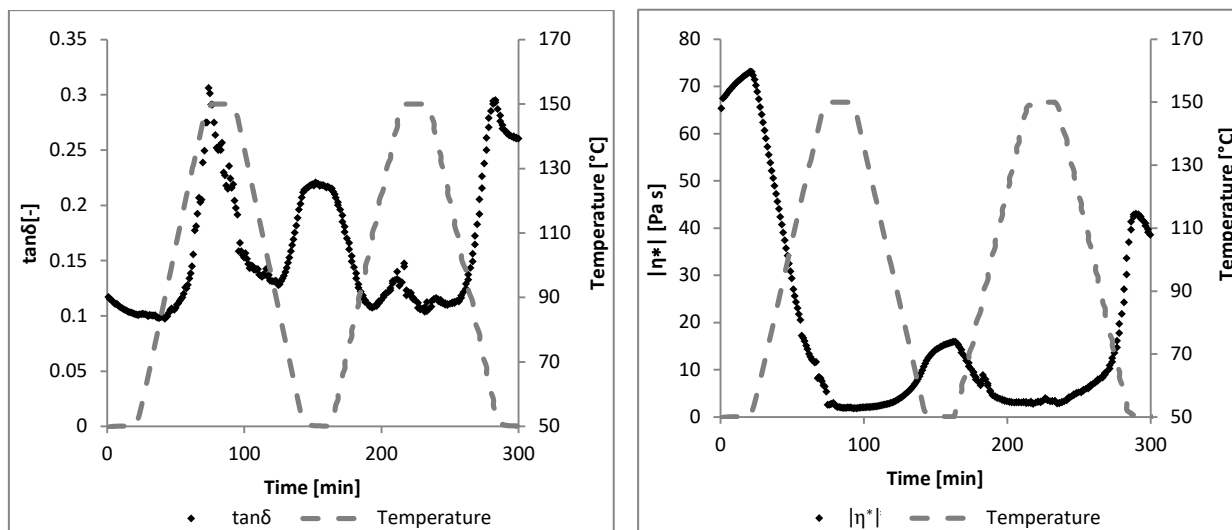


Figure 58: Viscoelastic properties ( $\tan\delta$  (a) and absolute value of complex viscosity (b)) of protein dispersion of PPI 1 with w.b. moisture content of 65% (w/w) obtained by temperature sweep experiments using a parallel plate geometry with 20 mm diameter (PP25, Anton-Paar, Graz, Austria) and 1 mm gap size at constant angular frequency  $\omega$  of  $10 \text{ s}^{-1}$ . Head pressure of 15 bar using nitrogen was applied to prevent moisture evaporation.

Both curves showed obvious dependencies on the temperature. The  $\tan\delta$  curve remained constant during heating, which relates to the simultaneous decrease of both  $G'$  and  $G''$  shown in Figure 57. The increase of  $\tan\delta$  from 0.1 to  $\sim 0.3$  during the first heating period indicates the softening of the mass. During the low temperature holding phase,  $\tan\delta$  stabilizes at around 0.2. In the second heating cycle,  $\tan\delta$  decreases to the initial value of 0.1 without a pronounced maximum during the second holding phase at  $150 \text{ }^\circ\text{C}$ .

The absolute value of the complex viscosity shown in Figure 58b was calculated from  $|G^*|$  and angular frequency, thus following a similar trend compared to the elastic modulus  $G'$ . Similar trends of the curve progressions during the second heating-cooling cycle indicate that the thermally induced molecular interactions seem to be partially reversible. Table 23 shows the mean values of the mechanical spectra as a function of temperature.

Table 23: Viscoelastic properties of a protein dispersion of PPI 1 with w.b. moisture content of 65% (w/w) as a function of temperature. Data were obtained by temperature sweep experiments using a parallel plate geometry with 20 mm diameter (PP25, Anton-Paar, Graz, Austria) and 1 mm gap size at a constant angular frequency  $\omega$  of  $10 \text{ s}^{-1}$ .

Temperature [ $^\circ\text{C}$ ]	50	150	50	150	50
$G'$ [Pa]	710.0	20.6	122.4	24.3	317.3
$G''$ [Pa]	77.9	6.5	28.7	4.3	81.4
$ \eta^* $ [Pa s]	71.4	2.2	12.6	2.5	32.7

The methodology of small strain oscillatory temperature sweeps to study the gelation behavior of globular protein dispersions has been previously applied by a number of researchers (Renkema *et al.* 2000; Renkema and van Vliet 2002; O'Kane *et al.* 2004; Sun and

Arntfield 2010; Sun and Arntfield 2011). In most cases, native protein was used to monitor physico-chemical changes such as unfolding, denaturation, aggregation and cross-linking during gel forming. In contrast, the observations in the current study are based on protein dispersions with (1) a comparatively high protein content that was (2) readily denatured and (3) showed the behavior of a viscoelastic solid already before the heating and cooling cycle applied for usual thermally-induced gelation of globular proteins. Therefore, data interpretation considerably differs from the usual methodology.

Several conclusions can be drawn from the mechanical spectra. The data suggest that the rheological behavior of the protein dispersion can be described as a viscoelastic solid in the temperature range up to 150 °C, which is typical for high moisture extrusion. This is based on the observation that  $G'$  remained higher than  $G''$  throughout the heating and cooling cycle. Consequently, no evidence for a sol/gel transition could be observed. This could be attributed to the high initial protein concentration of the protein dispersion typically used for high moisture extrusion. Hydration of the protein produced a crumbly paste- or dough- like structure at room temperature with high  $G'$ -values and a low  $\tan\delta$ . The decrease of  $G'$  during heating reflects the weakening of protein-protein interactions until the heating plateau is reached, yet  $G'$  remains higher than  $G''$ . In this state,  $G'$  and  $G''$  exhibit minimal values and  $\tan\delta$  maximum values, indicating decreasing interactions stabilizing the network and a softening of the texture. The slight changes in the moduli during the heating phase might be explained by protein rearrangement as described by Renkema (2002).

Based on the mechanical spectra from small strain temperature sweep experiments of a denatured protein dispersion, the following temperature-induced physico-chemical changes could be expected during high moisture extrusion: With increasing temperature, the paste-like mass becomes softer with decreasing elastic and viscous moduli. As the yield stress decreased rapidly with increasing temperature from 30 to 90 °C during amplitude sweep experiments (Table 21), it can be assumed that the yield stress would be close to zero at elevated temperatures i.e. in the cooking zone. This is corroborated by the absolute value of the complex viscosity which decreased to 2.2 Pa s at 150 °C. Hence, the material could be characterized as a low-viscosity fluid with a shear thinning flow behavior. Although the fluid is close to its sol/gel- transition point, the rheological behavior remains that of a viscoelastic solid as indicated by  $G' > G''$ . Following these assumptions, the terms “melting” or “liquefaction” would not accurately describe the changes occurring during heating of the proteinaceous mass. Taking into account the important role of water as a plasticizer for the biopolymers to be processed, the term “plasticization” would be more suitable to describe the

physical changes at elevated temperatures. Upon cooling, the increase of viscosity and elastic modulus due to a crosslinking of mainly protein interactions results in an increase of the three-dimensional structural rigidity that could be referred to as “solidification”. With respect to extrusion cooking, the data from small strain oscillation indicate that the pea protein dispersion plasticizes in the cooking zone of the extruder into a low-viscosity fluid. In the cooling zone, both viscosity and yield stress increase due to crosslinking and network formation.

#### 4.2.3.2 Apparent viscosity

The pressure rheometer was further used for steady shear rotational experiments to investigate the apparent viscosity as a function of temperature. For these experiments, only PPI 2 could be used due to its comparatively low viscosity at room temperature in the concentration range (55-65% w/w, wet basis). In contrast, the consistency of PPI 1 and PPI 3 was that of a solid paste with a high yield stress and a crumbly appearance that resulted in measuring errors due to predominating wall slip. The viscosity of PPI 2 as affected by temperature is shown in Figure 59.

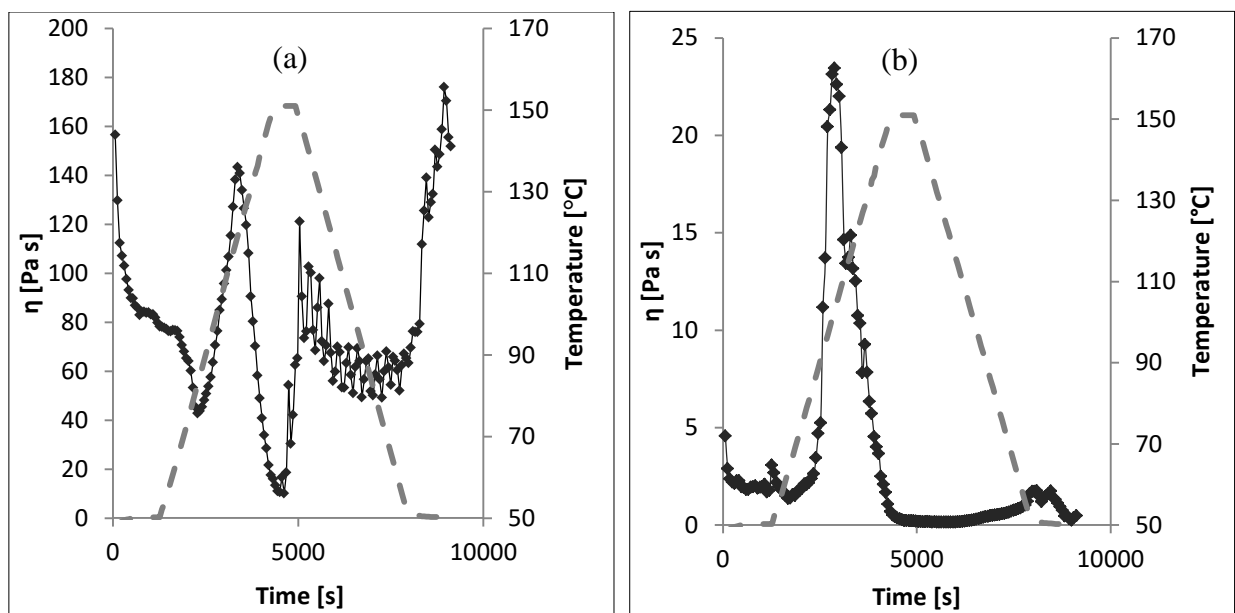


Figure 59: Apparent viscosity of PPI 2 with w.b. moisture content of 65% (w/w) during temperature sweep experiments as a function of time at a shear rate of (a)  $1\text{s}^{-1}$  and (b)  $20\text{s}^{-1}$ . Temperature profile was holding at  $50\text{ }^{\circ}\text{C}$  for 45 minutes, heating to  $150\text{ }^{\circ}\text{C}$  at  $2\text{ }^{\circ}\text{C}/\text{minute}$ , holding at  $150\text{ }^{\circ}\text{C}$  for 45 minutes, cooling to  $50\text{ }^{\circ}\text{C}$  and finally holding at  $50\text{ }^{\circ}\text{C}$  for 45 minutes. Head pressure of 15 bar using nitrogen was applied to prevent moisture evaporation.

The viscosity curves in Figure 59 show a distinct shear rate - and temperature dependency. An inverse relationship was observed between shear rate and viscosity as can be seen from comparing Figure 59a and b. This was expected as the protein dispersion showed shear

thinning behavior as evaluated by frequency sweep oscillation experiments (Table 22). At an angular frequency of  $1 \text{ s}^{-1}$ , the viscosity decreased from about 80 to 40 Pa s with increasing temperature from 50 to around 80 °C. When the temperature exceeded 80 °C, the viscosity increased to 143 Pa s. This increase can be attributed to denaturation of the native or partly native protein. Around 120 °C, the viscosity reached a peak value and decreased rapidly to a minimum of 11 Pa s during the holding phase at 150 °C. During cooling, the viscosity increased to values between 50 and 70 Pa s with maximum values of 150 Pa s during the final holding phase at 50 °C. These observations are generally in accordance with the results from temperature sweep experiments. However, it should be noted that the rheological characterization by rotational shear flow is limited to flowable materials to avoid measuring errors related to wall slip. As the protein dispersion exhibited a solid rubbery texture upon opening the measuring container following the experiment, it could be assumed that both viscosity and yield stress increase during the cooling phase up to a critical stage where structural rigidity during solidification would facilitate wall slip between measuring cylinder and the protein dispersion. To address these potential measurement errors, data interpretation from temperature sweep rotational shear flow should be limited to the heating phase where flowability can be expected in order to avoid misinterpretation. At a higher angular frequency of  $20 \text{ s}^{-1}$ , the viscosity curve showed a similar progression at lower viscosity values (Figure 59b) as previously observed.

In summary, rotational as well as small strain amplitude sweep experiments within elevated temperature ranges revealed some insights into the network formation of a protein dispersion. Regarding the shear thinning behavior of the protein dispersions, it could be expected that the extruded materials should exhibit low-viscosity values in the extruder barrel. For example, the shear rate in the cooking zone of the laboratory extruder was estimated to be up to  $\sim 600 \text{ s}^{-1}$  at a rotational screw speed of  $150 \text{ s}^{-1}$  (section 0). During cooling in the cooling die channel, the shear rate was estimated at  $\sim 20 \text{ s}^{-1}$  between the die wall and the extrudate, similar to the shear rate in Figure 59b. Regardless of shear rate, curves exhibited similar patterns that could be attributed to temperature-induced changes in the physico-chemical properties. As far as pressure effects on the rheological properties, it could be expected that the observations from pressure rheology should be sufficiently conferrable to high moisture extrusion as the pressure in the cooking zone of the extruder remained lower than 20 bar for most experiments, which was in the range of the pressure during temperature sweep experiments set at 15 bar.

A similar approach was reported by Morales and Kokini (1999) using a pressure rheometer equipped with a parallel-plate geometry to obtain the temperature-induced transitions of soy



proteins. They applied a pressure of 14 bar enabling the investigation of frequency- and temperature dependent changes of viscoelastic properties by monitoring changes in the elastic modulus. Ahmed *et al.* (2016) studied the effect of pressure treatment (3500-6500 bar) on soy protein isolate and observed no significant change in the elastic modulus of soy protein isolate dispersions at 10-20% protein (w/w), whereas protein concentration played an important role on the viscoelastic gel properties.

Although the experimental conditions were similar to extrusion conditions in terms of temperature and pressure, several parameters could not be adjusted to typical extrusion conditions. Obviously, the heating rate of 2 °C/min is lower compared to extrusion. It was previously shown that a slower heating rate facilitated a gel formation at lower temperatures (O'Kane *et al.* 2004), which is consistent with the observations of Renkema and van Vliet (2002) that a faster heating rates of soy protein dispersions initiated higher gelation temperatures. Taking into account these restrictions, the methodology applied allowed for some valuable insights into the mechanical response of protein dispersions under thermal conditions similar to those during high moisture extrusion cooking.

#### **4.2.4 Residence time distribution during extrusion**

The residence time distribution (RTD) provides information on how long temperature-sensitive biopolymers are treated at the processing temperature or shear level (Jager *et al.* 1995). As described in section 2.5.1, the thermal energy input during high moisture extrusion plays a crucial role for the physico-chemical reactions during the texturization process. The mean residence time of the protein in the extruder and in the cooling die is an important process parameter as it determines the extent of chemical reaction of the extruded material (Peng *et al.* 1994). The following section describes the residence time distribution in the laboratory scale and pilot-scale extrusion equipment in order to calculate the average time a particle remains subjected to the temperature conditions in the extrusion equipment. First, experimental residence time distribution was experimentally evaluated as affected by the flow rate and the theoretical mean residence time was calculated. In addition, the degree of fill was visually examined along the extruder barrel length in order to estimate the mean residence time in different zones of the extrusion equipment.

The experimental residence time distribution was determined by a manual impulse injection of a color tracer into the feeding zone of the extruder and the color intensities of the extruded samples were analyzed spectrophotometrically according to the procedure in section 3.2.1.7.

Figure 60 shows the residence time distribution curve  $E(t)$  and the cumulative residence time distribution  $F(t)$  in the lab scale extrusion equipment at different flow rates.

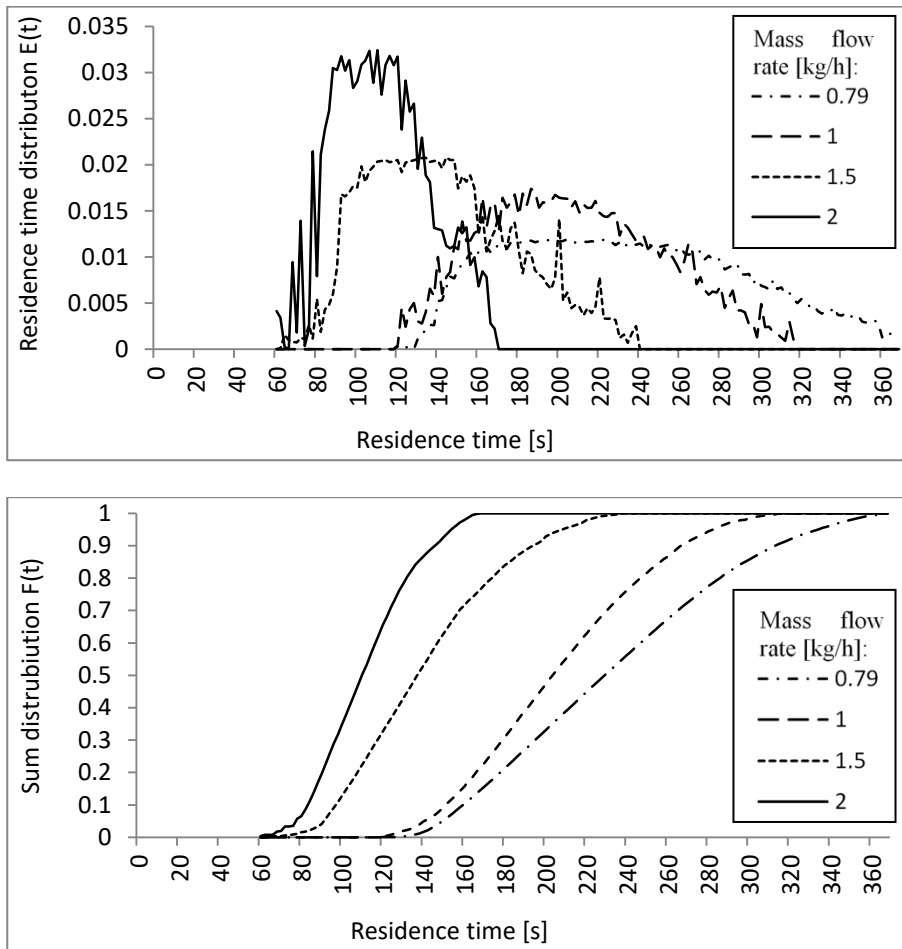


**Figure 60:** Residence time distribution function (a) and sum function (b) of pea protein isolate (PPII) in the laboratory extrusion equipment. Extrusion operating conditions were set at  $150 \text{ min}^{-1}$ ,  $140^\circ \text{C}$  cooking temperature, 60% w.b. moisture content (w/w) and mass flow rates between 0.79 and 2 kg/h.

The residence time distribution curves in Figure 60a represent the variation of the tracer concentration at the exit of the cooling die at varying mass flow rates. It can be seen that for a given rotational screw speed, a higher flow rate resulted in a sharper residence time distribution and smaller time delay as well as an increase in color intensity as indicated by the peak height of the curves. At a low mass flow rate of 0.79 kg/h, the first color appearance was observed around 130 seconds after the color was injected into the extruder barrel until the color disappeared around 360 seconds after injection. Increasing the mass flow rate to 2 kg/h reduced the residence time as indicated by a first color appearance around 60 seconds after the color was injected into the extruder barrel until the color disappeared 170 seconds after injection. Furthermore, data shows that the shape of the distribution curves becomes narrower with increasing flow rate. This can be attributed to the relationship between flow rate and

filling degree in the extruder. A lower degree of fill during processing usually results in a higher axial mixing rate, while a higher degree of fill reduces the mixing efficiency (Guy 2004). These observations are in accordance with previous studies. Lafleur and Vergnes (2014) obtained the distribution curves for different flow rates and screw rotation speeds and observed that when the flow rate increased at a constant rotational screw speed, the residence time distribution moved towards shorter times and became narrower. When the screw speed was increased at a constant flow rate, a shift in the curves towards a shorter time was observed without a noticeable change of the shape of the curve.

The cumulative residence time distribution  $F(t)$  represents the accumulated quantity of tracer at the exit at a given time. Based on  $F(t)$ , the experimental mean residence time  $\bar{t}_e$  was calculated for different mass flow rates (Figure 61).

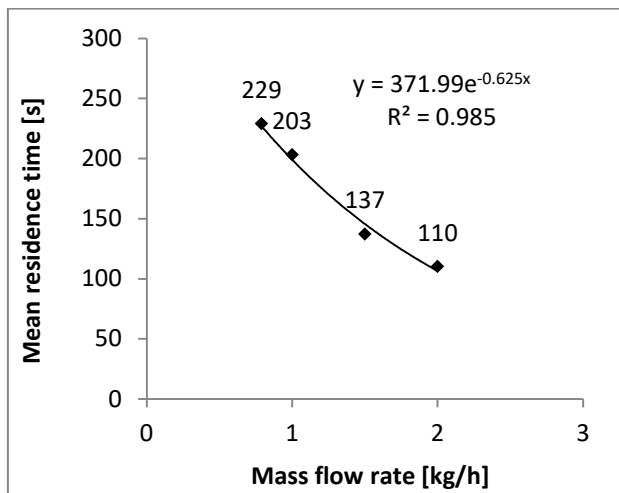


**Figure 61:** Mean residence time of pea protein isolate (PPI1) in the laboratory extrusion equipment as a function of flow rate. Extrusion operating conditions were set at  $150 \text{ min}^{-1}$ ,  $140 \text{ }^\circ\text{C}$  cooking temperature and 60% w.b. moisture content (w/w).

With increasing mass flow rate, the mean residence time decreased from 229 seconds at  $0.79 \text{ kg/h}$  to 110 seconds at  $2 \text{ kg/h}$ . An inverse correlation between the mean residence time and the mass flow rate was observed, that means that the higher the flow rate, the lower the mean residence time and the lower the thermal energy input during processing. These observations are in accordance with previous studies. Kao and Allison (1984) studied the effect of throughput, screw rotational speed, barrel temperature and screw configurations on the residence time distribution of a styrene-based copolymer in a corotating twin screw extruder and reported that throughput had the largest effect on the RTD, followed by the screw configuration and the screw rotational speed while barrel temperature had no effect.

They suggested that with increasing flow rate, the axial velocity and the filling degree of the screws increase which results in a decrease of the mean residence time.

An important factor to consider during discussion of the residence time is the filling degree in the screw channel as it affects shear forces, the amount of mixing of the material being processed, thermal energy transfer from the barrel into the material as well as the residence time (Guy 2004). In order to estimate the degree of fill along the extruder barrel length, the extruder was stopped after the extruder reached steady state conditions and the distribution of the extruded material inside the barrel was visually examined. The method is similar to the screw pull and carcass analysis technique, which has been used to visualize the flow of solid pellets and melting in twin screw extruders (Manas-Zloczower 2012) (Figure 62).

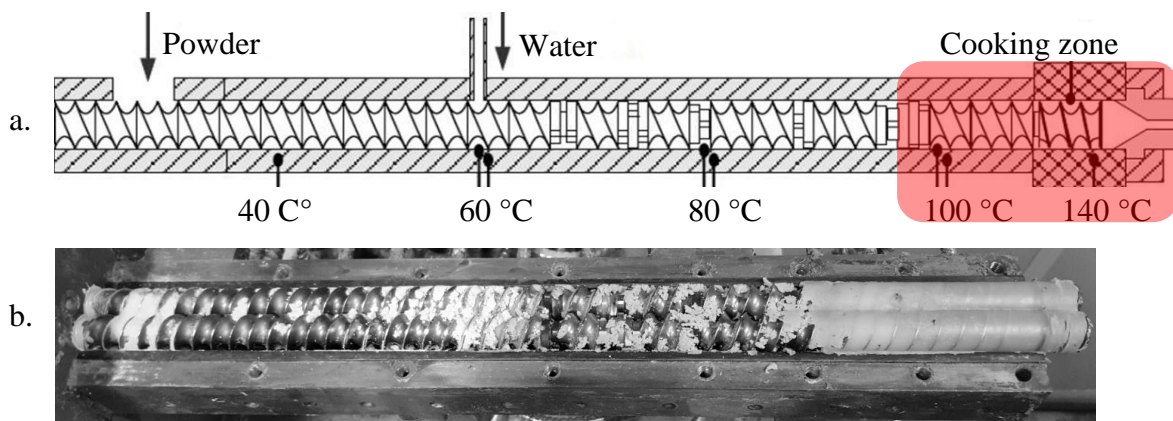


**Figure 62:** (a) Schematic screw profile showing the screw configuration and the heating profile. (b) Image of exemplary distribution of extruded material inside the barrel of the lab scale extruder after extrusion of pea protein isolate (mass flow rate 1kg/h, rotational screw speed  $150 \text{ min}^{-1}$ , cooking temperature  $140 \text{ }^{\circ}\text{C}$ , 60% w.b. moisture content (w/w)).

The image in Figure 62b shows that the screws were partially filled in the powder conveying zone and the mixing zone where water was injected, which means that the screw channel is not pressurized. In the cooking zone with temperatures  $> 100 \text{ }^{\circ}\text{C}$ , the screws were fully filled with extruded material having a cohesive gelled appearance. Furthermore, the cooling die channel was fully filled with extrudate upon disassembling. As previously reported by Mercier *et al.* (1989), much of the channel of twin screw extruders is not completely filled, unlike the screw channel in single screw extruders. This is attributed to the restricted flow by the screw configuration (mixing elements, die) which causes the material to accumulate upstream, creating a fully filled cooking section.

The screw filling degree was calculated as described in 3.2.1.6 varying the mass flow rate (Table 24).

**Table 24: Screw filling degree in the cooking zone of the lab scale extruder as a function of flow rate. Extrusion conditions were: rotational screw speed 150 min<sup>-1</sup>, cooking temperature 140 °C, 60% w.b. moisture content (w/w).**

Mass flow rate [kg/h]	Filling degree [%]
0.79	98.4
1	98.1
1.5	98.5
2	97.3

The table shows that the screw filling degree in the cooking zone was between 97 and 99% with regard to the free screw volume.

In partially filled screw sections, the residence time depends only on screw pitch and rotational screw speed, while in fully filled screw sections it is dependent on the flow rate (Kohlgrüber 2012). Therefore, it is possible to calculate the theoretical mean residence time in the fully filled zones of the extruder using the free volume in these sections and the flow rate. It should be noted, however, that a number of assumptions and simplifications have to be considered such as the assumption of an incompressible Newtonian fluid, a constant free screw volume and a steady isothermal operation due to the complexity of screw geometry and rheological behavior of food materials (Kao and Allison 1984).

Based on the dimensions of the rectangular cooling die used in this experiment, the theoretical mean residence time was calculated in both the extruder and the die (Table 25).

**Table 25: Experimental mean residence time in the laboratory extruder equipment from feed hopper to die exit at constant rotational screw speed of 150 min<sup>-1</sup>. The theoretical mean residence time in the fully filled cooking zone and the die was calculated using the free volume and the flow rate.**

Flow rate [kg/h]	Mean residence time [s]			
	Experimental*	Theoretical		
	Extruder barrel + die	Die	Cooking zone	Partially filled barrel
0.79	229	16	87	126
1	203	12	69	122
1.5	137	8	46	83
2	110	6	35	69

\* = experimentally measured residence time using a color tracer. Calculations based on a number of assumptions and simplifications such as the assumption of an incompressible Newtonian fluid, a constant free screw volume and a steady isothermal operation as previously described by Kao and Allison (1984).

The time a particle was moved through the laboratory extrusion equipment was between 110 and 229 seconds on average, depending on the flow rate. The calculated mean residence time in the cooking zone was between 35 and 87 seconds and in the cooling die between 6 and 16

seconds, respectively. Although an uncertainty in the theoretical residence time should be noted with regard to the simplification of the material properties, the data can help to estimate the extend of thermal energy intake of a particle in the cooking zone of the extruder. As for temperature-induced changes in the viscosity of the mass, Lafleur and Vergnes (2014) observed that the viscosity of a very fluid polymer had the same mean residence time as a very viscous one and did not affect the mean residence time at a constant flow rate. Similar findings were described by Leeb et al. (2008) who studied the residence time distribution during thermoplastic starch extrusion and found that increasing the water content - and therefore reducing the viscosity - had little effect on the mean residence time, but resulted in a narrower distribution curve.

Furthermore, the mean residence time in the pilot-scale extruder was evaluated at a constant flow rate of 10 kg/h at 180 min<sup>-1</sup> rotational screw speed. Based on the dimensions of the cooling dies used for offline flow visualization (section 4.3.5), the residence time was calculated in both the extruder and the die. It should be noted that, in contrast to the laboratory extruder, it was not possible to investigate the degree of fill inside the pilot scale extruder barrel because the carcass of residual protein material around the screws would disintegrate upon pulling the screws out of the barrel.

**Table 26: Experimental mean residence time in the pilot-scale extrusion equipment from feed hopper to die exit depending on the dimensions of the cooling die at 180 min<sup>-1</sup> rotational screw speed. The theoretical mean residence time in the fully filled cooling die was calculated using the free volume and the flow rate.**

Height [cm]	Volume [cm <sup>3</sup> ]	Cross sectional area [cm <sup>2</sup> ]	Mean residence time* [s]	Residence time die [s]	Residence time extruder [s]
0.5	120	2	97	47	50
1	240	4	150	94	56

\* = experimentally measured residence time using a color tracer.

The mean residence time of the protein-water-mixture in the extrusion equipment using a narrow cooling die (height 0.5 cm) was 97 seconds and 150 seconds using a larger cross section of the channel (height 1 cm). As expected, a smaller die channel increased the flow velocity inside the die which in turn reduced the residence time in the cooling section. Additionally, the residence time in the different sized extrusion equipment was compared under the extrusion conditions used for most of the experiments in this work (Table 27).

**Table 27: Comparison of experimental mean residence time between laboratory and pilot-scale extrusion equipment. The theoretical mean residence time in the cooling die and in the extruder was calculated using the free volume of the respective equipment section and the flow rate.**

Equipment Size	Flow rate [kg/h]	Rotational screw speed [min <sup>-1</sup> ]	Mean residence time* [s]	Residence time die [s]	Residence time extruder [s]
Laboratory scale	1	150	203	12	191
Pilot-scale	10	180	150	94	56

\*= experimental residence time measured using a color tracer

The comparison shows that the mean residence time in the laboratory extruder was longer compared to the larger pilot-scale equipment. Furthermore, it can be seen that extruded particles in the laboratory equipment spend the majority of their time – more than 3 minutes – in the extruder barrel and only little time (12 seconds) in the cooling die, while in the pilot scale equipment the opposite relation can be observed. These findings are limited to the specific processing conditions during the experiments and cannot be used to derive general assumption regarding scale-up of the process. For example, the design of the cooling die allows certain variations that would have an impact on the residence time distribution.

Up to now, literature offers relatively limited data on the extrusion time of vegetable materials (Moscicki 2011). However, knowledge about the mean residence time in the cooking zone of an extruder is of crucial importance for estimating the thermal energy input into the extruded mass that is required for the chemical reactions during protein texturization. The assessment of the residence time in the laboratory and pilot-scale equipment provided the basic understanding of the thermal history of particles for further investigations regarding fiber formations as well as protein-protein interactions.

### 4.3 Mechanical properties of high moisture extrudates

The microstructures of high moisture extrudates were visually examined using microscopic methods and compared to animal tissue with a focus on anisotropic structures. In order to quantify the formation of fibrous structures, the texture properties of high moisture extrudates were investigated by texture analysis as affected by the cooking temperature. This was achieved by evaluation of the cutting strength in longitudinal and transverse directions, with respect to the flow direction in the cooling die. Furthermore, the structure formation of the protein dispersion inside the cooling die was investigated by offline flow visualization.

#### 4.3.1 Visual microstructure and texture of extrudates and fibrous meat samples

Although texture properties and microstructure of texturized soy protein extruded at low moisture are well known, there is still little published data available for those extruded under high moisture conditions (Noguchi 1990; Thiebaud *et al.* 1996; Chen *et al.* 2010b). In addition, quantitative relationships among process parameters, product texture, and microstructure for high moisture extrudates based on pea protein have not been reported up to now. Thus, the objective of this section was to study the effect of the protein ingredients and extrusion parameters including cooking temperature, cooling temperature and moisture content on the fiber formation of high moisture extrudates. In order to validate the method of textural profiling for quantifying the fiber formation in extrudates, chicken and beef samples were used as an example for fibrous foods with anisotropic texture properties as described in section 3.4.2. The visible fibers in the meat samples are shown in Figure 45. As an example for foods without visible anisotropic structure, flat pasta was used and compared to extrudates (Figure 63).

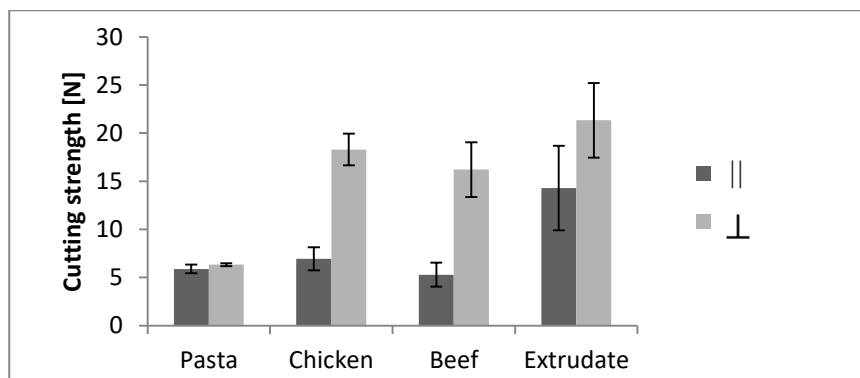
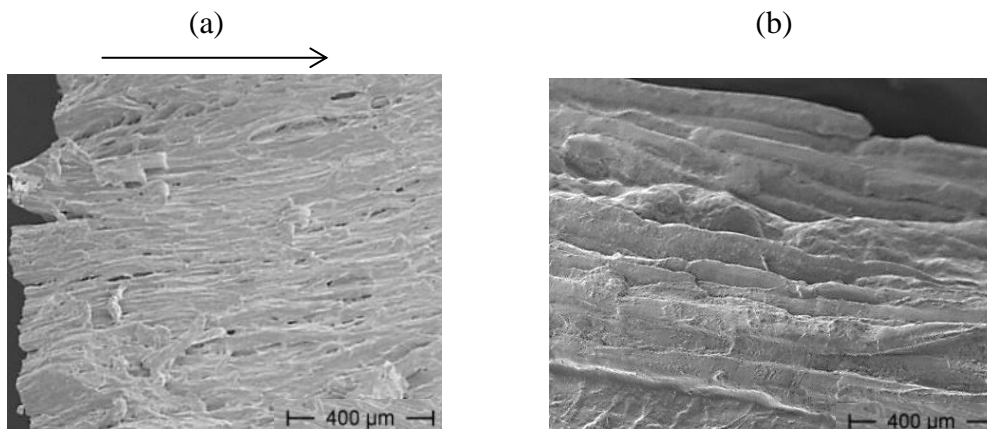


Figure 63: Cutting strength of different foods cut parallel to the visible fibers  $\parallel$  and cut perpendicular  $\perp$  to the visible fibers ( $n = 12$ ). Extrudates were extruded at 55% w.b. moisture content (w/w) and 140 °C cooking temperature. Mass flow rate was 1kg/h, rotational screw speed was 150  $\text{min}^{-1}$ , cooling die temperature was 80 °C.



The cutting strength of pasta was similar when samples were cut in orthogonal direction (texture analysis method described in section 3.4.2). In contrast, the meat and extrudate samples showed higher cutting strength when cut perpendicular to the visible fibers compared to the cutting strength parallel to the fibers which correlates with their anisotropic texture properties as shown in Figure 64. Similar texture properties were reported for other anisotropic foods such as mozzarella cheese (Ak and Gunasekaran 1997; Bast *et al.* 2015) or plant protein gels (Hartman 1978; Krintiras *et al.* 2014). Regarding the extrudate specimen in Figure 63, it should be noted that for texture analysis, a sample with characteristic fibrous structures was exemplary chosen.

Figure 64 shows the microstructure of high moisture extrudates and animal tissue samples (chicken breast) that were used for the textural profiling (sample preparation procedure described in section 3.4.1.1).



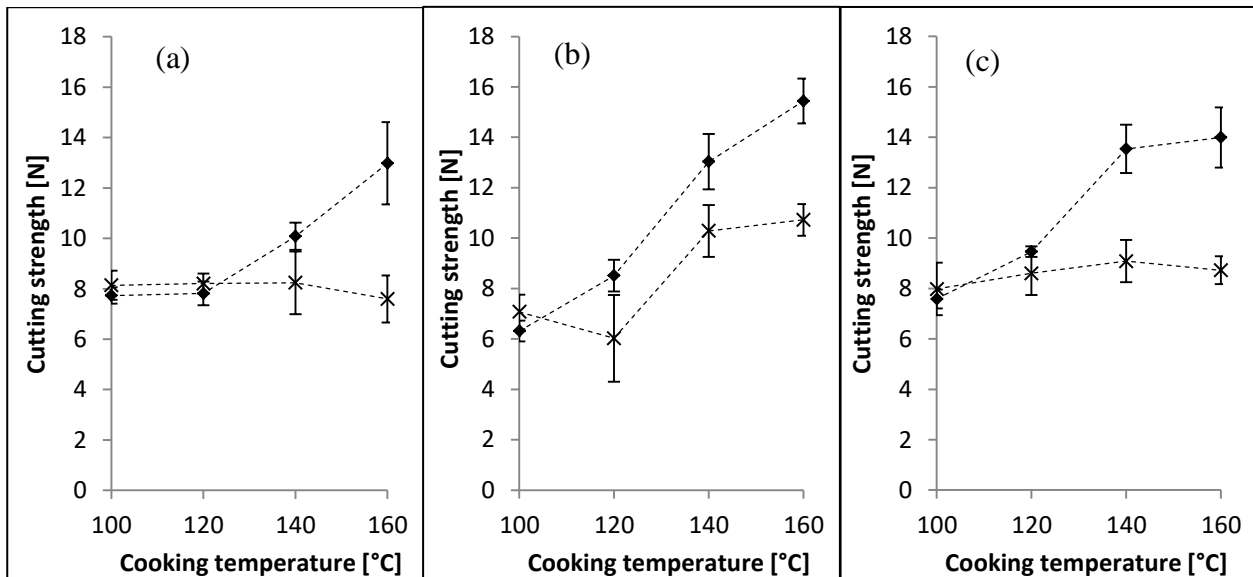
**Figure 64:** Scanning electron microscopic images of longitudinal sample sections of (a) extrudate (arrow indicates flow direction) and (b) chicken. Extrusion was performed using PPI 1 at 60% w.b. moisture content (w/w) and 140 °C cooking temperature. Mass flow rate was 1kg/h, rotational screw speed was 150 min<sup>-1</sup>, cooling die temperature was 80 °C.

Figure 64a shows the longitudinal cutting side of a sample extruded at 60% w.b. moisture content and 140 °C cooking temperature. Fiber structures are visible with diameters of about 50 μm that are aligned along the flow direction in the cooling die channel. In the chicken sample, longitudinal fiber structures with about 150 μm in diameter can be observed. These correspond to thin fibers typical for cooked chicken breast meat. The results show that the extrudates exhibit similar texture properties to meat in terms of fibrousness as evaluated by textural profiling and microscopy.

As described in 2.5.2, it is assumed that the generation of anisotropic properties from biopolymeric materials requires two thermodynamically incompatible phases (Tolstoguzov 1993). In the present study, it was observed that anisotropic fibrous structures could be generated by high moisture extrusion cooking using only pea protein isolate and water without the addition of any further ingredients. According to the “suspension model” proposed by Areas (Mitchell and Areas 1992), extrusion of a single component may yield small amounts of insoluble particulate material that act as a disperse phase in a continuous protein network, providing the breaking points for phase separation into filamentous structures. The generation of fibrous structures might be attributed to such a separation of a protein- and nonprotein-fraction during the texturization process, considering that the lipids- and ash content in the protein ingredients amounting to more than 10% of the dry mass (Table 15).

#### 4.3.2 Effect of protein ingredients and cooking temperature

The effect of cooking temperature on the cutting strength of extrudates made from pea protein isolates is shown in Figure 65a-c.



**Figure 65:** Cutting strength of extrudates cut in longitudinal direction ( $\ast F_L$ ) and cut in transverse direction ( $\diamond F_T$ ) with respect to the flow direction in the cooling die channel. Equal values ( $F_L = F_T$ ) indicate uniform texture with low material anisotropy and without fibrous texture, whereas  $F_L > F_T$  indicates predominantly transverse fibers and  $F_T > F_L$  predominantly longitudinal fibers. All determinations were performed with at least 12 replicates. Experiments were performed as a function of cooking temperature of PPI 1 (a), PPI 2 (b) and PPI 3 (c) at 55% w.b. moisture content (w/w). Mass flow rate was 1kg/h, rotational screw speed was  $150 \text{ min}^{-1}$ , cooling die temperature was  $80 \text{ }^\circ\text{C}$ . The lines connecting the data points are only to guide the eye. Modified from Osen *et al.* (2014), with permission of Elsevier.

At temperatures below 100 °C, the structure of the protein-water mixture was not yet generated and therefore cutting strength values are not shown within that temperature range. The individual protein ingredients as well as the cooking temperature significantly affected the extrudate texture, with a significant interaction among the factors ( $p < 0.05$ ). At low temperature (100 °C), both the longitudinal and transverse cutting strength were similar and in the range of 6-8 N. Increasing cooking temperature resulted in an increased transverse cutting strength whereas the longitudinal strength remained constant, except for PPI 2 where it increased from 7 to 11 N. This can be attributed to the formation of longitudinal fibrous structures. Although fiber formation was affected by both the cooking temperature and the protein ingredients used, the latter had only a minor effect. This is because the major difference between the protein ingredients, namely their functional properties, becomes less relevant at temperatures above the proteins' denaturation temperature. Similar results were previously reported by number of researchers. Noguchi (1990) extruded defatted soy flour under high moisture conditions and found that the longitudinal strength of extrudates was larger than the transverse strength. Thiebaud *et al.* (1996) studied the influence of process variables on the resistance to stretching of extrudates from a mix of fish surimi and soy protein concentrate and found that an increase in cooking temperature increased longitudinal tensile strength but did not affect the transverse tensile strength of extrudates. Chen *et al.* (2010b) showed that cooking temperature had a significant effect on tensile strength and degree of texturization during HMEC of soy protein isolate.

The positive correlation between cooking temperature and longitudinal fiber strength can be further seen in the microstructure of extrudates in the transverse direction Figure 66.

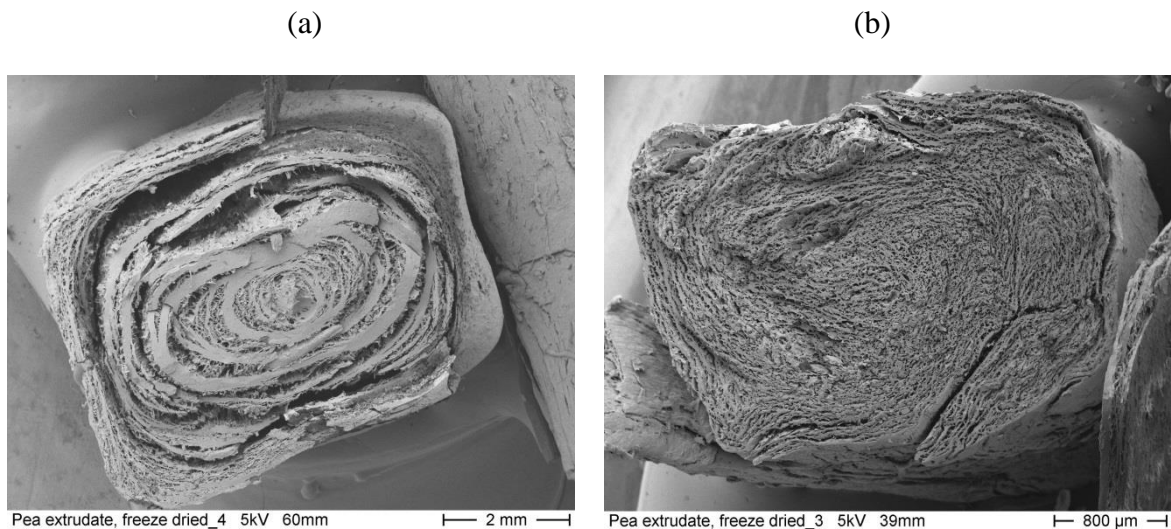


**Figure 66:** Scanning electron microscopic images of transverse sample sections of extruded PPI 1 with 60% w.b. moisture content (w/w) at (a) 160 °C (b) 120 °C extrusion temperature. Mass flow rate was 1kg/h, rotational screw speed was 150 min<sup>-1</sup>, cooling die temperature was 80 °C.

Samples extruded at high cooking temperatures (Figure 66a) displayed an elliptical pattern around the center of the sample in the transverse section. The friction induced by shearing inside the cooling die might have facilitated the formation of high- and low density material fractions causing rupture of the material in the vacuum chamber of the microscope. In contrast, the transverse section of a sample extruded at low cooking temperature (Figure 66b) did not exhibit elliptical patterns. Instead a continuous porous surface with an equal distribution of round cavities in a continuous protein network could be observed.

The effect of cooking temperature on the visual fiber formation is further shown in Figure 67.

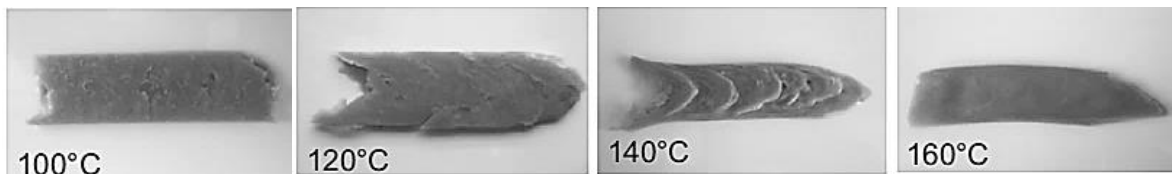


**Figure 67:** Images of samples of pea protein isolate (PPI 1) extruded at different cooking temperature at 55% w.b. moisture content (w/w). Mass flow rate was 1kg/h, rotational screw speed was 150 min<sup>-1</sup>, cooling die temperature was 80 °C. Reprinted from Osen and Schweiggert-Weisz (2016) with permission of Elsevier.

At extrusion temperatures below 120 °C, the samples exhibited a paste-like soft texture without any fibrous structures. With increasing barrel temperature the extrudates started to display multilayered structures with layers parallel to the die wall and fine fibers appearing upon tearing, especially at 140 °C. At temperatures as high as 160 °C, the samples became less fibrous with a smooth surface. Only upon tearing, predominant longitudinal oriented fibers appeared.

A similar relationship between fiber formation and cooking temperature was reported by Thiebaud *et al.* (1996). They proposed that the fiber formation requires a complete melting of the protein. At low temperature, the non-melted mix may be dispersed in between the forming fibers causing low rigidity and low anisotropy of the extrudate. With increasing temperature, the food mix would melt completely, thus reducing the viscosity of the melt causing fiber formation to appear. Upon further increasing the temperature, the reduction of the viscosity may induce laminar flow in the die that would result in longer fibers and corresponding high tensile strength.

In summary, the results indicate a minimal texturization temperature between 100 °C and 120 °C, with an optimum around 140 °C, while high temperatures (160 °C) produced samples that were already rigid and dense.

### 4.3.3 Specific mechanical energy

Evaluation of the specific mechanical energy, which is the amount of work input from driver motor into the extruded raw material, is a common method used in extrusion (Harper 1989). In the context of this thesis, taking the specific mechanical energy into consideration can help to monitor and compare changes in the proteinaceous matrix during extrusion texturization. Characterization of protein ingredients as discussed in chapter 4.1 showed that they possess different technofunctional properties. These in turn affected the network formation as indicated by their individual rheological behavior in chapter 4.2.

Yet, evaluation of the mechanical properties of fibrous extrudates in the previous section showed no difference between the protein ingredients. Upon thermal energy input in the extruder barrel, macromolecular transformations influence the rheological properties of the protein dispersion both in the extruder barrel as well as the cooling die. Therefore, the effects of the protein ingredients and extrusion conditions on network formation and final product texture should be reflected by their influence on extruder responses such as motor torque, die pressure and specific mechanical energy.

The effect of raw material and cooking temperature on specific mechanical energy are shown in Figure 68.

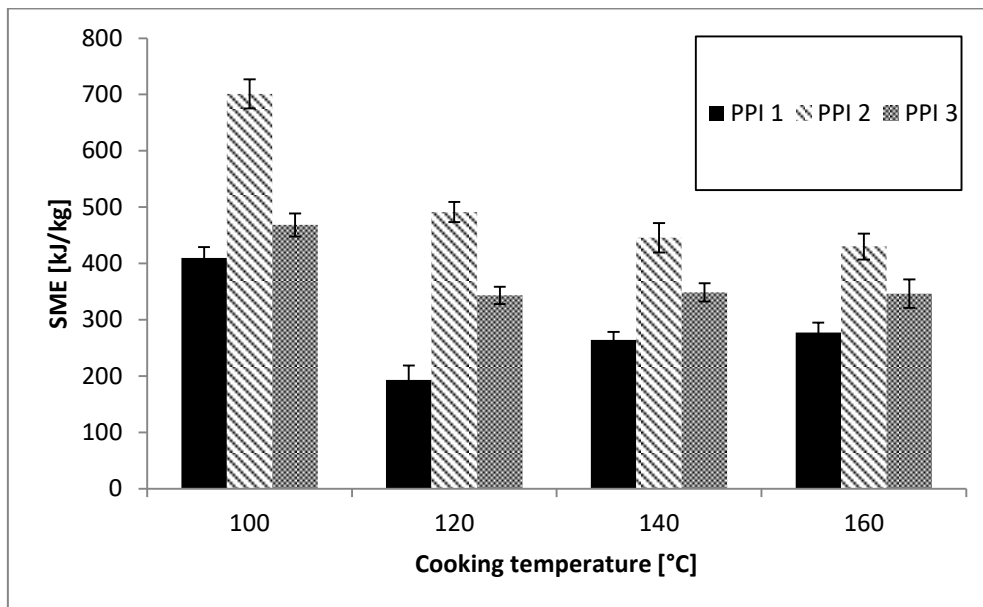


Figure 68: The effect of raw material (PPI 1, PPI 2 and PPI 3) and cooking temperature on specific mechanical energy during three consecutive experiments at a constant mass flow rate of 1 kg/h, rotational screw speed of  $150 \text{ min}^{-1}$  and 55% w.b. moisture content (w/w). Reprinted from Osen *et al.* (2014) with permission of Elsevier.

The specific mechanical energy was affected by the protein ingredients and cooking temperature with a significant factor interaction ( $p < 0.05$ ). The specific mechanical energy was highest at 100 °C among all proteins and decreased upon further heating to 120 °C, which is according to the general expectation that a higher temperature produces a lower viscosity resulting in a lower specific mechanical energy. With regard to the curve progressions during the initial start-up heating phase, it can be seen how a decrease in moisture content from 65% w.b. in Figure 51 to 55% w.b. in Figure 68 results in higher specific mechanical energy. Furthermore, above 100 °C extrusion temperature, the individual proteins showed slightly different dependencies between temperature and specific mechanical energy. The specific mechanical energy increased for PPI 1, decreased for PPI 2 and remained constant for PPI 3. Similar measurements are described in the literature. Lin *et al.* (2002) observed that during HMEC of soy protein isolate and starch at a 9:1 ratio and moisture contents of 60-70%, extruder responses revealed little changes at temperatures between 138 and 160 °C. They accounted protein denaturation and texturization to be responsible for affecting the temperature-viscosity relationship. Furthermore, Chen *et al.* (2010b) found that during HMEC of SPI at moisture contents of 60%, increasing cooking temperature from 140 to 160 °C decreased inline viscosity at the die. At the same time, specific mechanical energy decreased between 140 and 150 °C and increased at 160 °C.

In view of previous research studies, the relationship between cooking temperature and extruder responses is not only dependent on the fluid viscosity in the extruder barrel but also dependent on the friction during texturization inside the cooling die (Lin *et al.* 2000; Wang *et al.* 2001; Kang *et al.* 2007; Chen *et al.* 2010b). By comparison of the three protein ingredients regarding their extruder system responses, different specific mechanical energy at elevated temperature were observed, indicating protein interactions during the texturization process that will be addressed in chapter 4.3.5. These observation are in accordance with previous studies suggesting that the fiber formation results from several simultaneous phenomena taking place in the extruder barrel and in the cooling die, which are the type and intensity of interactions between food constituents (protein, carbohydrate, water, etc.), the extent of melting of the food mix as well as the flow regime inside the cooling die (Noguchi 1990; Thiebaud *et al.* 1996; Chen *et al.* 2010b).

#### 4.3.4 Effect of cooling die and moisture content

It was shown that the cooking temperature affected the fiber formation during high moisture extrusion. Accordingly, it could be inferred that the temperature during cooling would further affect the viscosity of the fluid, the flow regime and concurrently fiber formation. Hence, the effect of the cooling temperature on the cutting strength of extrudates was evaluated as a factor of cooking temperature (Figure 69).

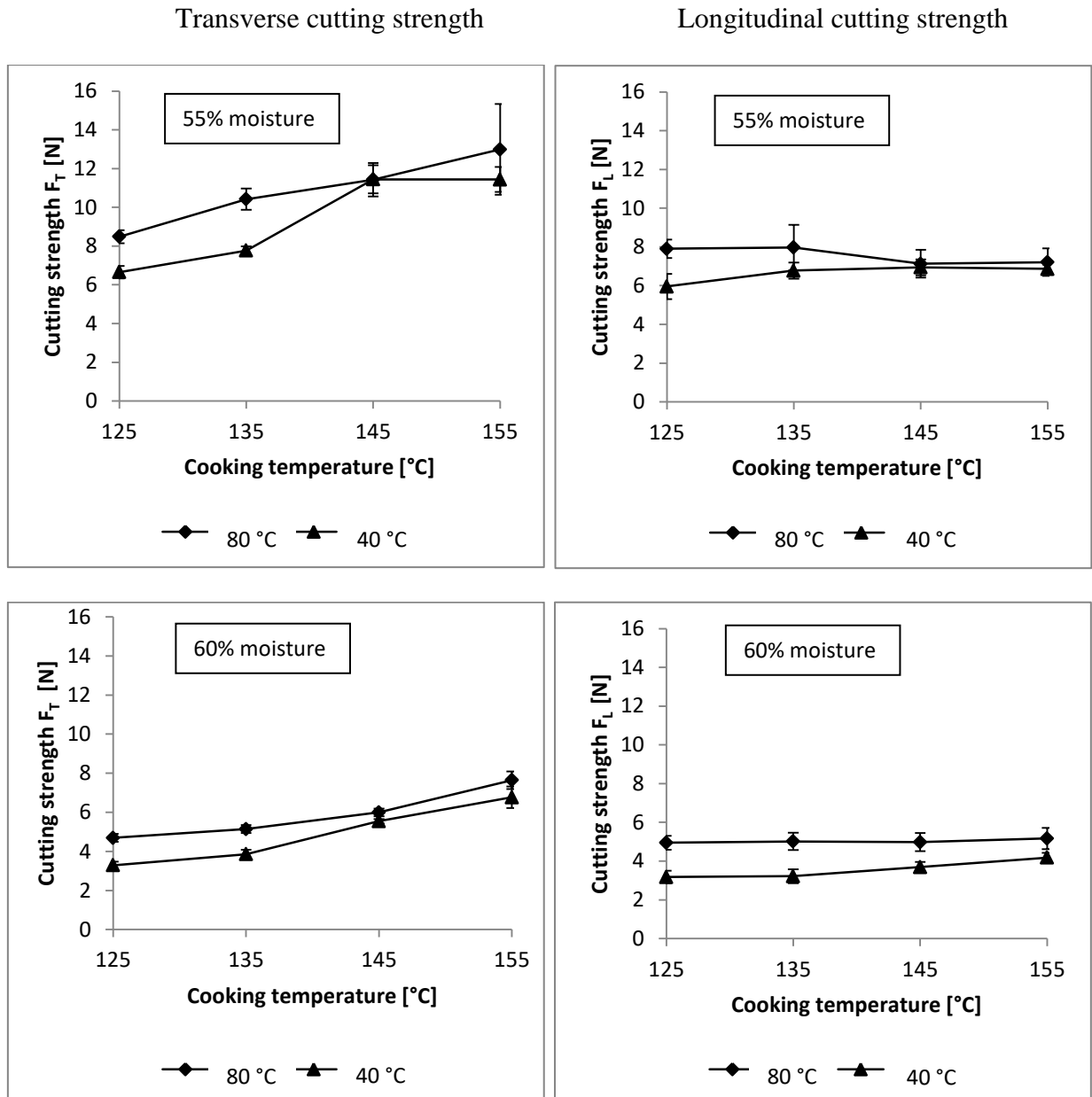


Figure 69: Effect of cooling die temperature (80 °C, diamond symbol; 40 °C, triangle symbol) and w.b. moisture content (% w/w) on cutting strength of extrudates cut in transverse direction ( $F_T$ ) and cut in longitudinal direction ( $F_L$ ) with respect to the flow direction in the cooling die channel. Equal values indicate uniform texture with low material anisotropy and without any fibrous texture, whereas  $F_L > F_T$  indicates predominantly transverse fibers and  $F_T < F_L$  predominantly longitudinal fibers. Evaluation as a function of moisture content and cooking temperature. Mass flow rate was 1 kg/h, rotational screw speed was 150  $\text{min}^{-1}$ .

The temperature of the cooling die as well as the moisture content affected the extrudate texture. The cutting strength of extrudates with 55% moisture content was in the range of 6 - 12 N. Increasing the moisture content reduced the cutting strength of extrudates to 3 – 8 N. Similar results were reported by several authors (Thiebaud *et al.* 1996; Lin *et al.* 2002; Chen *et al.* 2010b). They suggested that increasing the protein concentration increased the bonding sites for protein crosslinking resulting in higher rigidity of the extrudates.

Regarding the effect of the cooling die temperature on texture, Figure 69 shows that higher cooling die temperatures led to an increase in the cutting strength of specimen in both directions. Samples extruded using a die temperature of 80 °C exhibited higher resistance to cutting compared to samples extruded at 40 °C. One explanation could be that the higher die temperature allows the product to cool and solidify slower. Hence, there is more time for the product to texturize, which could lead to higher cutting strengths. This is in accordance with Alvarez *et al.* (1990).

In summary, it was shown in the previous section that the cooking temperature, the moisture content and the temperature of the cooling die affect the fiber formation during high moisture extrusion as indicated by cutting strength of extrudates in longitudinal and transverse direction. Similar observations were described in previous studies (Noguchi 1990; Thiebaud *et al.* 1996; Lin *et al.* 2000; Lin *et al.* 2002; Chen *et al.* 2010b). In order to explain the appearance of predominantly longitudinal oriented fibers with increasing cooking temperature, they suggested a concept that takes into account the flow properties during solidification in the cooling die. It was proposed that the reduction of the viscosity at high cooking temperatures would induce laminar flow in the die that would result in longer fibers and corresponding high longitudinal tensile strength. As described by Akdogan (1999), the temperature and the corresponding viscosity of the fluid is lowest at the cooled die wall and highest at the center of the die channel, which considerably affects the flow properties of the fluid in the die channel. Bounie and Van Hecke (1997) presented a model for a parabolic velocity profile in a cooled die channel as affected by the viscosity (Figure 70).



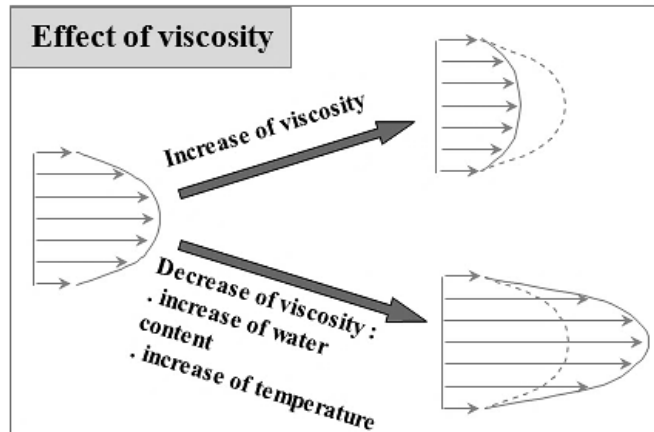


Figure 70: Effect of process parameters on the velocity profile of a non-Newtonian protein fluid in a cooled die channel. Top right: flat parabolic velocity profile. Bottom right: extended velocity profile (Bounie and Van Hecke 1997).

The figure shows that the increase of viscosity results in a flat velocity profile while the reduction of viscosity e.g. by increase of water content and/or cooking temperature has the opposite effect, resulting in an extended velocity profile. According to Bouvier and Campanella (2014), the shearing inside the die channel then facilitates the development of flow lines or lamellae within the melt. Upon further cooling, the melt changes from a liquid to a gelled state allowing fiber formation to occur.

#### 4.3.5 Offline flow visualization in the cooling die

The flow properties of the protein mass in the cooling die are clearly complex and a direct investigation inside the cooling die during processing is difficult (Bouvier and Campanella 2014). Visual assessment of gelled samples from inside the cooling die could assist in a better understanding of the complex fiber formation process and concerted adjustment of the process. Continuous process visualization has been applied in plastic extrusion to study the dynamics of melting, mixing and reactions during twin screw extrusion. Experimental process visualization methods developed include on-line visual observation by a glass window mounted through the barrel, in situ sample collection and offline sample analysis, model fluid extrusion and simulation. One early visualization method is the screw pull and carcass analysis technique, which has been used to visualize the flow of solid pellets and melting in twin screw extruders (Manas-Zloczower 2012).

In this section, the concept of offline flow visualization is applied on extruded samples from inside the cooling die in order to provide insights into the flow properties in the cooling channel. Due to the limited sample size from the laboratory extruder, the pilot scale extruder

equipped with an easy-to-open cooling die was used in order to generate extrudate samples large enough for offline visual and textural evaluation. In contrast to extrusion experiments on laboratory scale, it was found that high moisture extrusion on the pilot scale equipment using pea protein isolate was inherently difficult in terms of process fluctuations. These fluctuations led to irregular flow properties in the die channel as well as irregular texture properties. The process fluctuations might be attributed to the low viscosity of the pea protein isolate and a narrow process window using the pilot-scale extruder. As previously reported by Cheftel *et al.* (1992), it is relatively easy to extrude and texturize soy protein concentrate (64% protein in dry matter) but difficult to texturize soy protein isolate (84% protein in dry matter). They suggested that the use of non-protein ingredients with a high water binding activity e.g. insoluble fiber or starch can assist a laminar flow and facilitate the formation of anisotropic structures as addressed in chapter 2.5.2. Since the objective of this section was to investigate the flow visualization in the cooling die, it was fundamental to achieve constant flow properties and produce extruded samples with distinct anisotropic structures. Therefore, soy protein concentrate (Alpha 10 IP, Solae, USA) and defatted soy flour (Supro TB 200, Solae, USA) was used during pilot-plant trials instead of pea protein isolate as a model formulation.

In a first experiment, a dead-stop method as described in section 3.2.2.4 was conducted after a color tracer was visible in the extrudate at the cooling die exit. Figure 71 shows a stained extrudate that was removed from the inside of the cooling die after the extruder was stopped.

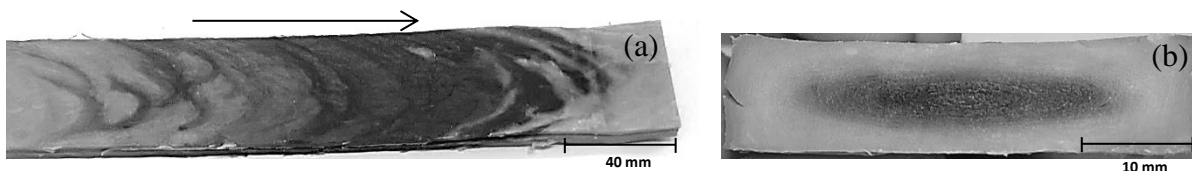


**Figure 71:** Extrudate stained with color tracer carmine. (a) top view of longitudinal sample section (arrow indicates flow direction) and (b) an elliptical color profile (front view, transverse sample section). Extrusion conditions of soy protein concentrate were: 55% w.b. moisture content (w/w), 160 °C cooking temperature, mass flow rate 10 kg/h, rotational screw speed 180 min<sup>-1</sup>, cooling die temperature 80 °C.

The stained sample in Figure 71a shows patterns which resemble parabolic structures with a clearly visible lane separation between the unstained sample and the first color appearance at the right end of the sample. Instead of being centered on the axial centerline as expected for laminar flow, parts of the visible stained patterns were distributed in the transverse direction. This could be attributed to the pulsation from the screws and temporary irregular conveyance of the fluid, especially in the entrance region of the die channel. Despite these deviations from constant flow properties, the patterns correspond to the velocity profile of a protein melt in a cooled die channel as shown in Figure 70. The color distribution in the corresponding front

view in Figure 71b shows elliptical patterns around the center of the sample. These observations infer that the visible pattern in the stained sample represents an image of the solidified velocity profile inside the cooling die at the moment the extruder was stopped. As expected, this indicates a maximum flow velocity in the center of the die channel that decreased towards the cooled die wall.

In order to further characterize the flow behavior of the fluid in the die channel, the residence time distribution (RTD) was evaluated. This is a common experimental method to investigate mixing in a complex flow field in the extruder by means of the time history of particles in the flow system (Stevens and Covas 1995). RTD curves were obtained after manual impulse injection of a color tracer into the feeding zone of the extruder and the color intensities of the extruded samples were analyzed spectrophotometrically according to the procedure in section 3.2.1.7. Figure 72 shows the residence time distribution curve  $E(t)$  and the cumulative residence time distribution  $F(t)$  in the pilot scale extrusion equipment using dies with different lengths (30cm, solid line, 60 cm dashed line) to evaluate the distribution of the flow velocities inside the cooling die.

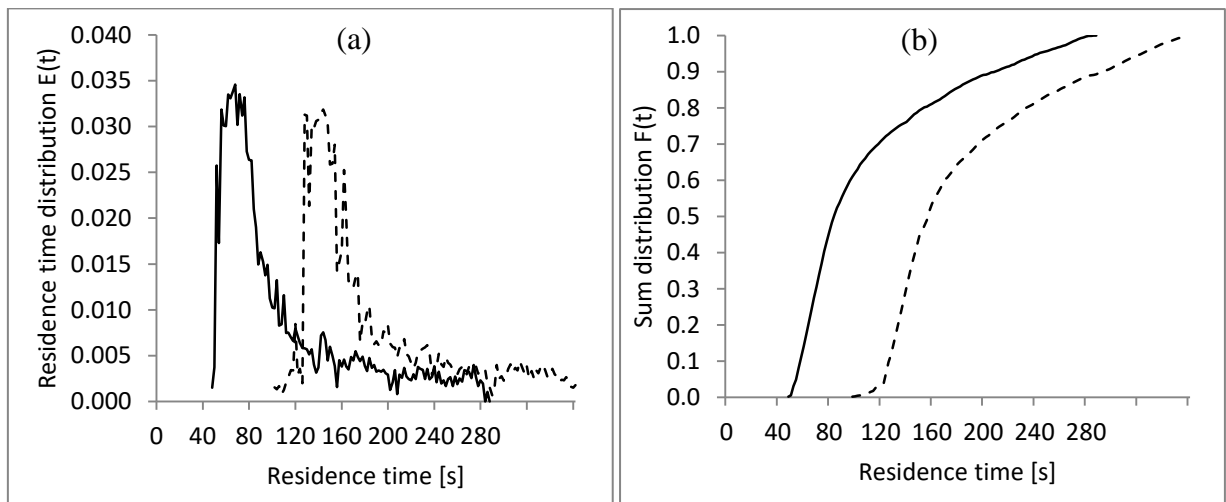


**Figure 72: Residence time distribution function (a) and sum function (b) in the pilot scale extrusion equipment using a cooling die with a length of 30 cm (solid line) and 60 cm (dashed line). Extrusion conditions of soy protein concentrate were: 55% w.b. moisture content (w/w), 160 °C cooking temperature, mass flow rate 10 kg/h, rotational screw speed 180 min<sup>-1</sup>, with water at a flow rate of 3.4 l/min at 80 °C as a cooling medium for the cooling die.**

In both experiments, the extruded samples exhibited a rigid elastic network upon exiting the cooling die, similar to the stained samples shown in Figure 71. The first color appearance in the short die (single segment,  $L = 30\text{cm}$ ) was observed after 52 seconds and after 100 seconds using the long die (two segments,  $L = 60\text{cm}$ ), respectively. The mean residence time, represented by the time when 50% of the colorant left the cooling die, was 86 seconds in the

short and 160 seconds in the long die. In contrast to the effect of mass flow rate on the residence time distribution functions in the laboratory extrusion equipment in Figure 60, the shape of the RTD curves in Figure 72 were similar in the short and the long die channel.

In the study of continuous flow systems, measurement and analysis of residence time distribution has been applied to provide insights into the flow patterns. It is possible to describe the mixing within the extruder using average total strain applied to the material during its passage through the extruder (Harper, 1981) as well as the estimation of the extent of reactions (e.g., protein denaturation, starch gelatinization) from characteristics of the distribution (Levenspiel, 1972). With regard to the flow properties in the cooling die, the observation of similar RTD curves indicate that the flow velocity profile was fully developed at the point where the material exits the first die segment (0-30cm) and that there were no major changes in the flow velocity profile during the passage through the second die channel (30-60cm). Hence, the shape of the curve could be attributed to the axial mixing in the extruder barrel rather than a change in the velocity profile in the cooling die channel.

As the fluid is exposed to shear stress inside the cooling die, it could be assumed that the texture properties as well as the anisotropic structure changes along the die channel. Therefore, the anisotropic structures of specimen from inside the die were evaluated at different axial positions in the die channel (from cooling die entrance to exit) by measuring the cutting strength of longitudinal and transverse fiber structures with respect to the flow direction. Texture analysis was performed after the extruder was stopped and the cooled samples were removed from inside the cooling die channel (Figure 73).

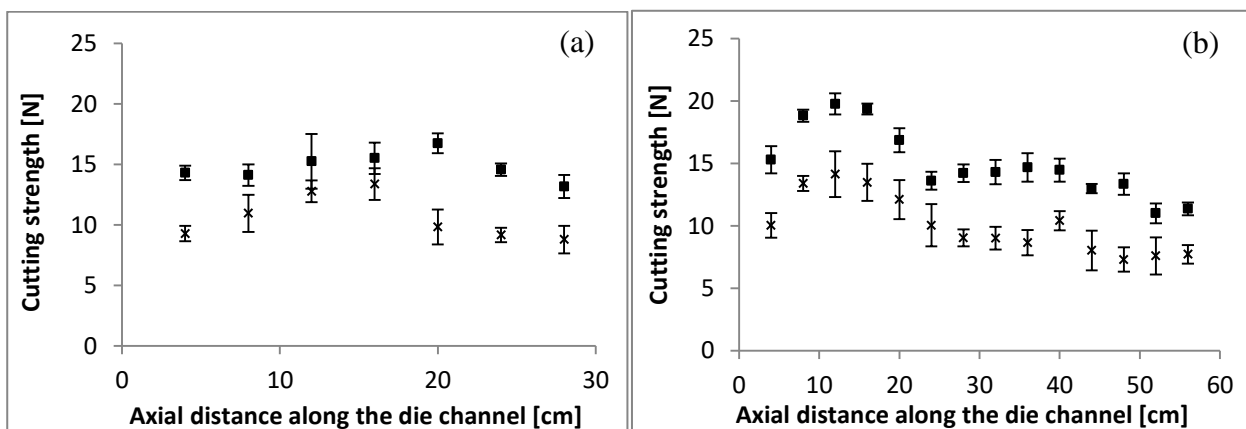


**Figure 73:** Cutting strength of extrudates cut in longitudinal direction ( $\times$ - $F_L$ ) and cut in transverse direction ( $\rightarrow$ - $F_T$ ) with respect to the flow direction in the cooling die channel with 5 mm (a) and 10 mm channel height (b). Samples were taken from different axial positions along the die channel. Equal values ( $F_L = F_T$ ) indicate uniform texture with low material anisotropy and without fibrous texture, whereas  $F_L > F_T$  indicates predominantly transverse fibers and  $F_T > F_L$  predominantly longitudinal fibers. Samples were removed from inside the cooling die channel after the extruder was stopped. Extrusion conditions of soy protein concentrate were: 55% w.b. moisture content (w/w), 160 °C cooking temperature, mass flow rate 10 kg/h, rotational screw speed 180 min<sup>-1</sup>, with water as a cooling medium for the cooling die at a flow rate of 3.4 l/min at 80 °C.

The results show that the transverse cutting strength was always higher than the longitudinal cutting strength which is indicative for longitudinal anisotropic structures. A height of the die channel of 5 mm resulted in slightly lower cutting strength values (Figure 73a) compared to a die channel height of 10 mm at similar positions inside the channel. These observations are in accordance with Noguchi (1990). They observed that the height of the cooling die channel considerably affects the texture formation under high moisture conditions. If the die channel is too narrow, the extruded products are fragile and possess low tensile strength. That means that decreasing the channel height results in increased shear stress of the protein dispersion during the passage through the die and, as a consequence, a reduction of the cohesive texture.

The data in Figure 73b also show a slight decrease of the cutting strength towards the end of the long die channel. As said before, this could be attributed to a reduced structural rigidity due to the increasing shear stress of the material with increasing die channel length.

In order to observe changes in the velocity profile along the cooling die channel, the visible anisotropic pattern in the solidified sample was investigated as described in chapter 3.4.1.2. The patterns were evaluated by measuring the axial length of visible fibers in samples with respect to the direction of extrudate outflow from the extruder. Samples were evaluated at different axial positions from inside the cooling die channel after the cooling die was disassembled. However, it should be noted that the high moisture extrusion process is frequently accompanied by minor process fluctuations resulting in various degrees of irregular structural patterns. As an example for constant process conditions with a laminar flow profile, Figure 74 exemplary shows the quantification of anisotropic structures of a sample from inside the cooling die.

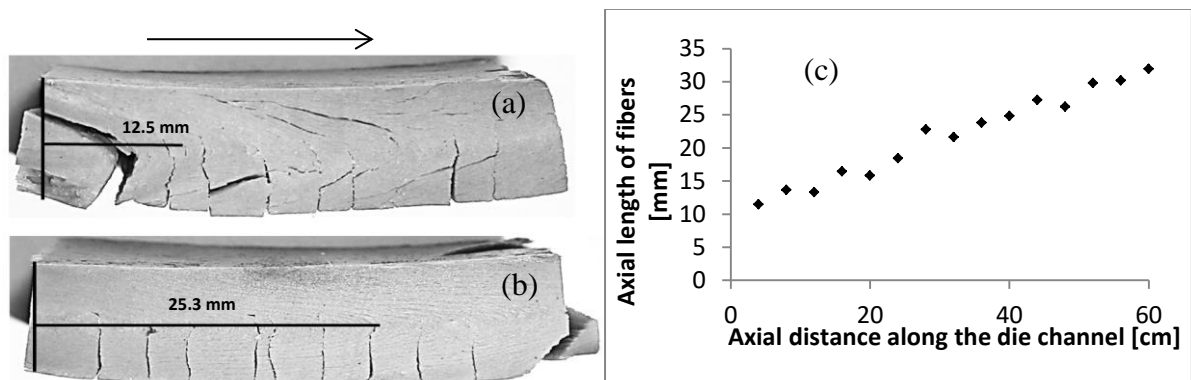
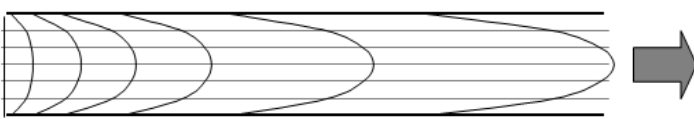


Figure 74: Side view of dissected extrudates from inside the die channel at different locations. Specimen (a) from the front part (die entrance) and specimen (b) from the end part (die exit) of the die channel. The arrow indicates flow direction. Axial length of fibers in samples (c) from inside the cooling die channel. Samples were taken from different axial positions. Extrusion conditions of soy protein concentrate were: 55% w.b. moisture content (w/w), 160 °C cooking temperature, mass flow rate 10 kg/h, rotational screw speed 180 min<sup>-1</sup>, with water as a cooling medium for the cooling die at a flow rate of 3.4 l/min at 80 °C.

The samples in Figure 74 were characterized by anisotropic structures. Sample a, which was taken from the front part of the die channel (die entrance), exhibited different patterns compared to sample b, which was taken from the end part of the die channel (die exit). The anisotropic pattern in sample b exhibited a stretched shape with longer axial fibers compared to sample a. Regarding Figure 74c, it can be seen that samples exhibited a constant increase in axial fiber length along the die channel from around 10 mm at the die front to 30 mm at the die exit. Following the hypothesis that the visible pattern in the sample represents an image of the solidified velocity profile inside the cooling die, the results suggest that the flow velocity profile changed continuously during the passage through the cooled die channel.

As the extruded mass did not expand upon exiting the cooling die, it can be assumed that the temperature of the fluid was below 100 °C at the die exit. Considering adequate heat transfer between the cooling medium and the extruded mass, the latter should have exhibited the same temperature as the cooling medium, which was set at 80 °C. This was confirmed by temperature measurement of the extrudate at the moment of exiting the die channel. As the anisotropic pattern of the specimen from inside the die channel continued to become more stretched towards the die exit as shown in Figure 74c, this indicates that extrudates showed textural deformation even at temperatures as low as 80 °C. These observations suggest that the extrudate was subjected to considerable shear forces during the passage through the die channel resulting in a constant change of the flow velocity profile. These observations are in accordance with the model of flow patterns of a protein during high moisture extrusion processing presented by Bounie and Van Hecke (1997).



**Figure 75: Schematic illustration of a constant change of the velocity profile of a protein melt at different positions inside a die channel from a flat velocity profile in the die front to an extended velocity profile (Bounie and Van Hecke 1997).**

In order to evaluate the effect of cooling die temperature on the visible flow pattern inside the die channel, another experiment was conducted using a longer die channel (90 cm) and a lower cooling temperature (60 °C). The same procedure for visual evaluation of the flow patterns was applied. Samples were evaluated at different axial positions from inside the cooling die channel after the cooling die was disassembled.

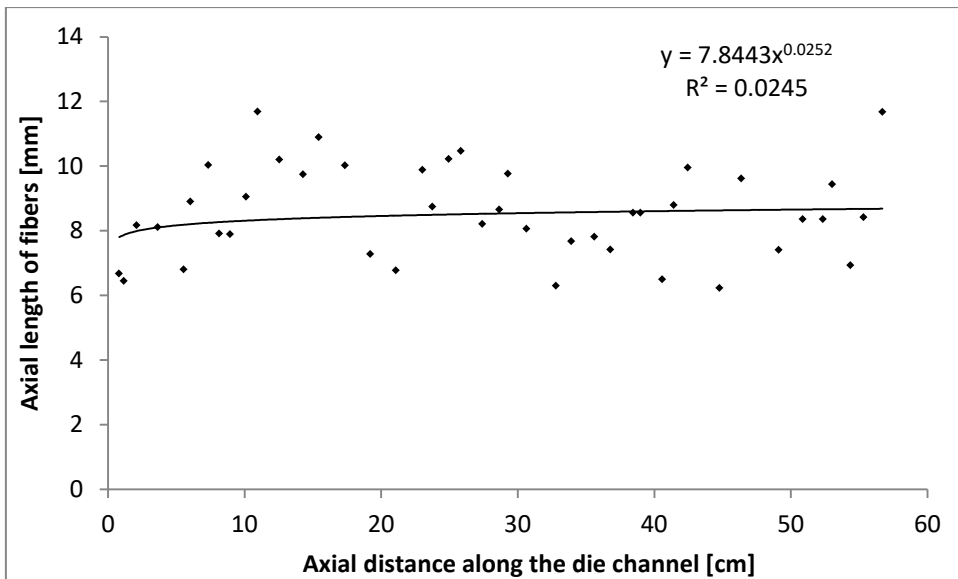
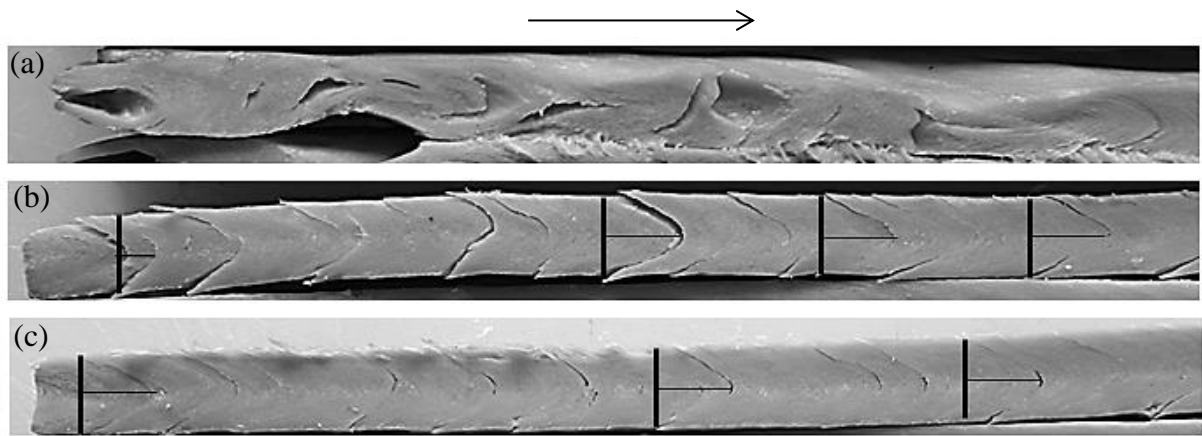


Figure 76: Side view of dissected extrudates from inside the die channel at different axial positions. Specimen (a) from the first segment (0-30 cm, no cooling) specimen (b) from the middle segment (30-60 cm) and specimen (c) from the third segment (60-90 cm, die exit) of the die channel. Temperature of segment 2 and 3 was set at 60 °C. Extrusion conditions of soy protein concentrate were: 55% w.b. moisture content (w/w), 160 °C cooking temperature, mass flow rate 10 kg/h, rotational screw speed 180 min<sup>-1</sup>.

The samples in Figure 76 were characterized by anisotropic structures. Sample (a) was taken from the front part (0-30 cm channel length, no cooling) of the die channel. It exhibited different anisotropic patterns compared to sample (b) and (c), which were taken from the middle and the end (30-90 cm channel length, 60 °C) of the die channel. The anisotropic pattern in sample (a) exhibited irregular patterns. The specimen from the middle part exhibited regular anisotropic patterns with increasing axial fiber length from ~ 6 mm to ~8 mm. In contrast to the previous observation of changing flow patterns along the die channel shown in Figure 74 and Figure 75, the anisotropic pattern remained constant in the remaining specimen (b) as well as sample (c).

Following the hypothesis that the visible pattern in the sample represents an image of the solidified velocity profile inside the cooling die, the results suggest that the changing flow

velocity profile was confined to the passage through the first cooled die channel, until a constant flow pattern was established (Figure 76b,c).

Several assumptions can be derived from these observations: The irregular flow patterns in the first die segment could be attributed to irregular flow velocities as a result of pulsation from the screws in the entry region of the die channel. In the region where the fluid was not cooled, a low viscosity could be expected that would further contribute to the observed irregular flow pattern. In the zone where the fluid entered the second cooled die segment, the flow profile changed into a regular pattern which could be explained by the effect of the cooling temperature on the rheological properties of the fluid. As shown in chapter 4.2, decreasing the temperature of a protein dispersion resulted in an increase of its viscosity as well as yield stress. Hence, cooling of the fluid in the die channel would increase viscosity and yield stress resulting in the visible flow pattern. The observation of a constant anisotropic pattern, as indicated by constant axial fiber contour in the middle part of the die channel, suggests that the fluid solidified as soon as the shear forces that would induce a change of the flow pattern were lower than the yield stress of the viscoelastic mass. Consequently, the flow properties changed to plug flow conditions during the remaining passage through the die channel until exiting the die channel. The effect of temperature-induced solidification of a proteinaceous mass on the flow properties in a cooling die channel was previously described by Bounie and Van Hecke (1997) (Figure 77).

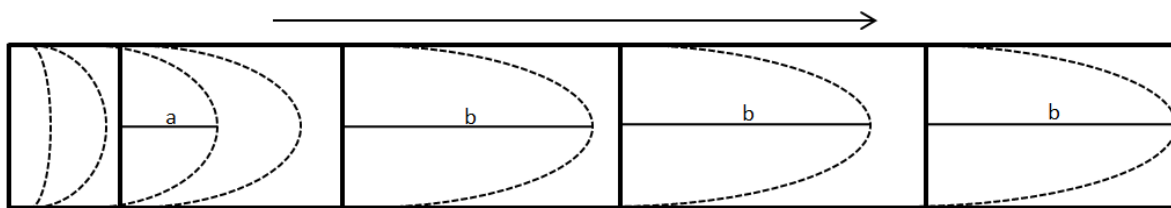


**Figure 77: Model for the effect of solidification on flow conditions of a non-Newtonian protein fluid in a cooled die channel (modified from Bounie and Van Hecke (1997)).**

The figure schematically shows a constant extension of the velocity flow profile (a) until the material solidifies and the flow profile of the solidified material changes to a plug flow with a constant flow velocity (b) over the transverse section of the channel.

In summary, these observations are in accordance with literature and provide further evidence for the importance of the thermal process conditions on the rheological properties and concomitantly the texture properties of the extruded mass during high moisture extrusion



cooking. Regarding the mechanism for structure formation discussed in chapter 2.5.2.1, the following assumption can be formulated: The shear forces during the temperature-induced solidification process in the cooling die channel could be one possible explanation for the anisotropy of the extrudates during high moisture extrusion cooking. In other words, the texture formation into anisotropic structures would be driven by solidification as the material is cooled under continuous shear stress. If shear forces were the only factor responsible for anisotropic structures in extrudates, the extrudate from the die exit should exhibit maximum anisotropy as it was subjected to the highest shear due to the long passage through the die channel. Consequently, the fluid protein dispersion from the entry region of the die should exhibit no anisotropy, because it was not subjected to any shear in the die channel during the cooling and solidification process due to the dead-stop operation.

However, the texture properties shown in Figure 73 as well as the axial fiber length in Figure 74 indicate that the material from inside the front part of the die exhibited anisotropic fibrous structures. Both samples exhibited anisotropic structures with visible fibers along the cutting side of the samples. Although the axial length of the fibers in the sample from the die front is lower than in the sample from the end part, it exhibits anisotropic fibrous structures. Regarding the observation above, it could be concluded that the fibrous structures of extrudates are affected not only by the shear forces between the die wall and the extruded protein in the cooling die during solidification, but also by the orientation of the biopolymer domains in the low-viscosity fluid state.

Similar observations were previously reported by Noguchi (1990). They observed anisotropic structures in injection-molded samples using defatted soy flour under high moisture conditions. When a previously heated protein melt was cooled under static no-shear conditions in an injection molding unit, the solidified product showed a continuous dense structure with coarse multilayers in the cross section that exhibited a higher tensile strength in the direction of the product flow, which is similar to the texture properties of extrudates. The appearance of the layered structures in the molded samples indicated that the protein molecules were aligned in the molten state during the passage in the molding unit forming predetermined breaking points during rupture. It was suggested that the proteins were first molten in the cooking zone, and then fused to each other to create a large elastic protein mass that is stretched in the extrusion direction to form the observed fibers (Noguchi 1990).

In summary, these examinations showed that the flow profile in the cooling die depends on a number of factors that need to be controlled in order to obtain the desired texture properties.

## 4.4 Protein reactions during high moisture extrusion

This chapter describes the bonding pattern of pea protein ingredients before and after high moisture extrusion cooking in order to provide an insight in the way proteins interact during HMEC and to further elucidate the formation of the fibrous meat-like texture.

Therefore two sets of experiments were conducted. First, the same protein ingredients that were characterized in the first chapter were used to investigate changes in the amino acid profile, molecular weight distribution as well as protein-protein interaction as a result of high moisture extrusion. Second, the effect of cooking temperatures between 40 °C and 160 °C on protein alteration of one exemplary protein ingredient (PPI 1) were investigated.

### 4.4.1 Amino acid composition

To monitor protein alterations inside the extruder, the amino acid profiles of the protein ingredients before and after extrusion were evaluated by reversed phase HPLC as described in chapter 3.4.4.1. Table 28 shows the amino acid composition of pea protein isolates (PPI) and extrudates (EPPI).

**Table 28: Amino acid composition of pea protein isolates (PPI) and extrudates (EPPI). Extrusion operating conditions were set at 150 min<sup>-1</sup>, 140 °C cooking temperature and 55% w.b. moisture content (w/w) (Osen *et al.* 2015).**

amino acid	Content [g/16g N]					
	PPI 1	PPI 2	PPI 3	EPPI 1	EPPI 2	EPPI 3
<b>Cys</b>	0.4±0.0	0.3±0.1	0.2±0.0	0.3±0.0	0.2±0.1	0.3±0.1
<b>Asn</b>	10.3±0.1	10.1±0.5	9.6±1.2	10.3±0.8	10.2±0.5	10.2±0.1
<b>Gln</b>	16.0±0.2	16.1±1.6	17.6±1.2	16.2±1.2	18.9±4.1	18.2±2.1
<b>Ser</b>	4.6±0.1	4.5±0.2	4.4±0.5	4.7±0.3	4.7±0.3	5.1±0.9
<b>Gly</b>	15.3±2.7	10.7±4.3	10.7±3.5	9.8±1.7	9.7±0.3	16.3±3.9
<b>His</b>	1.1±0.1	0.8±0.2	0.8±0.1	0.9±0.1	0.7±0.1	0.8±0.1
<b>Thr</b>	1.5±0.1	1.2±0.2	1.0±0.0	1.2±0.1	1.1±0.1	1.2±0.3
<b>Arg</b>	4.8±1.9 <sup>ab</sup>	3.2±0.5 <sup>a</sup>	2.9±0.2 <sup>a</sup>	4.2±1.8 <sup>ab</sup>	6.9±1.1 <sup>b</sup>	4.2±2.4 <sup>ab</sup>
<b>Ala</b>	2.2±0.2	1.6±0.2	1.4±0.1	1.7±0.2	1.4±0.3	1.6±0.3
<b>Tyr</b>	1.9±0.1	1.6±0.5	1.4±0.2	1.4±0.1	1.2±0.1	1.4±0.4
<b>Val</b>	2.6±0.2	2.3±0.5	1.8±0.1	2.1±0.2	1.8±0.3	2.2±0.5
<b>Phe</b>	2.7±0.2	2.2±0.4	1.8±0.1	2.1±0.3	1.8±0.4	2.1±0.4
<b>Ile</b>	2.2±0.2	2.0±0.5	1.5±0.1	1.8±0.2	1.5±0.3	1.8±0.4
<b>Leu</b>	4.5±0.3	3.8±0.6	3.1±0.3	3.6±0.5	3.1±0.6	3.5±0.7
<b>Lys</b>	2.8±0.2	3.3±1.5	2.1±0.1	2.4±0.3	2.1±0.3	2.6±0.5
<b>Pro</b>	4.1±0.8	5.1±1.3	4.5±0.7	4.0±0.4	4.0±0.4	4.6±1.5

Four measurements were performed for each sample. Different letters in the same row indicate significant differences ( $p < 0.05$ ).

The amino acid contents of the samples were in the same range reported by Holt and Sosulski (1979) and Leterme *et al.* (1990). Extrusion of pea protein isolates under high moisture conditions did not result in a significant reduction of amino acids ( $p > 0.05$ ). Previous studies have reported that thermoplastic extrusion under high temperature conditions can reduce the availability of amino acids through Maillard reactions, in particular lysine as the most reactive protein-bound amino acid due to its free  $\epsilon$ -amino group (Björck and Asp 1983; Björck *et al.* 1984). The loss of amino acids corresponds to the intensity of the extrusion cooking process e.g. higher cooking temperature, lower feed moisture and higher residence time (Noguchi *et al.* 1982; Björck and Asp 1983). As previously reported, the feed moisture has a protective effect on the amino acid loss in extrusion cooking under high moisture conditions as the moisture reduces the shearing and dissipation of mechanical energy in the extruder (Noguchi *et al.* 1982; Björck and Asp 1983). For instance, MacDonald *et al.* (2009) evaluated the nutritional value of extruded soy protein isolate and showed that the high moisture extrusion cooking process (160 °C and 60% moisture) did not cause a reduction in protein digestibility.

Figure 78 shows the effect of cooking temperature on the amino acid composition of PPI 1.

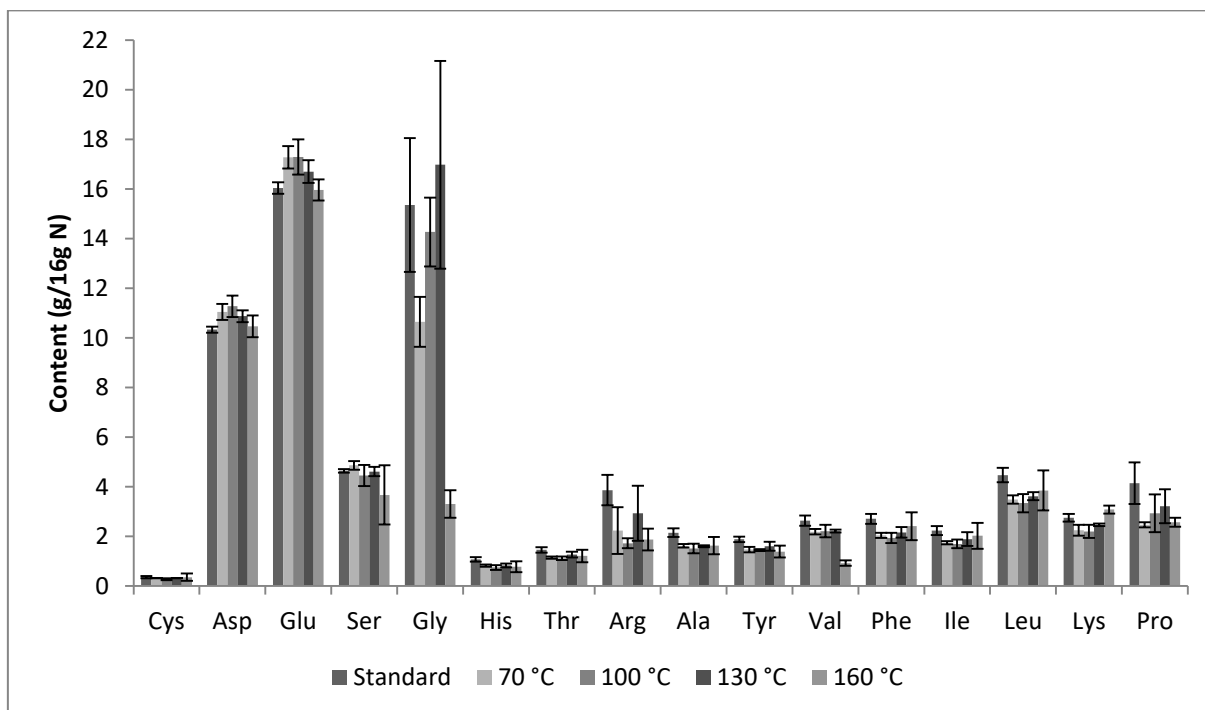


**Figure 78:** Amino acid composition of PPI 1 before (standard) and after extrusion depending on cooking temperature. Extrusion operating conditions were set at  $150 \text{ min}^{-1}$  and 55% w.b. moisture content (w/w).

Temperatures in the cooking zone between 70 °C – 160 °C did not significantly affect the amino acid composition of PPI 1 under high moisture conditions, except for glycine which

was reduced in samples extruded at 160 °C. The results are in accordance with previous studies showing that the feed moisture has a protective effect on the amino acid loss in extrusion cooking (Noguchi *et al.* 1982; Björck and Asp 1983).

#### 4.4.2 Molecular weight distribution

In order to assess the effect of HMEC on the bonding nature, the molecular weight distribution of three protein ingredients before (a) and after extrusion (b) were determined using electrophoresis under reducing and non-reducing conditions as described in chapter 3.4.4.2 (Figure 79).

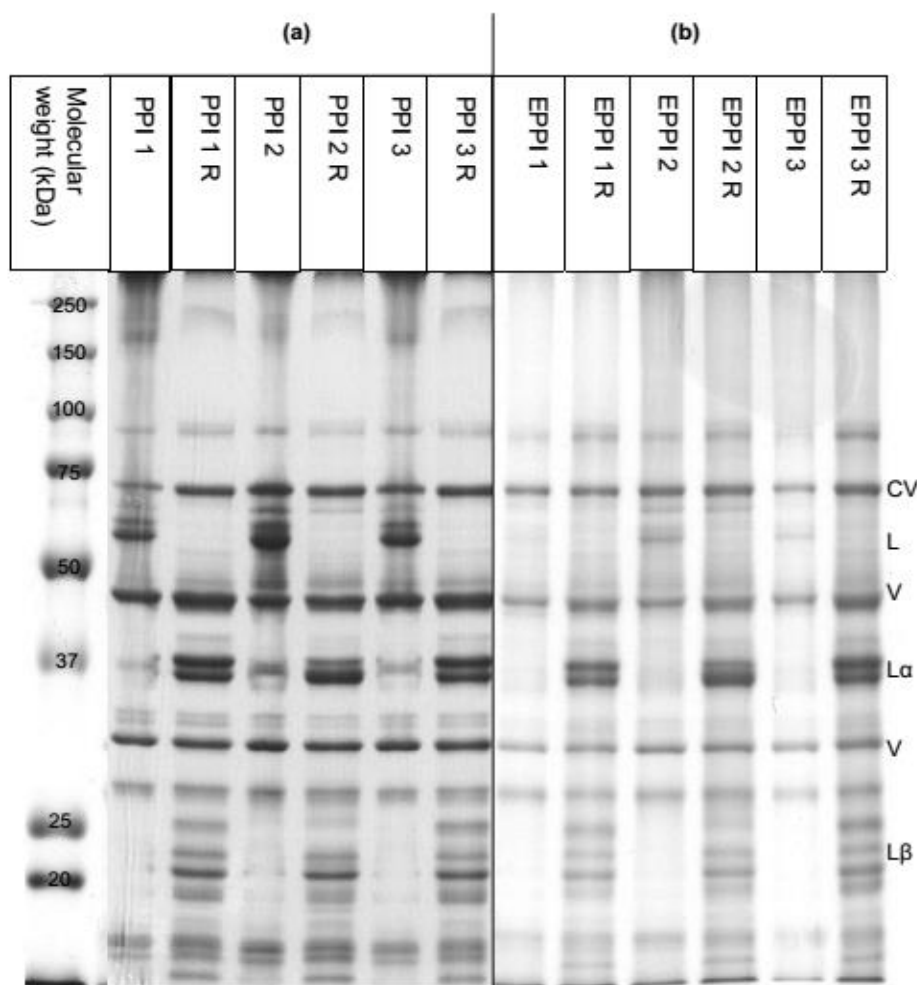


**Figure 79:** Sodium dodecylsulfate-polyacrylamide gel electrophoresis (SDS-PAGE) pattern (10% acrylamide, 60  $\mu$ g protein on gel) of pea protein isolates under reducing (R) and non-reducing conditions (a) before and (b) after extrusion at 60% w.b. moisture content (w/w) and 140 °C barrel temperature. PPI = pea protein isolate, EPPI = extruded pea protein isolate, V = vicilin, CV = convicilin, L = legumin, L $\alpha$  = legumin acidic subunit and L $\beta$  = legumin basic subunit. Reprinted from Osen *et al.* (2015) with permission of Elsevier.

As equal concentrations of each protein extracts were loaded onto the gel, changes in the relative amounts of the individual protein fractions could be compared. The band patterns of

the protein ingredients showed minor variations and were in accordance with previous studies (Alonso *et al.* 2000; Shand *et al.* 2007). It could be shown that the pea protein is mainly composed of the 11S fractions legumin and the 7S fraction vicilin (V) and Convicilin (CV) (O'Kane *et al.* 2004). Under non-reducing conditions, a protein fraction at about 60 kDa (L) was found that originated from legumin in all protein ingredients with the highest intensity in PPI 2. This finding can be related to the high protein solubility of PPI 2 compared to the other protein ingredients. Under reducing conditions, legumin dissociated which revealed new bands at around 40 (L $\alpha$ ) and 20 kDa (L $\beta$ ). Legumin consists of an acidic (L $\alpha$ , around 40 kDa) and a basic (L $\beta$ , 20 kDa) subunit covalently linked by a disulfide bond (O'Kane *et al.* 2004). Vicilin is non-covalently associated in trimers. The presence of bands above 150 kDa in PPI samples in the gels may represent polymerized proteins which were formed during commercial processing of protein isolates, which was previously reported by Shand *et al.* (2007). A protein with an apparent MW of about 90 kDa present in all protein ingredients has been reported to be an enzyme with lipoxygenase activity (Shand *et al.* 2007). A low molecular weight band at 30 kDa, which was observed in all protein ingredients under both conditions, can be attributed to albumins (Alonso *et al.* 2000).

The gel pattern of the extruded proteins revealed changes in the molecular weight distribution as affected by extrusion texturization. The pea protein molecules extracted from the respective extrudates showed lower intensities on the gel. As reported by Chen *et al.* (2011), it can be assumed that extrusion processing caused proteins to aggregate during texturization forming large molecular weight proteins or protein-non-protein macromolecules that were unable to penetrate the pores of the separating gel. Extrusion processing had different effects on the polypeptide subunits. The bands of legumin (L) disappeared, which can be attributed to their participation in a macromolecular network cross-linked by disulfide bonds. Interestingly, extrusion did not affect vicilin (V) and convicilin (CV), which were present in the extrudates both under reducing and non-reducing conditions. It could be assumed that vicilin and convicilin do not contribute to a network formation because they lack cysteine residues necessary for covalent crosslinking during texturization.

In order to evaluate the temperature necessary for legumin crosslinking, the molecular weight distribution of PPI 1 was evaluated as a factor of cooking temperature between 100 and 120 °C (Figure 80).

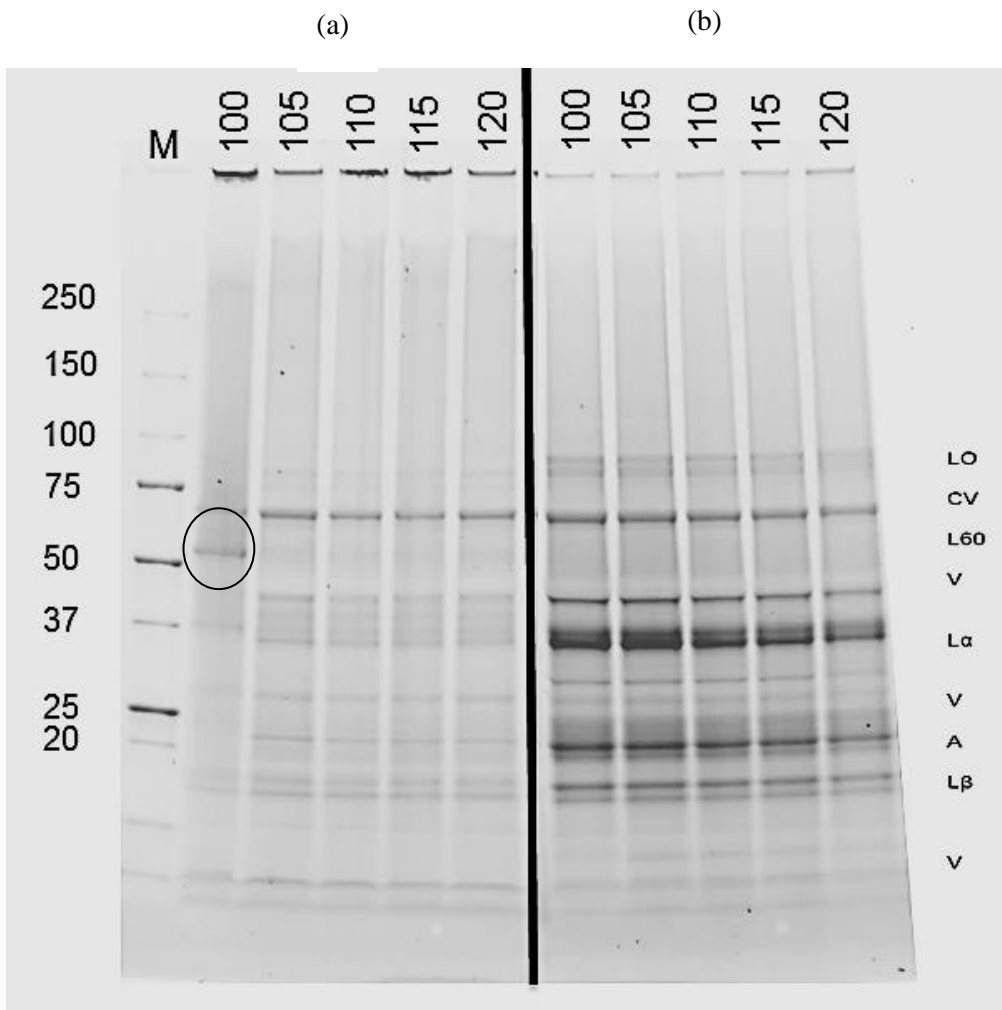


**Figure 80:** Sodium dodecylsulfate-polyacrylamide gel electrophoresis (SDS-PAGE) pattern (10% acrylamide, 60  $\mu\text{g}$  on Bio-Rad minigel) of PPI 1 as a function of cooking temperature under (a) non-reducing and (b) reducing conditions at 60% w.b. moisture content (w/w) and a rotational screw speed of  $150 \text{ min}^{-1}$ . Electrophoresis conditions were 300 V, 60 mA, 100 W at room temperature,

Only the protein extruded at 100 °C showed a band at 60 kDa that could be attributed to legumin (marked in Figure 80). When the protein was extruded at temperatures of 105 °C or higher, the bands of legumin disappeared. One explanation is that the thermal energy during extrusion at temperatures above 100 °C induced thiol-disulfide-exchange reactions and rearrangements of the cysteine-residues in the legumin fraction, which could have resulted in intermolecular crosslinking to larger insoluble legumin-aggregates. This “activation temperature” seemed to correlate with the minimum texturization temperature shown in Figure 65. These observations suggest that the texturization of pea protein isolate could be explained by the network formation of legumin at around 100 -110 °C due to the participation of the 11S subunit legumin in a macromolecular network that is aggregated and cross-linked via disulfide bonds. The 7S subunits vicilin and convicilin do not contribute to a network formation. These findings indicate that covalent disulfide bonding plays an important role during HMEC of PPI, which will be further addressed in the following sections.

#### 4.4.3 Degree of hydrolysis

To assess the effect of HMEC on protein alterations inside the extruder, the formation of covalent peptide bonding was subsequently investigated as described in chapter 3.4.5.2. These crosslinkings might be promoted by the thermal and mechanical energy input as previously described (Burgess and Stanley 1976). The degree of hydrolysis (DH) is defined as the ratio of cleaved peptide bonds and the amount of free amino groups (Nielsen *et al.* 2001). A hydrolysis of proteins would result in an increased DH, whereas the formation of covalent crosslinking involving free amino-groups would lower the DH (Table 29).

**Table 29: Degree of hydrolysis of pea protein isolates and extrudates. Extrusion operating conditions were set at 140 °C cooking temperature, 150 min<sup>-1</sup> and 55% w.b. moisture content (w/w). Reprinted from Osen *et al.* (2015) with permission of Elsevier.**

	Degree of hydrolysis [%]	
	Isolate	Extrudate
<b>PPI 1</b>	3.2±0.1	3.3±0.2
<b>PPI 2</b>	3.4±0.2	3.6±0.3
<b>PPI 3</b>	3.3±0.2	3.5±0.1

Average of duplicate determinations. Means do not differ significantly ( $p > 0.05$ ).

The DH was similar among the protein ingredients and among the extrudates ( $p > 0.05$ ). In addition, a significant difference between the DH of the protein ingredients and their respective extrudates could not be detected. These results suggest that a significant crosslinking via peptide bonds did not occur under the experimental high moisture conditions in this study, because the formation of new peptide bonds would induce a decrease of the DH. Referring to Figure 79, if a significant alteration of peptide-bonding would have occurred, the protein subunit of the SDS-PAGE should exhibit a different distribution between the extrudates and the isolates.

Furthermore, the effect of cooking temperature on degree of hydrolysis is shown in Table 30.

**Table 30: Degree of hydrolysis of PPI 1 at different cooking temperatures. Extrusion operating conditions were set at 150 min<sup>-1</sup> and 55% w.b. moisture content (w/w).**

Cooking temperature [°C]	Degree of hydrolysis [%]
0	3.4±0.0
40	3.3±0.0
70	2.9±0.0
100	3.1±0.0
120	2.7±0.0
130	2.7±0.0
140	2.7±0.0
160	3.3±0.0

Average of duplicate determinations.

It can be seen from the data in Table 30 that cooking temperatures between 40 – 160 °C did not significantly affect the amount of free amino groups in PPI 1 under high moisture conditions. Although literature data about the changes in the protein structure during extrusion are disparate, these findings are in accordance with recent studies on HMEC of soy protein isolate (Liu and Hsieh 2008; Chen *et al.* 2011). Both work groups could not observe the formation of peptide crosslinking during HMEC.

#### 4.4.4 Protein solubility

To assess the effect of HMEC on the protein-protein interactions with focus on the relative importance between covalent bonds and non-covalent interactions, the amounts of protein solubilized by four different solvent systems from protein ingredients and extrudates were determined as described in chapter 3.4.5.1. Figure 81 shows the protein solubility of protein ingredients before and after extrusion cooking.



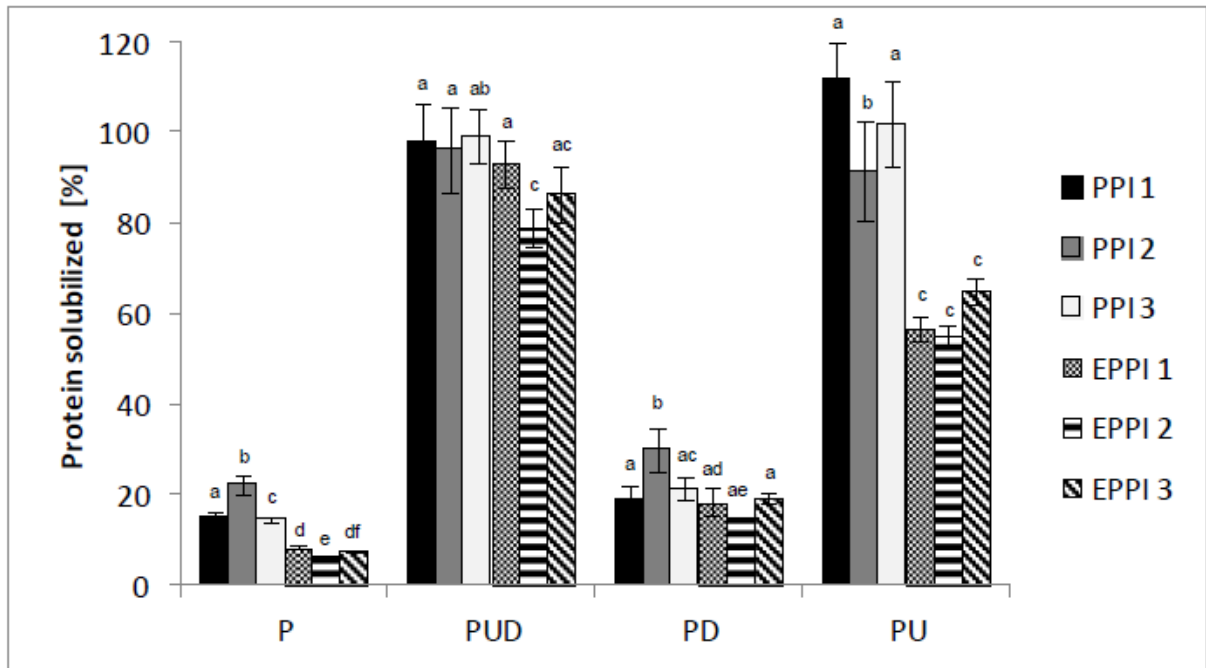


Figure 81: Effect of extrusion cooking (60% w.b. moisture content (w/w), 140 °C cooking temperature) on protein solubility from protein ingredients and their respective extrudates induced by extraction solvents. Protein solubility was expressed as percentage of total protein. P, phosphate buffer; D, dithiothreitol; U, urea. The same letter for the same extraction solution indicates no significant difference ( $p > 0.05$ ). Reprinted from Osen *et al.* (2015) with permission of Elsevier.

Following the recommendation of Liu and Hsieh (2008) on the design of protein solubility studies, a methodology was used based on omission of one or more reagents from an all-dissolving buffer (PUD) to evaluate protein-protein interactions in protein ingredients and extrudates.

Protein solubility was between 6% to around 100% with respect to the total protein content and in the range reported in previous studies (Liu and Hsieh 2007; Liu and Hsieh 2008; Chen *et al.* 2011). Protein solubility was affected by the protein ingredients and cooking temperature during extrusion ( $p < 0.05$ ), with a significant interaction between the factors.

The first extraction solution (P) is known to extract proteins in their native state. Compared to the other extraction solutions, the least amount of protein was extracted in all samples. This could be expected, because the protein ingredients were vastly denatured during their commercial preparation. When both disulfide bonds and non-covalent interactions were broken (PUD-solution), the solubility increased to 80-100%. This is in accordance with previous studies suggesting that the chemical bonding responsible for the rigid structure of high moisture extrudates is limited to disulfide bonds and non-covalent interactions (Hager 1984; Noguchi 1990; Liu and Hsieh 2008). The third extraction solution was used for cleavage of disulfide bonds only (PD). Compared to the phosphate buffer, the solubility

increased ( $p < 0.05$ ), indicating that some disulfide bonds were broken in both isolates and extrudates. When compared to the PUD-solution, the amount of extracted proteins decreased to around 20% for all samples, suggesting that non-covalent interactions played a more important role than disulfide bonding in holding the structure in both protein isolates and extrudates likewise. However, as there was no significant change in the solubility between the protein ingredients and extrudates, this would not explain the structural stabilization of extrudates, but indicate that both hydrogen and disulfide bonding remained unchanged during extrusion. When non-covalent interactions were broken (PU-solution,) the protein solubility decreased from around 100% in protein ingredients to around 60% in extrudates ( $p < 0.05$ ). In contrast to the PD-solution, the decrease of solubility in extrudates indicated that linkages other than non-covalent interactions emerged during high moisture extrusion cooking. As no indications for peptide bonding were found, these observations support the notion that the linkages that lead to insolubility in extrudates can be ascribed to disulfide bonding, possibly by thiol-disulfide-exchange and rearrangement from intra-to intermolecular disulfide crosslinking.

Comparing the effect of urea and DTT on the protein solubility, the total amount of soluble protein after breaking disulfide bonds (PD-solution) was lower compared to the amount of soluble protein after cleavage of non-covalent interactions (PU-solution). This might be attributed to the high number of non-covalent bonding sites compared to the small number of thiol-groups in pea proteins. Hence, it could be concluded that although the number of non-covalent interactions outweighs disulfide bonding in both isolates and extrudates, the decrease of solubility after extrusion in the PU-solution can be attributed to covalent disulfide crosslinking. This is in accordance with previous studies suggesting that the role of disulfide bonding outweighs non-covalent interactions in forming the rigid structure of high moisture extrudates (Hager 1984; Noguchi 1990; Liu and Hsieh 2008).

Regarding the insolubility of legumin (L) during electrophoresis (Figure 79), these observations further indicate that legumin participated in a macromolecular network that is aggregated and cross-linked via disulfide linkages. That would explain why the bands of vicilin and convicilin are visible after extrusion because they lack cysteine residues necessary for covalent disulfide crosslinking during texturization.

Furthermore, the effect of cooking temperature on the amount of protein solubilized by six different solvent systems from protein ingredients and extrudates were determined as shown in Figure 82.

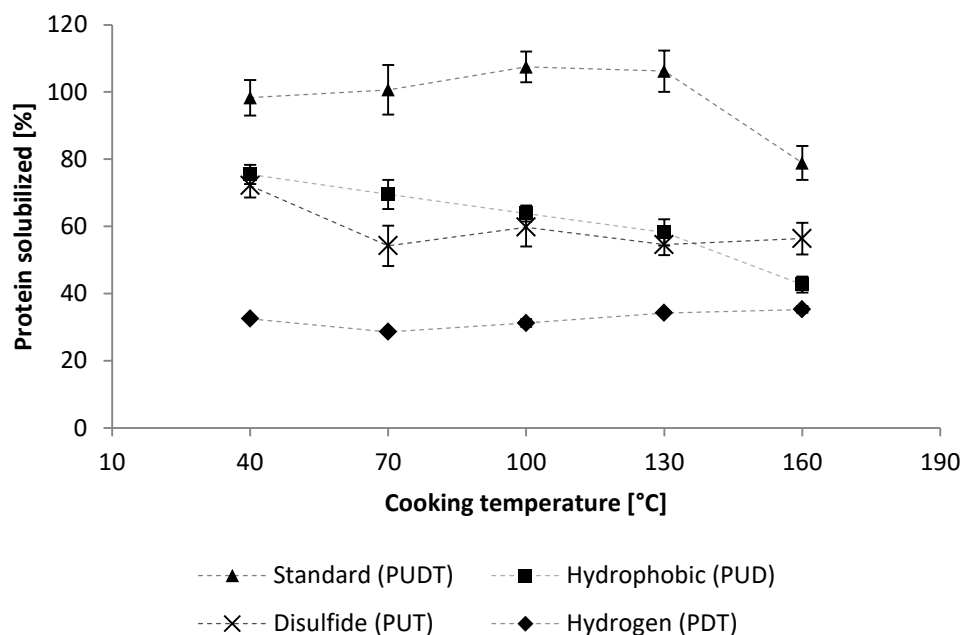


**Figure 82:** Effect of cooking temperature during HMEC of PPI 1 (60% w.b. moisture content (w/w)) on protein solubilized induced by extracting solutions. Protein solubility was expressed as percentage of total protein. P, phosphate buffer; D, dithiothreitol; U, urea; T, thiourea. The legend indicates the specific protein-protein interactions responsible for insolubility of the protein. The lines connecting the data points are only to guide the eye.

Figure 82 shows the protein solubility of PPI 1 as a factor of cooking temperature. The amount of solubilized protein was affected by the extraction solution and the cooking temperature. The highest amount of protein was extracted by the standard solution containing all selective reagents. Only in samples extruded at 160 °C the solubility decreased to ~ 80%. Since there was no indication for peptide bonding as evaluated by the amount of free amino acids, it is not clear which interactions could be attributed to the decrease of solubility in that particular sample.

The second data set represent protein solubility in the solution without thiourea, hence the decrease of solubility compared to the standard buffer could be attributed to hydrophobic interactions. Data show that solubility decreases from 75% in samples extruded at 40 °C to ~ 40% in samples extruded at 160 °C. A similar trend could be observed in the solution without DTT. In contrast, the amount of soluble protein in the solution without urea was not affected by the cooking temperature. These observations indicate that both hydrophobic interactions and covalent disulfide bonds increased with increasing cooking temperature. Considering the dissociation energy for hydrophobic interactions (4-12 kJ/mol) and disulfide bonds (268 kJ/mol), it could be assumed that the role of covalent disulfide bonds for the structural stabilization of extrudates outweighs hydrophobic interactions.



## 5 Conclusions

A promising solution to reduce the impacts of meat production on the environment may be offered by a partial replacement of meat proteins with plant protein products in the human diet (Smil 2000). A recent development for obtaining meat-like structures from plant protein is high moisture extrusion cooking (HMEC). The products derived thereof are characterized by a high water content of >50% and a fibrous, non-expanded texture (Noguchi 1990). During extrusion, the protein-rich materials undergo chemical and structural changes induced by a combination of high temperature, pressure and shear that greatly influence the texture quality of the extruded products (Ilo and Berghofer 2003). However, the reaction mechanisms of the proteins during extrusion are not fully understood and current studies investigating this topical research issue are scarce (Areas 1992; Cheftel *et al.* 1992; Liu and Hsieh 2008; Chen *et al.* 2011). For the structural stabilization of extrudates, alterations of both covalent bonds (peptide-, disulfide bonds) as well as non-covalent bonds such as hydrogen-, hydrophobic-, and ionic linkages could be expected (Areas 1992; Liu and Hsieh 2008). Until now, such studies under high moisture extrusion conditions have been limited to soy as the plant protein source.

Since there was no literature data on high moisture extrusion cooking of pea as a highly potential raw material, the characterization of technofunctional properties of three commercially available pea protein isolates was presented in chapter 4.1 as the basis for further studies in the following chapters. The comparison of the protein ingredients showed that commercial protein products from the same species can vary in terms of their functional, thermal and rheological properties. These characteristics are most likely attributed to the manufacture conditions (mechanical loads from grinding, high temperatures e.g. during spray-drying) during protein isolation. Regarding the texturization using high moisture extrusion cooking, these findings suggest that rheological properties of pea protein ingredients should be taken into account during processing to avoid blocking of the extruder barrel or the backing up of water. Further work should be carried out upon the effect of processing conditions during the manufacture of pea protein isolates on their functional and rheological properties. Other important criteria are the influences of environmental conditions on the protein content and protein functionality. These findings might be transferred to other potential plant proteins such as sunflower or rapeseed protein and could facilitate the production of tailor-made protein ingredients for high moisture extrusion cooking.

The rheological properties inside the extrusion equipment play an important role for the texturization to fibrous meat substitutes. Because of the difficulty to study physical changes of the protein-water mixture inside the extruder, small strain oscillatory experiments under thermal conditions similar to those during extrusion cooking were applied (chapter 4.2). The results suggest a plasticization of the protein suspension in the cooking zone forming a low viscosity fluid with viscoelastic solid characteristics and a subsequent solidification of the fluid upon cooling. The present work is a basis for further investigations on the interdependencies between protein properties, fluid properties inside the extruder and texture formation of extrudates. This is of high interest in order to understand the role of the rheological fluid behavior for the structure formation to fibrous meat substitutes.

Since the visual and textural appearance is a key requirement for meat substitutes, the mechanical properties of high moisture extrudates were presented in chapter 4.3. All of the commercial protein ingredients characterized in this thesis could be texturized to highly fibrous extrudates, as indicated by their texture properties that were similar to meat in terms of fibrousness and microstructure. Additionally, the potential of protein concentrates or protein enriched flours regarding fiber formation should be investigated in order to elucidate the possibilities of combined processing lines for protein enrichment and subsequent texturization. Further improvement of the texture could be achieved by addition of functional additives such as mono- or bivalent salts, hydrocolloids, plant fibers as well as pH-regulating agents.

The structural stabilization of extrudates is determined by alterations of protein-protein interactions during extrusion under high moisture conditions. Therefore, the bonding patterns of pea protein ingredients before and after extrusion were presented in chapter 4.4 in order to provide an insight in the way proteins interact and to further elucidate the formation of the fibrous meat-like texture. The occurrence of disulfide crosslinking during extrusion suggested that energy input might have caused macromolecules to unravel, making bonding sites available for further crosslinking that were previously buried within the macromolecules. As the amino acid profile of the pea protein remained unchanged after processing, it can be concluded that extrusion under high moisture conditions is a comparatively mild process for the production of high-quality meat substitutes. This knowledge about the reaction mechanisms for the network formation of high-moisture extrudates could be used for screening new plant proteins by evaluating the cysteine amount and adjusting the texture properties using e.g. sulphur-containing additives. In order to explore the limitations of HMEC regarding the chemical and structural changes that greatly influence the quality of

---

extruded products, further investigations on the effect of cooking temperature on protein properties are necessary.

Altogether, the results of this thesis provide a better understanding of the high moisture extrusion process for the development of high-quality meat substitutes using pea protein as a model ingredient. These results might be applied to other potential protein ingredients to improve the flavor, texture and nutritional value by a combination of different raw materials. In order to increase the acceptance of meat substitutes produced by high moisture extrusion cooking, it is important to inform the consumers about the benefits of the technology. Therefore, the carbon footprint of the products should be further optimized and the use of local raw materials promoted.





## 6 Summary

Due to the resource-consuming meat production, high-quality meat substitutes represent a major challenge for science and industry as a sustainable alternative. A promising technology to generate textured plant proteins is high moisture extrusion cooking (HMEC). Biopolymers such as proteins are plasticized with water and subjected to mechanical and thermal energy treatment to achieve a desired texture resembling meat. However, the texturization mechanisms of the proteins during extrusion have not been fully understood.

The aim of the present work was to elucidate the formation of fibrous meat-like structures during high moisture extrusion cooking by assessing the effect of temperature and moisture content on the texturization process. Several pea protein ingredients were characterized regarding their chemical composition and functional properties. Thermally induced network formation of protein dispersions was described using high pressure rheology. Furthermore, the mechanical properties of high moisture extrudates were determined and the structure formation of anisotropic fibrous extrudates inside the cooling die was monitored. Finally, protein reactions during texturization under high-moisture conditions were identified with focus on protein-protein interactions.

Three commercial pea protein isolates were compared in order to investigate which protein properties affect extruder responses and product texture properties. The comparison of the protein ingredients revealed that the functional and rheological properties of the pea proteins correlated with their thermal properties. As indicated by differential scanning calorimetry studies, only one out of three pea protein ingredients had partly native protein fractions and exhibited higher protein solubility and lower water binding capacity, oil binding capacity, and emulsifying capacity. These properties in turn affected the viscosity profile during heating to 95 °C. The current observations indicate that commercial protein products can vary in terms of their functional properties, which might affect their behavior during extrusion as well as their extrudate texture properties. Because of the black box conditions during extrusion, direct investigation of material properties inside the extruder is a difficult task. Small strain oscillation in combination with high pressure rheology allowed the characterization of the viscoelastic properties of protein dispersions as a function of temperature and moisture content typical for high moisture extrusion. The mechanical spectra suggested that the hydrated protein ingredients can be described as colloidal networks with viscoelastic solid characteristics, shear thinning behavior as well as a predominant yield stress. Upon heating to

temperatures typical for high moisture extrusion cooking, the elastic modulus decreased due to a reduction in the network strength. Although both viscosity and yield stress decreased rapidly, the moduli suggested viscoelastic solid properties of the protein mass at temperature conditions as high as 150 °C. These observations corroborated the hypothesis that the protein-water mixture is plasticized during the cooking zone in the extruder and solidified upon cooling into a rigid network. Investigation of the mean residence time in the laboratory scale and pilot-scale extrusion equipment provided information about the average time a particle is subjected to the temperature conditions in the extrusion equipment. The heating phase in the laboratory extruder was longer compared to the pilot-scale extruder whereas the cooling phase was shorter. All pea protein isolates that were investigated could be texturized to highly fibrous extrudates, as indicated by a higher cutting strength in the transverse compared to the longitudinal direction. The texture properties were similar to meat in terms of fibrousness and their microstructure. Based on the rheological properties discussed in section 4.2, the texturization process could be described and interpreted as follows: Different macrostructures were observed within the experimental domain. Below 120 °C, samples exhibited a paste-like soft texture without any fibrous structures. This could be attributed to insufficient thermal energy during the residence time in the cooling die that is necessary for cleaving network interactions resulting in incomplete unraveling of macromolecules. Upon further increase of the cooking temperature, extrudates started to display multilayered structures with layers parallel to the die wall and fine fibers appeared upon tearing the specimen. Increasing the cooking temperature facilitated a temperature- and velocity gradient of the low-viscosity fluid at the cross section of the die channel, which resulted in an extended flow profile indicated by increasing axial fiber length. During this stage, energy input might have caused macromolecules to unravel, making bonding sites available for further crosslinking that were previously buried within the macromolecules. This would explain the positive correlation between the cooking temperature and the cutting strength of the extrudates. At temperatures as high as 160 °C, the macrostructures became more homogenous with a smooth surface without aligned structures. Predominantly longitudinal oriented fibers appeared when the samples were manually dissected. Altogether, it appears that functional properties played a minor role during fiber formation due to the elevated cooking temperature, which exceeded the proteins' denaturation temperature. Also, particle size did not affect the product texture properties as the particles were already hydrated, melted to a protein water mixture, and solidified prior to texture analysis.

Furthermore, the effect of HMEC on the proteins with focus on the bonding nature was assessed. Comparison of the raw materials showed that the protein composition and bonding pattern was similar among the isolates and among their respective extrudates. Electrophoresis revealed the participation of the 11S subunit legumin in a macromolecular network that is aggregated and cross-linked via disulfide bonds during HMEC. The 7S subunits vicilin and convicilin did not contribute to a network formation. With regard to the controversy in literature about the relative importance of covalent bonding and non-covalent interactions, these observations support the hypothesis that disulfide bonding plays a major role for structural stabilization during HMEC as previously reported for soy protein (Liu and Hsieh 2007; Liu and Hsieh 2008). This is in accordance with the findings that crosslinking via peptide bonds did not occur, because the degree of hydrolysis of the proteins was not affected by extrusion temperature. Furthermore, these results were corroborated by the observation that legumin participated in a network cross-linked by disulfide bonds. Although the proteins aggregated and crosslinked via disulfide bonds as a result of HMEC, the thermal and mechanical energy did not cause the degradation of amino acids due to Maillard reactions. Compared to thermoplastic extrusion the high moisture reduced the shearing action and dissipation of mechanical energy in the extruder.

The present work described the potential of high moisture extrusion cooking for the texturization of pea protein ingredients to fibrous meat substitutes. The findings suggest that high moisture extrusion cooking is a comparatively mild process compared to conventional thermoplastic extrusion for the production of high-quality meat substitutes.



## 7 Literature

- AACC (1982). Hydration capacity of pregelatinized cereal products. St- Paul, MN, USA: American Association of Cereal Chemists.
- AACC (1997). General pasting method for wheat or rye flour or starch using the rapid visco analyser. St. Paul, MN, USA: American Association of Cereal Chemists International.
- Abberton, M. (2010). Enhancing the role of legumes: potential and obstacles. In: Grasslands carbon sequestration: management, policy and economics (edited by Abberton, M., Conant, R. & Bartello, C.). Pp. 177-187. FAO.
- Adebiyi, A. P. & Aluko, R. E. (2011). Functional properties of protein fractions obtained from commercial yellow field pea (*Pisum sativum* L.) seed protein isolate. *Food Chemistry*, **128**, 902-908.
- Adler-Nissen, J. (1986). Enzymic hydrolysis of food proteins. Pp. 110-169. New York: Elsevier Applied Science Publishers.
- Aguilera, J. M. & Stanley, D. W. (1999). Microstructural principles of food processing and engineering. Pp. XIV, 432. Springer.
- Ahmed, J. & Ramaswamy, H. S. (2007). Dynamic rheology and thermal transitions in meat-based strained baby foods. *Journal of Food Engineering*, **78**, 1274-1284.
- Ahmed, J., Ramaswamy, H. S. & Alli, I. (2006). Thermorheological characteristics of soybean protein isolate. *Journal of Food Science*, **71**, E158-E163.
- Ahmed, J., Ramaswamy, H. S., Kasapis, S. & Boye, J. I. (2016). Novel food processing: effects on rheological and functional properties. CRC Press.
- Aigner, M., Lepschi, A., Aigner, J., Garmendia, I. & Miethlinger, J. (2014). Experimental study and verification of the residence time distribution using fluorescence spectroscopy and color measurement. In: 30th International Conference of the Polymer Processing Society.
- Ak, M. M. & Gunasekaran, S. (1997). Anisotropy in tensile properties of mozzarella cheese. *Journal of Food Science*, **62**, 1031-1033.
- Akdogan, H. (1999). High moisture food extrusion. *International Journal of Food Science and Technology*, **34**, 195-207.
- Akdogan, H. & McHugh, T. H. (1999). Twin screw extrusion of peach puree: Rheological properties and product characteristics. *Journal of Food Processing and Preservation*, **23**, 285-305.
- Akdogan, H. & McHugh, T. H. (2000). Flow characterization of peach products during extrusion. *Journal of Food Science*, **65**, 471-475.
- Alonso, R., Orúe, E. & Marzo, F. (1998). Effects of extrusion and conventional processing methods on protein and antinutritional factor contents in pea seeds. *Food Chemistry*, **63**, 505-512.

- Alonso, R., Orue, E., Zabalza, M. J., Grant, G. & Marzo, F. (2000). Effect of extrusion cooking on structure and functional properties of pea and kidney bean proteins. *Journal of the Science of Food and Agriculture*, **80**, 397-403.
- Aluko, R. E., Mofolasayo, O. A. & Watts, B. A. (2009). Emulsifying and foaming properties of commercial yellow pea (*Pisum Sativum* L.) seed flours. *Journal of Agricultural and Food Chemistry*, **57**, 9793-9800.
- Alvarez, V., Smith, D., Morgan, R. & Booren, A. (1990). Restructuring of mechanically deboned chicken and nonmeat binders in a twin-screw extruder. *Journal of Food Science*, **55**, 942-946.
- AOAC International (1990). Official methods of analysis. Arlington, USA.
- Areas, J. A. G. (1992). Extrusion of food proteins. *Critical Reviews in Food Science and Nutrition*, **32**, 365-392.
- Arnfield, S. D. & Murray, E. D. (1981). The influence of processing parameters on food protein functionality. I. Differential scanning calorimetry as an indicator of protein denaturation. *Canadian Institute of Food Science and Technology Journal*, **14**, 289-294.
- Augusto, P. E. D., Cristianini, M. & Ibarz, A. (2012). Effect of temperature on dynamic and steady-state shear rheological properties of siriguela (*Spondias purpurea* L.) pulp. *Journal of Food Engineering*, **108**, 283-289.
- Augusto, P. E. D., Ibarz, A. & Cristianini, M. (2013). Effect of high pressure homogenization (HPH) on the rheological properties of tomato juice: Viscoelastic properties and the Cox–Merz rule. *Journal of Food Engineering*, **114**, 57-63.
- Barac, M., Cabrilo, S., Pesic, M., Stanojevic, S., Zilic, S., Macej, O. & Ristic, N. (2010). Profile and functional properties of seed proteins from six pea (*Pisum sativum*) Genotypes. *International Journal of Molecular Sciences*, **11**, 4973-4990.
- Barac, M., Cabrilo, S., Stanojevic, S., Pesic, M., Pavlicevic, M., Zlatkovic, B. & Jankovic, M. (2012). Functional properties of protein hydrolysates from pea (*Pisum sativum* L.) seeds. *International Journal of Food Science & Technology*, **47**, 1457-1467.
- Barrett, A. H., Cardello, A. V., Leshner, L. L. & Taub, I. A. (1994). Cellularity, mechanical failure, and textural perception of corn meal extrudates. *Journal of Texture Studies*, **25**, 77-95.
- Barth, A. (2007). Infrared spectroscopy of proteins. *Biochimica et Biophysica Acta (BBA) - Bioenergetics*, **1767**, 1073-1101.
- Bast, R., Sharma, P., Easton, H. K. B., Dessev, T. T., Lad, M. & Munro, P. A. (2015). Tensile testing to quantitate the anisotropy and strain hardening of mozzarella cheese. *International Dairy Journal*, **44**, 6-14.
- Berrios, J. d. J. (2011). Extrusion processing of main commercial legume pulses. In: *Advances in food extrusion technology* (edited by Maskan, M. & Altan, A.). CRC Press.

- Bialleck, S. (2012). Herstellung von Polysaccharidpellets mittels Schmelzextrusion (Doctoral Dissertation). Rheinische Friedrich-Wilhelms-Universität Bonn.
- Biliaderis, C. G. (2009). Structural transitions and related physical properties of starch. In: Starch (edited by Bemiller, J. & Whistler, R.). Pp. 293-372. San Diego: Academic Press.
- Björck, I. & Asp, N. G. (1983). The effects of extrusion cooking on nutritional value - A literature review. *Journal of Food Engineering*, **2**, 281-308.
- Björck, I., Asp, N. G., Birkhed, D., Eliasson, A. C., Sjöberg, L. B. & Lundquist, I. (1984). Effects of processing on starch availability In vitro and In vivo. II. Drum-drying of wheat flour. *Journal of Cereal Science*, **2**, 165-178.
- Björck, I., Noguchi, A., Asp, N. G., Cheftel, J. C. & Dahlgvist, A. (1983). Protein nutritional-value of a biscuit processed by extrusion cooking - Effects on available lysine. *Journal of Agricultural and Food Chemistry*, **31**, 488-492.
- Borwankar, R. P. (1992). Food texture and rheology: A tutorial review. *Journal of Food Engineering*, 1-16.
- Bounie, D. & Van Hecke, E. (1997). High moisture extrusion: optimisation of texturisation through control of rheological and textural parameters. In: Smart extrusion workshop. Pp. 22. Sydney.
- Bourne, M. C. (2002). Chapter 3 - Physics and Texture. In: Food Texture and Viscosity (Second Edition) (edited by Bourne, M. C.). Pp. 59-106. London: Academic Press.
- Bouvier, J.-M. & Campanella, O. H. (2014). Extrusion processing technology: Food and non-food biomaterials. Pp. 530. Wiley.
- Bouvier, J.-M., L., B., Durand, D., Le Royer, S. & J.-J., H. (2003). Method and installation for the continuous preparation of a retextured product. (edited by Intellectuelle, O. M. D. L. P.). France.
- Boye, J., Zare, F. & Pletch, A. (2010). Pulse proteins: Processing, characterization, functional properties and applications in food and feed. *Food Research International*, **43**, 414-431.
- Bredahl, L., Grunert, K. G. & Fertin, C. (1998). Relating consumer perceptions of pork quality to physical product characteristics. *Food Quality and Preference*, **9**, 273-281.
- Breitenbach, J. (2002). Melt extrusion: from process to drug delivery technology. *European journal of pharmaceuticals and biopharmaceuticals*, **54**, 107-17.
- Bryant, C. M. & McClements, D. J. (1998). Molecular basis of protein functionality with special consideration of cold-set gels derived from heat-denatured whey. *Trends in Food Science & Technology*, **9**, 143-151.
- Bur, A. J. & Gallant, F. M. (1991). Fluorescence monitoring of twin screw extrusion. *Polymer Engineering & Science*, **31**, 1365-1371.

- Burgess, L. D. & Stanley, D. W. (1976). Possible mechanism for thermal texturization of soybean protein. *Canadian Institute of Food Science and Technology Journal*, **9**, 228-231.
- Buzzi, O., Pedroso, D. M. & Giacomini, A. (2008). Caveats on the implementation of the generalized material point method. *Computer Modeling in Engineering & Sciences*, **31**, pp.85-106.
- Caine, W. R., Aalhus, J. L., Best, D. R., Dugan, M. E. R. & Jeremiah, L. E. (2003). Relationship of texture profile analysis and Warner-Bratzler shear force with sensory characteristics of beef rib steaks. *Meat Science*, **64**, 333-339.
- Camire, M. (1991). Protein functionality modification by extrusion cooking. *Journal of the American Oil Chemists' Society*, **68**, 200-205.
- Camire, M. E. (1998). Chemical changes during extrusion cooking - Recent advances. *Process-Induced Chemical Changes in Food*, **434**, 109-121.
- Catsimpolas, N. & Meyer, E. W. (1970). Gelation phenomena of soybean globulins.1. Protein-protein interactions. *Cereal Chemistry*, **47**, 559-&.
- Chang, Y. K., Martinez-Bustos, F., Park, T. S. & Kokini, J. L. (1999). Influence of specific mechanical energy on cornmeal viscosity measured by an on-line system during twin-screw extrusion. *Brazilian Journal of Chemical Engineering*, **16**, 285-295.
- Chao-Chi Chuang, G. & Yeh, A.-I. (2004). Effect of screw profile on residence time distribution and starch gelatinization of rice flour during single screw extrusion cooking. *Journal of Food Engineering*, **63**, 21-31.
- Cheftel (1992). *Lebensmittelproteine*. Hamburg, Behr's.
- Cheftel, J. C., Kitagawa, M. & Queguiner, C. (1992). New protein texturization processes by extrusion cooking at high moisture levels. *Food Reviews International*, **8**, 235-275.
- Chen, F. L., Wei, Y. M. & Zhang, B. (2010a). Characterization of water state and distribution in textured soybean protein using DSC and NMR. *Journal of Food Engineering*, **100**, 522-526.
- Chen, F. L., Wei, Y. M. & Zhang, B. (2011). Chemical cross-linking and molecular aggregation of soybean protein during extrusion cooking at low and high moisture content. *LWT - Food Science and Technology*, **44**, 957-962.
- Chen, F. L., Wei, Y. M., Zhang, B. & Ojokoh, A. O. (2010b). System parameters and product properties response of soybean protein extruded at wide moisture range. *Journal of Food Engineering*, **96**, 208-213.
- Clark, A. H., Kavanagh, G. M. & Ross-Murphy, S. B. (2001). Globular protein gelation-theory and experiment. *Food Hydrocolloids*, **15**, 383-400.
- Copeland, L., Blazek, J., Salman, H. & Tang, M. C. (2009). Form and functionality of starch. *Food Hydrocolloids*, **23**, 1527-1534.
- Cousin, R. (1997). Peas (*Pisum sativum* L.). *Field Crops Research*, **53**, 111-130.



- Damodaran, S. (1997). *Food Proteins and Their Applications*. Taylor & Francis.
- Davidson, V. J. (1992). The rheology of starch-based materials in the extrusion process. In: *Food Extrusion Science and Technology* (edited by L., K. J., Ho, C. & Karwe, M. V.). Pp. 263-275. New York: Marcel Dekker.
- Day, L. (2013). Proteins from land plants – Potential resources for human nutrition and food security. *Trends in Food Science & Technology*, **32**, 25-42.
- Day, L., Augustin, M. A., Batey, I. L. & Wrigley, C. W. (2006). Wheat-gluten uses and industry needs. *Trends in Food Science & Technology*, **17**, 82-90.
- De Huidobro, F. R., Miguel, E., Blázquez, B. & Onega, E. (2005). A comparison between two methods (Warner–Bratzler and texture profile analysis) for testing either raw meat or cooked meat. *Meat Science*, **69**, 527-536.
- DGF-Einheitsmethoden (2004). Deutsche Gesellschaft für Fettwissenschaft e.V. Münster, WVG, Stuttgart, Germany.
- El-Adawy, T. (2002). Nutritional composition and antinutritional factors of chickpeas (*Cicer arietinum* L.) undergoing different cooking methods and germination. *Plant Foods for Human Nutrition*, **57**, 83-97.
- El-Niely, H. F. G. (2007). Effect of radiation processing on antinutrients, in-vitro protein digestibility and protein efficiency ratio bioassay of legume seeds. *Radiation Physics and Chemistry*, **76**, 1050-1057.
- Elzerman, J. E., Hoek, A. C., van Boekel, M. A. J. S. & Luning, P. A. (2011). Consumer acceptance and appropriateness of meat substitutes in a meal context. *Food Quality and Preference*, **22**, 233-240.
- Emin, M. A. (2015). Modeling extrusion processes In: *Modeling food processing operations*. Pp. 235-253. Woodhead Publishing.
- Faller, J. & Unlu, E. (2010). Extrudate Rheology. In: *Encyclopedia of Agricultural, Food, and Biological Engineering, Second Edition*. Pp. 1480-1484. Taylor & Francis.
- Fang, Y., Zhang, B. & Wei, Y. (2014). Effects of the specific mechanical energy on the physicochemical properties of texturized soy protein during high-moisture extrusion cooking. *Journal of Food Engineering*, **121**, 32-38.
- Fang, Y., Zhang, B., Wei, Y. & Li, S. (2013). Effects of specific mechanical energy on soy protein aggregation during extrusion process studied by size exclusion chromatography coupled with multi-angle laser light scattering. *Journal of Food Engineering*, **115**, 220-225.
- FAO (2011). *Crops statistics. Concepts, definitions and classifications.*: Food and Agriculture Organization of the United Nations.
- FAO (2017). *Crop statistics. Production quantities of selected crops*.
- Figura, L. & Teixeira, A. A. (2007). *Food Physics: Physical Properties - Measurement and Applications*. Springer Berlin Heidelberg.

- Gao, Y., Muzzio, F. J. & Ierapetritou, M. G. (2012). A review of the residence time distribution (RTD) applications in solid unit operations. *Powder Technology*, **228**, 416-423.
- German Food Act (2005). Methods L. 16.01-2, L. 17.00-1, L. 17.00-3. In BVL Bundesamt für Verbraucherschutz und Lebensmittelsicherheit (Ed.), *Amtliche Sammlung von Untersuchungsverfahren nach § 64 LFGB, § 35 Vorläufiges Tabakgesetz, § 28b GenTG - I - Lebensmittel - Band I (L) Verfahren zur Probenahme und Untersuchung von Lebensmitteln*. Berlin, Germany: Beuth Verlag GmbH.
- Giles, H. F., Mount, E. M. & Wagner, J. R. (2004). *Extrusion: The Definitive Processing Guide and Handbook*. Elsevier Science.
- Godavarti, S. & Karwe, M. V. (1997). Determination of specific mechanical energy distribution on a twin-screw extruder. *Journal of Agricultural Engineering Research*, **67**, 277-287.
- González, R. J., Torres, R. L., De Greef, D. M. & Guadalupe, B. A. (2006). Effects of extrusion conditions and structural characteristics on melt viscosity of starchy materials. *Journal of Food Engineering*, **74**, 96-107.
- Grabowska, K. J., Tekidou, S., Boom, R. M. & van der Goot, A.-J. (2014). Shear structuring as a new method to make anisotropic structures from soy–gluten blends. *Food Research International*, **64**, 743-751.
- Grabowska, K. J., Zhu, S., Dekkers, B. L., de Ruijter, N. C. A., Gieteling, J. & van der Goot, A. J. (2016). Shear-induced structuring as a tool to make anisotropic materials using soy protein concentrate. *Journal of Food Engineering*.
- Gupta, Y. P. (1987). Anti-nutritional and toxic factors in food legumes: a review. *Plant Foods for Human Nutrition*, **37**, 201-228.
- Guy, R. (2001). *Extrusion cooking: Technology and applications* Cambridge, England, CRC Press.
- Guy, R. C. E. (2004). Extrusion technologies. In: *Encyclopedia of Grain Science* (edited by Wrigley, C.). Pp. 366-371. Oxford: Elsevier.
- Guy, R. C. E. & Horne, A. W. (1988). Extrusion and co-extrusion of cereals. In: *Food Structure* (edited by Blanshard, J. M. V. & Mitchell, J. R.). Pp. 331-349. Woodhead Publishing.
- H. Aiking, J. de Boer & Vereijken, J. (2006). Sustainable protein production and consumption: Pigs or peas? Pp. 229. Dordrecht, The Netherlands Springer.
- Hager, D. F. (1984). Effects of extrusion upon soy concentrate solubility. *Journal of Agricultural and Food Chemistry*, **32**, 293-296.
- Harper, J. M. (1989). Food extruders and their applications. In: *Extrusion cooking* (edited by Mercier, C., Linko, P. & Harper, J. M.). Pp. 1-15. AACC.
- Harper, J. M. & Harmann, D. V. (1973). Research needs in extrusion cooking and forming. *Transactions of the Asae*, **16**, 941-943.

- Hartman, W. E. (1978). Texturization through spinning. *Journal of Texture Studies*, **9**, 125-134.
- Hayashi, N., Hayakawa, I. & Fujio, Y. (1993). Flow behaviour of soy protein isolate melt with low and intermediate moisture levels at an elevated temperature. *Journal of Food Engineering*, **18**, 1-11.
- Hermansson, A. M. (1975). Functional properties of proteins for food-flow properties. *Journal of Texture Studies*, **5**, 425-439.
- Herrmann, J., Brito Alayón, A., Trembley, J. & Grupa, U. (2013). Development of a rheological prediction model for food suspensions and emulsions. *Journal of Food Engineering*, **115**, 481-485.
- Hochstein, B., Kizilbay, Z., Horvat, M., Schuchmann, H. P. & Willenbacher, N. (2015). Innovatives Inline-Rheometer zur Bestimmung des Stärkeabbaus im Extruder. *Chemie Ingenieur Technik*, **87**, 90-94.
- Holt, N. W. & Sosulski, F. W. (1979). Amino-acid composition and protein-quality of field peas. *Canadian Journal of Plant Science*, **59**, 653-660.
- Horvat, M., Emin, M. A., Hochstein, B., Willenbacher, N. & Schuchmann, H. P. (2013a). Influence of medium-chain triglycerides on expansion and rheological properties of extruded corn starch. *Carbohydrate Polymers*, **93**, 492-498.
- Horvat, M., Emin, M. A., Hochstein, B., Willenbacher, N. & Schuchmann, H. P. (2013b). A multiple-step slit die rheometer for rheological characterization of extruded starch melts. *Journal of Food Engineering*, **116**, 398-403.
- Hu, G.-H., Kadri, I. & Picot, C. (1999). One-line measurement of the residence time distribution in screw extruders. *Polymer Engineering & Science*, **39**, 930-939.
- Hua, Y., Cui, S. W., Wang, Q., Mine, Y. & Poysa, V. (2005). Heat induced gelling properties of soy protein isolates prepared from different defatted soybean flours. *Food Research International*, **38**, 377-385.
- Huang, H. C., Hammond, E. G., Reitmeier, C. A. & Myers, D. J. (1995). Properties of fibers produced from soy protein isolate by extrusion and wet-spinning. *Journal of the American Oil Chemists' Society*, **72**, 1453-1460.
- Ilo, S. & Berghofer, E. (2003). Kinetics of lysine and other amino acids loss during extrusion cooking of maize grits. *Journal of Food Science*, **68**, 496-502.
- Isobe, S. & Noguchi, A. (1987). High moisture extrusion with twin screw extruder - fate of soy protein during the repetition of extrusion cooking. *Journal of the Japanese Society for Food Science and Technology*, **34**, 456-461.
- Jager, T., Santbulte, P. & van Zuilichem, D. J. (1995). Residence time distribution in kneading extruders. *Journal of Food Engineering*, **24**, 285-294.
- Jeunink, J. & Cheftel, J. C. (1979). Chemical and physicochemical changes in field bean and soybean proteins texturized by extrusion. *Journal of Food Science*, **44**, 1322-1325.

- Kang, L. N., Wei, Y. M. & Zhang, B. (2007). Effects of technological parameters on system pressure and torque in soy protein texturization by high moisture extrusion. *Journal of the Chinese Cereals and Oils Association*, **22**, 43-49.
- Kao, S. V. & Allison, G. R. (1984). Residence time distribution in a twin screw extruder. *Polymer Engineering & Science*, **24**, 645-651.
- Kelley, J. J. & Pressey, R. (1966). Studies with soybean protein and fiber formation. *Cereal Chemistry Journal*, **43**, 195-206.
- Kinkema, M., Scott, P. T. & Gresshoff, P. M. (2006). Legume nodulation: successful symbiosis through short- and long-distance signalling. *Functional Plant Biology*, **33**, 707-721.
- Kinsella, J. E. & Melachouris, N. (1976). Functional properties of proteins in foods: A survey. *C R C Critical Reviews in Food Science and Nutrition*, **7**, 219-280.
- Kinsella, J. E. & Whitehead, D. M. (1989). Proteins in whey: chemical, physical, and functional properties. *Advances in Food and Nutrition Research*, **33**, 343-438.
- Kitabatake, N. & Doi, E. (1991). Denaturation and texturization of food protein by extrusion cooking. In: Food extrusion science and technology (edited by Kokini, J. L., Ho, C.-T. & Karwe, M. V.). Pp. 361-371. New York: Marcel Dekker, Inc.
- Kitabatake, N., Mégard, D. & Cheftel, J. C. (1985). Continuous gel formation by HTST extrusion-cooking: Soy proteins. *Journal of Food Science*, **50**, 1260-1265.
- Köhler, P. (2003). Amino acid and protein sequence analysis. In: Wheat Gluten Protein Analysis (edited by Shewry, P. R. & Lookhart, G. L.). Pp. 137-158. St. Paul, MN, USA: American Association of Cereal Chemists.
- Kohlgrüber, K. (2012). Co-rotating twin-screw extruder. Carl Hanser Verlag GmbH & Company KG.
- Kosson, R., Czuchajowska, Z. & Pomeranz, Y. (1994). Smooth and wrinkled peas. 1. General physical and chemical characteristics. *Journal of Agricultural and Food Chemistry*, **42**, 91-95.
- Krintiras, G. A., Gadea Diaz, J., van der Goot, A. J., Stankiewicz, A. I. & Stefanidis, G. D. (2016). On the use of the Couette Cell technology for large scale production of textured soy-based meat replacers. *Journal of Food Engineering*, **169**, 205-213.
- Krintiras, G. A., Gobel, J., Bouwman, W. G., Jan van der Goot, A. & Stefanidis, G. D. (2014). On characterization of anisotropic plant protein structures. *Food & Function*, **5**, 3233-3240.
- Krintiras, G. A., Göbel, J., van der Goot, A. J. & Stefanidis, G. D. (2015). Production of structured soy-based meat analogues using simple shear and heat in a Couette Cell. *Journal of Food Engineering*, **160**, 34-41.
- Kulicke, W. M. & Porter, R. S. (1980). Relation between steady shear-flow and dynamic rheology. *Rheologica Acta*, **19**, 601-605.

- Laemmli, U. K. (1970). Cleavage of structural proteins during the assembly of the head of bacteriophage 4. *Nature*, 680-685.
- Lafleur, P. G. & Vergnes, B. (2014). *Polymer Extrusion*. Wiley.
- Lai, L. S. & Kokini, J. L. (1991). Physicochemical changes and rheological properties of starch during extrusion. (A review). *Biotechnology Progress*, 7, 251-266.
- Lampart-Szczapa, E., Konieczny, P., Nogala-Kałużka, M., Walczak, S., Kossowska, I. & Malinowska, M. (2006). Some functional properties of lupin proteins modified by lactic fermentation and extrusion. *Food Chemistry*, 96, 290-296.
- Leeb, C. V., Maiser, B. & Schuchmann, H. R. (2008). Bestimmung der Verweilzeitverteilung bei der Kochextrusion von Maisgrieß in einem Hochgeschwindigkeitsextruder. *Chemie Ingenieur Technik*, 80, 1175-1179.
- Leterme, P., Monmart, T. & Baudart, E. (1990). Amino acid composition of pea (*Pisum sativum*) proteins and protein profile of pea flour. *Journal of the Science of Food and Agriculture*, 53, 107-110.
- Li, M. & Lee, T. C. (1996). Effect of extrusion temperature on solubility and molecular weight distribution of wheat flour proteins. *Journal of Agricultural and Food Chemistry*, 44, 763-768.
- Li, P. X., Campanella, O. H. & Hardacre, A. K. (2004). Using an in-line slit-die viscometer to study the effects of extrusion parameters on corn melt rheology. *Cereal Chemistry Journal*, 81, 70-76.
- Lillford, P. J. (2008). Extrusion. In: *Food Materials Science* (edited by Aguilera, J. M. & Lillford, P. J.). Pp. 415-435. Springer New York.
- Lin, M. J. Y., Humbert, E. S. & Sosulski, F. W. (1974). Certain functional properties of sunflower meal products. *Journal of Food Science*, 39, 368-370.
- Lin, S., Huff, H. E. & Hsieh, F. (2000). Texture and chemical characteristics of soy protein meat analog extruded at high moisture. *Journal of Food Science*, 65, 264-269.
- Lin, S., Huff, H. E. & Hsieh, F. (2002). Extrusion process parameters, sensory characteristics, and structural properties of a high moisture soy protein meat analog. *Journal of Food Science*, 67, 1066-1072.
- Little, C., Aguilera, J. M., Morales, A. & Kokini, J. (1997). Changes in soy protein during heating analyzed by pressure rheometry. *Food Science and Technology International, Tokyo*, 3, 130-133.
- Liu, K. S. & Hsieh, F. H. (2007). Protein-protein interactions in high moisture-extruded meat analogs and heat-induced soy protein gels. *Journal of the American Oil Chemists Society*, 84, 741-748.
- Liu, K. S. & Hsieh, F. H. (2008). Protein-protein interactions during high-moisture extrusion for fibrous meat analogues and comparison of protein solubility methods using different solvent systems. *Journal of Agricultural and Food Chemistry*, 56, 2681-2687.

- MacDonald, R. S., Pryzbyszewski, J. & Hsieh, F.-H. (2009). Soy protein isolate extruded with high moisture retains high nutritional quality. *Journal of Agricultural and Food Chemistry*, **57**, 3550-3555.
- Mackey, K. L. (1989). A generalized viscosity model for the cooking extrusion of starch based products (Doctoral dissertation). Michigan State University.
- Manas-Zloczower, I. (2012). *Mixing and Compounding of Polymers: Theory and Practice*. Carl Hanser Verlag GmbH & Company KG.
- Maninder, K., Sandhu, K. S. & Singh, N. (2007). Comparative study of the functional, thermal and pasting properties of flours from different field pea (*Pisum sativum* L.) and pigeon pea (*Cajanus cajan* L.) cultivars. *Food Chemistry*, **104**, 259-267.
- Mariotti, F., Pueyo, M. E., Tomé, D., Bérot, S., Benamouzig, R. & Mahé, S. (2001). The influence of the albumin fraction on the bioavailability and postprandial utilization of pea protein given selectively to humans. *The Journal of Nutrition*, **131**, 1706-1713.
- Martelli, F. G. (1983). *Twin screw extruders: a basic understanding*. Springer.
- Martínez-Villaluenga, C., Gulewicz, P., Frias, J., Gulewicz, K. & Vidal-Valverde, C. (2008). Assessment of protein fractions of three cultivars of *Pisum sativum* L.: Effect of germination. *European Food Research and Technology*, **226**, 1465-1478.
- Mathanker, S. K., Weckler, P. R. & Bowser, T. J. (2013). X-ray applications in food and agriculture: A review. *Transactions of the ASABE*, **56**, 1227-1239.
- Mathmann, K., Kuhn, M. & Briesen, H. (2014). Application of micro-computed tomography in food and beverage technology using the examples of textured vegetable protein and filtration steps in the brewing process. In: iCT Conference 2014. Haifa, Israel.
- Mélo, T. J. A. & Canevarolo, S. V. (2002). An optical device to measure in-line residence time distribution curves during extrusion. *Polymer Engineering & Science*, **42**, 170-181.
- Mensa-Wilmot, Y., Phillips, R. D. & Hargrove, J. L. (2001). Protein quality evaluation of cowpea-based extrusion cooked cereal/legume weaning mixtures. *Nutrition Research*, **21**, 849-857.
- Mercier, C., Linko, P. & Harper, J. M. (1989). *Extrusion Cooking*. American Association of Cereal Chemists.
- Meuser, F. & Van Lengerich, B. (1984). System analytical model for the extrusion of starches. In: *Thermal processing and quality of foods*. (edited by Zeuthen, P., Cheftel, J. C. & Eriksson, C.). Pp. 175-179. London: Elsevier.
- Mezger, T. G. (2006). *The rheology handbook: for users of rotational and oscillatory rheometers*. Vincentz Network.
- Mitchell, J. R. & Areas, J. A. G. (1992). Structural changes in biopolymers during extrusion. In: *Food extrusion science and technology* (edited by Kokini, J. L., Ho, C. & Karwe, M. V.). Pp. 345-360. New York: Marcel Dekker Inc.

- Moisio, T., Forssell, P., Partanen, R., Damerou, A. & Hill, S. E. (2015). Reorganisation of starch, proteins and lipids in extrusion of oats. *Journal of Cereal Science*, **64**, 48-55.
- Moore, J. C., DeVries, J. W., Lipp, M., Griffiths, J. C. & Abernethy, D. R. (2010). Total protein methods and their potential utility to reduce the risk of food protein adulteration. *Comprehensive Reviews in Food Science and Food Safety*, **9**, 330-357.
- Moore, S. (1963). On the determination of cystine as cysteic acid. *The Journal of Biological Chemistry*, **238**, 235-237.
- Morales, A. & Kokini, J. L. (1999). State diagrams of soy globulins. *Journal of Rheology*, **43**, 315-325.
- Moraru, C. I. & Kokini, J. L. (2003). Nucleation and expansion during extrusion and microwave heating of cereal foods. *Comprehensive Reviews in Food Science and Food Safety*, **2**, 147-165.
- Morr, C. V., German, B., Kinsella, J. E., Regenstein, J. M., Van Buren, J. P. & Kilara, A. (1985). A collaborative study to develop a standardized Food protein solubility procedure. *Journal of Food Science and Technology*, **50**, 1715-1718.
- Moscicki, L. (2011). Extrusion cooking techniques. Pp. 220. Wiley-VCH, Weinheim.
- Munialo, C. D., Martin, A. H., van der Linden, E. & de Jongh, H. H. J. (2014). Fibril formation from pea protein and subsequent gel formation. *Journal of Agricultural and Food Chemistry*, **62**, 2418-2427.
- Munialo, C. D., van der Linden, E., Ako, K. & de Jongh, H. H. J. (2015). Quantitative analysis of the network structure that underlines the transitioning in mechanical responses of pea protein gels. *Food Hydrocolloids*, **49**, 104-117.
- Naczki, M., Rubin, L. J. & Shahidi, F. (1986). Functional properties and phytate content of pea protein preparations. *Journal of Food Science*, **51**, 1245-1247.
- Nakai, S. & Modler, H. W. (2000). Food proteins: processing applications. Wiley-VCH.
- Nielsen, P. M., Petersen, D. & Dambmann, C. (2001). Improved method for determining food protein degree of hydrolysis. *Journal of Food Science*, **66**, 642-646.
- Noguchi, A. (1990). Extrusion cooking of high moisture protein foods. In: Extrusion Cooking (edited by Mercier, C. L., P.; Harper, J.M.). Pp. 343-369. Minnesota: AACC.
- Noguchi, A., Jaekag, L. & Wakamiya, S. (1986). Extrusion cooking in high moisture meat analog from defatted soy flour with twin screw extruder. *Journal of the American Oil Chemists Society*, **63**, 407-408.
- Noguchi, A., Mosso, K., Aymard, C., Jeunink, J. & Cheftel, J. C. (1982). Maillard reactions during extrusion cooking of protein-enriched biscuits. *Lebensmittel-Wissenschaft und Technologie*, **15** 105-110.
- Nowak-Wegrzyn, A., Sampson, H. A., Wood, R. A. & Sicherer, S. H. (2003). Food protein-induced enterocolitis syndrome caused by solid food proteins. *Pediatrics*, **111**, 829-835.

- O'Kane, F. E., Happe, R. P., Vereijken, J. M., Gruppen, H. & van Boekel, M. A. J. S. (2004). Heat-induced gelation of pea legumin: comparison with soybean glycinin. *Journal of Agricultural and Food Chemistry*, **52**, 5071-5078.
- Onomi, S., Okazaki, Y. & Katayama, T. (2004). Effect of dietary level of phytic acid on hepatic and serum lipid status in rats fed a high-sucrose diet. *Bioscience, Biotechnology, and Biochemistry*, **68**, 1379-81.
- Onwulata, C. I., Tunick, M. H. & Thomas-Gahring, A. E. (2014). Rapid visco analysis of food protein pastes. *Journal of Food Processing and Preservation*, **38**, 2083-2089.
- Osen, R. & Schweiggert-Weisz, U. (2016). High-Moisture Extrusion: Meat Analogues. In: Reference Module in Food Science. Elsevier.
- Osen, R., Toelstede, S., Eisner, P. & Schweiggert-Weisz, U. (2015). Effect of high moisture extrusion cooking on protein-protein interactions of pea (*Pisum sativum* L.) protein isolates. *International Journal of Food Science & Technology*, **50**, 1390-1396.
- Osen, R., Toelstede, S., Wild, F., Eisner, P. & Schweiggert-Weisz, U. (2014). High moisture extrusion cooking of pea protein isolates: Raw material characteristics, extruder responses, and texture properties. *Journal of Food Engineering*, **127**, 67-74.
- Owusu-Ansah, Y. J. & McCurdy, S. M. (1991). Pea proteins: A review of chemistry, technology of production, and utilization. *Food Reviews International*, **7**, 103-134.
- Pelgrom, P. J. M., Boom, R. M. & Schutyser, M. A. I. (2015). Functional analysis of mildly refined fractions from yellow pea. *Food Hydrocolloids*, **44**, 12-22.
- Peng, J., Huff, H. E. & Hsieh, F. (1994). An RTD determination method for extrusion cooking. *Journal of Food Processing and Preservation*, **18**, 263-277.
- Petrucelli, S. & Anon, M. C. (1995). Soy protein isolate components and their interactions. *Journal of Agricultural and Food Chemistry*, **43**, 1762-1767.
- Prudencio-Ferreira, S. H. & Areas, J. G. (1993). Protein-protein interactions in the extrusion of soya at various temperatures and moisture contents. *Journal of Food Science*, **58**, 378-381.
- Ranasinghesagara, J., Hsieh, F. & Yao, G. (2006). A photon migration method for characterizing fiber formation in meat analogs. *Journal of Food Science*, **71**, E227-E231.
- Ranasinghesagara, J., Hsieh, F. H., Huff, H. & Yao, G. (2009). Laser scanning system for real-time mapping of fiber formations in meat analogues. *Journal of Food Science*, **74**, E39-E45.
- Ranasinghesagara, J., Hsieh, F. H. & Yao, G. (2005). An image processing method for quantifying fiber formation in meat analogs under high moisture extrusion. *Journal of Food Science*, **70**, E450-E454.
- Ranasinghesagara, J. & Yao, G. (2007). Imaging 2D optical diffuse reflectance in skeletal muscle. *Opt. Express*, **15**, 3998-4007.



- Rao, M. A. (2007). Flow and Functional Models for Rheological Properties of Fluid Foods. In: *Rheology of Fluid and Semisolid Foods: Principles and Applications*. Pp. 27-58. Boston, MA: Springer US.
- Rao, M. A. & Cooley, H. J. (1992). Rheological behavior of tomato pastes in steady and dynamic shear. *Journal of Texture Studies*, **23**, 415-425.
- Ratnayake, W. S., Hoover, R. & Warkentin, T. (2002). Pea starch: composition, structure and properties - a review. *Starch*, **54**, 217-234.
- Rauh, C., Baier, D., Heinz, V., Toepfl, S., Schuchmann, H. P. & Emin, A. (2015). Aufklärung der Texturierungsmechanismen bei der Nassextrusion von Soja- und Erbsenprotein unter besonderer Berücksichtigung biothermofluidodynamischer und proteinchemischer Aspekte auf Basis experimenteller und numerischer Untersuchungen. Project proposal (AiF 18727 N), Forschungsbereich der Ernährungsindustrie e.V. (FEI).
- Renkema, J. M. & van Vliet, T. (2002). Heat-induced gel formation by soy proteins at neutral pH. *Journal of Agricultural and Food Chemistry*, **50**, 1569-73.
- Renkema, J. M. S. (2004). Relations between rheological properties and network structure of soy protein gels. *Food Hydrocolloids*, **18**, 39-47.
- Renkema, J. M. S., Lakemond, C. M. M., de Jongh, H. H. J., Gruppen, H. & van Vliet, T. (2000). The effect of pH on heat denaturation and gel forming properties of soy proteins. *Journal of Biotechnology*, **79**, 223-230.
- Riaz, M. N. (2000). *Extruders in food applications*. CRC Press.
- Riaz, M. N. (2004). Texturized soy protein as an ingredient. In: *Proteins in food processing* (edited by Yada, R. Y.). Pp. 517, 558 p. Cambridge, Eng.: CRC Press ; Woodhead Pub.
- Riaz, M. N. (2006). *Soy applications in food*. Pp. 288 p. Boca Raton, Fla., CRC.
- Riedel, E. (2010). *Allgemeine und anorganische Chemie*. Pp. 452. De Gruyter.
- Roberts, I. (2001). In-line and on-line rheology measurement of food. In: *Instrumentation and Sensors for the Food Industry* (edited by Kress-Rogers, E. & Brimelow, C. J. B.). Pp. 403-422. Elsevier Science.
- Román, L., Dura, Á., Martínez, M. M., Rosell, C. M. & Gómez, M. (2016). Combination of extrusion and cyclodextrin glucanotransferase treatment to modify wheat flours functionality. *Food Chemistry*, **199**, 287-295.
- Roos, Y. H. & Drusch, S. (2015). *Phase Transitions in Foods*. Elsevier Science.
- Rosentrater, K. A., Muthukumarappan, K. & Kannadhasan, S. (2009). Effects of ingredients and extrusion parameters on properties of aquafeeds containing DDGS and corn starch. *Journal of Aquaculture Feed Science and Nutrition*, **1**, 44-60.
- Sahin, S. & Sumnu, S. G. (2006). *Rheological Properties of Foods*. In: *Physical Properties of Foods*. Pp. 39-105. Springer New York.

- Sathe, S. K. (2002). Dry bean protein functionality. *Critical Reviews in Biotechnology*, **22**, 175-223.
- Saunders, J., Levin, D. B. & Izydorczyk, M. (2011). Limitations and Challenges for Wheat-Based Bioethanol Production. INTECH Open Access Publisher.
- Schneider, A. & Lacampagne, J. P. (2000). Peas: a European production of protein-rich materials for feed and food. *Industrial Proteins*, 3-6.
- Schuchmann, H. P. (2008). Extrusion zur Gestaltung von Lebensmittelstrukturen. *Chemie Ingenieur Technik*, **80**, 1097-1106.
- Schutyser, M. A. I., Pelgrom, P. J. M., van der Goot, A. J. & Boom, R. M. (2015). Dry fractionation for sustainable production of functional legume protein concentrates. *Trends in Food Science and Technology*, **45**, 327-335.
- Shand, P. J., Ya, H., Pietrasik, Z. & Wanasundara, P. K. J. P. D. (2007). Physicochemical and textural properties of heat-induced pea protein isolate gels. *Food Chemistry*, **102**, 1119-1130.
- Sheard, P. R., Fellows, A., Ledward, D. A. & Mitchell, J. R. (1986). Macromolecular changes associated with the heat treatment of soya isolate. *International Journal of Food Science & Technology*, **21**, 55-60.
- Shenoy, A. V., Chattopadhyay, S. & Nadkarni, V. M. (1983). From melt flow index to rheogram. *Rheologica Acta*, **22**, 90-101.
- Shevkani, K., Singh, N., Kaur, A. & Rana, J. C. (2015). Structural and functional characterization of kidney bean and field pea protein isolates: A comparative study. *Food Hydrocolloids*, **43**, 679-689.
- Shewry, P. R. & Halford, N. G. (2002). Cereal seed storage proteins: structures, properties and role in grain utilization. *Journal of Experimental Botany*, **53**, 947-58.
- Shih, F. & Daigle, K. (2000). Preparation and characterization of rice protein isolates. *Journal of the American Oil Chemists' Society*, **77**, 885-889.
- Sikorski, Z. E. (2001). Chemical and Functional Properties of Food Proteins. Taylor & Francis.
- Smil, V. (2000). Feeding the world: a challenge for the twenty-first century. Pp. xxxviii, 360 p. Cambridge, Mass., MIT Press.
- Smonskey, R. W. & Stanley, D. W. (1982). Texture-structure relationships in textured soy protein. V. Influence of pH and protein acylation on extrusion texturization. *Canadian Institute of Food Science and Technology Journal*, **15**, 294-301.
- Sorba, A. & Sopade, P. A. (2013). Changes in rapid visco-analysis (RVA) viscosity reveal starch digestion behaviours. *Starch - Stärke*, **65**, 437-442.
- Sosulski, F. W. & Mccurdy, A. R. (1987). Functionality of flours, protein-fractions and isolates from field peas and faba bean. *Journal of Food Science*, **52**, 1010-1014.

- Sousa, I. M. N., Mitchell, J. R., Ledward, D. A., Hill, S. E. & daCosta, M. L. B. (1995). Differential scanning calorimetry of lupin and soy proteins. *Zeitschrift Fur Lebensmittel-Untersuchung Und-Forschung*, **201**, 566-569.
- Steinfeld, H., Gerber, P., Wassenaar, T., Castel, V., Rosales, M. & De Haan, C. (2006). *Livestock's long shadow: Environmental issues and options*. Rome, Italy: FAO.
- Stephen, A. M. & Phillips, G. O. (2006). *Food polysaccharides and their applications*. CRC Press.
- Stevens, M. J. & Covas, J. (1995). *Extruder Principles and Operation*. Springer Netherlands.
- Stone, A. K., Karalash, A., Tyler, R. T., Warkentin, T. D. & Nickerson, M. T. (2015). Functional attributes of pea protein isolates prepared using different extraction methods and cultivars. *Food Research International*, **76, Part 1**, 31-38.
- Storz, H., Zimmermann, U., Zimmermann, H. & Kulicke, W.-M. (2010). Viscoelastic properties of ultra-high viscosity alginates. *Rheologica Acta*, **49**, 155-167.
- Su, J.-F., Huang, Z., Yuan, X.-Y., Wang, X.-Y. & Li, M. (2010). Structure and properties of carboxymethyl cellulose/soy protein isolate blend edible films crosslinked by Maillard reactions. *Carbohydrate Polymers*, **79**, 145-153.
- Sumner, A. K., Nielsen, M. A. & Youngs, C. G. (1981). Production and evaluation of pea protein isolate. *Journal of Food Science*, **46**, 364-366.
- Sun, X. D. & Arntfield, S. D. (2010). Gelation properties of salt-extracted pea protein induced by heat treatment. *Food Research International*, **43**, 509-515.
- Sun, X. D. & Arntfield, S. D. (2011). Gelation properties of salt-extracted pea protein isolate induced by heat treatment: Effect of heating and cooling rate. *Food Chemistry*, **124**, 1011-1016.
- Swanson, B. G. (1990). Pea and lentil protein extraction and functionality. *Journal of the American Oil Chemists Society*, **67**, 276-280.
- Tabilo-Munizaga, G. & Barbosa-Cánovas, G. V. (2005). Rheology for the food industry. *Journal of Food Engineering*, **67**, 147-156.
- Thiebaud, M., Dumay, E. & Cheftel, J. C. (1996). Influence of process variables on the characteristics of a high moisture fish soy protein mix texturized by extrusion cooking. *Food Science and Technology-Lebensmittel-Wissenschaft & Technologie*, **29**, 526-535.
- Thompson, M., Puaux, J. P., Hrymak, A. N. & Hamielec, A. E. (1995). Modeling the residence time distribution of a non-intermeshing twin screw extruder. *International Polymer Processing*, **10**, 111-119.
- Tiziani, S. & Vodovotz, Y. (2005). Rheological effects of soy protein addition to tomato juice. *Food Hydrocolloids*, **19**, 45-52.

- Tolstoguzov, V. (1988). Creation of fibrous structures by spinneretless spinning. In: Food Structure-Its Creation and Evaluation (edited by Blanshard, J. M. V. & Mitchell, J. R.). Pp. 181–196. Butterworths, London.
- Tolstoguzov, V. (1993). Thermoplastic extrusion-the mechanism of the formation of extrudate structure and properties. *Journal of the American Oil Chemists' Society*, **70**, 417-424.
- Tolstoguzov, V. B., Grinberg, V. Y. & Gurov, A. N. (1985). Some physicochemical approaches to the problem of protein texturization. *Journal of Agricultural and Food Chemistry*, **33**, 151-159.
- Tomoskozi, S., Lasztity, R., Haraszi, R. & Baticz, O. (2001). Isolation and study of the functional properties of pea proteins. *Nahrung-Food*, **45**, 399-401.
- Tsitzikas, E. N. (2005). Exploring variation in pea protein composition by natural selection and genetic transformation (Doctoral Dissertation). Wageningen University, The Netherlands.
- Tung, M. A. (1978). Rheology of protein dispersions. *Journal of Texture Studies*, **9**, 3-31.
- Utsumi, S. & Kinsella, J. E. (1985). Forces Involved in soy protein gelation - Effects of various reagents on the formation, hardness and solubility of heat-induced gels made from 7s, 11s, and soy isolate. *Journal of Food Science*, **50**, 1278-1282.
- Van Der Borgh, A., Goesaert, H., Veraverbeke, W. S. & Delcour, J. A. (2005). Fractionation of wheat and wheat flour into starch and gluten: overview of the main processes and the factors involved. *Journal of Cereal Science*, **41**, 221-237.
- Van Der Poel, A. F. B. (1990). Effect of processing on antinutritional factors and protein nutritional value of dry beans (*Phaseolus vulgaris* L.). A review. *Animal Feed Science and Technology*, **29**, 179-208.
- Vélez-Ruiz, J. F. & Barbosa-Cánovas, G. V. (1998). Rheological properties of concentrated milk as a function of concentration, temperature and storage time. *Journal of Food Engineering*, **35**, 177-190.
- Vidal-Valverde, C., Frias, J., Hernández, A., Martín-Alvarez, P. J., Sierra, I., Rodríguez, C., Blazquez, I. & Vicente, G. (2003). Assessment of nutritional compounds and antinutritional factors in pea (*Pisum sativum*) seeds. *Journal of the Science of Food and Agriculture*, **83**, 298-306.
- Wang, H. W., Zhou, J. G. & Lin, B. J. (2001). Effect of processing variables of twin-screw extrusion on texturization of compound soybean protein. *Journal of the Chinese Cereals and Oils Association*, **16**, 54-58.
- Wang, S. M., Bouvier, J. M. & Gelus, M. (1990). Rheological behaviour of wheat flour dough in twin-screw extrusion cooking. *International Journal of Food Science and Technology*, **25**, 129-139.
- Wang, Y. (2000). Compounding in Co-Rotating Twin-Screw Extruders. Rapra Technology Ltd.

- Wäsche, A., Müller, K. & Knauf, U. (2001). New processing of lupin protein isolates and functional properties. *Nahrung/Food*, **45**, 393-395.
- Wild, F. (2012). Herstellung und Charakterisierung von Proteinprodukten aus Pelerbsen und deren Potential zur Bildung von Proteinmatrices mit hohen Lipidanteilen in Futtermitteln für Salmoniden (Doctoral Dissertation). Technischen Universität Berlin.
- Wolf, D. & White, D. H. (1976). Experimental study of the residence time distribution in plasticating screw extruder. *AIChE Journal*, **22**.
- Wu, F., Meng, Y., Yang, N., Tao, H. & Xu, X. (2015). Effects of mung bean starch on quality of rice noodles made by direct dry flour extrusion. *LWT - Food Science and Technology*, **63**, 1199-1205.
- Yada, R. Y. (2004). Proteins in food processing. Pp. xviii, 686 p. Cambridge, Eng., CRC Press ; Woodhead Pub.
- Yao, G., Liu, K. S. & Hsieh, F. (2004). A new method for characterizing fiber formation in meat analogs during high-moisture extrusion. *Journal of Food Science*, **69**, 303-307.
- Yaşar, K., Kahyaoglu, T. & Şahan, N. (2009). Dynamic rheological characterization of salep glucomannan/galactomannan-based milk beverages. *Food Hydrocolloids*, **23**, 1305-1311.
- Yin, S.-W., Tang, C.-H., Wen, Q.-B., Yang, X.-Q. & Li, L. (2008). Functional properties and in vitro trypsin digestibility of red kidney bean (*Phaseolus vulgaris* L.) protein isolate: Effect of high-pressure treatment. *Food Chemistry*, **110**, 938-945.
- Yu, G. Q., Warkentin, T., Niu, Z., Khan, N. A. & Yu, P. (2015). Molecular basis of processing-induced changes in protein structure in relation to intestinal digestion in yellow and green type pea (*Pisum sativum* L.): A molecular spectroscopic analysis. *Spectrochimica Acta Part A: Molecular and Biomolecular Spectroscopy*, **151**, 980-988.
- Zayas, J. F. (1997). Functionality of proteins in food. Pp. x, 373 p. New York, Springer.
- Zhang, B., Zhang, Y., Dreisoerner, J. & Wei, Y. (2015). The effects of screw configuration on the screw fill degree and special mechanical energy in twin-screw extruder for high-moisture texturised defatted soybean meal. *Journal of Food Engineering*, **157**, 77-83.



## 8 Appendix

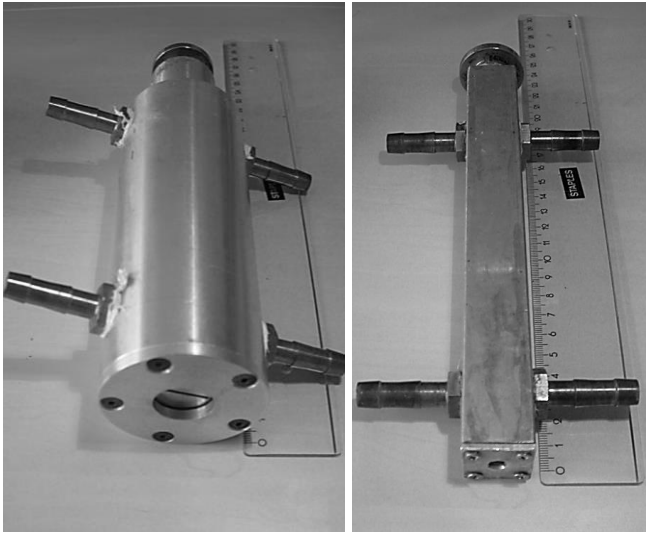


Figure 83: Cooling dies used for lab scale experiments with (a) rectangular and (b) slit-shaped die opening.

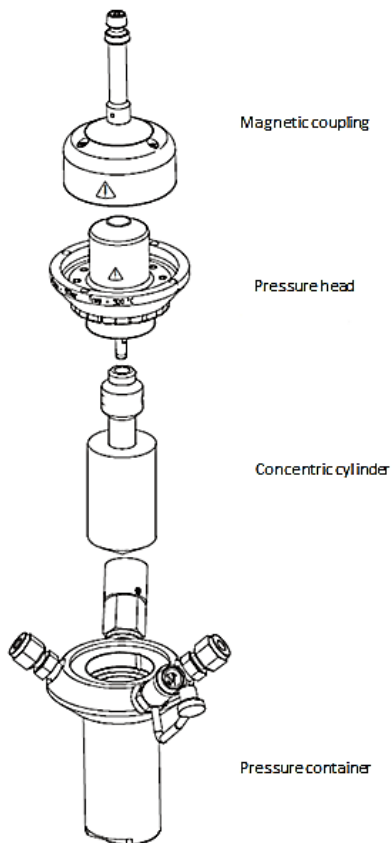


Figure 84: Schematic view of pressure cell for temperature sweep measurements of high moisture extrudates (Anton-Paar, Graz, Austria).

**Table 31: Water activity of protein dispersions of PPI 1 as a factor of protein concentration.**

<b>moisture content [%]</b>	<b>water activity</b>
55	0.985±0.000
60	0.989±0.000
65	0.991±0.001

**Table 32: Screw elements used during pilot plant trials.**

<b>Quantity</b>	<b>Label</b>
1 x	16/16
5 x	36/36
2 x	KB45/5/12
1 x	36/36
2 x	24/24
1 x	24/12
1 x	KB90/5/24
2 x	36/36
1 x	36/18
1 x	KB90/5/24
2 x	36/36
4 x	24/24
1 x	24/12
1 x	24/24 RECESSED



## 9 Curriculum Vitae

### Contact details

Raffael Osen                      Fischergasse 5  
85354 Freising  
Email: raffael.osen@ivv.fraunhofer.de  
Phone: +49 176 56766747



### Date and place of birth

25/05/1982                      Offenburg, Germany

### Education

- 09/2010- current              PhD candidate, Technical University Munich, Freising
- PhD topic.: Texturization of pea protein isolates using high moisture extrusion cooking. Advisor: Prof. Dr. H.C. Langowski
- 04/2004- 06/2010              Dipl.-Ing. Food Technology, Bonn University
- Thesis: Applicability of dielectric time domain reflectometry for the detection of added water in fish and seafood
- 1992- 2002                      Werner Heisenberg Gymnasium, Weinheim
- 1988- 1992                      Johann-Rupprecht Grundschule, Reinstetten Forchheim

### Work experience

- 04/2017 – current              Deputy Head Department for Food Process Engineering, Fraunhofer IVV, Freising
- 02/2016 – 04/2017              Team Leader Food Technology, Department for Food Process Engineering, Fraunhofer IVV, Freising
- 02/2015 – 02/2016              Research Scientist, Department for Food Process Engineering, Fraunhofer IVV, Freising
- 09/2010- 02/2015              PhD candidate, Department for Food Process Engineering Fraunhofer IVV, Freising
- Research projects:
  - Meat Surrogates: Determination of the formation mechanisms of fibrous microstructures during the production of vegetable meat surrogates. Project leader. BMBF Federal Ministry of Research and Education.

- LikeMeat: High quality meat-like products - from niche markets to widely accepted meat alternatives. Subproject leader. FP 7 EU project.
- Preparation for founding a spin-off of the Fraunhofer IVV for the production and marketing of high moisture meat alternatives. Project leader. FhG Fraunhofer project “Fraunhofer fosters entrepreneurs”.
- Selected for Fraunhofer career program “Step forward”

### Journal Articles (peer reviewed)

Muranyi, I. S., Otto, C., Pickardt, C., Osen, R., Koehler, P., & Schweiggert-Weisz, U. (2016). Influence of the Isolation Method on the Technofunctional Properties of Protein Isolates from *Lupinus angustifolius* L. *Journal of Food Science*, **81**(11), C2656-C2663.

Tyapkova, O., Osen, R., Wagenstaller, M., Baier, B., Specht, F., & Zacherl, C. (2016). Replacing fishmeal with oilseed cakes in fish feed – A study on the influence of processing parameters on the extrusion behavior and quality properties of the feed pellets. *Journal of Food Engineering*, **191**, 28-36.

Osen, R., Schweiggert-Weisz, U., 2016. High-Moisture Extrusion: Meat Analogues. *Reference Module in Food Sciences*. Elsevier, pp. 1–7.

Osen, R., Toelstede, S., Eisner, P., Schweiggert-Weisz, U. (2015). Effect of high moisture extrusion cooking on the protein composition and protein-protein interactions of pea (*Pisum Sativum* L.) protein isolates. *International Journal of Food Science and Technology* **50**, 1390-1396.

Osen, R., Toelstede, S., Wild, F., Eisner, P., Schweiggert-Weisz, U. (2014). High moisture extrusion cooking of pea protein isolates: Raw material characteristics, extruder responses, and texture properties. *Journal of Food Engineering* **127**, 67-74.

### Oral presentations

Osen, R. (2017). Texturization of plant protein using extrusion cooking. Innovations in Food Science and technology. Erding, Germany.

Osen, R. (2014). Texturization of pea proteins by high moisture extrusion cooking. Advances in Food Processing: Challenges for the Future; Campinas, Brasil

Osen, R. (2014). High moisture extrusion cooking of pea protein isolate: Effect of extrusion temperature on the protein composition and protein-protein interactions. IUFoST, Montreal, Canada

Mathmann K., Osen, R., Eisner, P., Briesen, H. (2013). Comparison of the microstructure of meat and meat-like extruded vegetable proteins. Delivery of Functionality in Complex Food Systems- Physically-Inspired Approaches from the Nanoscale to the Microscale, Haifa, Israel

Osen, R., Limbrunner, S., Wild, F., Ute Weisz (2012). Interactions of proteins during high-moisture extrusion cooking of pea protein. European Federation of Food Science and Technology (EFFoST), Montpellier, France

**Poster presentations**

Osen, R., Toelstede, S., Wild, F., Eisner, P., Schweiggert-Weisz, U.(2014). High moisture extrusion cooking of pea protein isolates: Raw material characteristics, extruder responses, and texture properties. Food Structure Symposium: From molecules to functionality, Amsterdam, Netherlands

Osen, R., Limbrunner, S., Wild, F., Schweiggert-Weisz, U. (2013). The role of covalent disulfide-bonding during high-moisture extrusion cooking of pea protein isolate. Capabilities of Vegetable Proteins, 19th International Scientific Conference, IGV Institut für Getreideverarbeitung GmbH, Nuthetal, Germany

Osen, R., Hemmy, B. (2009). A rapid method to detect added water in seafood by its dielectric properties; European Federation of Food Science and Technology, Budapest, Hungary

**Patent applications**

Einser, P., Osen, R. (2014). Extruded plant protein product with colouring plant ingredients and production method (WO 2016000940 A1)

**Reviewer activities**

Innovative Food Science and Emerging Technologies

**Co-supervision of thesis**

2016	Rheologische Eigenschaften von Erbsenprotein dispersionen in Abhängigkeit von der Temperatur
2014	Effekt proteinreicher Saaten auf Farbe und sensorische Eigenschaften von Nasstexturaten aus Erbsenprotein
2014	Trockentexturierung pflanzlicher Proteine mittels Extrusion: Einfluss von Rohstoff- und Prozessparametern auf Produkteigenschaften
2013	Texturization of plant protein during high moisture extrusion cooking
2012	Proteinbasierte Kochextrusion mit hohem Wasseranteil: Einfluss von Stärken auf die Texturierung
2011	Einfluss der Extrusionsprozessparameter auf die Faserausbildung von kochextrudiertem Erbsenproteinisolat mit hohem Feuchtegehalt
2011	Vernetzungseigenschaften von Erbsenprotein während dem Kochextrusionsprozess